



저작자표시-비영리-변경금지 2.0 대한민국

이용자는 아래의 조건을 따르는 경우에 한하여 자유롭게

- 이 저작물을 복제, 배포, 전송, 전시, 공연 및 방송할 수 있습니다.

다음과 같은 조건을 따라야 합니다:



저작자표시. 귀하는 원저작자를 표시하여야 합니다.



비영리. 귀하는 이 저작물을 영리 목적으로 이용할 수 없습니다.



변경금지. 귀하는 이 저작물을 개작, 변형 또는 가공할 수 없습니다.

- 귀하는, 이 저작물의 재이용이나 배포의 경우, 이 저작물에 적용된 이용허락조건을 명확하게 나타내어야 합니다.
- 저작권자로부터 별도의 허가를 받으면 이러한 조건들은 적용되지 않습니다.

저작권법에 따른 이용자의 권리는 위의 내용에 의하여 영향을 받지 않습니다.

이것은 [이용허락규약\(Legal Code\)](#)을 이해하기 쉽게 요약한 것입니다.

[Disclaimer](#)

Thesis for a Ph. D. Degree

Role of Vegetation and Cloud on Arctic
Climate Change: A Modeling Study

북극지역에서 식생과 구름이 기후변화에 미치는
영향의 모델링 연구

Sang-Yoon Jun

February 2014

School of Earth and Environmental Sciences
Graduate School
Seoul National University

이학박사학위논문

북극지역에서 식생과 구름이 기후변화에
미치는 영향의 모델링 연구

Role of Vegetation and Cloud on Arctic Climate Change:
A Modeling Study

2014년 2월

서울대학교 대학원

지구환경과학부

전 상 운

Role of Vegetation and Cloud on Arctic Climate Change: A Modeling Study

by
Sang-Yoon Jun

Dissertation Submitted to the Faculty of the Graduate School of the
Seoul National University in Partial Fulfillment of the Requirement
for the Degree of Doctor of Philosophy

Degree Awarded:
February 2014

Advisory committee:

Professor	Rokjin Park, Chair
Professor	Chang-Hoi Ho, Advisor
Doctor	Seong-Joong Kim
Professor	Soon-Il An
Professor	Myong-In Lee

북극지역에서 식생과 구름이 기후변화에 미치는
영향의 모델링 연구
Role of Vegetation and Cloud on Arctic Climate Change:
A Modeling Study

지도교수 허 창 회

이 논문을 이학박사 학위논문으로 제출함
2013년 10월

서울대학교 대학원
지구환경과학부
전 상 윤

전 상 윤 의 이학박사 학위논문을 인준함
2013년 12월

위 원 장 _____ (인)
부위원장 _____ (인)
위 원 _____ (인)
위 원 _____ (인)
위 원 _____ (인)

ABSTRACT

The Arctic has experienced substantial warming in recent decades of which degree and rate is much larger than global averages. This phenomenon, which is also widely predicted from future climate modeling for several climate change assessment reports of the Intergovernmental Panels for Climate Change, is called as the Arctic amplification. Various climate factors on the globe could contribute to the amplified warming over the Arctic because of the highly sensitive Arctic climate system and the northward transport into the high latitude region. Much of understanding for these contributing factors come from modeling study because of lack of observation datasets owing to severe weather and climate conditions of the Arctic. In particular, less consideration of climate factors such as vegetation, cloud, and sea ice in modeling could bring large uncertainties in understanding the Arctic climate. Thus present thesis examines the contributions of vegetation and cloud to the Arctic amplification through modeling work with adopting a global dynamic vegetation model (DGVM) and improving physical processes related to sea ice and cloud.

First, modeling result from simulating the Community Climate System Model 3 (CCSM3) coupled with a DGVM indicates that potential vegetation change under a doubled CO₂ situation and its feedback have an influence on

surface warming over the Arctic/high-latitude region. This dissertation performed two baseline experiments under the present and doubling CO₂ concentration using the CCSM3-DGVM. Then, an additional simulation without DGVM was performed under doubling CO₂ concentration with the prescribed vegetation taken from the present CO₂ simulation. Model experiments indicate that a vegetation change in high-latitudes may induce substantial alteration of climate in the Arctic/high-latitude during warm and cold seasons. When the interactive vegetation process is included in the future climate simulation, vegetation in high-latitudes increases during growing season and the warming in the Arctic and high-latitude continent appears to be significantly amplified. Furthermore, and the Arctic sea ice exhibits considerable decline both in areal extent and thickness associated with the vegetation feedback effect. The present results demonstrate that a conspicuous climatic change can take place in the Arctic region from the vegetation-climate feedback, and suggest a possible positive vegetation feedback over the Arctic and high-latitude region in association with anthropogenic global warming.

Next, diagnosis and modeling on recent Arctic cloud change are conducted. The dissertation first examines changes in Arctic cloud during winter (December to February) in recent three decades and their impacts on atmospheric circulation with multiple datasets from satellite and reanalysis products. From change point

analysis applied to both datasets, it was shown that Arctic cloud decreases gradually during the late 20th century and increases considerably after late 1990s. The gradual decrease and substantial increase in each period are also seen simultaneously in the temperature and moisture at lower troposphere over the Arctic. In particular, the recent profound cloud increasing emerges over the most Arctic and expands to higher altitude compared to decreasing period, accompanying increasing in precipitation. Between decreasing and increasing periods, the relationship between cloud and the Arctic Oscillation does not change, and the region where cloud increasing and moisture upward transport are linked to sea ice reducing moves from the margin to the center of the Arctic. Changes in surface conditions between two periods indicate that reduced sea ice cover in cloud-increasing period leads to an increase in turbulent fluxes from surface, a decrease in lower tropospheric static stability, and deepening of planetary boundary layer. As a result, these altered conditions provide a favorable condition for cloud to be more formed through enhancing upward moisture transport. In addition, these changes tighten the local relationship between cloud at lower troposphere and atmospheric states over the Arctic. Diagnosis on recent cloud change suggests that sea ice change could play a crucial role on changes in cloud and its effect on the Arctic climate, also suggests that further modeling is needed due to weakness in datasets.

The modeling of the impact of sea ice on recent cloud change first performs an investigation of surface boundary condition related to sea ice change in order to obtain more accurate modeling result. It is found that the atmospheric responses related to Arctic sea ice melt in the cold season (October–March) depend on sea ice fraction and are very sensitive to *in-situ* sea surface temperature (SST) from a series of atmospheric general circulation model (AGCM) simulations in which multiple combinations of SSTs and sea ice concentrations are prescribed in the Arctic Ocean. The amplitude of surface warming over the melted sea ice region is controlled by concurrent *in-situ* SST even if these simulations are forced by the same sea ice concentration. Much of the sensitivity of surface warming to *in-situ* SST are related with large changes in surface heat fluxes such as the outgoing long-wave flux in early winter (October–December) and the sensible and latent heat fluxes for the entire cold season. Vertical extension of surface warming and moistening is sensitive to these changes as well; the associated condensational heating modulates a static stability in the lower troposphere. Thus, changes in SST fields in AGCM simulations must be implemented with extra care, especially in the melted sea ice region in the Arctic. In addition, the statistical method in the thesis for adjusting SSTs in conjunction with a given sea ice change can help to model the atmospheric response to sea ice loss more accurately.

Finally, modeling result of recent Arctic climate change with refined surface boundary condition and cloud amount parameterization suggests that recent changes in cloud and its effect on the Arctic climate are closely linked to surface condition change due to sea ice retreat even during winter. As seen in reanalyses, modeling result also describes that reduced sea ice cover leads to an increase in turbulent fluxes from surface, deepening of planetary boundary layer, and enhancing of convective process, thereby causing an increasing in cloud and closer relationship between cloud and local atmospheric state over the Arctic. Further investigation from the fifth phase the Coupled Model Intercomparison Project, of which the winter Arctic cloud increases and its impact on the Arctic becomes enhanced in future climate under global warming condition, also confirms this modeling result. The results from diagnosis and modeling emphasize that the cloud may amplify the surface warming over the Arctic during winter in recent decade, under sea ice retreat condition.

Keywords: Arctic, Arctic amplification, climate modeling, vegetation, cloud, sea ice

Student number: 2008-30822

TABLE OF CONTENTS

Abstract	i
Table of Contents.....	vi
List of Tables	viii
List of Figures	ix
1. Introduction	1
1.1. Background	1
1.2. Motivation and Objectives	4
1.3. Thesis Organization.....	8
2. Model and Data	9
2.1. Model	9
2.2. Data	13
3. Modeling the role of vegetation on the Arctic warming under greenhouse warming	17
3.1. Vegetation over the high-latitudinal region and its change	17
3.2. Modeling vegetation change and its effect under greenhouse warming 19	
3.3. The vegetation change under a doubled CO ₂ climate	21
3.4. Vegetation feedback effect on SAT and circulation changes	24
3.5. Sea ice change and atmospheric northward energy transport	30

3.6. Discussion	37
4. Modeling the role of cloud on the recent Arctic warming during winter	39
4.1. Recent change in the winter Arctic cloud.....	39
4.1.1. Year-to-year variation and trends in cloud-related variables.....	43
4.1.2. Effect of AO on the change in Arctic cloud	51
4.1.3. Effect of sea ice retreat on recent changes in Arctic cloud	53
4.1.4. Discussion	60
4.2. Refinement of surface boundary condition for reduced sea ice in AGCM Experiment	76
4.2.1. Surface condition according to sea ice change for AGCM Experiment	76
4.2.2. Experimental Design.....	80
4.2.3. Responses in surface air temperature and heat fluxes.....	84
4.2.4. Vertical structure of responses in temperature and specific humidity	91
4.2.5. Discussion	95
4.3. Modeling the change in cloud and its effect in relation to sea ice	115
4.3.1. FREEZEDRY cloud amount parameterization	115
4.3.2. Response over the Arctic on reduced sea ice cover in AGCM Experiment	118
4.3.3. Discussion	121
5. Summary and Discussion	130
References	137

LIST OF TABLES

Table 2.1 Description of the CMIP5 models used in this study.....	16
Table 3.1 Change in model simulated variables by vegetation feedback effect (<i>F-FPV</i>).....	36
Table 4.1 Mean, standard deviation, and trends of total cloud fraction over the Arctic Ocean (north of 67°N) in each dataset.....	64
Table 4.2 Mean, standard deviation, and trend of surface skin temperature over the Arctic Ocean (north of 67°N) in each dataset.	65
Table 4.3 The 3rd polynomial fitting coefficients for the relationship between SST and sea ice fraction for each month during the cold season.....	100
Table 4.4 Summary of surface conditions of experiments in this study.	101

LIST OF FIGURES

- Fig. 3.1 Mean leaf area index (LAI) in growing season (May to September) for a) present (P) and b) future (F) simulation, and c) the fractional coverage of plant species (NET: needleleaf evergreen tree, BDT: broadleaf deciduous tree, C3: grasses with C3 pathway. T, B, and Arc in the suffix indicate temperate, boreal, and the Arctic respectively) over high-latitude, north of 60°N. The LAI represent the leaf abundance, the fractional area of plant's leaf surface relative to the surface area.23
- Fig. 3.2 (left panel) SAT difference between *F* and *P* simulation (upper) and *FPV* and *P* simulation (lower). (right panel) zonal mean of SAT difference between *F* and *FPV* simulation.28
- Fig. 3.3 Zonal mean temperature (shading) and u-wind (contour) changes by vegetation feedback effect (*F-FPV*) in JJA and SON.29
- Fig. 3.4 Shading indicates simulated average sea ice extent and thickness for September to October in *P* simulation. Lines in the left panel indicate sea ice extents where the ocean is covered with more than 15% sea ice. White line is the observed sea ice extent averaged from 1981-2000 HadISST data. Lines in the right panel indicate 25cm levels of mean sea ice thickness.33
- Fig. 3.5 (left panel) *NET* change by vegetation feedback effect (*F-FPV*). (right panel) changes in the components of *NET* at 70°N. 10-day running average is applied for the time dimension. Here atmospheric energy is estimated by moist static energy – summation of atmospheric latent, potential, and internal energy.34
- Fig. 3.6 Zonal mean *NET* change by vegetation feedback effect (*F-FPV*).35

- Fig. 4.1 Time-series of (a) cloud amount, (b) surface temperature, (c) sea ice cover over the Arctic Ocean (north of 67°N), and (d) AO index in winter (December to February) from the NCEP CFSR, ERA-Interim, APP-x, and TPP datasets. Trend lines are denoted with dashed line. Time series of cloud amount, surface temperature, and sea ice cover are re-scaled to have the mean and standard deviation of ERA-Interim for comparison.66
- Fig. 4.2 Changing trends in winter total cloud amount and surface air temperature during late 20th century (1979–1997) and early 21st century (1998–present) from the ERA-Interim and NCEP CFSR. Stippled region indicates that trend is significant at the 95% confidence level. Oblique and cross checked region in c and g (d and h) indicate that region sea ice cover is increasing (decreasing) with above (below) 0.2 %/year and 0.5 %/year, respectively.67
- Fig. 4.3 (left panels) changing trends in zonal-averaged winter temperature (shading) and specific humidity (contour) during late 20th century (1979–1997) and early 21st century (1998–present) from the ERA-Interim and NCEP CFSR. (right panels) same as left panels except for cloud water contents (shading) and fractional cloud cover (contour).68
- Fig. 4.4 Zonal-averaged total northward moisture transport ($vq + v'q'$, shading) and northward transport by mean flow (vq , contour) at 67°N.69
- Fig. 4.5 Changing trends in winter evaporation and precipitation during late 20th century (1979–1997) and early 21st century (1998–present) from the ERA-Interim and NCEP CFSR. Stippled region indicates that trend is significant at the 95% confidence level.70
- Fig. 4.6 Regressions of the AO index with zonal-averaged (a) cloud water

content [10^6 kg kg^{-1}], (b) horizontal moisture convergence [$10^9 \text{ kg kg}^{-1} \text{ s}^{-1}$], and (c) upward moisture transport [$10^5 \text{ kg Pa kg}^{-1} \text{ s}^{-1}$] from the ERA-interim and NCEP CFSR. Stipple regions indicate that values are significant at the 95% confidence level. 71

Fig. 4.7 Partial correlations of sea ice cover averaged over the Arctic Ocean (north of 67°N) with zonal-averaged cloud water content (shading) and mean upward moisture transport (contour) independent on the AO index during the late 20th century and the early 21st century from the ERA-interim and NCEP CFSR. Stippled (cross-checked) regions indicate that values with shading (contour) are significant at the 95% confidence level. 72

Fig. 4.8 Differences in (a and e) 850 hPa thickness (shading) and surface air temperature (contour), (b and f) PBL height (shading) and sea ice fraction (contour), (c and g) longwave cloud radiative forcing (shading) and cloud amount (contour), and sea level pressure (shading) and 500 hPa geopotential (contour) between averages for the early 21st century and the late 20th century. Stippled region indicates differences in shading values are significant at the 95% confidence level. 73

Fig. 4.9 Regression of winter low-level cloud amount [%] averaged over the Arctic Ocean (North of 67°N) with zonally averaged temperature (shading, [K]) and specific humidity (contour, [g kg^{-1}]) during late 20th century (1979 – 1997) and early 21st century (1998 – present) from the ERA-Interim and NCEP CFSR. All trends are removed. Stippled and cross-checked regions indicate that regression is significant at the 95% confidence level. 74

Fig. 4.10 Regression of winter low-level cloud amount averaged over the Arctic Ocean (North of 67°N) with sea level pressure (shading, [hPa]) and geopotential at 500 hPa (contour, [$\text{m}^2 \text{ s}^{-2}$]) during the late 20th century

(1979 – 1997) and the early 21st century (1998 – present) from the ERA-Interim and NCEP CFSR. All trends are removed in calculation. Stippled and cross-checked regions indicate that regressions are significant at the 95% confidence level.	75
Fig. 4.11 Scatter plot between sea ice concentration (SIC; fraction) and sea surface temperature (SST) over the Arctic (north of 60°N) for the cold season (October through March) of the period 1982–2000 from OISST v2. White lines indicate the third-degree polynomial fitting between SIC below 0.9 fraction and SST, in each month.	102
Fig. 4.12 Differences of sea surface temperature (shade) and sea ice concentration (contour) boundary conditions from (a and e) CTRL, (b and f) CONV, and (c and g) POLY experiments compared to the baseline experiment during early winter (October-November-December) and late winter (January-February-March); (d and h) Differences between mean sea surface temperature during early and late winters for 2006–2010 and 1982–2000 from the OISST v2. Differences are plotted only over the region where sea ice reduced above 0.01 fraction. In all panels, the contour interval is 0.1 fraction.	103
Fig. 4.13 Change in surface air temperature from (a) CTRL, (b) CONV, (c) POLY compared to the baseline experiment during the cold season, and (d) 2 m air temperature difference between 2006–2010 and 1982–2000 during the cold season from the ERA-Interim data.	104
Fig. 4.14 Change in surface air temperature from (a) CONV and (b) POLY compared to CTRL experiment during the cold season. Oblique and cross regions indicate that surface air temperature response is significant at the 90% and 95% confidence level, respectively.	105

- Fig. 4.15 Changes in net longwave flux (positive in the upward direction), sensible heat flux, and latent heat flux at the surface from CTRL (contour in all figures) compared to the baseline experiment, and changes in (a–c) CONV and (d–f) POLY experiments compared to CTRL experiment (shade in all figure) during the cold season. Contour interval is 5 W m^{-2} . Oblique and cross regions indicate that surface fluxes are significant at the 90% and 95% confidence level, respectively..... 106
- Fig. 4.16 Monthly changes in (a) net longwave flux (positive in the upward direction), (b) sensible heat flux, and (c) latent heat flux averaged over the Arctic Ocean (north of 67°N) from CTRL, CONV, and POLY experiments compared to the baseline experiment..... 107
- Fig. 4.17 Vertical profiles in temperature and specific humidity averaged over the Arctic Ocean (north of 67°N) in the baseline, CTRL, CONV, and POLY experiments during early and later winter (left panel) and their differences to the baseline experiment (right panel)..... 108
- Fig. 4.18 Changes in zonal-averaged heating by longwave radiation, diffusion, and moist processes during the cold season. Contour in the figure indicates a change between CTRL and the baseline experiments, and shade indicates the change in CONV and POLY against CTRL. Contour interval is 0.03 K day^{-1} . Oblique and cross regions indicate that surface fluxes are significant at the 90% and 95% confidence level, respectively..... 109
- Fig. 4.19 Changes in zonal-averaged temperature (shade) and specific humidity (contour) during early winter (October–November–December) and late winter (January–February–March) from CTRL, CONV, and POLY experiments compared to the baseline experiment. Oblique and cross regions indicate that surface fluxes are significant at the 90% and 95%

confidence level, respectively; (d and h) changes in the same variables for the periods 2006–2010 and 1982–2000 from the ERA-Interim data. Contour interval is 0.03 g kg^{-1} 110

Fig. 4.20 Change in surface air temperature from CTRL compared to the baseline experiment (contour), and changes in (a) POLY, (b) HadISST over the MSR, and (c) OISSTv2 over the MSR compared to CTRL (shade) during the cold season. Contour interval is 0.5 K. Oblique and cross regions indicate that surface air temperature response is significant at the 90% and 95% confidence level, respectively. 111

Fig. 4.21 Comparisons between simulated SST (model; left figure in each panel) and adjusted SST by polynomial fitting with SIC change (fitting; right figure in each panel) among 14 model results with future experiment of the RCP4.5 scenario in the fifth phase of the Climate Model Intercomparison Project. Model differences are calculated with simulated SSTs averaged for 2051–2055 and simulated SSTs averaged for 2006–2010. Fitting differences are calculated with fitted SSTs by using polynomial coefficients in the POLY method, SIC values averaged for 2051–2055 and simulated SSTs averaged for 2006–2010. Shading indicates sea surface temperature, and contour indicates sea ice concentration with an interval of 0.1. 112

Fig. 4.22 (a) relative humidity, (b) layered cloud amount by cloud amount parameterization in CAM3, and (c) layered cloud amount by FREEZEDRY modified parameterization under varying in temperature and specific humidity. 124

Fig. 4.23 Low level cloud amount during winter from (a) CAM3 original cloud amount parameterization, (b) FREEZEDRY cloud amount parameterization, and (c) their difference. 125

- Fig. 4.24 Changes in (a) surface air temperature (contour) and 850 hPa thickness (shading), (b) sea ice cover (contour) and planetary boundary layer height (shading), (b) total cloud amount (contour) and longwave cloud radiative forcing (shading), and (c) 500 hPa geopotential (contour) and sea level pressure (shading) from SIC experiment compared to CTRL experiment.126
- Fig. 4.25 Changes in (a) zonal-averaged temperature (contour) and specific humidity (shading), (b) heating by diffusion (contour) and moistening process (shading), and (c) cloud amount (contour) and regressed temperature of low-level cloud amount over the Arctic (shading) from SIC experiment compared to CTRL experiment.....127
- Fig. 4.26 Annual cycles of changes in (a) surface air temperature, (b) cloud amount, (c) longwave cloud radiative forcing, (d) shortwave cloud radiative forcing, (e) latent heat flux, and (f) sensible heat flux averaged over the Arctic (north of 70°N) between RCP4.5 and PIctrl experiments from climate models in the CMIP5. Solid thick lines in each figure indicate their ensemble mean values.....128
- Fig. 4.27 Annual cycles of regressions of (a) cloud amount onto surface air temperature, and (b) surface air temperature onto cloud amount averaged over the Arctic (north of 70°N) from PIctrl experiment, and (c) cloud amount onto surface air temperature, and (d) surface air temperature onto cloud amount from RCP4.5 experiment in the CMIP5. Solid thick lines indicate their ensemble mean values.....129

1. INTRODUCTION

1.1. Background

The Arctic is the northern polar component of the global climate system, the coldest region in the Northern Hemisphere. The Arctic is characterized by severe climate system during winter due to a low amount or absence of sunlight in winter and long days during summer. The absence of sunlight during cold season induces extremely low temperature, and the cryosphere, which is present as snow, ice sheets, glaciers, sea ice, and permafrost, becomes a prominent feature of the Arctic. In particular, a high reflectivity of the cryosphere makes the Arctic climate highly sensitive system passively through the ice-albedo feedback. It could help unusually large and rapid climate change by small temperature changes in the Arctic (ACIA, 2005).

In Earth's radiation budget, the Arctic is a less receiver for net solar radiative flux than lower latitudinal region because of an incoming angle of solar radiation. In the annual averages of top of atmosphere (TOA) radiation budget from the Earth Radiation Budget Experiment (ERBE), the region between about 38°N and 38°S receives more radiation than it emits to space. Poleward regions of these latitudes, the earth emits more radiation than it receives (Trenberth and Caron, 2001). The imbalance in energy budget along latitude implies that there

must be poleward transports of energy by the atmosphere and oceans that warm the Arctic region in order to keep global energy budget in balance.

These major characteristics, a highly sensitive climate system of the Arctic and an existence of poleward energy transport into the Arctic, could bring a unique phenomenon for the Arctic under the global climate change. The globe has experienced a large increasing in surface air temperature since the mid-1800s called as 'global warming', which might be caused by increasing in concentration of greenhouse gases (IPCC, 2007). Under the global warming, the Arctic has experienced larger warming almost twice as large as the global average increasing rate. This phenomenon is known as the 'Arctic amplification' (Graversen, 2006; Holland and Bitz, 2003; Serreze and Francis, 2006). Global warming may reinforce poleward energy transport by atmosphere and ocean (Alexeev et al., 2005; Bitz et al., 2006; Graversen et al., 2008), and the warming could be amplified by highly sensitive climate system of the Arctic (Bintanja et al., 2011; Boe et al., 2009; Screen and Simmonds, 2010a). Consequently, warming over the Arctic becomes larger than that over the globe.

Although major underlying cause for the Arctic amplification between the sensitive Arctic climate system due to the cryosphere and enhanced poleward energy transport is in debate (Bitz and Fu, 2008; Graversen et al., 2008; Screen and Simmonds, 2010a; Serreze and Francis, 2006), numerous studies have

attempted to find the other factors which affect the Arctic amplification. The cloud, which could compose positive process over the Arctic, has received much attention as one of amplifying factor from the earlier studies (Curry et al., 1996; Wetherald and Manabe, 1988). Water vapor feedback also has attracted attention for the factor since mid-1990s (Curry et al., 1995; Sinha and Harries, 1995). Recent studies have persisted in investigating the effect of these factors focused on earlier (Graversen and Wang, 2009; Vavrus, 2004; Vavrus et al., 2009), and tried to find the effect of other factors such as surface inversion at near surface over the Arctic (Bintanja et al., 2011; Boe et al., 2009), vegetation over the high-latitude region (Chapin et al., 2005; Swann et al., 2010), ocean heat uptake (Bitz et al., 2006; Winton et al., 2010), chemical feedback by methane emission in the Arctic region (Isaksen et al., 2011), and remotely induced warming from lower latitude (Chung and Räisänen, 2011).

These studies, which investigate the effect of various factors on the Arctic amplification, utilize a numerical model broadly. There might be two major reasons why the modeling is extensively adopted. First, because of extreme weather and climate condition over the Arctic, observational data are quite limited. In particular, extremely harmful condition in cold season causes hardship in both surface and satellite observations. Next, because the Arctic is the highly complex and sensitive system which has many climatic elements to

affect each other, modeling study can be an efficient way to investigate the isolated effect of climate factor on the Arctic climate. Namely, much of our current understanding of the Arctic climate system comes from numerical models (Serreze and Barry, 2009).

However, extreme weather and complex climate conditions also bring large difficulties into modeling the Arctic (Walsh et al., 2005). In intercomparison of multi-model results, it has been reported that the Arctic region has large discrepancies in principle variables such as surface air temperature (SAT) among the models (IPCC, 2007). This might be caused by the uncertainties in the cloud and related surface energy budget over the Arctic (Vavrus and Waliser, 2008; Walsh et al., 2005), and unrealistic longwave feedback at the near surface (Boe et al., 2009). In addition, uncertainties in the properties of sea ice also could bring a wide sensitivity into coupled models (Rampal et al., 2011; Winton, 2011). Moreover, the important physical elements excluded in the Arctic modeling such as glacier could induce error into the Arctic modeling. Namely, for the Arctic, while modeling is one of the most important tools for understanding the climate system, modeling result must always be handled with appropriate caveats.

1.2. Motivation and Objectives

Nevertheless, the modeling can give a great motivation to the study on the

Arctic. As modeling becomes refined and modeling area becomes extended, an understanding on the Arctic could grow. For instance, because the effect of vegetation on the Arctic warming could not be fully understood without interaction with other climatic elements, earlier modeling studies could investigate fragmentary effect of vegetation. Meanwhile, recent land surface model includes dynamical vegetation process, thus we can investigate the role of vegetation on the Arctic climate in much detail (Swann et al., 2010). In addition, reducing uncertainties by improving cloud properties over the Arctic also gives better understanding for the role of cloud on the Arctic climate system (Vavrus et al., 2011a; Vavrus and Waliser, 2008; Vavrus et al., 2011b). In other words, the Arctic climate modeling with refinement and extension of processes of climatic elements may facilitate more detailed study for the Arctic.

The role of vegetation on the Arctic warming still remains as one of challenges in modeling study on the Arctic. Warming and moistening over the Arctic and high latitudes provide a favorable condition for vegetation to grow. In practice, recent observations suggest that the shrubs and grasses in the Arctic tundra and trees in the boreal forests have expanded more northward and increased in its growth during recent decades (Bunn et al., 2007; Goetz et al., 2005; Jia et al., 2003; McMahon et al., 2010). An increasing in vegetation has a positive feedback effect – more warming with more vegetation growth, which is

mainly caused by decreased surface albedo as relatively darker vegetation cover replaces snow-covered or barren surface of high-reflectivity (Levis et al., 1999; Notaro and Liu, 2008; Notaro et al., 2007; O'ishi and Abe-Ouchi, 2009). Thus, the vegetation may, in turn, amplify the warming over the high latitudinal regions under global warming.

Although it is evident that such vegetation-feedbacks may provoke profound consequences in the Arctic climate system, much mechanism are still poorly understood due to lack of physical understanding and observations. In addition, only a few climate models include dynamic vegetation models, and most climate models' future climate predictions – even multi-model climate model predictions of the Intergovernmental Panels on Climate Change (IPCC) the Fourth Assessment Report (AR4) (IPCC, 2007) – neglect the vegetation feedback effect. Thus, modeling work with dynamic vegetation model could promote our understanding for role of the vegetation on the Arctic warming. In a chapter 3, the dissertation examines the role of vegetation on the Arctic climate under global warming condition by performing the doubled CO₂ simulation with dynamic vegetation model.

As mentioned previously, the cloud has been attracted attention as one of the major amplifying factors for the Arctic warming from earlier studies. However, much of understanding for the role of cloud on the Arctic climate

change still remains uncertain. In particular, for the cold season when uncertainties in both observation and modeling become stronger, only a few studies have focused on the change and the role of cloud under the Arctic climate (Liu et al., 2007; Miller et al., 2007).

The lack of studies for the winter Arctic cloud also is also seen in the recent Arctic climate change. Since the late 1990s, the accelerated melting of sea ice and associated ice-albedo feedback led to considerable warming throughout the troposphere (Screen and Simmonds, 2010a) and even caused hemispheric-scale atmospheric circulation changes (Francis et al., 2009; Overland and Wang, 2010). These changes are conspicuous especially during winter (Screen and Simmonds, 2010b), and numerous studies have pointed out the cloud as possible cause for amplifying the Arctic warming in winter because cloud-radiation feedback process works positively due to absence of solar radiation (Graversen et al., 2008; Graversen and Wang, 2009; Palm et al., 2010).

However, previous studies for the Arctic cloud with respect to recent Arctic climate change have been concentrated in melting season although winter Arctic cloud could play a crucial role on the recent Arctic warming (Cuzzone and Vavrus, 2011; Kay and Gettelman, 2009; Palm et al., 2010; Schweiger et al., 2008). Accordingly, whereas much of role of Arctic sea ice loss for the associated changes in Arctic clouds in melting season have been investigated, the

change in cloud and its impact on the Arctic climate system according to recent Arctic change during winter still remains poorly understood. Thus it is necessary to understand the change and effect of winter Arctic cloud in recent Arctic climate. In a chapter 4, this dissertation further diagnose the change in cloud and its impact on the Arctic during winter in recent decades, and model the recent Arctic change related to cloud with refinement in surface condition and modified cloud amount parameterization.

1.3. Thesis Organization

This dissertation is organized as the following.

Chapter 2 describes the model and data used in this thesis. Chapter 3 denotes the role of vegetation on the Arctic climate change under global warming condition by modeling work with dynamic vegetation model. Chapter 4 reveals the diagnosis and modeling on the change in cloud and its impact on the Arctic during winter in recent decades. Modeling works to improve modeling result are also documented. Lastly, the results of this dissertation are summarized, and the limitation of the study and possible future works are also discussed in Chapter 5.

2. MODEL AND DATA

2.1. Model

For modeling the role of vegetation and cloud on the Arctic climate change, the Community Climate System Model version 3 (CCSM3; Collins et al., 2006) is used. The CCSM3 is a fully coupled climate model with component models representing atmosphere, ocean, land surface, and sea ice, allowing researchers to conduct fundamental research into the earth's past, present and future climate states. The CCSM3 is a one of models participating the Coupled Model Intercomparison Project phase 3 (CMIP3) for the IPCC AR4, and the performance of CCSM3 for simulating global and regional climate system has been verified by numerous studies – El Niño/Southern Oscillation (McGregor et al., 2009; Merkel et al., 2010; Schneider et al., 2009; Zhang et al., 2009), regional climate such as monsoon and storm track (Finnis et al., 2007; Lee et al., 2008; Meehl et al., 2006a; Yu et al., 2009), global warming by greenhouse gases (Kiehl et al., 2006; Kirkevåg et al., 2008; Meehl et al., 2006b; Yoshida et al., 2008), and paleo-climate (Andersson et al., 2010; Brandefelt and Otto-Bliesner, 2009; Eldrett et al., 2009; Shellito et al., 2009). In addition, numerous studies also have been done for the Arctic climate with giving much of knowledge on the Arctic climate system (Deser et al., 2010; Gorodetskaya et al., 2008;

Graversen and Wang, 2009; Lawrence et al., 2008a; Lawrence et al., 2008b; Skific et al., 2009a, b; Teng et al., 2006; Vavrus and Waliser, 2008; Xin et al., 2008).

This study utilizes the CCSM3 by using two main component models and two additional models in each main component model instead of using fully coupled model. First, the Community Atmosphere Model version 3 (CAM3), the atmospheric component of CCSM3, and the Community Land Model version 3 (CLM3), the land surface component of CCSM3, are used to simulate atmosphere and land surface, respectively. These two component models are used to study the role of both vegetation and cloud on the Arctic climate change.

Next, for investigating the role of vegetation, the Community Land Model's Dynamic Global Vegetation Model (CLM-DGVM), which simulates the distribution and structure of natural vegetation dynamically, is coupled to CLM3. The CLM-DGVM is based on the Lund–Potsdam–Jena (LPJ) DGVM (Sitch et al., 2003) and the IBIS which provides plant phenology to the CLM3 (Foley et al., 1996). It simulates the biogeographic distributions of potential vegetation plant functional types (PFTs) as a response of environmental conditions such as temperature, growing degree days, and precipitation. These climatic variables determine the survival and establishment of PFTs (Levis et al., 2004). The CLM-DGVM has been used in numerous studies for investigating the change in

vegetation and its effect on climate system for past, present and future climate (Bonan and Levis, 2006; Jeong et al., 2012; Jeong et al., 2010; Jeong et al., 2011; Notaro et al., 2007).

In addition to CLM-DGVM, the mixed-layer slab ocean model (SOM) is coupled to CAM3 for calculating prognostic ocean mixed-layer temperature instead of using the full-layered dynamical ocean and sea ice model. The governing equation for the slab mixed-layer temperature, which is usually treated as sea surface temperature (SST) in SOM, is

$$\rho_o C_o h_o \frac{\partial T_o}{\partial t} = (1 - A)F + Q + AF_{oi} + (1 - A)F_{fz} \quad (2.1)$$

where T_o is the ocean mixed layer temperature, ρ_o is the density of ocean water, C_o is the heat capacity of ocean water, h_o is the annual mean ocean mixed layer depth (m), A is the fraction of the ocean covered by sea ice, F is the net atmosphere to ocean heat flux (Wm^{-2}), Q is the internal ocean mixed layer heat flux (Wm^{-2}), F_{oi} is the heat exchanged with the sea ice (Wm^{-2}) and F_{fz} is the heat gained when sea ice grows over open water (Wm^{-2}).

In addition to ocean mixed layer model, thermodynamical sea ice model coupled to SOM calculates the prognostic fractional cover and thickness of sea ice. Sea ice thickness is calculated by following equations:

$$\frac{dh_i}{dt} = \frac{F_{TOP}}{q} + \frac{F_{LH}}{-q + \rho_i L_v} \quad (2.2)$$

$$\frac{dh_i}{dt} = \frac{F_{BOT}}{q} + \frac{k}{q} \frac{dT}{dz} \quad (2.3)$$

where F_{TOP} is heat flux from ice surface, h_i is the ice thickness, ρ_i is the ice density, q is the energy of melting of sea ice, F_{BOT} is the heat flux from the ocean to the ice, k is the thermal conductivity, and z is the vertical coordinate. In addition, sea ice cover A is prognostically calculated with three separate equations:

$$q_f \frac{\partial h_{new}}{\partial t} = F_{fz} (1 - A) \quad (2.4)$$

$$\left(A - \frac{\partial A}{\partial t} \right)^2 = \frac{A^2}{h_i} \left(h - \frac{\partial h_i}{\partial t} \right) \quad (2.5)$$

$$\frac{\partial A}{\partial t} = A \frac{F_{SID}}{E_{TOT}} \quad (2.6)$$

where q_f is the energy of melting for new ice growth, h_{new} is the thickness of the new ice, F_{SID} is the total flux from lateral boundary, and E_{TOT} is total energy of melting of snow and ice.

As the equilibrium climate sensitivity of the CCSM3 with SOM to anthropogenic forcing is known to be almost similar to that from fully-coupled version of CCSM3 (Danabasoglu and Gent, 2009; Kiehl et al., 2006). Therefore the using SOM gives an advantage of reducing computational time and bias reduction in remapping process between different grid systems compared to

using fully coupled model with ocean and sea ice models.

2.2. Data

The ERA-Interim, the latest European Centre for Medium-Range Weather Forecast (ECMWF) reanalysis, covers the period from the January 1979 to present with 0.75° by 0.75° horizontal resolution and 37 vertical levels. In the ERA-Interim, notable improvements have been made in its hydrological cycle by updating data assimilation system which newly includes rain-affected Special Sensor Microwave Image (SSM/I) radiances with updated cloud and convection schemes. In addition, a new bias correction to satellite radiances led to improvement in representing magnitude and vertical structure of temperature accurately with respect to the radiosonde observations over the Arctic (Dee and Uppala, 2009). These provide good performance of ERA-Interim in simulating accurate amount and properties of clouds in the Arctic (Dee et al., 2011; Walsh et al., 2009). The ERA-Interim provides two kind of horizontal resolution – full resolution (0.75° by 0.75°) and low resolution (1.5° by 1.5°), and low resolution dataset is used in this study.

The NCEP CFSR, a new reanalysis provided by the NCEP recently, covers the period from the January 1979 to December 2009 with 0.5° by 0.5° horizontal resolution and 37 vertical levels. The NCEP CFSR is produced by a coupled

forecast system model which has T382 (about 38 km) horizontal resolution and hybrid vertical sigma coordinate with 64 levels. The NCEP CFSR has many improvements in data quality by introducing a new satellite bias correction method with direct assimilation of radiances, and in prognostic cloud water from condensation based on diagnostic cloud cover compared to the previous version of the NCEP reanalyses (Saha et al., 2010). A better performance of the cloud data in the reanalysis from the NCEP in the Arctic region has been evaluated in the NARR reanalysis, which has 32 km horizontal resolution but covers limited area of the Arctic (Walsh et al., 2009). The NCEP CFSR also provides various horizontal resolutions – 0.5° by 0.5°, 1.5° by 1.5°, and 2.5° by 2.5°, and we use 2.5° by 2.5° horizontal resolution in this study.

For validation of the used reanalyses, we utilize clouds and surface temperature data from two long-term satellite observations – APP-x (Wang and Key, 2005a) and the Television and Infrared Observation Satellite (TIROS) Operational Vertical Sounder (TOVS) Polar Pathfinder (TPP) (Schweiger et al., 2002). These data were utilized for many previous studies on the Arctic cloud (Eastman and Warren, 2010a; Liu et al., 2007; Liu et al., 2009; Schweiger et al., 2008; Wang and Key, 2003, 2005a, b). The APP-x composites are a collection of products for both poles, consisting of calibrated satellite channel data and derived parameters at a 25 km spatial resolution. Skin temperature, cloud mask,

and clear sky surface albedo are provided from five AVHRR channels for the period 1982–2004. The APP-x provides daily composites at 04:00 and 14:00 local solar time (LST). We use monthly cloud and surface skin temperature data averaged from only 14:00 LST in daily dataset, but results from the data at 04:00 are very similar. The TPP dataset is another long-term satellite observation including atmospheric temperature, water vapor, skin surface temperature, total effective cloud fraction, cloud top pressure and temperature. Data are available for the period 1980–2005 with a resolution of 100 km. We use monthly cloud and surface skin temperature based on 1200 UTC daily values.

For validation of our modeling result, we use modeling outputs from the fifth phase of the Coupled Model Intercomparison Project (CMIP5). We use sea ice concentration and sea surface temperature (SST) in 14 model results from the RCP4.5 future simulation for checking the usability of our polynomial fitting method to generate SST distribution with respect to sea ice distribution. In addition, in order to check whether cloud increases during winter, total cloud amount, surface air temperature, CRF, and sensible and latent fluxes in 30 model results from the PIconrol and RCP4.5 simulations are used. Descriptions of all used CMIP5 models are summarized in Table 2.1.

Table 2.1 Description of the CMIP5 models used in this study.

Model Name	Institute	Country	Resolution
ACCESS1-0	CSIRO-BOM	Australia	192 × 145
ACCESS1-3	CSIRO-BOM	Australia	192 × 145
BCC-CSM1-1	BCC	China	128 × 64
BNU-ESM	BNU	China	128 × 64
CCSM4	NCAR	USA	288 × 192
CESM1-BGC	NSF-DOE-NCAR	USA	288 × 192
CSIRO-Mk3.6	CSIRO-QCCCE	Australia	192 × 96
FGOALS-G2	LASG-CESS	China	128 × 60
GFDL-CM3	NOAA GFDL	USA	144 × 90
GFDL-ESM2G	NOAA GFDL	USA	144 × 90
GFDL-ESM2M	NOAA GFDL	USA	144 × 90
GISS-E2-H	NASA-GISS	USA	144 × 90
GISS-E2-H-CC	NASA-GISS	USA	144 × 90
GISS-E2-R	NASA-GISS	USA	144 × 90
GISS-E2-R-CC	NASA-GISS	USA	144 × 90
HadGEM2-CC	MOHC	UK	192 × 145
HadGEM2-ES	MOHC	UK	192 × 145
INMCM4	INM	Russia	180 × 120
IPSL-CM5A-LR	IPSL	France	96 × 96
IPSL-CM5A-MR	IPSL	France	144 × 143
IPSL-CM5B-LR	IPSL	France	96 × 96
MIROC4h	MIROC	Japan	640 × 320
MIROC5	MIROC	Japan	256 × 128
MIROC-ESM	MIROC	Japan	128 × 64
MIROC-ESM-CHEM	MIROC	Japan	128 × 64
MPI-ESM-LR	MPI-M	Germany	192 × 96
MPI-ESM-MR	MPI-M	Germany	192 × 96
MRI-CGCM3	MRI	Japan	320 × 160
NorESM1-M	NCC	Norway	144 × 96
NorESM1-ME	NCC	Norway	144 × 96

3. MODELING THE ROLE OF VEGETATION ON THE ARCTIC WARMING UNDER GREENHOUSE WARMING

3.1. Vegetation over the high-latitude region and its change

The Arctic and northern high-latitude region have experienced substantial climate warming in recent decades, and its degree and pace is much larger and faster than the global average (ACIA, 2005). The extent of sea ice cover in the Arctic Sea and snow-cover in the sub-Arctic landmasses have reached their lowest recorded levels, and it is likely that associated feedback processes have exacerbated the warming (Chapin et al., 2005; Overpeck et al., 2005; Serreze et al., 2000). Accompanying with this warming is conspicuous change in vegetation in the Arctic and high-latitude regions. Contrasting to our great anxiety to it, anthropogenic climate change seems to provide the vegetation in the harsh Arctic climate environment with more pleasant conditions for living – higher temperature and increased water availability over longer growing season and fertilization by elevated CO₂ level. Much attention has been paid with this vegetation change, because it may, in turn, lead to considerable changes in surface energy budget and hydrological cycle. Therefore it has been widely

perceived that this vegetation-climate feedback has a great potential to alter natural or anthropogenic climate change, having different feedback effects depending on regional vegetation type and climate characteristics (Bonan et al., 1992; Chapin et al., 2005; Folley, 2005; Levis et al., 1999; Notaro and Liu, 2008).

Previous modeling studies have emphasized the potential significance of vegetation feedback on climate model's responses to anthropogenic and natural forcings in recent centuries, and to paleoclimatic perturbations (Bonan et al., 1992; Foley et al., 1994; Notaro et al., 2007). Regarding the recent warming in the Arctic and high-latitude climate, climate models generally indicate that the vegetation changes have a positive feedback effect – more warming with more vegetation growth, which is mainly caused by decreased surface albedo (reflectivity of the surface to sunlight) as relatively darker vegetation cover replaces snow-covered or barren surface of high-reflectivity (Levis et al., 1999; Notaro and Liu, 2008; Notaro et al., 2007; O'ishi and Abe-Ouchi, 2009). In addition, more suggested are an increased greenhouse effect by increased atmospheric water vapor from increased evapotranspiration and more ice-melt in the Arctic reinforcing both the Arctic warming and more vegetation growth (Swann et al., 2009).

Here we present the possible vegetation feedback effect on the Arctic and high-latitude climate under the anthropogenic climate change. Taking advantages

of the vegetation-climate coupled model, the potential vegetation change under doubled CO₂ concentration and its feedback effects on surface temperature and associated energy budgets in the Arctic/high-latitude climate system were investigated. In addition to the local feedback effect, the remote influence of vegetation change on the Arctic sea and sea ice through atmospheric energy transports and associated feedback mechanism are primary foci of present study.

3.2. Modeling vegetation change and its effect under greenhouse warming

For modeling vegetation change and its effect, CAM3, CLM3, and CLM-DGVM are utilized. The mechanistic parameterization of large-scale vegetation processes in CLM-DGVM simulates the distribution and structure of natural vegetation, and therefore synchronous climate-vegetation coupling enables to consider the two-way feedback between climate and vegetation. If not coupled to the CLM-DGVM, the CAM3 and CLM3 can be run with prescribed vegetation, where the fractional distribution of plant species and seasonal cycle of plant's leaf abundance are fixed during model simulation years. We utilized this CCSM3's functionality to be run with/without CLM-DGVM to isolate the vegetation feedback effect.

First, we performed two baseline experiments *P* and *F*, representing

‘Present’ and ‘Future’ respectively. 355 *ppmv* and 710 *ppmv* CO₂ concentration were used for the present and future simulation respectively. Each model simulation was run for 150 model years, and results for the last 30 years are utilized. Then, an additional ‘future’ simulation – *FPV* was performed. The *FPV* is identical to *F* simulation except performed with the prescribed vegetation taken from the *P* simulation. Namely, vegetation change caused by overlying climate change is not allowed in the *FPV* simulation. Therefore the difference between *F* and *FPV* is only contributed by vegetation changes caused by CO₂ doubling. Here we simply estimated the ‘vegetation feedback effect’ under CO₂-doubled climate change as *F* minus *FPV*, and the ‘all effect’ including CO₂-doubling and climate-vegetation feedback effects as *F* minus *P*.

The equilibrium climate sensitivity of annual and global averaged surface air temperature change (Δ SAT) associated with a doubling CO₂ (355 to 710 *ppmv*) was estimated as 2.78°C when all effect was considered (*F* vs. *P*), and 2.51°C when vegetation feedback effect was not considered (*FPV* vs. *P*). Both values are comparable to the sensitivity to a CO₂ doubling estimated by the CCSM3 with full dynamical ocean (without vegetation feedback) – 2.47°C and the transient simulation for IPCC AR4 under A1B emission scenario – 2.78°C (IPCC, 2007; Kiehl et al., 2006). Over the Arctic/high-latitudes (north of 60°N), the Δ SAT change becomes much higher compared to the global average; 5.53°C

when all effect was considered (F vs. P), and 3.92°C when vegetation feedback effect was not considered (FPV vs. P).

3.3. The vegetation change under a doubled CO_2 climate

We first examined potential vegetation over the Arctic and high-latitude region under present (P) and future (F) climate condition simulated by CLM-DGVM (Fig. 3.1). Overall, the replacement of low-vegetated land to densely grass-covered surface and the northward expansion and enhanced growth of boreal trees are salient. Over the northern high-latitude land, where the severe cold climate is the limiting factor for vegetation's growth, all simulated plant species have increased in their areal coverage and leave growth (leaf area index) during the warm season. In particular, increase in the coverage of the Arctic grass (+17%) and boreal deciduous tree species (+10%) are prominent. The most notable change is the encroachment of in the northern parts of continents where the major permafrost regions are located in the present climate. It is likely that the strong surface warming boosts the cold season temperature above the threshold for the establishment and survival of some plants species. Also it is plausible that the increase in available moisture and CO_2 fertilization effect contribute to this remarkable change. A larger CO_2 fertilization effect may have promoted the photosynthetic activity of vegetation owing to more available

moisture supply from the increased precipitation and the thawing of soil-ice in the permafrost region (Lawrence et al., 2008a; Long et al., 2006). But it should be noted that the simulated potential vegetation has discrepancies against observed vegetation. The CLM-DGVM tends to underestimate the forest cover but overestimate grass cover (Bonan and Levis, 2006), and this is also the case in the simulated vegetation in northern high-latitudes. Another important discrepancy is the missing treatment of the shrub species despite of its importance in the vegetation ecosystem in the sub-Arctic region. Recent observation indicated that an explosive shrub encroachment to the Arctic tundra in the northernmost part of continents is one of prominent vegetation change associated with the rapid climate warming (ACIA, 2005; Tape et al., 2006). However, the grass species seem to undertake the shrub's role in the present CLM-DGVM simulation results. Compared to the grass in tundra, shrubs have a lower albedo and a stronger interaction with snow, and therefore give a stronger positive feedback effect on the climate warming (Chapin et al., 2005; Sturm et al., 2001). Despite of these discrepancies, our simulation results indicating more greening in the Arctic/high-latitudes under climatic changes induced by the elevated CO₂ are generally consistent with observed trends and other model's predictions.

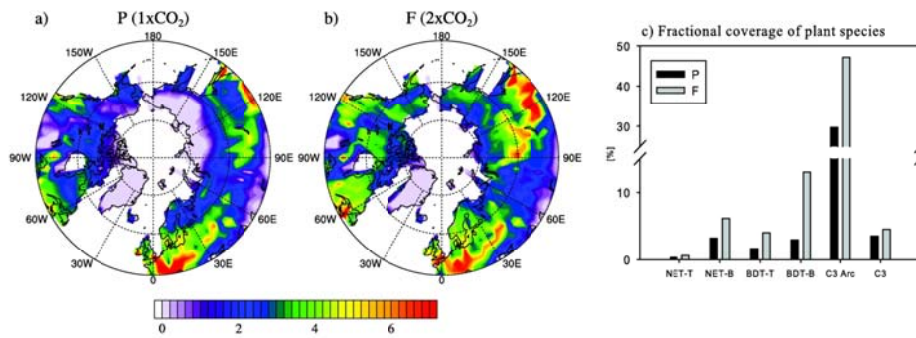


Fig. 3.1 Mean leaf area index (LAI) in growing season (May to September) for a) present (P) and b) future (F) simulation, and c) the fractional coverage of plant species (NET: needleleaf evergreen tree, BDT: broadleaf deciduous tree, C3: grasses with C3 pathway. T, B, and Arc in the suffix indicate temperate, boreal, and the Arctic respectively) over high-latitude, north of 60°N. The LAI represent the leaf abundance, the fractional area of plant's leaf surface relative to the surface area.

3.4. Vegetation feedback effect on SAT and circulation changes

Vegetation change in the high-latitudes induces substantial alternation of climate change in the Arctic/high-latitude in the warming seasons through winter. Figure 3.2 compares the simulated SAT changes under a doubling CO₂ concentration with/without the interactive vegetation. When the interactive vegetation is included in the future climate simulation, the warming in high-latitude continent appears to be substantially amplified. In summer, additional 2 to 3°K warming can be detectable over northern high-latitudes area where the major vegetation change is found. In autumn, this vegetation-related additional warming in land region becomes weaker, but it spreads over the entire Arctic sea. Seen from the direct estimation of vegetation feedback effect ($F\text{-FPV}$) on the zonal mean ΔSAT , interestingly, vegetation-related warm shows a northward propagation pattern of the warm season warming in high-latitude toward the Arctic region in autumn through winter.

The warming in spring to summer is mostly contributed by a great increase of absorbed shortwave radiation (SW, solar radiation) at surface: +6.93 W/m² in MAM and +16.82 W/m² in JJA. With relatively smaller increase net longwave radiation (LW, terrestrial radiation): -1.84 W/m² in MAM and -6.52 W/m² in JJA, the net absorbed radiation increases is +5.09 W/m² in MAM and +10.3 W/m² in JJA at surface. These surplus radiative energy is mostly transferred to sensible

(MAM: +1.12 and JJA: +5.08 W/m²) and latent heat (MAM: +2.31 and JJA: +6.47 W/m²) increases, which contributes to the strong surface warming (+1.58 and +2.53°K for land north of 60°N). In spring to early summer, the surface albedo decrease (-7.34% in MAM) by the replacement of snow-covered surface by vegetation (-6.17% snowcover change in MAM) appear to induce the increased absorption of SW at surface. The low cloud change associated with vegetation feedback effect seems to be another contributor to the increased SW absorption particularly in summer. Because low cloud has high-reflectivity to incoming SW, the notable decrease in low cloud in summer (-8.85%) may lead to more incoming SW at surface. We also note that high cloud amount slightly increases over all seasons, but is thought to be effective on the LW change. Being almost transparent to SW radiation, high cloud is known to invoke greenhouse effect by absorbing and re-emitting LW radiation (Vavrus, 2004). Thus high cloud increase seems to partly offset the increased LW emission at warmer and less ice-covered surface, which may also contribute surface warming.

The vegetation-induced changes are not only confined to near-surface, but significantly alter the tropospheric temperature and associated atmospheric circulation. Figure 3.3 represent vertical structure of temperature and zonal wind change associated with vegetation feedback effect. In summer, the vegetation-induced near-surface warming well extends above to mid-troposphere and also

northward over the Arctic sea; about 1.5°C air temperature increase can be found almost at 400 hPa in the Arctic/high-latitudes. Probably relatively weak vertical atmospheric stability in summer leads to the upward energy transport by vertical mixing process, while it is highly prevented by the strong atmospheric stability in the Arctic climate system during the rest of year. There is relatively modest warming at the near surface in the Arctic sea, which implies the large consumption of energy to melt sea ice and warm the upper ocean (Serreze and Francis, 2006). In autumn, the lower- to mid-tropospheric warming originated from high-latitude land surface is almost vanished, but substantial warming is found over the Arctic sea ice, mostly confined near surface. This lower-tropospheric warming pattern evokes the typical characteristic of the Arctic amplification when sea ice feedback mechanism provokes the near surface warming in cold season. Namely, as the Arctic atmosphere becomes very stably stratified, weak atmospheric vertical mixing traps the large warming signal to near surface. Accompanying with this tropospheric temperature change, the atmospheric zonal wind shows substantial change. Overall pattern is the weakening of tropospheric westerlies in the mid- to high-latitude in the south of maximum warming. As the center of maximum warming moves to the Arctic in autumn, the negative zonal mean wind pattern also moves northward. The change in westerlies and warming seems to be well consistent with the thermal

wind relationship. Also expected is the positive geopotential height (or pressure) anomaly in the mid- to high-latitudes, which may also contribute the decrease of low cloud in summer.

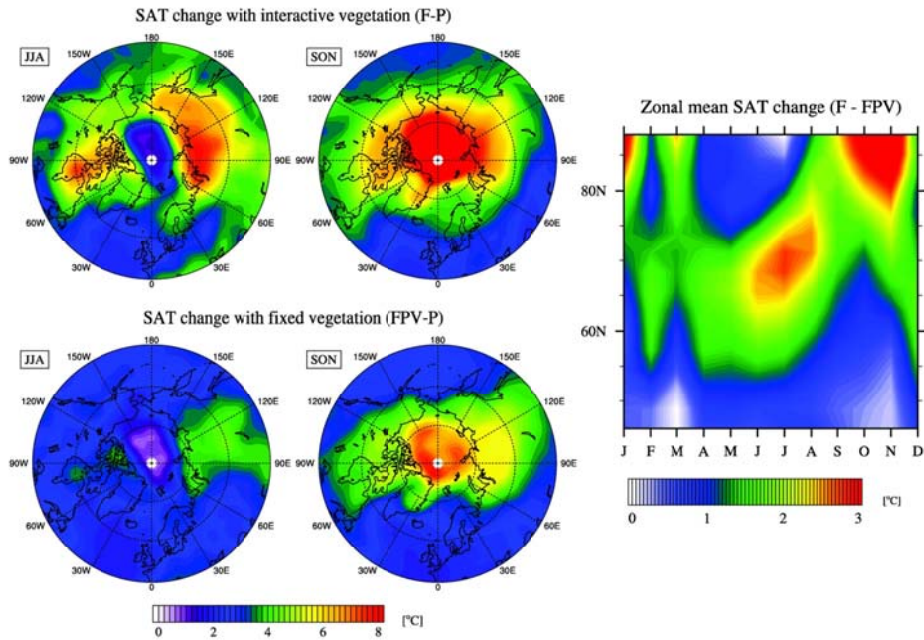


Fig. 3.2 (left panel) SAT difference between F and P simulation (upper) and FPV and P simulation (lower). (right panel) zonal mean of SAT difference between F and FPV simulation.

Zonal mean T and U difference (F - FPV)

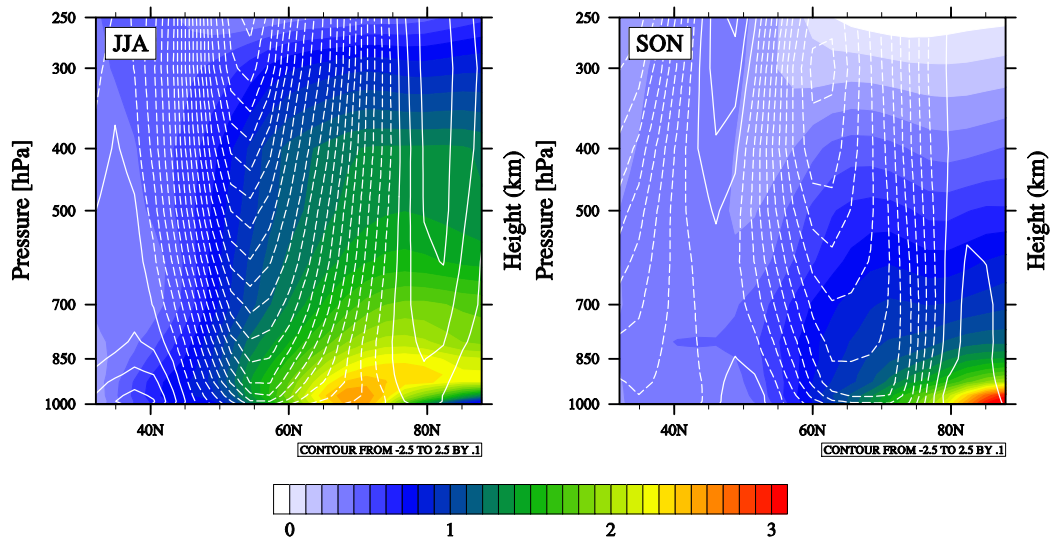


Fig. 3.3 Zonal mean temperature (shading) and u-wind (contour) changes by vegetation feedback effect (F - FPV) in JJA and SON.

3.5. Sea ice change and atmospheric northward energy transport

Easily expected from the temperature change, the Arctic sea ice exhibits considerable decline both in areal extent and thickness associated with the vegetation feedback effect. Much more decrease in sea ice extent and thickness are found owing to vegetation feedback effect (Figure 3.4 and Table 3.1). The greatest change in the Arctic sea ice is found in autumn, when the extent and thickness of sea ice reaches its minimum in a year, showing about 24% and -13cm decrease in areal extent and thickness respectively. The direct cause of this sea ice change may lie in the warmer atmospheric air (JJA: 1.60°K and SON: 2.15°K) and warmer ocean (JJA: 1.48°K and SON: 0.93°K). In summer, the positive feedback between the reduced sea ice extent (-10.57%) and more absorbed SW radiation (9.61 W/m²) may give the largest effect on the oceanic temperature rise, whereas the negative feedback effect from increased surface LW radiation is relatively modest (-1.43 W/m²). As a consequence, more latent heat (3.13 W/m²) and sensible heat (0.80 W/m²) release are emitted from the warmer and more opened Arctic Ocean. It is obvious that such energy fluxes associated with sea ice changes eventually cause the near-surface warming, of which processes exhibit a typical mechanism of sea ice feedback to invoke the Arctic amplification of surface warming.

Given that the horizontal energy transport within land surface is almost

negligible, the atmospheric transport of excess heat to the Arctic region could be the only mechanism to connect the vegetation-related warming in the continents with the remote changes in the Arctic sea. Actually, atmospheric circulation change and associated energy transports are important process accounting for the amplification of tropospheric warming in the Arctic region (Graversen, 2006; Graversen and Wang, 2009; Serreze and Francis, 2006). Figure 3.5 shows the tropospheric northward atmospheric energy transport (NET) change by the vegetation feedback effect. Zonal mean change of NET pattern appears well consistent with temperature change; the maximum NET occurs over and to the north of surface warming in the high-latitude land from spring through summer. This indicates that the surplus sensible energy and moisture from the increased vegetation activity are transported by atmosphere, presumably through strong atmospheric eddy activities in the high-latitudes. Seen at 70°N roughly about boundary between the Arctic sea and surrounding continents, the contribution of internal energy transport explains about half of total NET change, and the latent and potential energy transport explain the other half. Like as the temperature change, the increased NET well extends to mid- to upper-troposphere in summer (Fig. 3.6), which may contribute the considerable warming in the mid to upper troposphere in the Arctic region as well as near surface warming.

The maximum of NET increase is in summer but that of Arctic warming

occurs in autumn through winter. This lagged response is related with the seasonal cycle of the Arctic sea ice and associated the latent heat release/absorption. As the Arctic sea ice reaches its minimum around in September to October both in areal extent and thickness, the large amount of surplus energy input by NET in summer is consumed by the heat absorption to melt the Arctic sea ice as well as to warm the upper ocean. We estimated the latent heat content change by the Arctic sea ice loss associated with the vegetation feedback, manifested as an equivalent temperature change attained if the latent energy is used to warm the upper mixed layer of the Arctic Ocean. The heat content change by sea ice is found to be substantial; it is estimated as larger than that by warming of mixed layer ocean throughout a year. The maximum occurs in summer when the NET is largest in the Arctic region, and become smaller in winter through spring. Recalling that the Arctic sea ice begins to refreeze from mid-autumn, this is consistent with the less sea ice refreezing in the cold season.

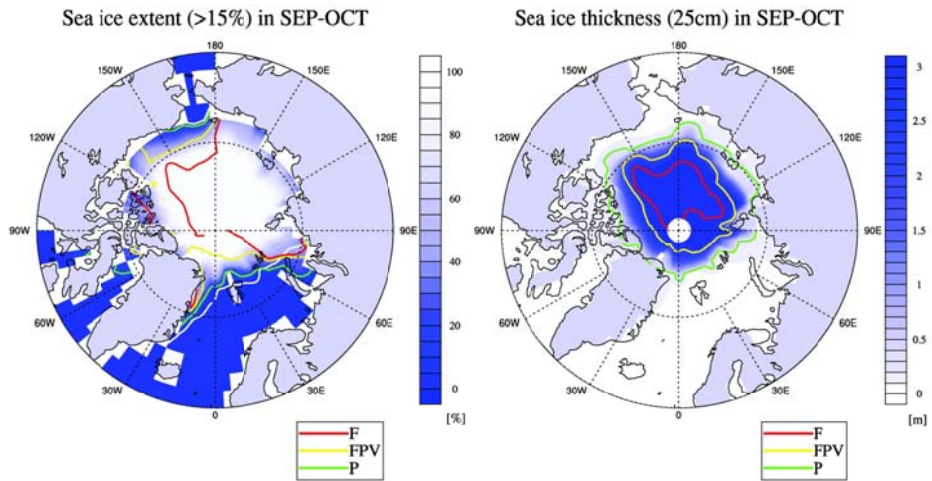


Fig. 3.4 Shading indicates simulated average sea ice extent and thickness for September to October in *P* simulation. Lines in the left panel indicate sea ice extents where the ocean is covered with more than 15% sea ice. White line is the observed sea ice extent averaged from 1981-2000 HadISST data. Lines in the right panel indicate 25cm levels of mean sea ice thickness.

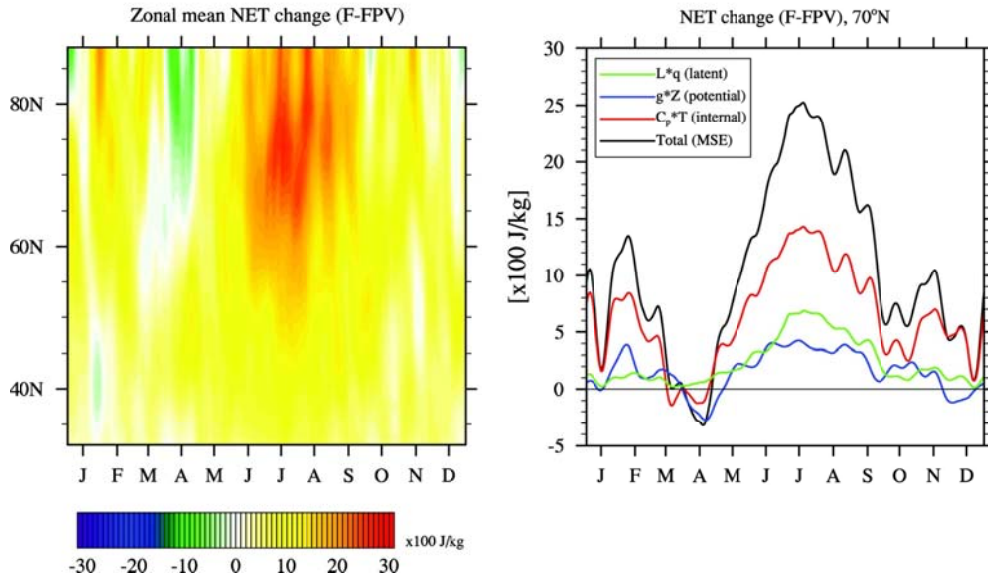


Fig. 3.5 (left panel) *NET* change by vegetation feedback effect (*F-FPV*). (right panel) changes in the components of *NET* at 70°N. 10-day running average is applied for the time dimension. Here atmospheric energy is estimated by moist static energy – summation of atmospheric latent, potential, and internal energy.

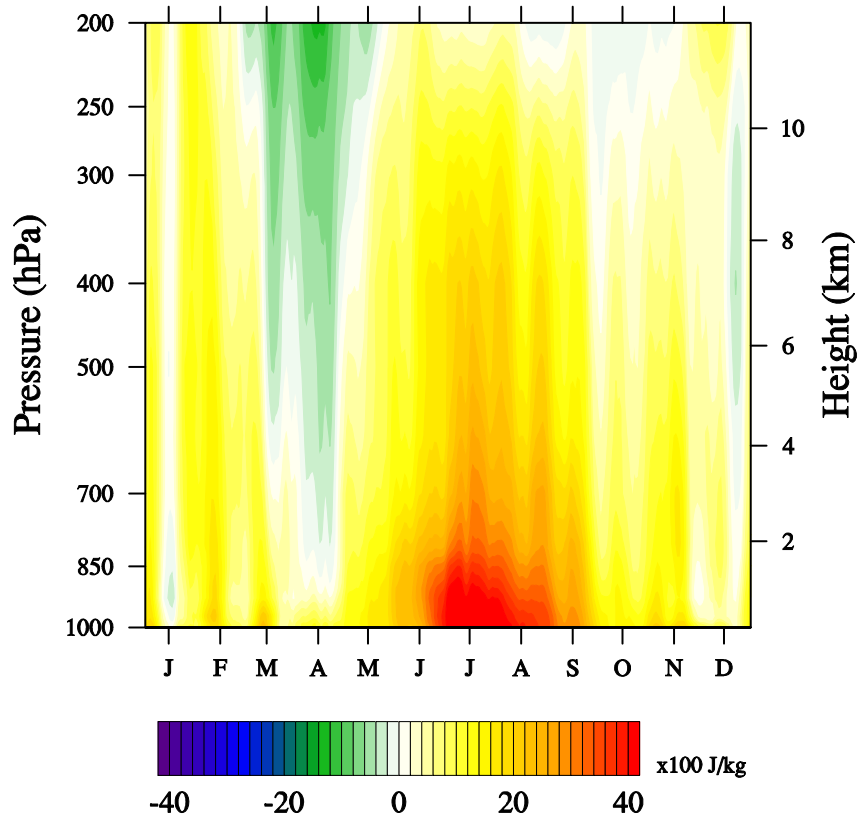


Fig. 3.6 Zonal mean NET change by vegetation feedback effect ($F-FPV$).

Table 3.1 Change in model simulated variables by vegetation feedback effect (*F-FPV*).

Variables	High-latitude land (north of 60°N)				Arctic sea (north of 70°N)			
	MAM	JJA	SON	DJF	MAM	JJA	SON	DJF
Sfc air temperature [K]	1.58	2.53	1.28	1.46	1.24	1.60	2.15	1.37
Net SW [Wm^{-2}]	6.93	16.82	0.24	0.22	1.72	9.61	0.49	0.00
Net LW [Wm^{-2}]	-1.84	-6.52	0.28	0.40	-0.23	-1.43	-0.99	-1.08
Latent heat [Wm^{-2}]	2.31	6.47	1.59	0.65	1.02	3.13	1.79	1.51
Sensible heat [Wm^{-2}]	1.12	5.08	-0.54	-0.13	-0.09	0.80	-0.35	0.75
Low cloud [%]	-1.93	-8.85	0.41	1.21	0.24	-2.21	0.40	-0.05
High cloud [%]	2.00	1.71	1.51	1.24	1.35	1.41	0.35	0.65
Sea ice extent [%]	-	-	-	-	-0.86	-10.57	-24.13	-1.64
Sea ice thickness [cm]	-	-	-	-	-7.64	-14.42	-13.37	-9.50
Oceanic temperature [K]	-	-	-	-	0.15	1.48	0.93	0.18
Snowcover fraction [%]	-6.17	-2.49	-3.46	-2.59	-	-	-	-

Values represent the climatological mean difference between the F and FPV simulation.

3.6. Discussion

Present modeling results clearly demonstrated that conspicuous climatic change can be arisen in the Arctic region from the vegetation-climate feedback. However, it should be noted again that the simulated vegetation and its change could be highly model-dependant, and limitations of CLM-DGVM restrict the direct application of present results to recorded climate change. Above all, anthropogenic vegetation change is not considered in the chosen modeling system. Because the CLM-DGVM only simulates the ‘potential’ vegetation under idealized present and future conditions, vegetation change from urbanization, deforestation, and cultivation were not taken into account despite of its huge impacts on the local vegetation biosphere. Also important limitation to note is that the carbon cycle is not considered in the present modeling system, despites profound impacts are anticipated in company with vegetation change. In the Arctic climate system, for instance, the enhanced carbon uptake by more vegetation activity may counteract the warming, and also possible is that the methane release from vegetation activity and accelerated thawing of permafrost may amplify the warming. There are still many controversial issues on the ecosystem-climate interaction under climate change, that need to be further accessed in order to increase the fidelity of our climate prediction. In addition, limitations also lie in the utilization of SOM instead of full-depth ocean

dynamics. Either possible changes in meridional transport of energy by ocean circulation or the redistribution of sea ice were not simulated, although it has a great potential to affect the vegetation-climate feedback process.

Most climate models underestimate the surface warming and Arctic sea ice loss in recent decades after late 1990s. This partly seems to be due to unrealistic, excessive negative LW feedback of climate models (Boe et al., 2009), but the reason is still controversial (Rampal et al., 2011; Stroeve et al., 2007; Winton, 2011). Our finding implies that the exclusion of vegetation-feedback in climate model can be one of underlying causes. This could not be examined due to the limitation of experiment design, but the transient simulations with fully-coupled ocean model may address this issue.

4. MODELING THE ROLE OF CLOUD ON THE RECENT ARCTIC WARMING DURING WINTER

4.1. Recent change in the winter Arctic cloud

The existence of cloud has immediate impacts on the surface radiation balance. Due to its unique physical properties, clouds tend to warm the surface by absorbing and re-emitting longwave radiation from the Earth's surface. At the same time, clouds have cooling effect by reflecting incoming shortwave radiation from space. These radiative properties of cloud are known to be very important for the Arctic climate and weather system and its change (Curry et al., 1996). Clouds cover the Arctic region by more than 50% throughout the year (Eastman and Warren, 2010a), interacting with other atmospheric and oceanic variables of Arctic climate system (Francis and Hunter, 2006; Schweiger et al., 2008). During the wintertime over Arctic region, net cloud radiative forcing (CRF) at surface is about $+20 \text{ W m}^{-2}$ in spite of nearly zero incoming solar radiation, which is due to the strong long wave radiative effect of Arctic cloud (Shupe and Intrieri, 2004). Therefore wintertime surface air temperature is largely controlled by Arctic clouds and a coherent change of Arctic clouds and surface temperature has been suggested by various observations. For instance,

Wang and Key (2003) reported that the both Arctic clouds and surface temperature have decreased by $-5.7 \text{ \% decade}^{-1}$ and $-0.34 \text{ K decade}^{-1}$, respectively, for the period 1982–1999 from APP-x data. Liu et al. (2009) found that change in Arctic clouds accounts for a cooling trend at surface at a rate of $-0.91 \text{ K decade}^{-1}$ for the period 1982–2004 from the same satellite product.

On the other hand, Arctic clouds are greatly affected by surface conditions as well. Curry et al. (1996) showed that the formation of Arctic clouds is enhanced by surface warming through enhanced turbulent heat fluxes and horizontal and vertical advection, suggesting a positive feedback effect to surface temperature. Vavrus (2004) argued that this positive feedback process plays a crucial role in amplifying Arctic warming under increased greenhouse forcing. Other studies have noted that variation of winter Arctic clouds in recent decades was much affected by large-scale atmospheric circulation in addition to the radiative feedback effect; Liu et al. (2007) showed that moisture convergence induced by large-scale atmospheric circulation change over the Nansen Basin and the Barents and Kara Seas had significant impacts on Arctic clouds during 1982–2000. Eastman and Warren (2010b) noted that the cloudiness in the Arctic is highly associated with the variation of Arctic Oscillation (AO) (Thompson and Wallace, 1998), a hemispheric pattern of atmospheric circulation anomalies.

Since the late 1990s, the Arctic climate has been exposed to radical changes.

The accelerated melting of sea ice and associated ice-albedo feedback led to considerable warming throughout the troposphere (Screen and Simmonds, 2010a) and even caused hemispheric-scale atmospheric circulation changes (Francis et al., 2009; Overland and Wang, 2010). These changes are conspicuous especially during early winter (Screen and Simmonds, 2010b). Numerous studies pointed out the cloud as possible cause for amplifying the Arctic warming in winter because cloud-radiative feedback process works positively due to absence of solar radiation (Graversen et al., 2008; Graversen and Wang, 2009; Palm et al., 2010).

However, previous studies for the Arctic cloud with respect to recent Arctic climate change have been concentrated in melting season although winter Arctic cloud could play a crucial role on the recent Arctic warming (Cuzzone and Vavrus, 2011; Kay and Gettelman, 2009; Palm et al., 2010; Schweiger et al., 2008). Accordingly, whereas much of role of Arctic sea ice loss for the associated changes in Arctic clouds in melting season have been investigated, the change in cloud and its impact on the Arctic climate system according to recent Arctic change during winter still remains poorly understood. Thus it is necessary to more understand the change and effect of winter Arctic cloud in recent Arctic climate.

The lack of study on winter Arctic cloud is mainly due to harmful weather and climate condition in Arctic winter (ACIA, 2005). Examining changes in

clouds and its feedback in winter is very difficult because extremely cold and dry conditions lead to large detection error in observation. Still there is large discrepancy in the interannual variation and even long-term trends of cloud cover observations among different satellites and surface measurement (Eastman and Warren, 2010a). In addition, the extreme condition also gives uncertainty to modeling for simulating the Arctic cloud (Vavrus and Waliser, 2008; Walsh et al., 2005).

Considering the uncertainties in cloud data from satellite products, cloud information from the reanalysis might be a useful complementary to study the Arctic clouds and associated feedback effects. Schweiger et al. (2008), for instance, used cloud data from the 40-yr the ECMWF Re-Analysis (ERA40) (Uppala et al., 2005) to investigate the relationship between the sea ice and cloud cover during autumn. Walsh et al. (2009) compared the fraction and radiative forcing of Arctic clouds estimated from four different reanalysis datasets with an observational dataset from the Atmospheric Radiation Measurement Program (ARM) (Stokes and Schwartz, 1994). They suggested that the reanalysis models could simulate cloud radiative forcing correctly when the cloud amount was simulated correctly.

Thus we examine the variation of Arctic clouds during winter (December through February) for the recent 3 decades from two reanalyses: ERA-Interim

reanalysis and NCEP CFSR. Long-term trends in Arctic cloud for the recent decades, and coherent changes in atmospheric variables (e.g., temperature and moisture) and large-scale atmospheric circulations are examined.

4.1.1. Year-to-year variation and trends in cloud-related variables

We examine overall changes in total cloud cover, surface temperature and sea ice cover during winter over the Arctic Ocean (oceanic and sea ice covered region in the north of 67°N), and AO index for last three decades (Fig. 4.1). The trends in cloud amount and surface temperature from all datasets are summarized in Tables 4.1 and 4.2. In considering the large differences in the mean and variability among the dataset (Table 4.1), each time-series in Fig. 4.1 is re-scaled to have the mean and standard deviation of the ERA-Interim for the period 1979–2011 for comparison. The most notable feature of the Arctic cloud amount variation for the analysis period is the long-term trend change occurred around the end of the 20th century. The Arctic cloud amount showed a clear negative trend for the last two decades in the 20th century but it was turned to a positive trend around the 2000s. Although the interannual variation of the Arctic cloud amount exhibits little consistency among datasets, even between two satellites ($r = -0.08$ for the period 1982–2004), these long-term trends and their changes agree fairly well with each other only except the APP-x which shows continuous

decrease until the mid 2000s. The variations in surface temperature and sea ice fraction are negatively correlated ($r = -0.86$ in the ERA-Interim and -0.80 in the NCEP CFSR). Interestingly, the surface temperature and sea ice cover in the Arctic seem to also have a notable trend change concurrent with the cloud amount. There was a weak decreasing (increasing) or nearly neutral trend in surface temperature (sea ice cover) for the 1980s to 1997 but it was replaced by a strong increasing (decreasing) trend from 1998 to 2011. This is commonly found in the both reanalyses. Here the APP-x again exhibits quite different long-term variation from other datasets.

We check whether there actually exists trend change in these year-to-year variations in late 1990s by performing the change point analysis (Tomé and Miranda, 2004). As a result, year-to-year variations of cloud amount, surface temperature, and sea ice cover have breakpoints to trend changes in late 1990s. In variation of the cloud, trend is changed in 1997 (NCEP CFSR) and 2000 (ERA-Interim). The trends of surface temperature and sea ice cover from both reanalyses also are changed in 1997 and 1998, respectively. Considering the concurrent trend changes in cloud and surface temperature around year 1997 and 1998, we divide whole period into two periods including the late 20th century (1979–1997, hereinafter L20C) and including the early 21st century (1998–present, hereinafter E21C).

In spatial distributions of linear trends in clouds over the Arctic during both L20C and E21C, clear trend changes appear between two periods (Figs. 4.2a–b, and 4.2e–f). Both reanalyses show consistent significant decrease in cloud amount over the Kara Sea, Laptev Sea, East Siberian Sea, north of the Queen Elizabeth Islands and central Arctic for the L20C, but the tendency is larger in the ERA-Interim. Satellite datasets also show similar decrease over the Arctic for the same period. In the E21C both reanalyses show increasing cloud amount over the most of the Arctic Ocean but regions of large increase slightly differ between the two reanalyses. The ERA-Interim shows significant increasing trend over the Kara Sea, Laptev Sea, East Siberian Sea, north of the Queen Elizabeth Islands, and Baffin Bay, but the NCEP CSFR does not show significant increasing trend mostly over the Kara Sea, north of the Queen Elizabeth Islands, Baffin Bay. The difference in significant regions for the E21C may be partly due to slightly different periods in two reanalyses (the ERA-Interim covers three more years: 2009–2011); the statistically significant regions for the period 1998–2008 are more similar.

Spatial pattern and strength of the cloud amount change consort with surface air temperature (SAT; 2-meter air temperature) changes in the Arctic Ocean (Figs. 4.2c–d, and 4.2g–h). Surface skin temperature is used in Fig. 4.1 for the comparison with satellite data, but we hereinafter use SAT rather than

surface skin temperature. During the L20C, both reanalyses show general cooling trend over the Arctic Ocean with significant cooling over the central Arctic, north of Queen Elizabeth Islands, East Siberian Sea, and Chukchi Sea. In the E21C, SAT shows prominent warming trend over the most Arctic Ocean and also over high-latitude continents. The significant warming trend is found over the Kara, East Siberian, and Chukchi Seas, and northern Greenland in both reanalyses (Figs. 4.2d and 4.2h). Most of these regions also are experiencing large sea ice retreat (see region with oblique lines in Fig. 4.2). However, very strong warming trend is found over the Barents Sea in both datasets, where a prominent decrease in sea ice is found in winter (Cavalieri and Parkinson, 2012), while vivid increasing in total cloud amount is not found over this region. Over this region, low level cloud cover decreases while mid level cloud increases during the E21C (figure not shown). Schweiger et al. (2008) suggested that less sea ice cover could affect decreasing in low level cloud and increasing in mid level cloud through changing in boundary layer height and static stability during autumn. The Barents Sea is relatively warmer than other Arctic regions because it is located at the location contacting with warm Atlantic water. In addition, over the Barents Sea, the PBL height increases and static stability decreases significantly during the E21C. Consequently, similar mechanism may underlie between changes in total cloud cover and SAT.

Trends in vertical distribution of zonal-averaged temperature, specific humidity, and cloud water content also show that there are gradual decreasing during the L20C and large increasing during E21C over the Arctic (Fig. 4.3). Although vertical distributions in temperature from two reanalyses are slightly different during L20C in weak warming region, weak cooling is dominant whole troposphere over the Arctic. The weak cooling trend over the Arctic is changed to substantial warming trend with particularly strong warming at near surface in the vicinity of 80°N during the E21C. This strong increasing at near surface is also found in the trend of specific humidity for same period. During the E21C, vigorous moistening trend occurs at surface over the 70-80°N and spreads to entire lower troposphere over the Arctic while weak drying trend is found at lower troposphere.

Changes in cloud properties are also observed mainly at the lower troposphere with the same manner of moisture change. In particular, vertical distributions of trends in cloud water content along with latitude in both reanalyses and both periods are almost analogous to each other. Trends during the L20C from both reanalyses reveal weak decreasing at near surface over around 70°N and relatively stronger decreasing over central Arctic (80–90°N). A spatial distribution of trend in cloud cover is consistent with cloud water content; strong decrease occurs primarily at near surface over the central Arctic. During

the E21C, explosive increasing in cloud water content compared to change in the L20C occurs at lower troposphere and the increasing spreads to mid-troposphere. In particular, both reanalyses show that cloud water content increases mainly at altitude of around 900 hPa over the most Arctic region. In addition, cloud water content above 900 hPa to about 500 hPa is also largely increasing. Meanwhile, the differences between reanalyses are observed at surface over central Arctic with larger amount of observed in the ERA-Interim.

The major distinctions in cloud change between in the E21C compared to the L20C are the different trend and vertical extent of cloud water content. The gradual decrease and steep increase are also observed in temperature and moisture change. However, spatial pattern in cloud water content change resembles that of humidity more than temperature. This implies that cloud trend might be closely linked to variation of moisture budget over the Arctic. Previous studies have noted this relationship; moisture inflow to the Arctic could be primarily attributable to cloud variation (Beesley and Moritz, 1999; Curry et al., 1996; Liu et al., 2007). Thus, we examine the contribution of moisture transport to the Arctic Ocean through northward moisture transport ($\bar{v}\bar{q} + v'q'$) at 67°N. Properly, as expected, the variation in total moisture inflow to the Arctic at 67°N with height resembles that in moisture over the Arctic (Fig. 4.4). In particular, moisture transport also presents largely increasing after winter of 1997/1998.

Tendency to vertical extension in cloud water content implies that other cloud type besides stratiform cloud can be more formed. Eastman and Warren (2010b) found that an increasing in formation of cumulonimbus and stratus over the Arctic Ocean is correlated with sea ice reduce even in winter based on long-term surface observation. They found that this kind of cloud type increases under low-ice cover winter by comparing cases in low-ice covered years and high-ice covered years. Thus, considering recent substantially reduced sea ice, the increasing in cloud water content during the E21C might indicate increases in low level stratus at about 900 hPa and cumulonimbus above 900 hPa.

Trend changes in precipitation and evaporation over the Arctic Ocean also suggest the possibility of increasing in cumulonimbus. Figure 4.5 shows spatial distribution of changing trend of evaporation and total precipitation over the Arctic Ocean during each period. Both evaporation and precipitation show decreasing during L20C and increasing during E21C over the most Arctic Ocean similarly with temperature and cloud amount. Trend in precipitation change appear more largely than evaporation for both periods, and this tendency that precipitation is larger than evaporation becomes stronger during the E21C. Difference between precipitation and evaporation averaged over the Arctic Ocean increases during the E21C. This also implies that formation of precipitating cloud such as cumulonimbus and nimbostratus increases during this

period.

Moreover, the spatial distributions of trend in evaporation and precipitation during the E21C are almost analogous to each other. Significant increasing in both variables emerges over the Kara, Laptev, East Siberian, and Chukchi Seas. These coherent changes in evaporation and precipitation are different from the L20C. This suggests that local hydrological cycle is being enhanced during the E21C. Additionally, the region where total cloud cover increases significantly is also consistent to these regions (Fig. 4.2). In this process, the relationship between cloud and surface condition could be closer through enhanced local hydrological cycle. We also find that the coherent change between SAT and cloud is being tightened in the E21C in Fig. 4.1. Correlation coefficients between SAT and cloud amount averaged over the Arctic Ocean increase in the E21C compared to the L20C: 0.68 to 0.81 in the ERA-Interim, 0.42 to 0.66 in the CFSR. Furthermore, the changing trends in the E21C also become larger than those in the L20C (Tables 4.1 and 4.2). Major underlying physical basis for the coherent changes in SAT and cloud cover is the cloud radiative effect (Liu et al., 2008; Wang and Key, 2005a). However, it can be suggested that the other factors such as the large-scale circulation change and substantial sea ice retreat can affect the tightened coherent change in SAT and cloud in the E21C.

4.1.2. Effect of AO on the change in Arctic cloud

The large-scale advective process also contributes to the variation of Arctic cloud in addition to local feedback processes (Eastman and Warren, 2010b; Liu et al., 2007; Wang and Key, 2005b). Thus, cloud change between the L20C and E21C also could be affected by the large-scale atmospheric circulation change. In particular, during the E21C, the large-scale circulation also has shown a notable change in association with sea ice melting (Overland and Wang, 2010). The AO, which represents the variation of large-scale atmospheric circulation over the Arctic, turned into opposite phase in this period (Stroeve et al., 2011). This implies that the phase change in the AO could affect trend change between two periods. Therefore, we examine the relationship between the Arctic cloud and the AO and its changes between two periods.

In the last three decades, the AO showed a clear interdecadal variation. The positive AO phase was dominant during the L20C including prominent positive trend from the 1980s to 1990s. However, the trend was sharply changed to neutral to weak negative in the 2000s and extreme negative AO in the recent years (Fig. 4.1d). The change in temperature-cloud relationship between two periods could be affected by the change in AO phase due to vertical and horizontal moisture flux associated with the AO.

In the both reanalyses the AO index is positively correlated with cloud water

content over mid- and upper troposphere and negatively correlated with that at near surface (Figs. 4.6a and 4.6d) and similarly with surface observation from Eastman and Warren (2010b). This contrasting relationship between low and upper tropospheric cloud is equally found in both L20C and E21C periods, suggesting that intrinsic relationship between cloud and the AO might be not much affected by recent changes in large-scale circulation and surface conditions. Examining moisture fluxes associated with AO, it seems that that lower clouds are affected more by horizontal moisture flux while upper clouds are affected more by vertical moisture flux from the lowest level of troposphere (Figs. 4.6b–c, and e–f). The horizontal moisture convergence is negatively correlated with the AO at the lower troposphere over the subarctic latitudes (60–75°N). In contrast, vertical moisture transport is positively correlated with the AO over the sub Arctic (60–75°N) and central Arctic (80–90°N) at the whole troposphere. This is associated with the low (high) pressure anomalies in the positive (negative) AO phase. The anomalous low pressure above planetary boundary layers supports lifting of moisture but leads to the divergence in the sub Arctic. This can strengthen cloud formation above near surface over the central Arctic while horizontal moisture divergence at lower troposphere decreases low clouds.

In the same manner to relationship between cloud water content and AO index, the moisture transport associated with the AO presented in Fig. 4.6 is also

found in both L20C and E21C periods. Namely, AO-related moisture transport does not change between two periods. This suggests that the AO contributes to the interannual variation of cloud mainly through its phase; the phase of wintertime AO changed from negative to positive in the L20C, but it was changed to decreasing trend in the E21C. Because low-level cloud mostly accounts for the total cloud amount, low-level moisture convergence associated with the AO might be mainly linked to cloud change in each period. In addition, it also suggests that the AO-related moisture transport has a weak effect on change in cloud and its relation to surrounding atmospheric states.

4.1.3. Effect of sea ice retreat on recent changes in Arctic cloud

The recent change in Arctic cloud during the E21C seems to be more linked to the change in Arctic surface than change in large-scale circulation represented with AO. This implies that change during the E21C could be more directly linked with accelerated sea ice retreat. Therefore, we examine change in cloud water content and upward moisture transport in relation to sea ice cover during the two periods. To minimize the correlation from the AO, we calculated the partial correlation between sea ice cover averaged over the Arctic Ocean and zonal-averaged cloud water content/upward moisture transport independent from the AO index during the L20C and E21C. First, cloud water content at troposphere is

tightly associated with sea ice fraction over the Arctic Ocean for the both L20C and E21C (Fig. 4.7). In particular, cloud water content at lower troposphere below 700 hPa is more closely linked to surface conditions. Surface evaporation, horizontal moisture flux, and longwave CRF may be major causes for this binding at lower troposphere (Beesley and Moritz, 1999; Shupe and Intrieri, 2004).

Comparing relationships between the L20C and E21C, strengthening of relationship over the local Arctic occurs for the E21C. At lower troposphere, significantly correlated region over the Arctic margin during the L20C moves and extends to the central Arctic during the E21C. Contrastingly, significant correlation between cloud water content and sea ice reduction at most troposphere over the Arctic margin (70–80°N) during the L20C disappears in the E21C. In addition, cloud water content at upper troposphere above 700 hPa over the central Arctic (80–90°N) is positively correlated to sea ice during the L20C (Figs. 6a and 6c), but it becomes to be negatively correlated to sea ice during the E21C same as cloud water content at the Arctic margin (Figs. 6b and 6d). Namely, during the E21C, the effect of sea ice on cloud at lower troposphere over the central Arctic becomes to be reinforced while effect on upper troposphere over the Arctic becomes weaker.

On the relationship of sea ice fraction with cloud water content, vertical

moisture transport seems to play an important role (see contour in Fig. 4.7). During the L20C, upward moisture transport is positively correlated with sea ice reduction over the Arctic margin, and negatively correlated over the central Arctic in common to correlation of cloud water content. It seems to be plausible that the ice-reduced surface condition might be linked to the increase in cloud water content through upward moisture transport. In addition, the significant linkages among sea ice reduction, cloud water content and vertical moisture flux at near the top of troposphere bring the hint of the possibility that these linkages are bound under large-scale circulation during the L20C. During the E21C, the influence of sea ice on vertical moisture transport move to the higher Arctic (75–90°N). The northward expansion of correlated region to higher Arctic is also seen in cloud water content. In addition, the change in upward moisture transport related to sea ice during the E21C is also consistent with the vertical expansion in cloud water content during the E21C in Fig. 4.3. Perhaps, enhanced upward moisture transport over this region might contribute to an increase in cumulonimbus over the Arctic.

The change in upward moisture transport related to sea ice during the E21C suggests that there could be surface condition change which enhances upward moisture transport over the central Arctic. At the surface, a decreasing in static stability and deepening in planetary boundary layer (PBL) could contribute to

this change as suggested for autumn by Schweiger et al. (2008). In Fig. 4.8, we examine changes in 850 hPa thickness ($\theta_{850 \text{ hPa}} - \theta_{1000 \text{ hPa}}$) and PBL height between the E21C and L20C. It is found that 850 hPa thickness and PBL height averaged for the E21C are larger than those for the L20C over the most Arctic Ocean. In particular, both reanalyses show that the Barents Sea, which region sea ice cover reduces substantially during the E21C, experiences significant changes in thickness and PBL height. These indicate that sea ice retreat induces increasing in PBL height and decreasing in static stability (increasing in thickness) even during winter. This also implies that upward moisture transport might be enhanced corresponding to these changes.

Meanwhile, two reanalyses show slightly different features over the Arctic Ocean except the Barents Sea. Although the ERA-Interim shows that atmospheric thickness expansion during the E21C occurs significantly over the most Arctic Ocean and PBL height increases over the Eurasian margins of the Arctic Ocean (Figs. 4.8a and 4.8b), the CFSR shows that the increases in atmospheric thickness and PBL height are limited in the vicinity of the Barents Sea (Figs. 4.8e and 4.8f). The discrepancy between two datasets seems to be mainly due to difference in sea ice change between two datasets. First, the ERA-Interim has three more years which period has experienced substantial sea ice retreat than the CFSR. In addition, the CFSR has less sea ice cover over the

Arctic than ERA-Interim during the L20C (Fig. 4.1c). Consequently, an amount of reduce sea ice during the E21C is smaller in the CFSR than the ERA-Interim. As a result, weaker changes at surface appear in the CFSR compared to the ERA-Interim. However, despite of this discrepancy, the relationship between sea ice retreat and near surface change is found consistently in both datasets. The increases in PBL height and atmospheric thickness are mainly found in sea ice retreated regions in each datasets (contour in Figs. 4.8b and 4.8f).

In addition, alterations in surface condition and cloud amount could bring a change in effect of cloud on surface, and this could amplify the change at surface. Figures 4.8c and 4.8g present the difference in CRF between two periods. Both datasets show that significant increase in CRF during the E21C occurs over the Barents Sea. As examined with PBL height and atmospheric thickness, this region has experienced substantial surface warming and consequent surface condition change due to sea ice retreat. According to surface warming outgoing longwave radiation increases, thus CRF increases because of more trapping increased longwave radiation by cloud. In addition, increased cloud amount also reinforces CRF. Consequently, the surface, in turn, can be more warmed. On the other hand, the large discrepancy between two datasets is also found in CRF over the Arctic Ocean except the Barent Sea in similar manner to PBL height and atmospheric thickness. This also seems to be linked to different change in sea ice

cover between two datasets.

The differences in sea level pressure and 500 hPa geopotential between two periods present the development of high pressure system across the Eurasian side of the Arctic Ocean and Eurasia continent (Figs. 4.8d and 4.8h). Significant change in sea level pressure appears over the Eurasian continent around 90°E from only the ERA-Interim, and 500 hPa geopotential near this region also shows large increases during the E21C. Larger differences from ERA-Interim are also probably relevant to difference in sea ice cover between datasets. It has been suggested that the development of winter high pressure over the Eurasian continent around 90°E is linked to sea ice melting (Jaiser et al., 2012), and the recent dipole-like atmospheric structure over the Arctic could contribute to modification of large-scale circulation patterns (Overland and Wang, 2010). Perhaps, recent change in vertical moisture transport related to sea ice may be closely linked with this pressure system change.

The overall changes in the Arctic climate between two periods also could induce the change in the impact of clouds on recent Arctic climate. Figure 4.9 presents the regression of zonally averaged air temperature and specific humidity onto low level cloud cover (below 750 hPa) averaged over the entire Arctic with removing the trends. Here we choose low-level clouds as it mostly accounts for total cloud cover and have strongest radiative effect at the surface (Eastman and

Warren, 2010b; Intrieri et al., 2002; Shupe and Intrieri, 2004). Overall, the underlying positive relationship between the cloud and SAT is found to be largely similar in both periods, but there is important difference between two periods. During the L20C, low-level cloud in the Arctic is positively correlated with lower tropospheric (below 700 hPa) temperature over the southern part of Arctic (60–75°N) rather than the central Arctic. In the E21C, contrastingly, the center of temperature associated with clouds moves to the high Arctic, north of 70°N with strengthened amplitude of the relationship. Atmospheric moisture exhibits positive relationship with the low-level cloud change similar to the temperature change pattern. Moreover, the positive relationship between low-level cloud and temperature more vertically extends further to mid- to even upper-troposphere above 500 hPa. In other words, the local connection between cloud and temperature/moisture over the Arctic became much tightened in the E21C.

Relationship between low-level cloud and atmospheric states in the L20C presented in Figs. 4.9a and 4.9c reflects the mechanism between cloud and the moisture over the marginal Arctic suggested by Liu et al. (2007). Arctic low clouds show largest correlation with subarctic moisture and temperature and the pattern seems to represent the influence of northward moisture fluxes to the Arctic. During the E21C, however, the changed pattern of strengthened local

connection presented in Figs. 4.9b and 4.9d implies that cloud might be more associated with profound changes in the Arctic climate system for this period – explosive warming and moistening associated with accelerated melting of sea ice. The strong surface warming would cause lower tropospheric warming and sea ice retreat might reinforce moistening by increased evaporation more over the central Arctic region. Warming and moistening of lower troposphere associated with melting sea ice might greatly reduce the atmospheric stability. Consequently, the near-surface warming could more easily propagate to mid- to upper troposphere by enhanced turbulent mixing and upward motion. In addition, this might reinforce increases in formation of precipitating cloud and precipitation, thus the local connection between clouds and temperature/moisture, in turn, is much tightened over the Arctic. This suggests that the impact of cloud on warming and moistening at lower troposphere over the local Arctic could be strengthened under sea ice retreated condition.

4.1.4. Discussion

We examined the long-term variations of cloud and its relationship to atmospheric state over the Arctic during winter for recent three decades, particularly focusing on changes for the early 21st century in relation to sea ice retreat. Two state-of-the-art reanalyses present that cloud decreases gradually

during late 20th century and increases largely in the 21st century. Coherent changes in each period also are found in temperature and moisture at lower troposphere, and the relation of cloud to local atmospheric states becomes stronger during the increasing period. Surface condition change due to reduced sea ice cover seems to be the major cause for the increasing in cloud and change in relationship between cloud and environmental atmospheric state. Reduced sea ice cover leads to an increasing in surface fluxes, a decrease in lower-tropospheric static stability, and deepening of planetary boundary layer. Consequently, low level stratiform cloud and convective cloud can be more formed over the more opened ocean. This reinforces the cloud radiative effect and precipitation over the Arctic, and, in turn, the local relationship between cloud at lower troposphere and atmospheric states becomes strengthened.

We divided whole analysis period into two periods with criterion based on the year of changing trends oppositely. In interannual variation of cloud amount, the change point analysis indicates that the criterion year could be 1997 or 2000. We checked both years as criterion to divide periods, and the results including relationship between cloud and surrounding atmospheric state are almost analogous to each other. In particular, most characteristics in sea ice melting period do not change. This result also emphasizes the role of sea ice retreat on recent Arctic climate changes related to cloud.

We compare cloud data from reanalyses with satellite data retrieved from APP-x and TOVS which cover the late 20th century, but we do not use recent cloud data retrieved from CloudSat and CALIPSO. Because this study focuses on long-term change more than decade, we think that data consistency in homogeneous dataset might give more reliable result to this study. For a similar reason, we choose satellite datasets which covers more than two decades for comparison. Recent satellite cloud dataset has relatively short-term period, so we do not compare with this dataset. However, Zygmuntowska et al. (2012) has mentioned that there are large discrepancy in winter cloud data between the ERA-Interim and recent satellite retrievals from CloudSat and CALIPSO from comparison for 4 years (2006–2009). Although the domains defined for the Arctic cloud are slightly different from this study, this suggests that more careful interpretation for result in this study should be needed.

Lastly, although the result of this study and prior studies suggest that the atmospheric circulation on cloud change plays also important role, the role of the atmospheric circulation is not investigated in detail. We examine interannual variation of sea level pressure and geopotential at 500 hPa in association with low level cloud (Fig. 4.10). Both analyses show that the variation in low level cloud is mainly related to low pressure over the most Arctic Ocean during the L20C. The relationship between low level cloud and pressure system over the

Arctic during the L20C indicates the low level cloud forms more frequently under low pressure system over the Arctic region. This relation between winter Arctic cloud and low pressure system is consistent with the result of prior study (see Fig. 3 in Liu et al. (2007)). During the E21C, the variation in low level cloud becomes to be related with high pressure system across the Eurasian coastal region and the Siberia region and low pressure over the central and North American side of the Arctic, which forms dipole-like structure. The dipole-like spatial pattern related to low level cloud during the E21C is also shown in geopotential at 500 hPa more clearly. The dipole-like pattern with high pressure over the Eurasian continent around 90°E and the low pressure over the Arctic Ocean is also seen in difference between two periods (Fig. 4.8). These resemblances strongly suggest that this dipole-like pressure system will be closely linked to recent variation of the Arctic winter cloud. Maybe, the factors such as storm track and cyclone activity related to this structure could affect the cloud formation over the Arctic.

Table 4.1 Mean, standard deviation, and trends of total cloud fraction over the Arctic Ocean (north of 67°N) in each dataset.

	mean (%)	standard deviation (%)	trend (% decade ⁻¹)		
			whole period	20th century	21st century
ERA-Interim	87.47	3.35	-1.39^{**} (1979–2011)	-5.08^{**} (1979–1997)	5.51^{**} (1998–2011)
NCEP CFSR	81.89	2.41	-1.36^{**} (1979–2008)	-2.43^{**} (1979–1997)	4.46^{**} (1998–2008)
TPP-x	72.67	7.38	-2.09 (1980–2005)	-3.06 (1980–1997)	19.66^{**} (1998–2005)
APP-x	70.55	8.12	-8.86^{**} (1982–2004)	-12.23^{**} (1982–1997)	-24.96[*] (1998–2004)

* significant at 90% confidence level

** significant at 95% confidence level

Table 4.2 Mean, standard deviation, and trend of surface skin temperature over the Arctic Ocean (north of 67°N) in each dataset.

	mean (K)	standard deviation (K)	trend (K decade ⁻¹)		
			whole period	20th century	21st century
ERA-Interim	253.91	1.51	0.88[*] (1979–2011)	-0.88^{**} (1979–1997)	2.80[*] (1998–2011)
NCEP CFSR	252.32	1.23	0.67^{**} (1979–2009)	-0.49 (1979–1997)	2.42^{**} (1998–2008)
TPP-x	248.82	1.25	0.67^{**} (1980–2005)	-0.33 (1980–1997)	4.81[*] (1998–2005)
APP-x	251.26	1.26	-1.20^{**} (1982–2004)	-2.27^{**} (1982–1997)	-3.03 (1998–2004)

^{*} significant at 90% confidence level

^{**} significant at 95% confidence level

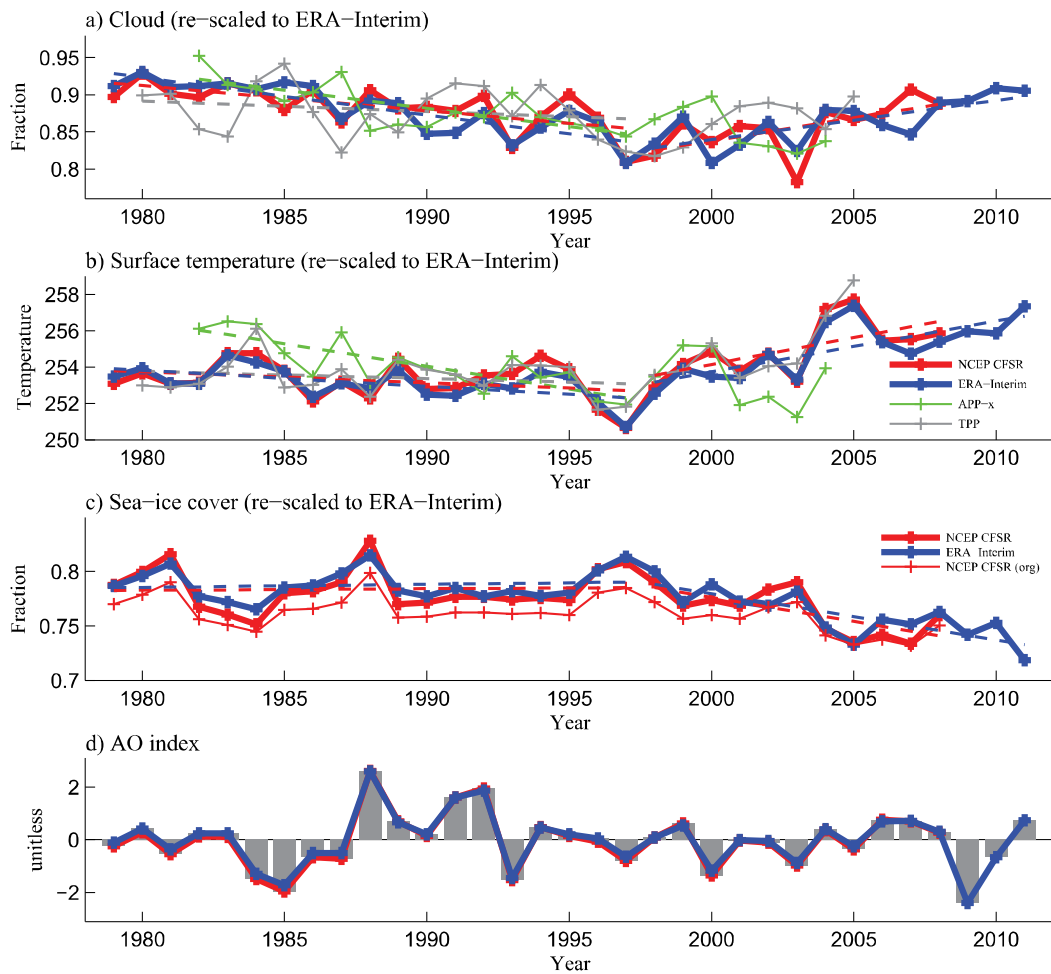


Fig. 4.1 Time-series of (a) cloud amount, (b) surface temperature, (c) sea ice cover over the Arctic Ocean (north of 67°N), and (d) AO index in winter (December to February) from the NCEP CFSR, ERA-Interim, APP-x, and TPP datasets. Trend lines are denoted with dashed line. Time series of cloud amount, surface temperature, and sea ice cover are re-scaled to have the mean and standard deviation of ERA-Interim for comparison.

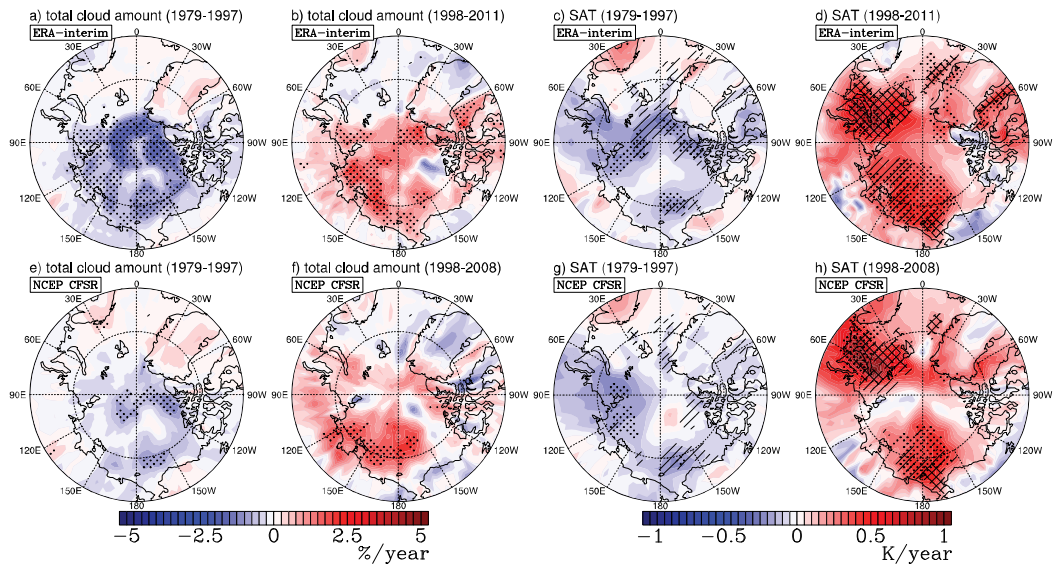


Fig. 4.2 Changing trends in winter total cloud amount and surface air temperature during late 20th century (1979–1997) and early 21st century (1998–present) from the ERA-Interim and NCEP CFSR. Stippled region indicates that trend is significant at the 95% confidence level. Oblique and cross checked region in c and g (d and h) indicate that region sea ice cover is increasing (decreasing) with above (below) 0.2 %/year and 0.5 %/year, respectively.

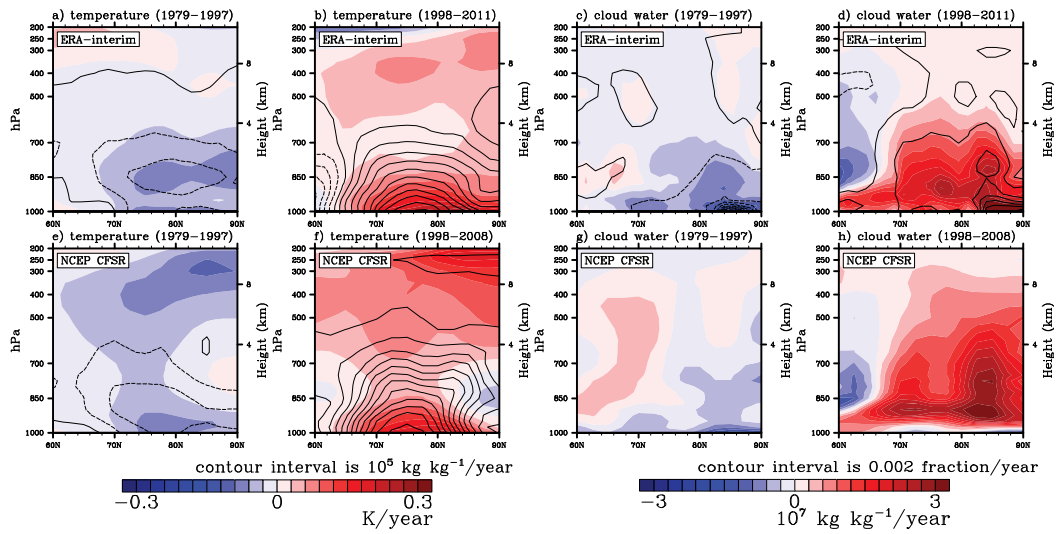


Fig. 4.3 (left panels) changing trends in zonal-averaged winter temperature (shading) and specific humidity (contour) during late 20th century (1979–1997) and early 21st century (1998–present) from the ERA-Interim and NCEP CFSR. (right panels) same as left panels except for cloud water contents (shading) and fractional cloud cover (contour).

northward moisture transport at 67N

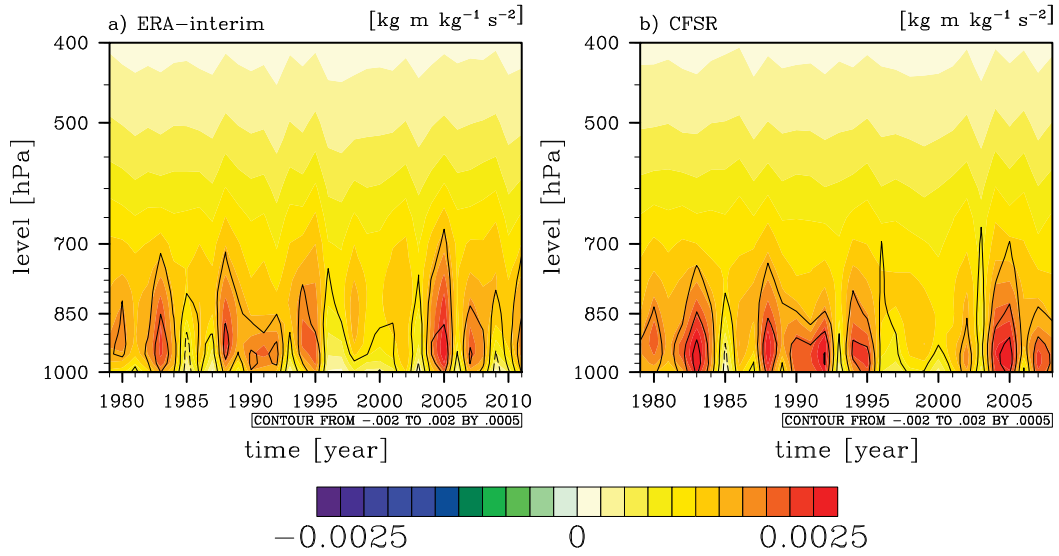


Fig. 4.4 Zonal-averaged total northward moisture transport ($\bar{v}\bar{q} + v'q'$, shading) and northward transport by mean flow ($\bar{v}\bar{q}$, contour) at 67°N.

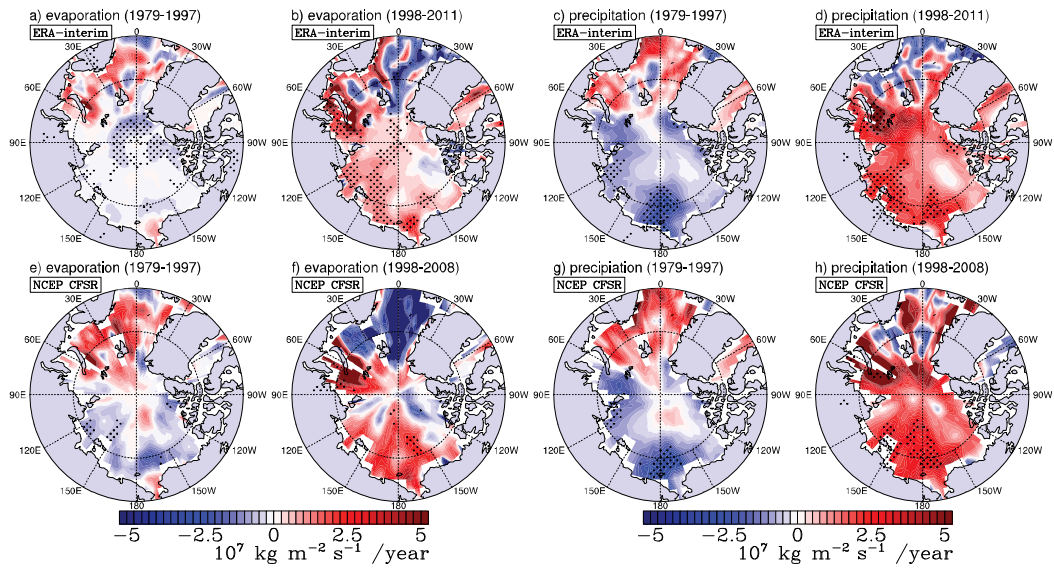


Fig. 4.5 Changing trends in winter evaporation and precipitation during late 20th century (1979–1997) and early 21st century (1998–present) from the ERA-Interim and NCEP CFSR. Stippled region indicates that trend is significant at the 95% confidence level.

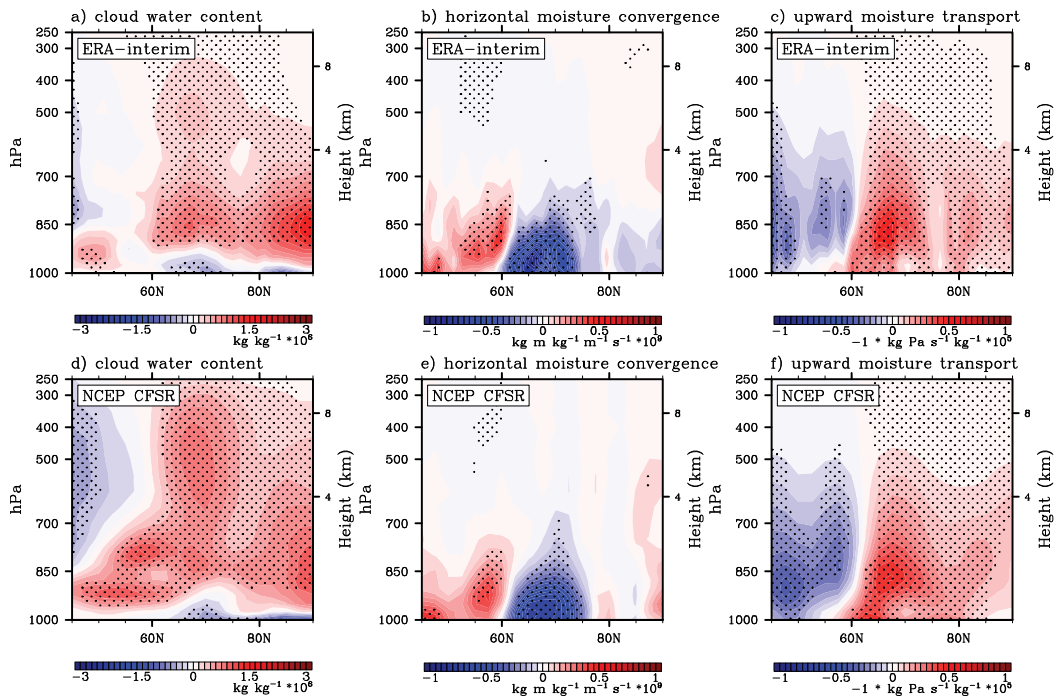


Fig. 4.6 Regressions of the AO index with zonal-averaged (a) cloud water content [10^6 kg kg^{-1}], (b) horizontal moisture convergence [$10^9 \text{ kg kg}^{-1} \text{ s}^{-1}$], and (c) upward moisture transport [$10^5 \text{ kg Pa kg}^{-1} \text{ s}^{-1}$] from the ERA-interim and NCEP CFSR. Stipple regions indicate that values are significant at the 95% confidence level.

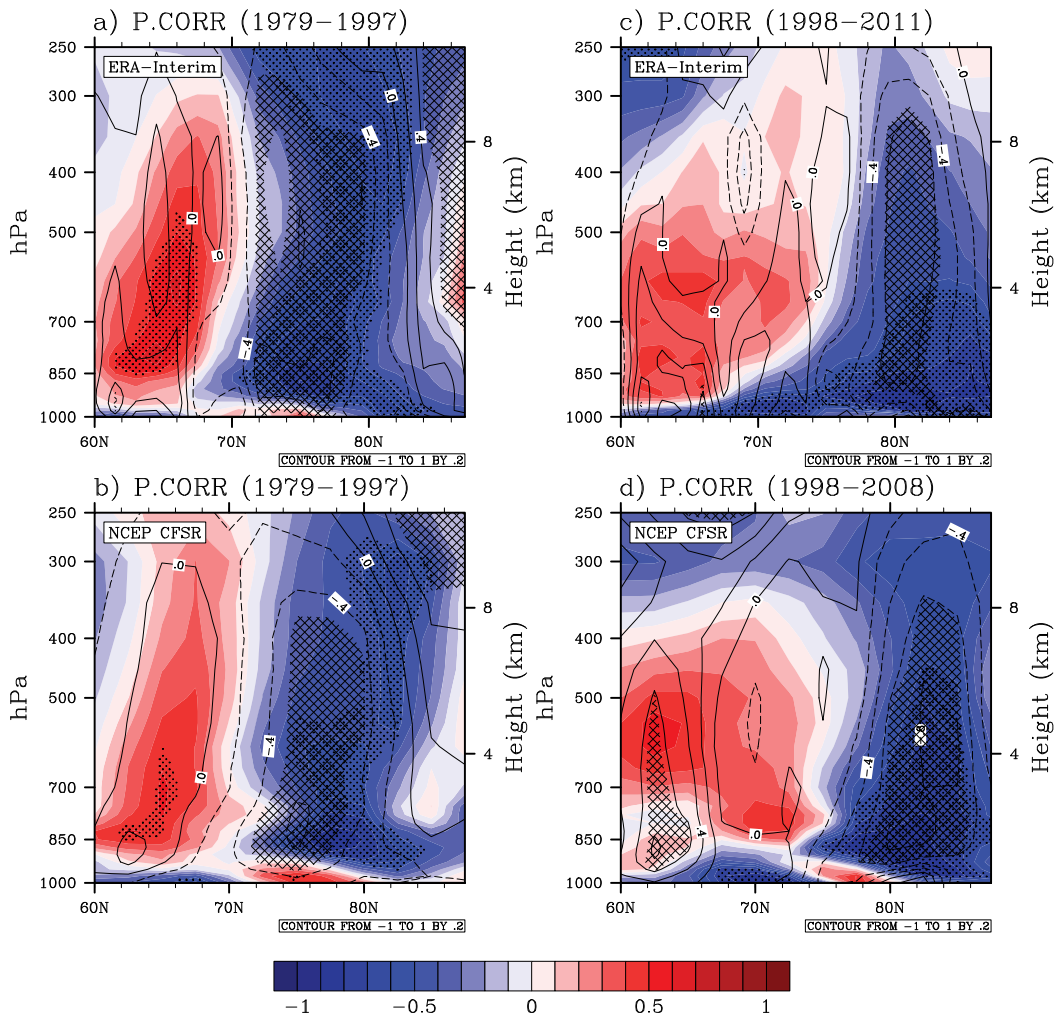


Fig. 4.7 Partial correlations of sea ice cover averaged over the Arctic Ocean (north of 67°N) with zonal-averaged cloud water content (shading) and mean upward moisture transport (contour) independent on the AO index during the late 20th century and the early 21st century from the ERA-interim and NCEP CFSR. Stippled (cross-checked) regions indicate that values with shading (contour) are significant at the 95% confidence level.

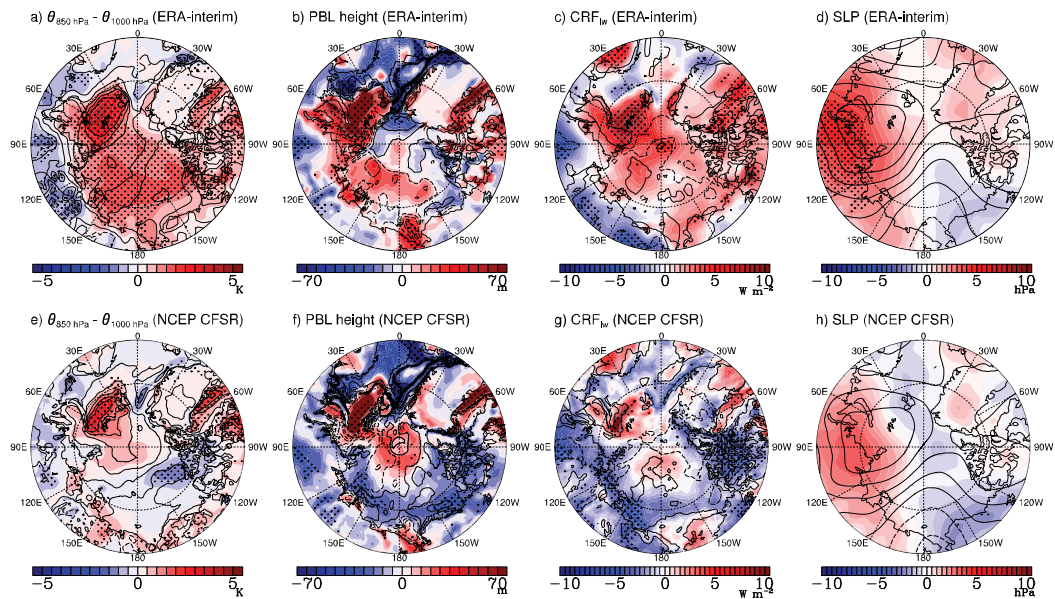


Fig. 4.8 Differences in (a and e) 850 hPa thickness (shading) and surface air temperature (contour), (b and f) PBL height (shading) and sea ice fraction (contour), (c and g) longwave cloud radiative forcing (shading) and cloud amount (contour), and sea level pressure (shading) and 500 hPa geopotential (contour) between averages for the early 21st century and the late 20th century. Stippled region indicates differences in shading values are significant at the 95% confidence level.

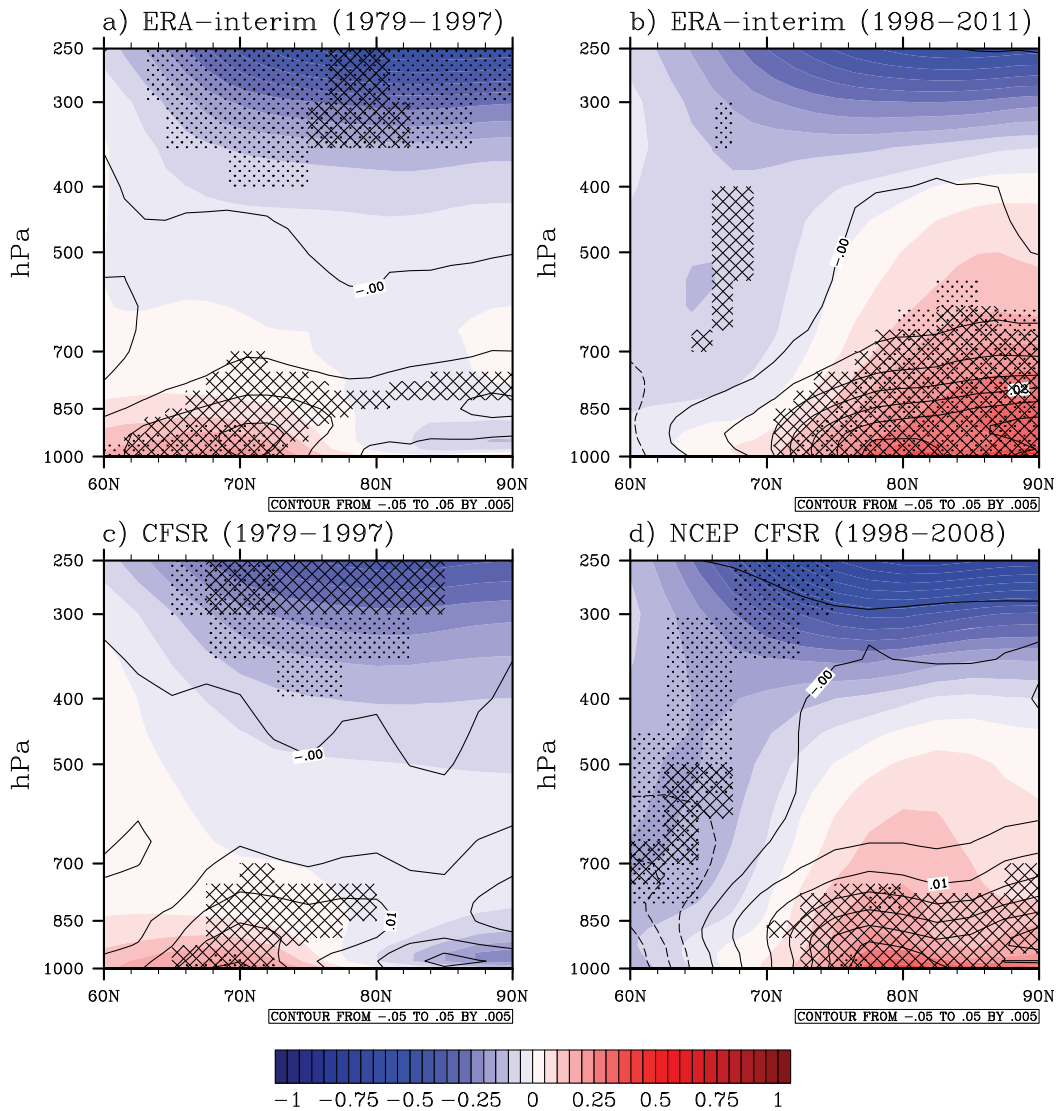


Fig. 4.9 Regression of winter low-level cloud amount [%] averaged over the Arctic Ocean (North of 67°N) with zonally averaged temperature (shading, [K]) and specific humidity (contour, [g kg⁻¹]) during late 20th century (1979 – 1997) and early 21st century (1998 – present) from the ERA-Interim and NCEP CFSR. All trends are removed. Stippled and cross-checked regions indicate that regression is significant at the 95% confidence level.

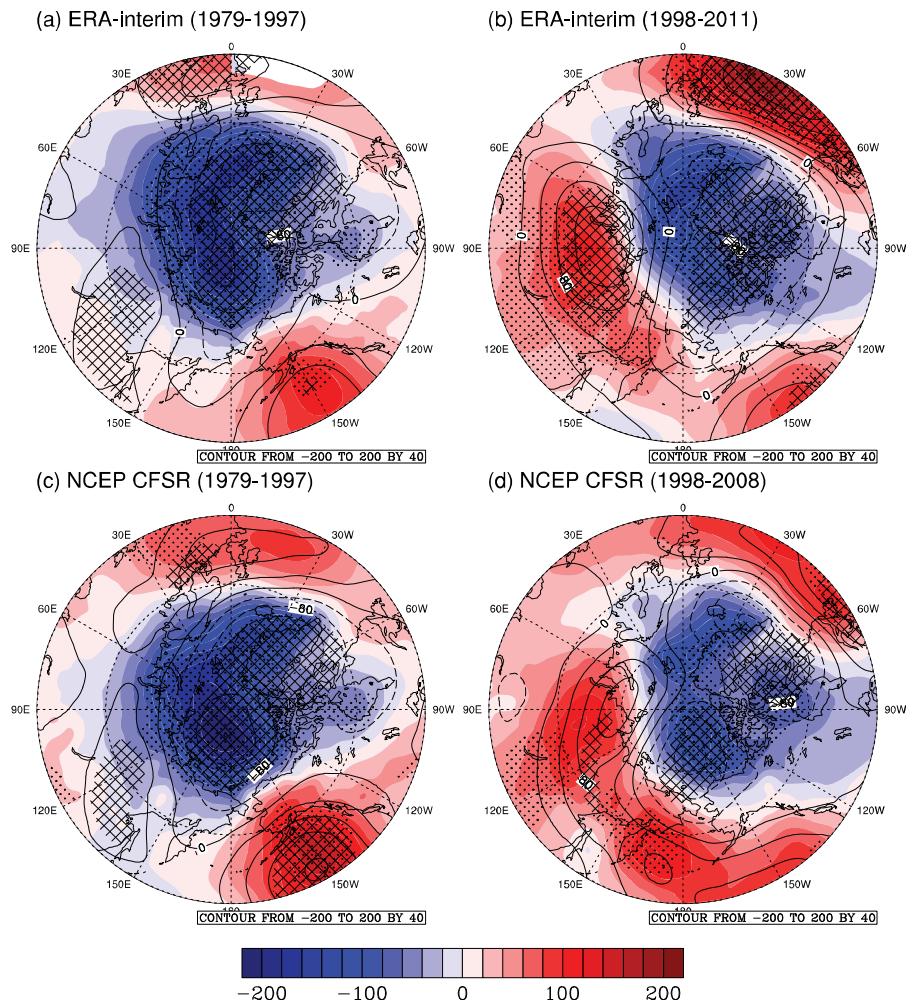


Fig. 4.10 Regression of winter low-level cloud amount averaged over the Arctic Ocean (North of 67°N) with sea level pressure (shading, [hPa]) and geopotential at 500 hPa (contour, [$\text{m}^2 \text{s}^{-2}$]) during the late 20th century (1979 – 1997) and the early 21st century (1998 – present) from the ERA-Interim and NCEP CFSR. All trends are removed in calculation. Stippled and cross-checked regions indicate that regressions are significant at the 95% confidence level.

4.2. Refinement of surface boundary condition for reduced sea ice in AGCM Experiment

A diagnosis on recent cloud change from reanalysis and satellite datasets in previous chapter suggests that surface condition change owing to reduced sea ice cover might play a crucial role on recent changes in cloud and its relation to adjacent atmospheric states over the Arctic during winter. Thus, we attempt to confirm these consequences through modeling work which examines the impact of the areal change in sea ice on the Arctic climate with atmospheric general circulation model (AGCM).

In this modeling, the accurate surface condition according to sea ice change is very important because of the highly sensitive Arctic climate system (Singarayer et al., 2005). The CAM3 uses SST and sea ice fractional coverage as oceanic surface boundary condition, and thus it is demanded evaluating a proper SST distribution according to sea ice change for more accurate surface boundary condition. Therefore, prior to modeling impact of the areal change in sea ice on the Arctic climate, we first examine the sensitivity of SST distribution on the Arctic climate and find proper method to generate the SST distribution according to sea ice change.

4.2.1. Surface condition according to sea ice change for AGCM

Experiment

The change of Arctic sea ice, particularly in the areal extent (i.e., the change of open ocean area occupied by water surface), is known to affect the Arctic and sub-Arctic climate from local temperature change in the Arctic during the boreal winter (Screen and Simmonds, 2010b) to winter weather patterns and large-scale atmospheric circulations over the midlatitudes (Francis et al., 2009; Overland and Wang, 2010). Thus, many previous studies have investigated the impact of Arctic sea ice on large-scale environments over the Northern Hemisphere using AGCMs (Budikova, 2009).

These studies have focused mainly on the atmospheric sensitivity to the changes in sea ice extent. In early 1970s, several studies examined the atmospheric response to a complete removal of Arctic sea ice (Newson, 1973; Warshaw and Rapp, 1973). Murray and Simmonds (1995) performed a perpetual January simulation by gradually reducing sea ice coverage; their results suggest that Arctic sea ice extent is non-linearly related to the changes in the 850 hPa temperature over the Arctic and mid-latitude westerlies. Alexander et al. (2004) correlated large-scale atmospheric teleconnection patterns, such as the Arctic Oscillation/North Atlantic Oscillation (AO/NAO), to anomalous sea ice cover. Deser et al. (2004) investigated an AO/NAO-type atmospheric response to changes in North Atlantic sea ice and sea surface temperature (SST) conditions

based on observations spanning over a 40-year period. Screen et al. (2012) suggested that the response pattern of atmospheric circulation in early winter to sea ice loss in the last three decades resembles the NAO negative phase. This NAO-type atmospheric response is also found in future climate projections under reduced Arctic sea ice conditions (Deser et al., 2010; Seierstad and Bader, 2009).

Arctic atmospheric response to local changes in sea ice conditions is quite sensitive and non-linear (Singarayer et al., 2005). To account for this sensitivity, researchers have been specifying more detailed and observation-based sea ice conditions in AGCM experiments. For instance, both the thickness and fractional coverage of sea ice are used to specify surface boundary conditions (Gerdes, 2006; Rind et al., 1995). Dethloff et al. (2006) achieved a realistic surface air temperature (SAT) simulation for the Arctic using an improved sea ice albedo scheme.

Changes in sea ice concentration (SIC) are a primary factor in driving atmospheric changes by inducing dramatic changes in energy and moisture exchanges between the sea surface and the lower troposphere. Based on this, a number of previous studies have investigated atmospheric responses to altered SIC (Alexander et al., 2004; Magnusdottir et al., 2004; Semmler et al., 2012; Singarayer et al., 2006). Typically, SST in the melted sea ice region (MSR) is estimated by using SST values at the adjacent grids (Alexander et al., 2004) or

by using sea ice surface temperature (Semmler et al., 2012); none of earlier studies use SIC fraction in the estimation of the SST over MSR.

This earlier approach in estimating SSTs in MSR is rather unrealistic and may produce erroneous results. As the sea ice and ocean interact, their changes are always concurrent. For instance, the heat absorbed by the Arctic Ocean when covered with broken sea ice is used in part to melt sea ice and in part to increase SST. Thus, the oceanic area exhibiting significant reduction in SIC is expected to show a significant increase in local SST. Because heat fluxes between two interfaces (i.e., atmosphere and ocean surface) increase the temperature difference between the two interfaces; the increased SST provides more heat and moisture fluxes into the lower troposphere. Hence, accurate determination of local SST in a region where SIC exhibits dramatic decreases is essential for improving the simulations in sea ice model experiments.

This study shows that the atmospheric response associated with sea ice variability depends on SIC, and the response is very sensitive to *in-situ* SST distributions. To isolate the atmospheric response to SSTs in a given SIC change, we compare the results from multiple AGCM simulations generated using various SST conditions in MSR. Model configurations for the sensitivity include: (1) no SST change; (2) SST adjusted by averaging a long-term climatology with a constant value for the lowest ice-free SST; and (3) SST from a statistical fitting

concurrent with the *in-situ* observed SIC. By comparing the three corresponding sensitivity experiments, we have examined the atmospheric responses during the cold season (October through March) and changes in the associated surface-heat fluxes.

4.2.2. Experimental Design

The version used in this study is configured with a finite volume dynamics core having a $4^\circ \times 5^\circ$ horizontal resolution and 26 vertical levels. Previous studies suggested that the sensitivity of the atmospheric response to surface boundary and doubling- CO_2 conditions in the CAM3 version increases with spatial resolution (Hack et al., 2006; Kiehl et al., 2006). Thus, results from this type of experiment using the model can vary according to the spatial resolutions; relatively low resolution used in this study may give results derived from conditions of relatively lower sensitivity.

To assess atmospheric responses to SST changes in MSR, a series of CAM3 experiments have been performed; one baseline and three sensitivity experiments. The baseline experiment prescribes the monthly climatological seasonal cycles of SST and SIC from the National Oceanic and Atmospheric Administration Optimum Interpolation version 2 (OISSTv2) (Reynolds et al., 2002) for 1982–2000. The three sensitivity runs employ the same reduced SIC averaged over

2006–2010, but with different MSR SST conditions. It is noted that, for the period 2006–2010, there is a dramatic decrease in Arctic sea ice extent in winter (Stroeve et al., 2012).

In the three sensitivity experiments, MSR is defined as the region where the time-mean SIC for 2006–2010 is reduced by over 1% compared to that for 1982–2000. Local SSTs are specified over MSR as follows: the first experiment (hereafter CTRL) prescribes the same SST field as in the baseline run in conjunction with the reduced SIC. The second experiment (hereafter CONV) adjusts SST at the MSR grid points using average of the mean climatological SSTs for 1982–2000 and the minimum value of -0.8°C . This method is designed to follow the conventional approach of Alexander et al. (2004) where the SST in grids adjacent to the sea ice is constrained with the average of value of -0.8°C (the lowest ice-free SST) and the warmest climatological SST in adjacent grid boxes. In the third experiment (hereafter POLY), the MSR SSTs are estimated to be more physically associated with the given sea ice reduction using a statistical relationship between SIC and SST over MSR derived from a 3rd-order polynomial regression method.

Figure 4.11 presents a scatter plot of the observed relationship between SST and SIC over the ocean, north of 60°N for the cold seasons (October through March) for the period 1982–2000. In general, regions of larger sea ice cover

show relatively colder SSTs, close to the sea-water freezing point (around -1.8°C); SSTs over areas with small sea ice cover vary widely. White lines in the figure represent a 3rd-degree polynomial fit to the observed data. These polynomials are calculated using data over the regions of $\text{SIC} < 0.9$. SSTs where $\text{SIC} > 0.9$ are excluded as SSTs over such regions are approximately constant (i.e. -1.8°C). These polynomials represent the seasonal variation reasonably in the relationship between the two variables (SST and SIC). This fitting method is currently applied to adjust bias in the Hadley Centre Sea ice and Sea Surface Temperature data (HadISST) using a 2nd-degree polynomial to estimate SSTs over MSR where SST observations are absent (Rayner et al., 2003). In our POLY experiment, SSTs over MSR are specified based on the third-degree polynomial fits; the SST corresponding to the given SIC from the fitting line is chosen as the SST over MSR. Table 4.3 presents the polynomial fitting coefficients between the two variables in the POLY experiment during the cold season.

The baseline and three sensitivity experiments have been run for 250 years by prescribing the annual cycles of SST- and SIC fields corresponding to each experiment as described above. In this study, we focused on the cold season responses when the atmospheric local response to an altered boundary condition is known to be strongest (Screen and Simmonds, 2010b; Screen et al., 2012). Table 4.4 summarizes the monthly-mean values of SST and SIC during the cold

season, averaged over the Arctic Ocean to the north of 67°N in all experiments. As expected, among the sensitivity experiments, POLY had mean values of SST for 2006–2010 that are closest to those obtained by the OISSTv2 product. The mean SST in CONV in October is considerably colder than in POLY; the colder SSTs in CONV affects values in autumn and December, perhaps because the method used in CONV is originally designed to model atmospheric response during December-January-February (Alexander et al., 2004).

Figure 4.12 shows the SIC differences between the sensitivity and baseline experiments (contour in all panels). Also shown are the SST differences in CONV (shading, Figs. 4.12b and 4.12f) and POLY (shading, Figs. 4.12c and 4.12g) from CTRL in early winter (October–December) (Figs. 2a–2d) and late winter (January–March) (Figs. 4.12e–h). Note that SSTs in CONV and POLY are explicitly calculated using the local SIC value. For comparison, the SST changes in OISSTv2 between 2006–2010 and 1982–2000 are presented in (Figs. 4.12d and 4.12h for the corresponding periods. In terms of the pattern and amplitude of SST anomalies, results from POLY are most similar to observations. Compared to POLY, CONV has apparently smaller SST increases over most of MSR. In addition, colder SSTs are generally found in the Barents Sea indicating that CONV is unable to capture the SST changes associated with the recent decline in early and late winter (Figs. 4.12b and 4.12f). Previous studies have noted that

SIC changes over the Barents Sea and Kara Sea play a crucial role in modulating large-scale atmospheric circulations (Honda et al., 2009; Petoukhov and Semenov, 2010). Thus, these results imply that using SST values adjusted to the lowest SST in the ice-free region cannot generate proper atmospheric responses because warming over the Barents and Kara Seas is much weaker than the observed. More detailed examination of early winter conditions shows that, over most of the Arctic Ocean, POLY captures the SST increase associated with the SIC decrease better than CONV (Figs. 4.12b and 4.12c). However, warming over the Barents Sea in POLY is overestimated compared to the observation (Figs. 4.12c and 4.12d). In late winter, CONV presents excessive warming over the Kara Sea and Laptev Sea (Figs. 4.12f and 4.12h). In contrast, those for POLY in late winter are closer to the observed SST changes associated with the changes in SIC. Still, a stronger warming tendency appears over the Barents Sea (Figs. 4.12g and 4.12h).

4.2.3. Responses in surface air temperature and heat fluxes

We first compare the CTRL with the baseline results to examine the SAT response related solely with changing sea ice conditions and fixed climatological SST (Fig. 4.13a). During the cold season, the reduced SIC induces overall warming over the Eurasian margins of the Arctic Ocean and Hudson Bay by

more than 1 K, with particularly strong warming over the Barents Sea of approximately 3 K. This spatial variation in SAT response also appears in CONV and POLY. Compared to CTRL, POLY shows stronger the warming over the Barents Sea; both CONV and POLY show further horizontal expansions of warming to the Eurasian margins (Figs. 4.13b and 4.13c). With the same SIC changes, the mean SAT difference between 2006–2010 and 1982–2000 is estimated from the ERA-Interim. The estimate shows warming > 3 K over major sea ice reduced regions and extreme warming > 6 K over the Barents Sea (Fig. 4.13d). All three experiments yield smaller warming compared to the ERA-Interim data, perhaps due to weaker internal variability since the results obtained in this study is the mean response averaged over much longer period than the averaging period of the ERA-Interim data. In addition, the lack of heat transport from lower latitudes in the three sensitivity experiments can be another reason for this weaker warming because they use the climatological SSTs where SIC does not change.

In Fig. 4.14, we compare SAT responses in CONV and POLY against CTRL. Under the same SIC change, SAT in POLY differs significantly from that in CONV. CONV generates slightly weaker SAT responses compared to CTRL over most of the Arctic Ocean, except for weak warming of about 0.2 K over the Chukchi Sea (Fig. 4.14a), consistently with the prescribed colder SSTs in the

Barents Sea and warmer SSTs in the Chukchi Sea in CONV (Figs. 4.12b and 4.12f). In contrast, POLY generates significant warming of 0.2 K over most of the Arctic Ocean, particularly by as much as 0.4 K over the Barents Sea (Fig. 4.14b). Considering the changes found in the ERA-Interim reanalysis data, POLY appears to simulate SAT response over the Arctic more reasonably, in both intensity and spatial distribution, than CONV. Even though warming in POLY is weaker than the observed, our results suggest that a careful choice of the SST field based on statistical estimation can improve model response. In addition, the relatively weaker warming found in the experiments, even in POLY, emphasizes that heat transport from lower latitudes is a major cause of Arctic warming (Chung and Räisänen, 2011; Graversen et al., 2008).

Screen and Simmonds (2010b) showed that, during the cold season, recent Arctic warming is largely associated with enhanced surface heat fluxes over the region of reduced sea ice. Here, we examine the changes in surface heat fluxes associated with SST distributions that might be closely associated with SAT responses. CAM3 formulates surface fluxes in the sea ice covered region as follows (Collins et al., 2004),

$$F_{LWUP} = \varepsilon\sigma_{sb}T_s^4 - (1 - \varepsilon)F_{LWDN} \quad (4.1)$$

$$F_{SW} = \rho_a c_a r_h u^* (T_s - \theta_a) \quad (4.2)$$

$$F_{LH} = \rho_a (L_i + L_v) r_e u^* (\bar{q} - q_a) \quad (4.3)$$

where, the upwelling longwave flux is F_{LWUP} ; sensible heat flux is F_{SH} ; latent heat flux is F_{LH} ; downwelling longwave flux is F_{LWDN} ; longwave emissivity is ε ; Stefan-Boltzmann constant is σ_{sb} , specific heat of air is c_a , exchange coefficients for sensible and latent heat are r_h and r_e , respectively; and latent heat of fusion of ice and vaporization are L_i and L_v , respectively. At the lowest model layer, the air density is ρ_a ; potential temperature is θ_a ; and specific humidity q_a . At the surface, the temperature is T_s ; friction velocity is u^* ; and saturation specific humidity is \bar{q}^* . In the equations, all surface fluxes are defined to be positive in upward direction.

When the ocean surface previously occupied by sea ice becomes warmer, MSR experiences a significant increase in surface fluxes. In Fig. 4.15, all of the SIC change experiments show a consistent increase in surface fluxes over MSR (see contours in the figure). Net longwave flux ($F_{LWUP} + F_{LWDN}$) increases over the Barents Sea, Laptev Sea, and East Siberian Sea; these regions also experience large increases in sensible (F_{SH}) and latent (F_{LH}) heat fluxes. In particular, a large reduction in sea ice over the Barents Sea leads to increases in both sensible and latent heat fluxes. Elsewhere, in the inner-Arctic, especially over the northeast of Greenland and Queen Elizabeth Islands, the sea ice expanded region undergoes a conspicuous decrease in sensible heat flux of more than 1 W m^{-2} . This occurs in all three experiments (contour in the Figs. 4.15b and 4.15e) due mainly to the

cold surface temperatures over the sea ice expanded region which are colder than in the baseline experiment.

In CONV and POLY, warmer SSTs increase the outgoing longwave flux as well as the sensible and latent heat fluxes. Compared to CTRL, POLY shows significant and larger increases in surface fluxes over most MSRs (Figs. 4.15d–f) than CONV (Figs. 4.15a–c). These increases in surface fluxes in POLY are roughly proportional to the reduction of sea ice because fluxes increase most over the Barents Sea and north of the Chukchi Sea and considerably less elsewhere. In particular, increases in the surface fluxes over the Barents Sea were above 3 W m^{-2} . These changes over MSR in POLY are significant at the 95% confidence level.

The SAT responses obtained in the three experiments are well explained by increases in surface flux changes. Surface flux changes might have different monthly variations due to diverse dependencies of the fluxes on the seasonal evolution of SST. Because longwave flux increases in proportion to the fourth power of SST, as indicated by Eq. (4.1), an increase in longwave flux becomes larger in early winter than in late winter because the early winter has a considerably warmer SST value. In Fig. 4.16a, changes in net longwave flux are largest over the Arctic Ocean, exceeding 3.6 W m^{-2} , and represent warmer SST conditions in October. In November, all experiments show a stronger longwave

flux, 2 W m^{-2} more than in the baseline experiment. Afterwards, the net longwave flux changes become much weaker as the Arctic becomes colder. Thus, differences among all methods are nearly zero in February and March; the impact of longwave flux is concentrated in the two months, October and November.

Changes in sensible heat flux for all experiments remain in a similar range of $1\text{--}2 \text{ W m}^{-2}$ in every month, except for October; the change is relatively small in October compared to the changes in other cold months (Fig. 4.16b). In Eq. (4.2), sensible heat flux mainly depends on the difference between the potential temperature at the lowest atmospheric level and the surface temperature. The temperature differences in all experiments closely match observed sensible heat fluxes during all cold months. These differences are smallest in October, although SST anomalies in all experiments are largest in October compared to the baseline experiment.

Among experiments, the sensible heat flux in POLY is consistently larger than that in CTRL during the whole cold season. However, sensible heat flux in CONV is smaller than that in CTRL for several months (Fig. 4.16b). This feature is coupled tightly to the SST change in MSR, especially over the Barents Sea. The SST in POLY bears a more accurate warming signal, corresponding to a reduction in SIC, while SST in MSR CONV is colder than in CTRL for most

periods. This SST difference occurs throughout the entire winter (see Fig. 4.12) and follows the sensible heat flux difference between CONV and CTRL quite well.

Changes in latent heat flux are more sensitive to changes in SST conditions than are other fluxes throughout the cold season in the models. As shown in Eq. (4.3), latent heat flux depends mainly on the difference between specific humidity in the lowest layer and saturated specific humidity at the surface. In the annual cycle, both the specific humidity at the lowest model layer and the saturated specific humidity at the surface have maximum values in July and August. However, saturated specific humidity declines more gradually in association with declines of SIC. Consequently, the latent heat flux over the Arctic peaks in October and declines through the remaining cold season. In addition, because specific humidity in the lowest layer changes least in all three sensitivity experiments, changes in the saturated specific humidity at the surface is more responsible than other factors for increasing latent heat fluxes. Because saturated specific humidity at the surface increases exponentially with SST, different SST distributions in each sensitivity experiments contribute largely to the differences in latent heat fluxes among the sensitivity experiments during the cold season (Fig. 4.16c).

In CTRL, CONV and POLY, changes in fluxes over the Arctic Ocean

average to 1.09, 1.01, and 1.42 W m^{-2} for net longwave flux, 1.32, 1.19, and 1.65 W m^{-2} for sensible heat fluxes, and 1.32, 1.26, and 1.73 W m^{-2} for latent heat fluxes, respectively. Different SST conditions yield changes in all surface fluxes, and latent heat fluxes are most sensitive to SST conditions in the cold season. Among the surface flux differences between POLY and CTRL, those for latent heat fluxes are significant at the 90% confidence level during the entire cold season. The sensible heat fluxes in October, November, and March, and the longwave fluxes in October and March are also significant at the 90% confidence level. In contrast, most differences between CONV and CTRL are not statistically significant. The longwave fluxes in November and January and latent heat flux in October are significant at the 90% confidence level.

4.2.4. Vertical structure of responses in temperature and specific humidity

The changes in surface fluxes related to SST eventually affect the vertical distributions of temperature and humidity, which, in turn, affects the atmospheric response to SIC and SST changes. Figure 4.17 shows the vertical profiles of temperature and specific humidity and their changes among the three experiments during early and late winter. For both periods, vertically extended warming and moistening are commonly found in all three sensitivity experiments. The effects of surface-induced warming and moistening on lower troposphere are

larger with warmer SSTs. CTRL and CONV generate similar magnitudes of warming and moistening near the surface compared to the baseline experiment, and POLY generates warming and moistening greater than the other two experiments. During late winter, CONV also generates lower tropospheric warming greater than CTRL (Fig. 4.17b) with larger surface flux differences (Fig. 4.16).

Near-surface warming in the sea ice reduced experiments is linked mainly to longwave radiation and sensible heat fluxes. First, longwave radiation flux from the surface is greater in MSR (Figs. 4.15a and 4.15d) and possibly warms the lower troposphere if the atmosphere absorbs the longwave flux. Over the Arctic, this effect of longwave flux can be stronger near the surface because of the abundance of longwave-absorbing low-cloud cover that reemits longwave radiation to the surface during the cold season (Curry et al., 1996). Figures 4.18a and 4.18d show longwave radiative heating at troposphere based on the SST change: CTRL generates larger longwave radiative heating over the Arctic region than baseline experiment (contour). CONV induces rather cooling compared to CTRL, and POLY induces weaker warming than CTRL (shade). Meanwhile, the difference in longwave radiative heating at lower troposphere between CONV (POLY) and CTRL is relatively weak compared to heating by other processes (Fig. 4.18). This may have been caused by seasonal variations in the Arctic

longwave radiation; longwave radiative heating in lower troposphere is effective only during early winter due to extremely cold conditions at the near surface during middle and late winters (Fig. 4.16a). In addition, longwave radiative heating in the lower troposphere does not represent the only effect of longwave emissions at the surface. Because it presents the difference in longwave radiative heating in equilibrium state, longwave radiative heating results from the total effects of factors that contribute to the temperature change in the lower troposphere. Thus, the effect of change in longwave radiation at surface could be underestimated in Figs. 4.18a and 4.18d.

Turbulent heat diffusion in lower troposphere below 850 hPa over 70°–80°N suggests that changes in sensible heat fluxes mainly contribute to the near-surface warming (Figs. 4.18b and 4.18e). CTRL induces greater diffusive heating in the lower troposphere than the baseline experiment. CONV generates greater diffusive heating than CTRL, and POLY generates even greater heating than CONV. In particular, diffusive heating effects associated with different SST conditions appear to induce stronger lower atmospheric warming, as compared to the effects from longwave radiation. The difference in sensible heat flux among our experiments became larger during late winter (Fig. 4.16b) and it appears that the different vertical temperature profiles between early and late winter, especially shown in the difference between CTRL and CONV, might be

influenced by sensible heat flux (Figs. 4.17a and 4.17b).

POLY simulates cooling near the surface and heating in the troposphere by moist processes that is the largest and most significant among experiments (Fig. 4.18f). In particular, tropospheric heating via moist processes over MSR (70–80°N) in POLY reaches around the 500 hPa level, much higher when compared to the altitude in CONV (Fig. 4.18c). This vertical extension of heating by moist processes should be affected by the strengthened vertical moisture transport such as shallow convection. Large increases in the surface fluxes and associated warming and moistening induces a decrease in static stability and thickening of the planetary boundary layer. The decrease in static stability occurs through an enhanced vertical mixing of heat and moisture that, consequently, contributes to warming and moistening in the mid-troposphere. This destabilization effect associated with the increase in surface fluxes has been suggested by observational relationships between an increase in mid-level cloud cover and a decrease in SIC during early winter (Schweiger et al., 2008).

In addition to affecting vertical propagation, warmer SST conditions over MSR can spread warming and moistening further into the mid-latitudes, even under the same sea ice condition. Figure 4.19 shows a vertical cross-section of changes in the zonal-averaged temperature (shade) and specific humidity (contours) during early and late winter for each method. It also shows

observational changes. As SST becomes warmer from CTRL to POLY, warming reaches a high altitude and spreads farther south to mid-latitudes, with a corresponding change in specific humidity. In particular, the SST condition in POLY leads to warming and moistening even to the mid-latitudes as south as 45°N (Figs. 4.19c and 4.19g). According to ERA-Interim, warming and moistening over the high latitudes, particularly amplified warming and moistening over the Arctic, occur between the cold seasons for 2006–2010 and 1982–2000 (Figs. 4.19d and 4.19h). Therefore, the strong warming and moistening over the Northern Hemisphere in POLY, are closest to the recent observed changes in the Arctic and high-latitude regions. In particular, among the experiments, POLY simulates well the vertically and horizontally expanded warming during both early and late winters as captured in ERA-Interim data (Figs. 4.19c and 4.19g). It has been suggested that these changes in the lower troposphere is linked closely with recent drastic sea ice melt (Screen and Simmonds, 2010a); the present results support this linkage.

4.2.5. Discussion

Sensitivity of atmospheric warming in response to the SST for reduced SIC in the Arctic Ocean has been examined. It has been found that temperature and moisture responses in the lower troposphere over the Arctic are sensitive to even a small amount of SST changes under the same sea ice condition. Warmer SSTs

generate substantially stronger warming near the surface, which expands vertically and horizontally compared to colder SST conditions with the same SIC. Surface heat fluxes play crucial roles in shaping these different atmospheric responses. Longwave radiation and sensible and latent heat fluxes perceptively respond to different SST conditions. Averaged over the entire cold season, latent and sensible heat fluxes are more responsible for altered atmospheric responses than longwave radiation. In particular, distribution of atmospheric heating into diffusive and condensational processes implies that sensible heat fluxes affect near-surface warming, and latent heat fluxes affect the warming in the mid-troposphere above 800 hPa. Static stability is decreased, and the air-column expands vertically due to warming and moistening in the lower troposphere.

This study suggests that the SST field in POLY may be most suitable for examining the effect of sea ice change on the climate over the Arctic and surrounding regions as the results in POLY compares most closely with observations based on recent observational changes and in terms of larger impact on the atmosphere, vertically and horizontally. Thus, the SST adjusting methodology used in POLY can be recommended for examining the effect of sea ice condition changes, including realistic and artificial changes. Meanwhile, because a part of SSTs used in the ERA-Interim is adjusted with sea ice concentration, a similarity between result from POLY and the ERA-Interim may

come from adjusting method. This suggests that present modeling result should be handled more carefully.

To address the validity of the polynomial fitting method more clearly, we have conducted additional experiments using observed and prescribed SSTs and comparing results with POLY (Fig. 4.20). For comparison, two different SST conditions, HadISST and OISSTv2, have been used over MSR. Comparison of the mean atmospheric surface air temperature response to the SST difference for the two periods (2006–2010 versus 1982–2000) against HadISST, POLY can capture qualitatively similar features, supporting the use of the polynomial fitting method (Figs. 4.20a–b). Rather unexpectedly, the SAT response from OISSTv2 is significantly different than that from HadISST (Figs. 4.20b–c). These results show that atmospheric circulation responses sensitively to small SST changes in the Arctic Ocean. It is also noted that the quality of SST observations over MSR is poor in both products and also is subjected to statistical fitting using slightly different methods (Appendix B in Rayner et al. (2003)).

The polynomial fitting method can be more useful for studies that do not use observed SST data, e.g., examining certain sea ice melting trends on the paleo- or future climates. To examine the usability of the POLY method for future climate projection studies, we have applied our polynomial fitting coefficients to 14 model results from future experiments of RCP 4.5 scenarios in

CMIP5. We have generated SST conditions by applying the polynomial coefficients to SIC differences between 2051–2055 and 2006–2010, and compared the generated SSTs with simulated SSTs (Fig. 4.21). As shown in the figure, the polynomial fitting method successfully reproduces the simulated SST distribution well in the sea ice retreated region. The method also well captures the SST warming pattern in most of these models, although the estimated SST is slightly warmer than the simulated ones. Among the models, the estimation method gives the best match for GFDL-CM3, GFDL-ESM2G, MIROC5, MRI-CGCM3, and NorESM1-M.

Warming and moistening responses in troposphere in our study, even in POLY, are still weaker than the observed (see Fig. 4.19), basically due to the difference in internal variability based on the differences in the averaging periods for the observed and simulated records. Nevertheless, this can occur if recent tropospheric warming and moistening over the Arctic is induced by additional factors other than sea ice retreat. For example, heat and moisture can be transported from the lower latitudes to the Arctic by atmospheric and oceanic circulations that also contribute to Arctic warming and moistening (Alexeev et al., 2005; Chung and Räisänen, 2011; Graversen et al., 2008). Perhaps, given the weak responses obtained in this study compared to observations, contributions from other factors are larger. This situation can be explored in additional

experiments using the observed global SST conditions for 2006–2010, which can replicate well the recent vertical warming structure that extends to the upper troposphere. This result also implies that there can be another important factor, in addition to melting sea ice, which contributes to the recently observed tropospheric warming over the Arctic. The SST condition over middle or lower latitudes can be one such factor.

Table 4.3 The 3rd polynomial fitting coefficients for the relationship between SST and sea ice fraction for each month during the cold season.

	Oct	Nov	Dec	Jan	Feb	Mar
a	1.4573	1.1727	1.4012	1.3413	1.1103	1.1486
b	-4.248	-4.716	-4.5208	-3.7716	-3.1089	-3.3505
c	3.3636	5.7375	6.0431	5.4956	4.3157	4.2713
d	-2.626	-4.278	-5.1979	-5.4454	-4.6410	-4.3526

* $y = \mathbf{a} + \mathbf{b}x + \mathbf{c}x^2 + \mathbf{d}x^3 + \varepsilon$ where x and y are sea ice (fraction) and SST ($^{\circ}\text{C}$), respectively, and ε is residual.

Table 4.4 Summary of surface conditions of experiments in this study.

Experiment	Sea ice	SST	SST averaged over the Arctic Ocean (north of 67°N, °C)						
			OC T	NO V	DEC	JAN	FEB	MA R	OND JFM
Baseline	averaged annual cycle for 1982–2000	averaged annual cycle for 1982–2000	0.10	-0.65	-0.89	-1.01	-1.08	-1.08	-0.77
CTRL		same as baseline	0.10	-0.65	-0.89	-1.01	-1.08	-1.08	-0.77
CONV	averaged annual cycle for 2006–2010	adjusted to average of climatology for 1982–2000 and -0.8°C	0.10	-0.56	-0.82	-0.93	-1.00	-1.01	-0.70
POLY		adjusted to the 3rd degree polynomial fitted SST where sea ice fraction is melted to below 0.9	0.47	-0.50	-0.80	-0.92	-1.01	-1.02	-0.63
*2006–2010	averaged annual cycle for 2006–2010	averaged annual cycle for 2006–2010	0.38	-0.49	-0.78	-0.88	-0.97	-1.03	-0.63

*only for comparison

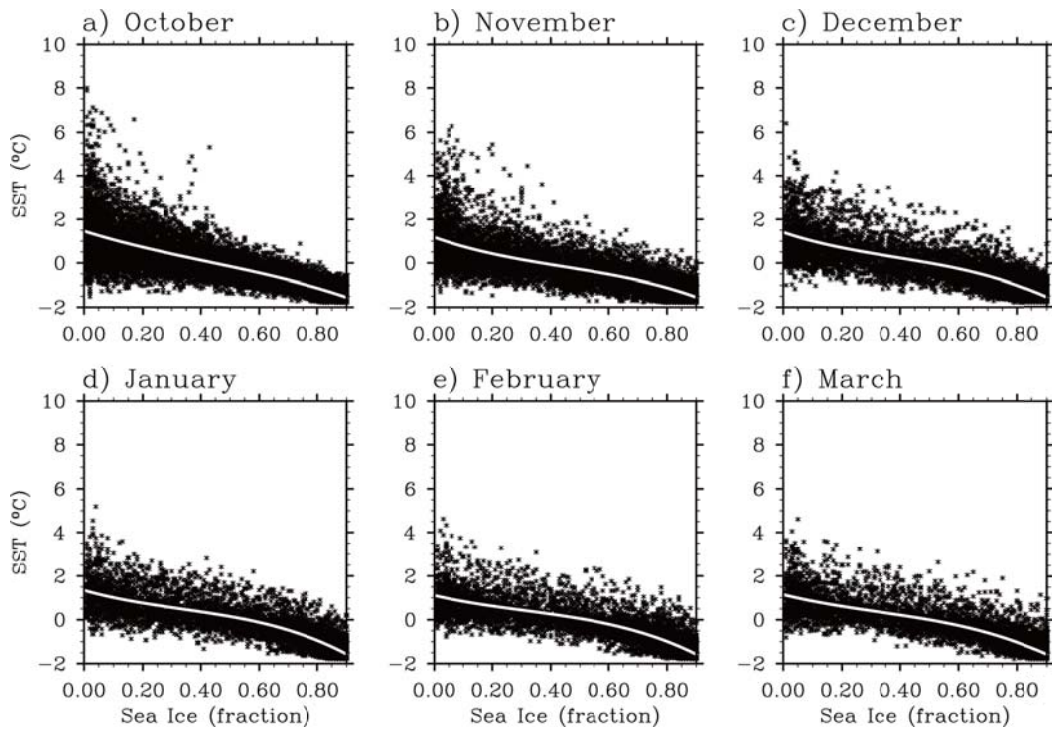
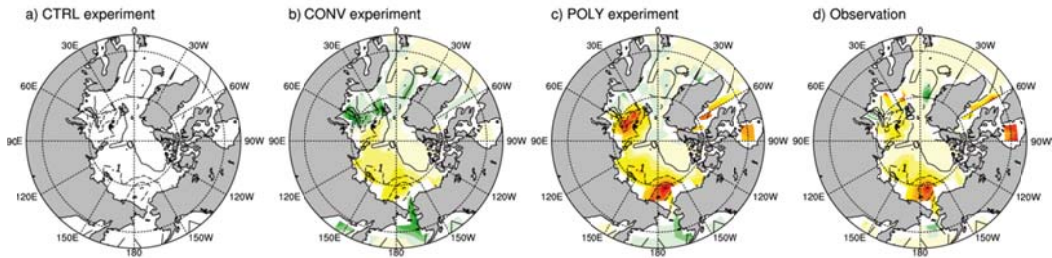


Fig. 4.11 Scatter plot between sea ice concentration (SIC; fraction) and sea surface temperature (SST) over the Arctic (north of 60°N) for the cold season (October through March) of the period 1982–2000 from OISST v2. White lines indicate the third-degree polynomial fitting between SIC below 0.9 fraction and SST, in each month.

Early winter (October–November–December)



Late Winter (January–February–March)

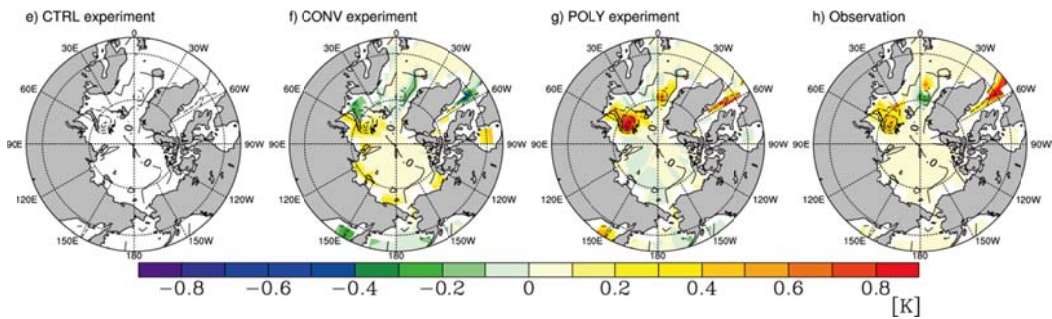


Fig. 4.12 Differences of sea surface temperature (shade) and sea ice concentration (contour) boundary conditions from (a and e) CTRL, (b and f) CONV, and (c and g) POLY experiments compared to the baseline experiment during early winter (October–November–December) and late winter (January–February–March); (d and h) Differences between mean sea surface temperature during early and late winters for 2006–2010 and 1982–2000 from the OISST v2. Differences are plotted only over the region where sea ice reduced above 0.01 fraction. In all panels, the contour interval is 0.1 fraction.

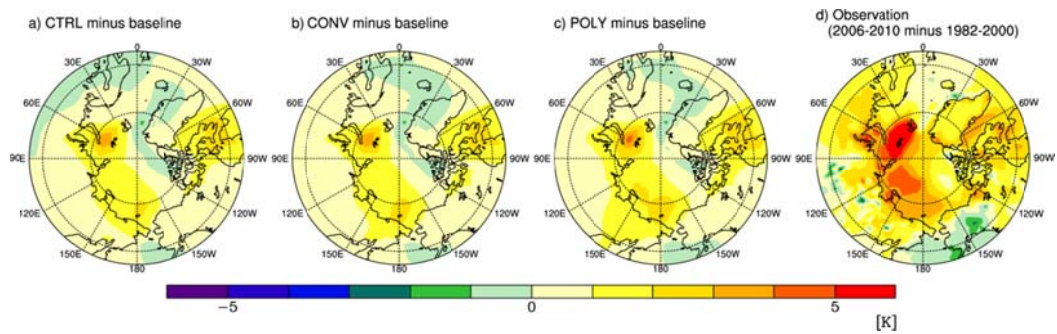


Fig. 4.13 Change in surface air temperature from (a) CTRL, (b) CONV, (c) POLY compared to the baseline experiment during the cold season, and (d) 2 m air temperature difference between 2006–2010 and 1982–2000 during the cold season from the ERA-Interim data.

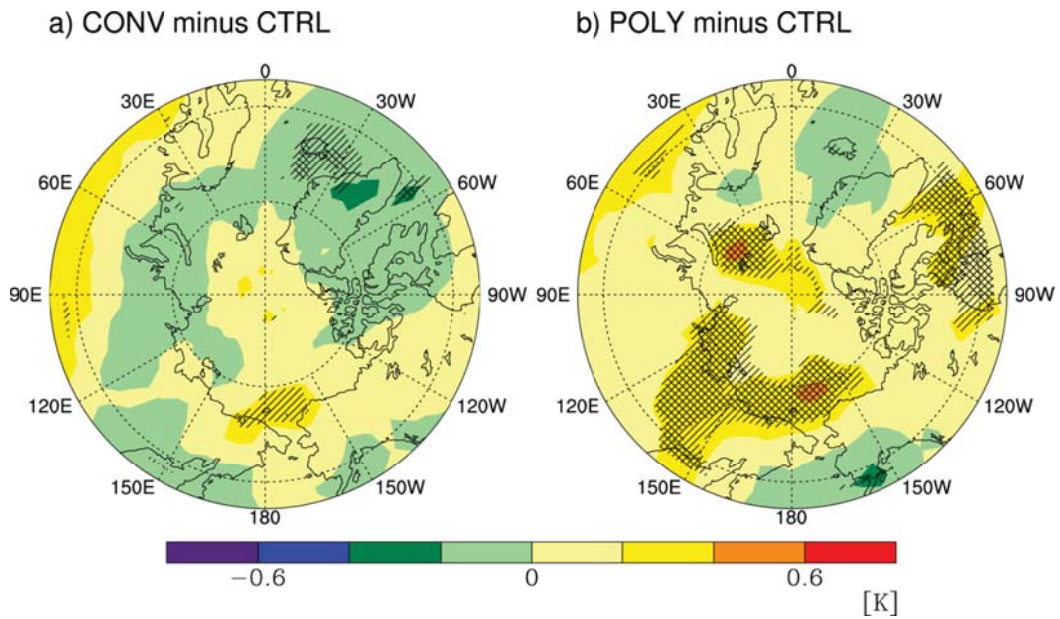


Fig. 4.14 Change in surface air temperature from (a) CONV and (b) POLY compared to CTRL experiment during the cold season. Oblique and cross regions indicate that surface air temperature response is significant at the 90% and 95% confidence level, respectively.

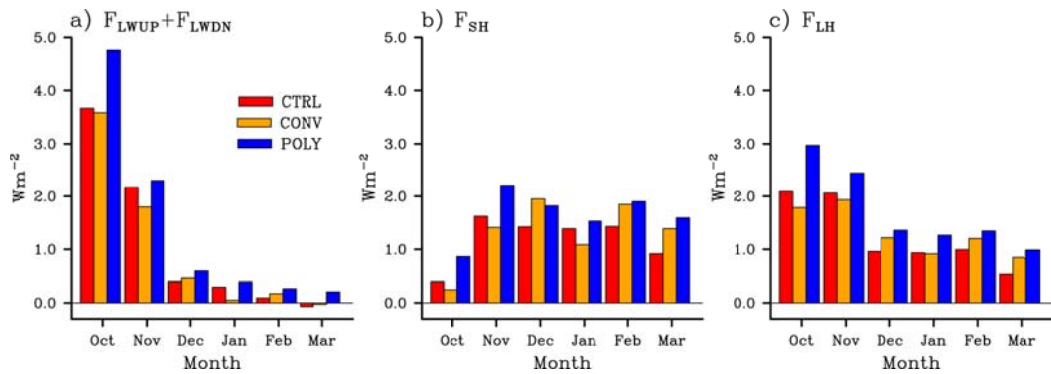


Fig. 4.16 Monthly changes in (a) net longwave flux (positive in the upward direction), (b) sensible heat flux, and (c) latent heat flux averaged over the Arctic Ocean (north of 67°N) from CTRL, CONV, and POLY experiments compared to the baseline experiment.

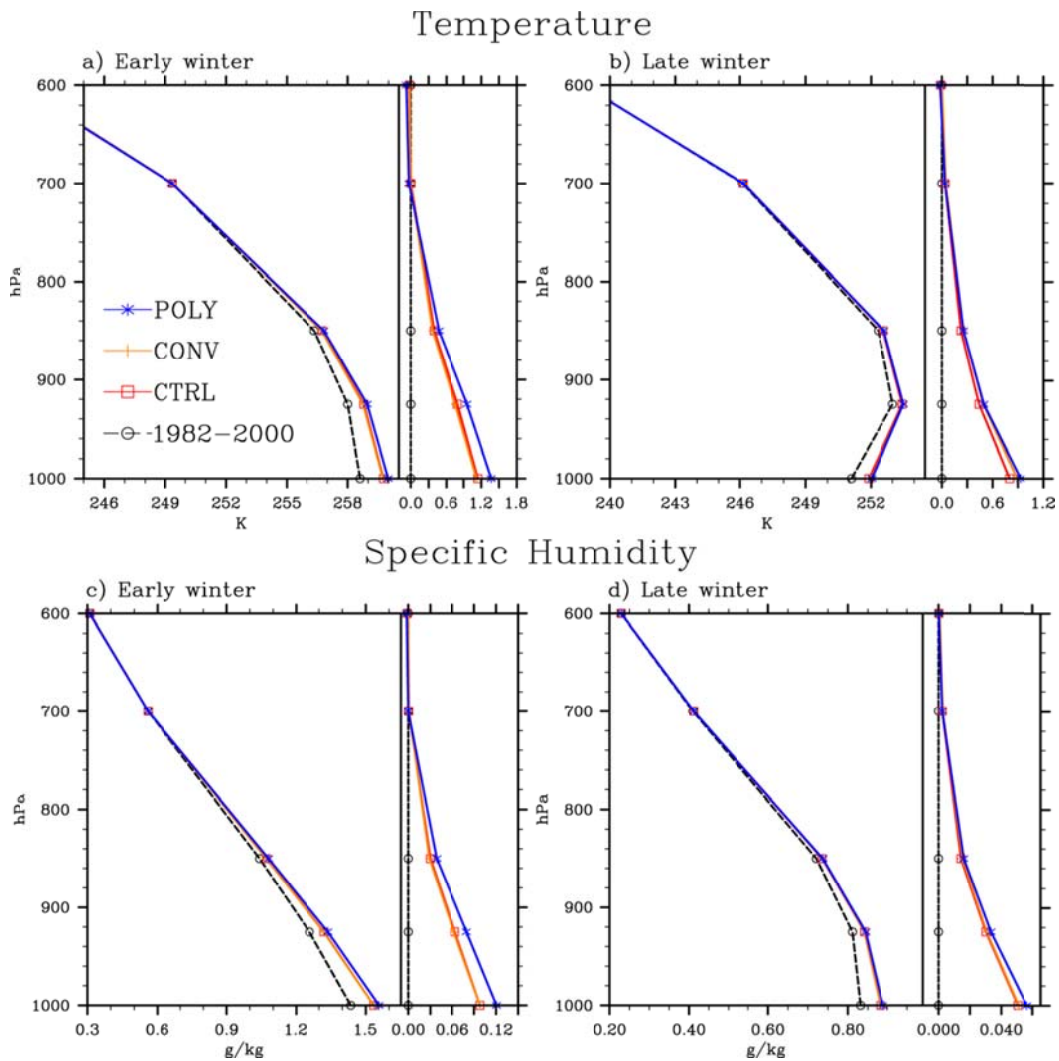


Fig. 4.17 Vertical profiles in temperature and specific humidity averaged over the Arctic Ocean (north of 67°N) in the baseline, CTRL, CONV, and POLY experiments during early and later winter (left panel) and their differences to the baseline experiment (right panel).

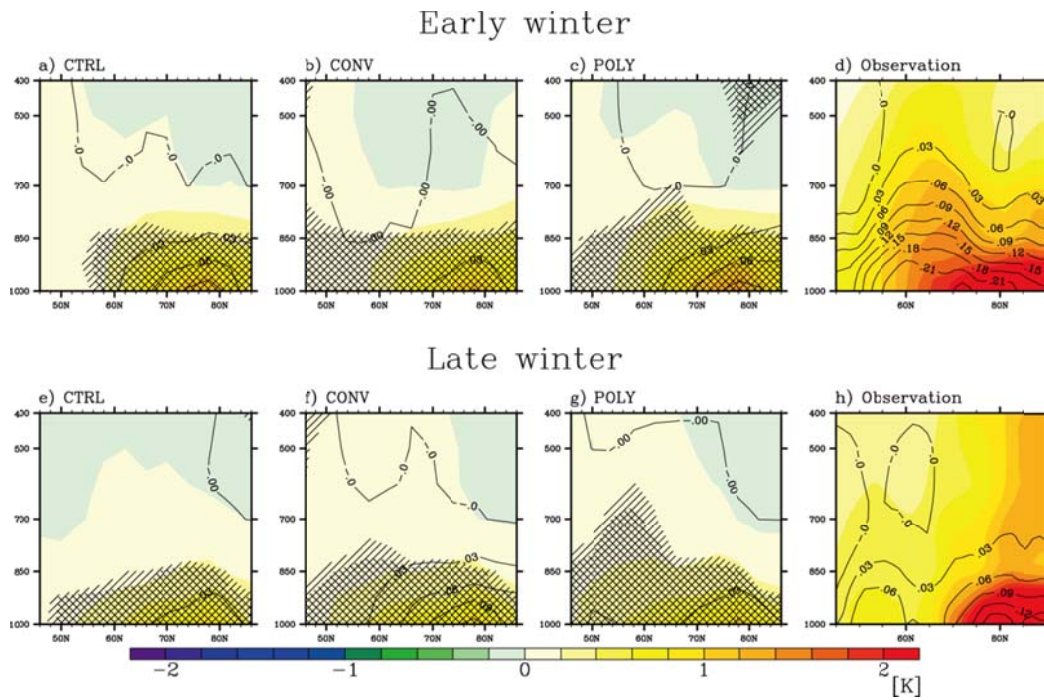


Fig. 4.19 Changes in zonal-averaged temperature (shade) and specific humidity (contour) during early winter (October–November–December) and late winter (January–February–March) from CTRL, CONV, and POLY experiments compared to the baseline experiment. Oblique and cross regions indicate that surface fluxes are significant at the 90% and 95% confidence level, respectively; (d and h) changes in the same variables for the periods 2006–2010 and 1982–2000 from the ERA-Interim data. Contour interval is 0.03 g kg^{-1} .

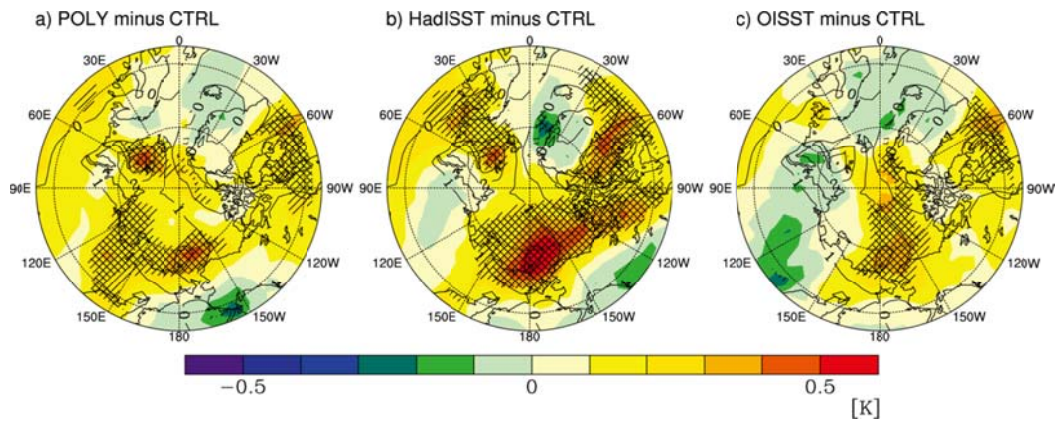


Fig. 4.20 Change in surface air temperature from CTRL compared to the baseline experiment (contour), and changes in (a) POLY, (b) HadISST over the MSR, and (c) OISSTv2 over the MSR compared to CTRL (shade) during the cold season. Contour interval is 0.5 K. Oblique and cross regions indicate that surface air temperature response is significant at the 90% and 95% confidence level, respectively.

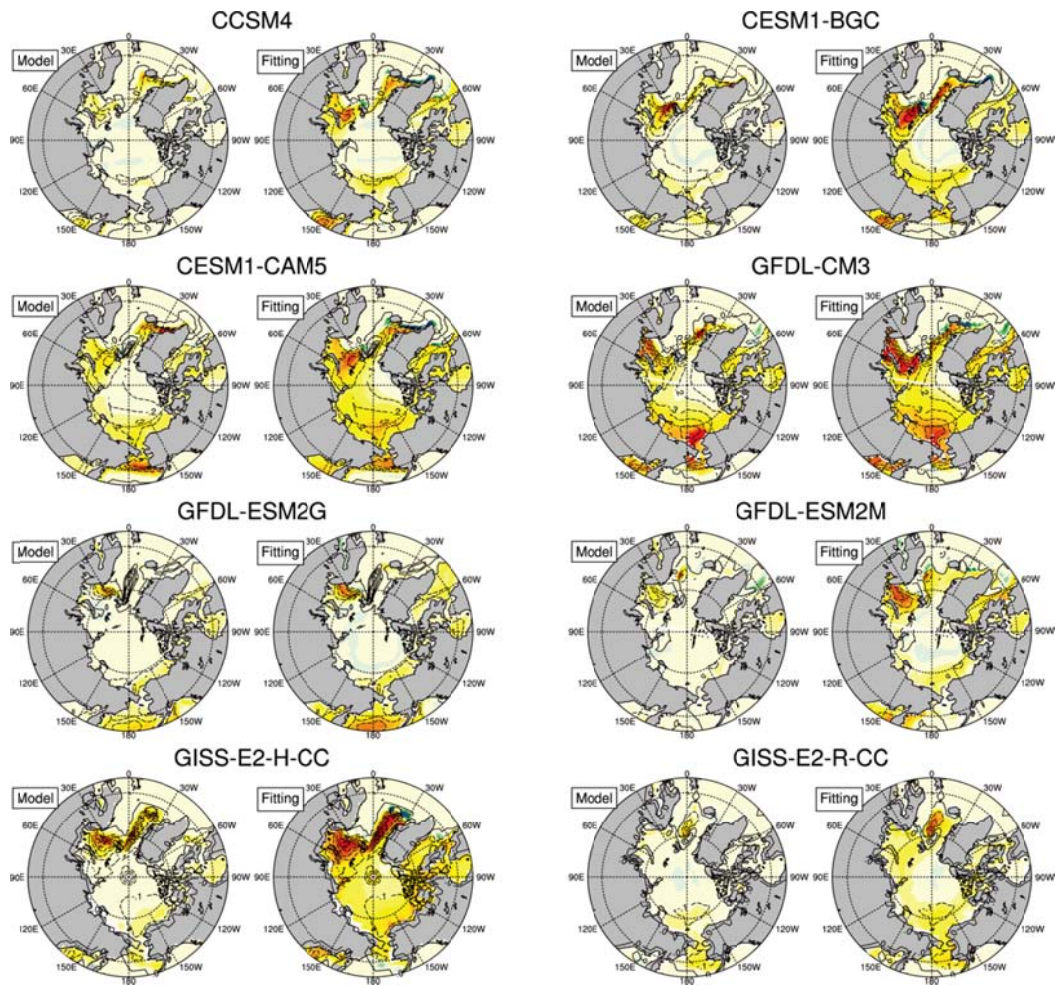


Fig. 4.21 Comparisons between simulated SST (model; left figure in each panel) and adjusted SST by polynomial fitting with SIC change (fitting; right figure in each panel) among 14 model results with future experiment of the RCP4.5 scenario in the fifth phase of the Climate Model Intercomparison Project. Model differences are calculated with simulated SSTs averaged for 2051–2055 and simulated SSTs averaged for 2006–2010. Fitting differences are calculated with fitted SSTs by using polynomial coefficients in the POLY method, SIC values averaged for 2051–2055 and simulated SSTs averaged for

2006–2010. Shading indicates sea surface temperature, and contour indicates sea ice concentration with an interval of 0.1.

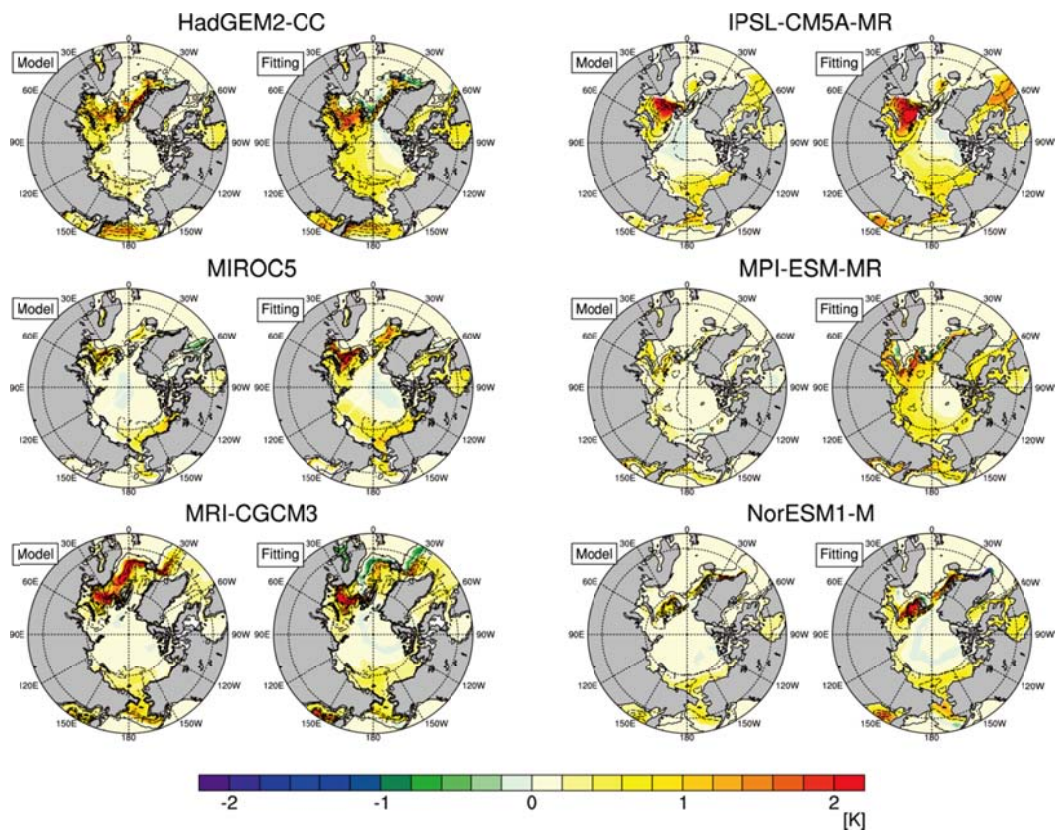


Fig. 4.21. (continued)

4.3. Modeling the change in cloud and its effect in relation to sea ice

As mentioned earlier, much of GCMs have difficulty in simulating cloud amount in the Arctic region (Jones et al., 2004; Vavrus and Waliser, 2008; Vavrus et al., 2009; Walsh et al., 2005), thereby displaying a large discrepancy in total cloud amount among models, particularly during winter (Karlsson and Svensson, 2011). Jones et al. (2004) has indicated climate models commonly produce excessive wintertime Arctic clouds, particularly at low levels, an error attributed to an insufficient treatment of cloud processes unique to polar region. It is known that the CAM3 also produce excessive low level cloud over the Arctic during cold season (Vavrus and Waliser, 2008). Since the focus of modeling work is cloud change in relation to sea ice, we adopt modified cloud amount parameterization into our modeling the impact of reduced sea ice on the recent Arctic climate change.

4.3.1. FREEZEDRY cloud amount parameterization

For improving parameterization of the Arctic low cloud, Vavrus and Waliser (2008) suggests the “FREEZEDRY” parameterization, which is designed to alleviate the bias of excessive low clouds during polar winter by reducing the cloud amount under very dry conditions. The CAM3 uses three types of cloud amount parameterizations: convective cloud, marine-stratus cloud, and layered

cloud. In these, layered cloud amount parameterization is used for low-level cloud in winter Arctic. Current layered cloud fraction in the CAM3 is function of relative humidity as follow:

$$f = \left[\frac{(RH - RH_{MIN})}{(1 - RH_{MIN})} \right]^2 \quad (4.4)$$

However this type of formula is not well suited for high latitudes, particularly the extremely cold and dry atmospheric conditions typical of polar winter. Thompson and Pollard (1995) suggests that reducing the relative humidity-derived low cloud fraction (f) when the gridbox mean specific humidity (q) falls below a threshold value (0.003 kg kg^{-1}):

$$f = f \times \left[\max(0.15, \min\left(1.0, \frac{q}{0.003}\right)) \right] \quad (4.5)$$

Thus, the originally calculated cloud fraction is only adjusted under very dry atmospheric conditions, in which case the low cloud amount is reduced by as much as 85% of its relative humidity-based value. Figure 4.22 presents relative humidity, layered cloud fraction in original CAM3, and layered cloud fraction by FREEZEDRY parameterization under varying temperature and specific humidity. Relative humidity is calculated with equation by Magnus approximation based on the Clausius-Clapeyron relationship. Figure 4.22a indicates that air becomes

supersaturated easily by less moisture under extremely cold condition. Thus, the CAM3 simulated excessively large amount in Arctic cloud in these condition (Fig. 4.22b). The FREEZEDRY modification, in meeting its own purpose, generates less cloud amount than original CAM3 under dry and cold conditions (Fig. 4.22c). Vavrus and Waliser (2008) performed simulation by using CCSM3 adopted the FREEZEDRY parameterization, and gained enhanced result with reduced polar low cloud in similar with observations.

We also perform 50 years test simulations with the original CAM3 and modified with FREEZEDRY parameterization in order to check whether adaptation has been done correctly and confirm the performance of FREEZEDRY parameterization. Figure 4.23 describes spatial distributions of low level cloud amount during winter from simulations with original cloud amount parameterization and FREEZEDRY parameterization. The FREEZEDRY parameterization successfully reduces a large amount of low level cloud over the Arctic and continents at high latitudes where are cold and dry during winter.

In addition, FREEZEDRY parameterization has another effect besides its own purpose that removes excessive cloud amount. In most extremely cold and dry region (below about 260 K and 3 g/kg), the original CAM3 always generates almost maximum cloud amount (Fig. 4.22b). In contrast, in this region, FREEZEDRY parameterization generates changed cloud amount by gradually

reduced with specific humidity (Fig. 4.22c). This effect could generate stronger relationship between temperature and cloud. In original CAM3, cloud amount has few or no response to temperature change during winter. It always generates almost maximum cloud under cold and dry condition during winter. However, in the FREEZEDRY parameterization, temperature change could bring change in cloud amount as well. Thus, tropospheric warming could be linked to increases in winter cloud. The FREEZEDRY modified cloud amount parameterization is currently adopted in recent fourth and fifth versions of CAM (Neale et al., 2012; Neale et al., 2011).

4.3.2. Response over the Arctic on reduced sea ice cover in AGCM

Experiment

To examine whether sea ice retreat is a key factor for changes in cloud and its relationship to environmental atmospheric states during recent decade, we perform AGCM experiments with sea ice retreat condition. We perform two 50 year experiments configured with a finite volume core having a 2x2.5 horizontal resolution; baseline and sensitivity experiments. For more realistic cloud amount simulation, we adopt the FREEZEDRY cloud amount parameterization for the cloud. The baseline experiment (hereinafter SIC_CTRL) uses monthly climatological SST and sea ice concentration from the OISSTv2 for 1982–2000,

and under CO₂ concentration of 369 ppmv. Sensitivity experiment (hereinafter SIC_REDUCE) is performed for same 50 year to examine effects of recent sea ice retreat. The SIC_REDUCE experiment prescribes reduced sea ice condition in the Arctic averaged over 2006–2010, with SST condition adjusted befittingly with reduced sea ice concentration by method suggested in earlier chapter.

First, modeling result shows that surface air temperature, PBL height, total cloud amount, longwave CRF increase mainly over the sea ice retreated region in SIC_REDUCE experiment compared to SIC_CTRL experiment. The Barents, Kara, Chukchi Seas, where sea ice reduces largely, induce large increases in these variables (Fig. 4.24). These changes related to sea ice retreat between experiments are consistent to differences between E21C and L20C in reanalyses (Fig. 4.8). In addition, atmospheric pressure system also resembles differences in reanalyses; high pressure system develops across the Eurasian side of the Arctic Ocean and Eurasia continent (Fig. 4.24c).

In addition, sea ice retreat induces tropospheric warming and moistening over the Arctic region during winter (Fig. 4.25a). Reduced sea ice is sufficient to increase temperature and specific humidity even under same CO₂ concentration with SIC_CTRL experiment. This might be because surface condition change by sea ice retreat supplies sufficient heat and moisture to troposphere by turbulent and radiative fluxes during cold season (Jun et al., 2013; Screen and Simmonds,

2010b). We examine the effect of change in turbulent heat fluxes due to sea ice retreat on atmosphere through atmospheric heating by diffusion and moistening process among experiments (Figure 4.25b). The diffusive heating over the sea ice retreated region (65–80°N) warms air at near surface, with particularly strong diffusive heating at around 80°N where sea ice cover reduces largely. In contrast, heating by moistening process cools air at near surface and warms air above cooling region. It is found that warming region by moistening becomes higher where sea ice cover reduced more (around 80°N). This indicates that evaporation and convection can occur more frequently over the sea ice retreat region, and convection over more opened ocean can be deeper. Namely, sea ice retreat leads to increase in PBL height and decrease in static stability at near surface by diffusive heating, and this could help frequency and strength of convection to be increased.

SIC_REDUCE experiment shows that an increase in cloud amount occurs over most Arctic regions with larger increasing, and its spatial distribution resembles heating distribution by moistening process (see contour in Fig. 4.25c). The region where strong condensation (heating by moistening) occurs also shows clearly the increasing in cloud amount. This result supports recent increasing in cloud above 900 hPa in both reanalyses. Meanwhile, the disparity between changes in cloud amount and moistening process is a larger increase in

cloud amount over the central Arctic region. Over this region, climatological temperature is extremely low, and increasing in moisture is relatively larger than increasing in temperature (Fig. 4.25a). This leads to large increasing in relative humidity, thus cloud can be more formed easily at this region.

The stronger increasing over the central Arctic region is also found in the change in relationship between low level cloud and zonal-averaged temperature. The relationship becomes stronger over the most Arctic region (north of 60°N), and the relationship becomes much stronger over the central Arctic compared to SIC_CTRL experiment (sea shading in Fig. 4.25c). In reanalyses, the enhancement in relationship between cloud and temperature over the central Arctic becomes stronger during the E21C (Fig. 4.9). Modeling results from sensitivity experiments well reproduce the relationship change over the Arctic during the E21C, and this suggests that sea ice retreat could induce the increasing in cloud amount and the enhancement of the effect of cloud on the Arctic climate in winter.

4.3.3. Discussion

Modeling result strongly suggests that recent changes in cloud and atmospheric state over the Arctic are associated with sea ice retreat. In AGCM experiments, reduced sea ice cover leads to an increasing in surface fluxes, a

decrease in lower-tropospheric static stability, and deepening of planetary boundary layer as seen in the Arctic surface during recent decade. Consequently, cloud in most Arctic troposphere increases according to reduced sea ice. In particular, modeling result also suggests that convection could be deeper where sea ice reduces more largely even during winter. Eventually, an increasing in cloud reinforces the CRF and precipitation over the Arctic, and, the local relationship between cloud at lower troposphere and atmospheric states, in turn, also becomes strengthened.

Modeling result in this study differs from prior modeling work in Vavrus et al. (2011a). Vavrus et al. (2011a) investigated cloud change in the case of rapid sea ice decline from CCSM3 future climate simulation. Their result presents that winter cloud decreases during rapid sea ice loss. Although major decreasing occurs in mid and high level cloud, low level cloud also decreases. In contrast, modeling result in this study shows the increasing in cloud under sea ice reduced condition. The difference between two modeling results is mainly due to cloud amount parameterization in each model. Both studies use same CAM3 for simulating atmosphere, but we utilize the modified cloud amount parameterization which is designed to reduce exceeded cloud amount at low level. This might produce different cloud response to sea ice retreat.

Meanwhile, much of modeling results predict that the Arctic warming under

global warming accompanies an increasing in winter Arctic cloud. Most climate models and their ensemble mean values in the CMIP3 predict that cloud increases during winter in future climate simulation (Vavrus et al., 2009). In future experiment from the CMIP5, most climate models also predict that cloud increases and its relationship to SAT is also closer during winter (Figs. 4.26 and 4.27). Most models and their ensemble mean from the CMIP5 predict that strong surface warming emerges over the Arctic during winter in future (RCP4.5 experiment) compared to present climate (PIcontrol experiment). Additionally, cloud amount also increases during cold season with the strongest increasing in November. Similarly to our experimental results, sensible and latent heat fluxes also increase largely during winter, and this may play an important role for increasing cloud (Fig. 4.26). In addition, longwave CRF increases largely during winter (Fig. 4.26c), and relationship between cloud and surface also becomes closer in future climate (Fig. 4.27).

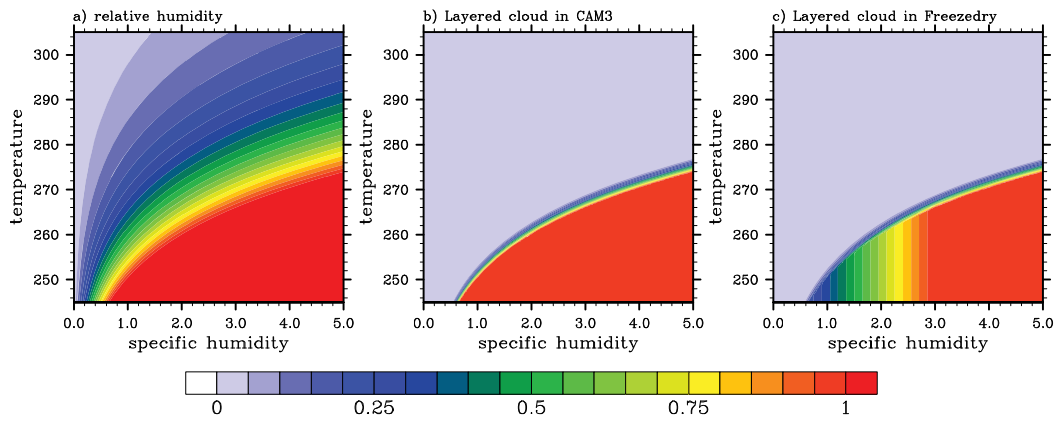


Fig. 4.22 (a) relative humidity, (b) layered cloud amount by cloud amount parameterization in CAM3, and (c) layered cloud amount by FREEZEDRY modified parameterization under varying in temperature and specific humidity.

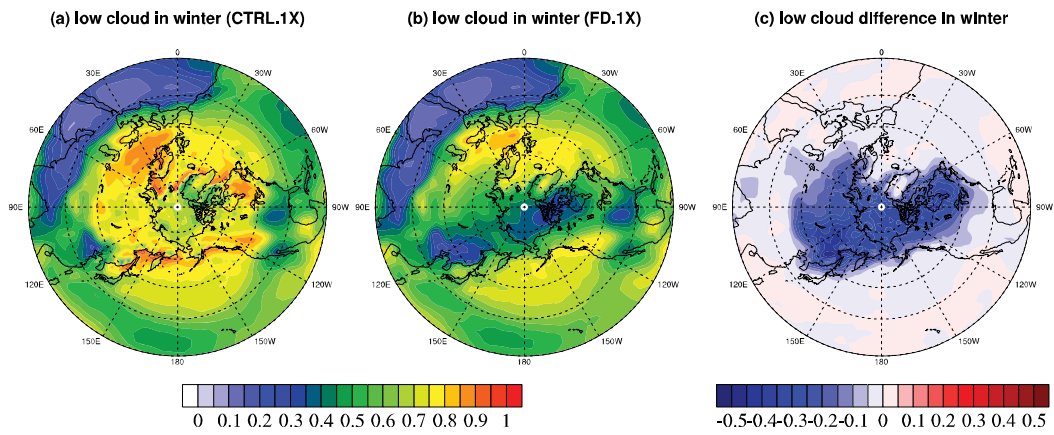


Fig. 4.23 Low level cloud amount during winter from (a) CAM3 original cloud amount parameterization, (b) FREEZEDRY cloud amount parameterization, and (c) their difference.

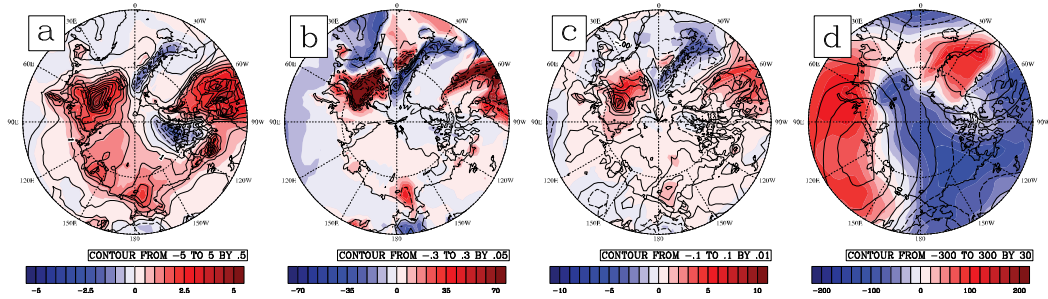


Fig. 4.24 Changes in (a) surface air temperature (contour) and 850 hPa thickness (shading), (b) sea ice cover (contour) and planetary boundary layer height (shading), (b) total cloud amount (contour) and longwave cloud radiative forcing (shading), and (c) 500 hPa geopotential (contour) and sea level pressure (shading) from SIC experiment compared to CTRL experiment.

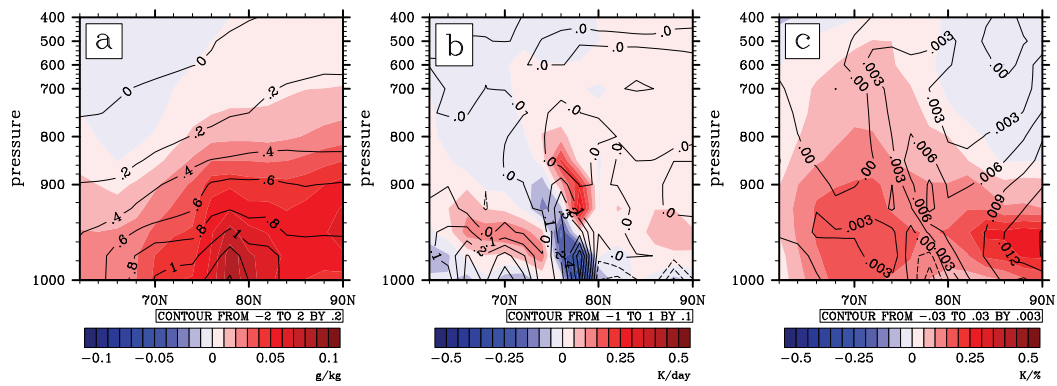


Fig. 4.25 Changes in (a) zonal-averaged temperature (contour) and specific humidity (shading), (b) heating by diffusion (contour) and moistening process (shading), and (c) cloud amount (contour) and regressed temperature of low-level cloud amount over the Arctic (shading) from SIC experiment compared to CTRL experiment.

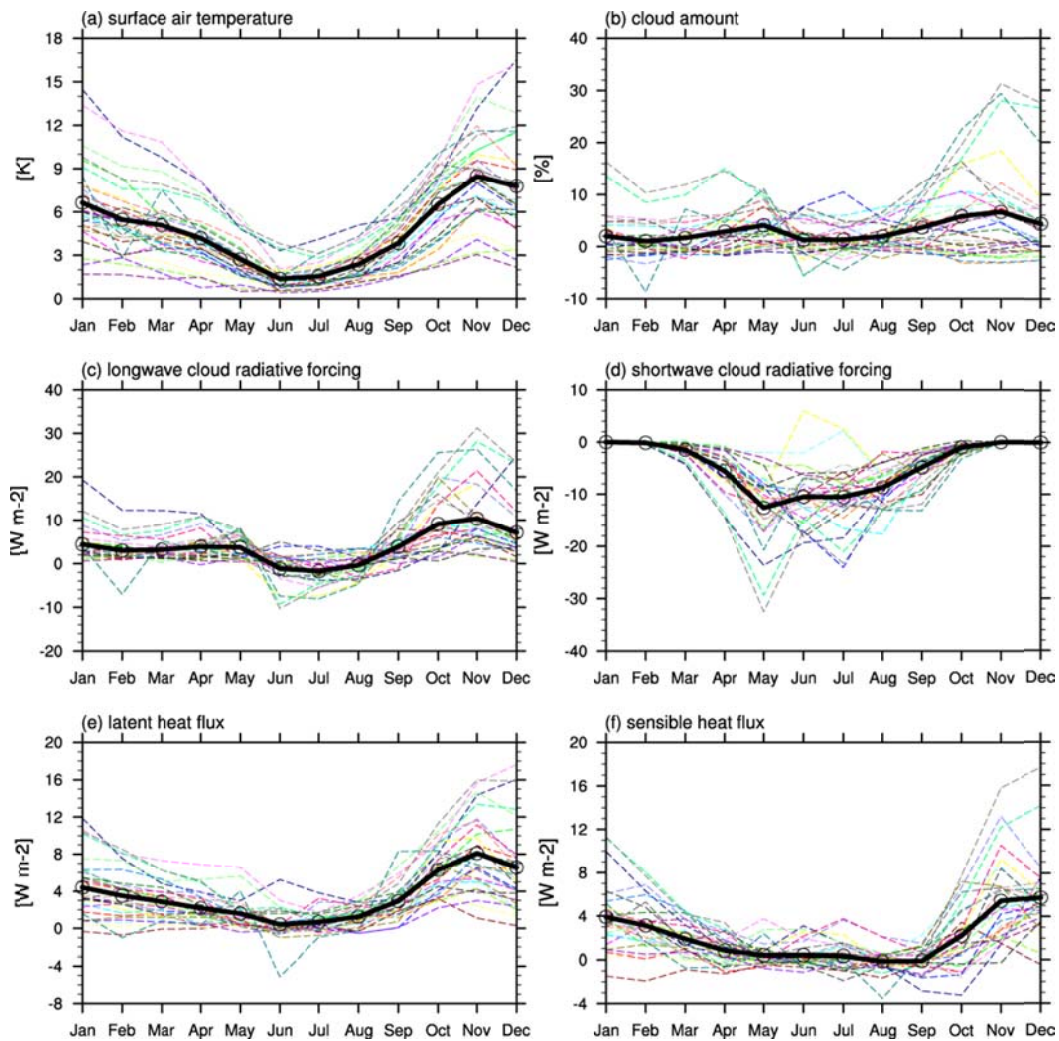


Fig. 4.26 Annual cycles of changes in (a) surface air temperature, (b) cloud amount, (c) longwave cloud radiative forcing, (d) shortwave cloud radiative forcing, (e) latent heat flux, and (f) sensible heat flux averaged over the Arctic (north of 70°N) between RCP4.5 and P1ctrl experiments from climate models in the CMIP5. Solid thick lines in each figure indicate their ensemble mean values.

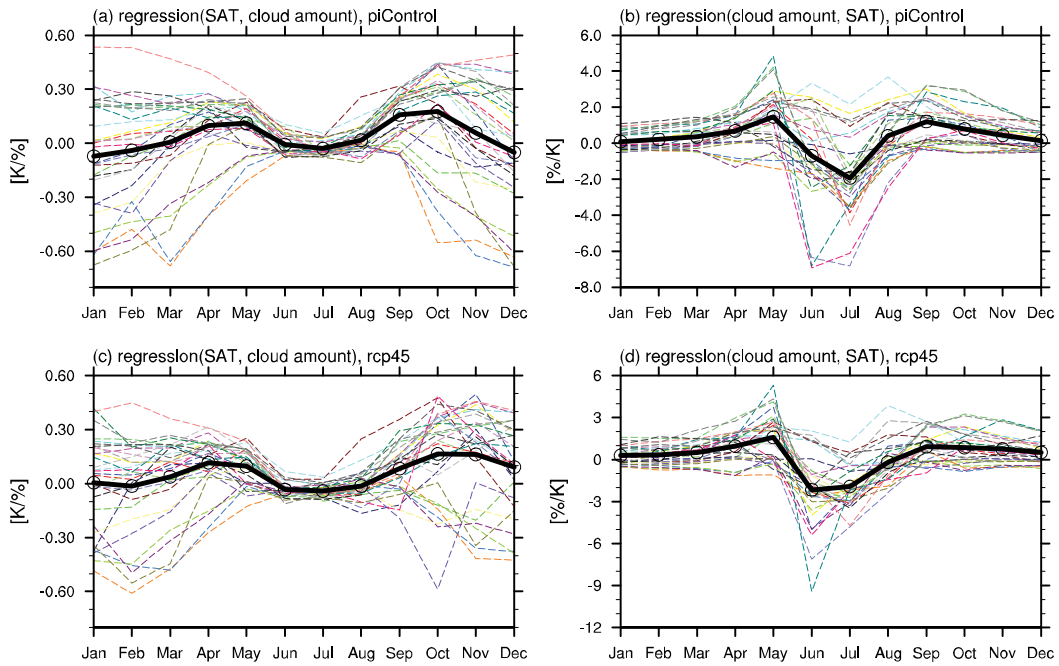


Fig. 4.27 Annual cycles of regressions of (a) cloud amount onto surface air temperature, and (b) surface air temperature onto cloud amount averaged over the Arctic (north of 70°N) from PIctrl experiment, and (c) cloud amount onto surface air temperature, and (d) surface air temperature onto cloud amount from RCP4.5 experiment in the CMIP5. Solid thick lines indicate their ensemble mean values.

5. SUMMARY AND DISCUSSION

The Arctic has experienced substantial warming in recent decades of which degree and rate is much larger than global averages. This phenomenon, which is also widely predicted from future climate modeling for several climate change assessment reports of the Intergovernmental Panels for Climate Change, is called as the Arctic amplification. Various climate factors on the globe could contribute to the amplified warming over the Arctic because of the highly sensitive Arctic climate system and the northward transport into the high latitude region. Much of understanding for these contributing factors come from modeling study because of lack of observation datasets owing to severe weather and climate conditions of the Arctic. In particular, less consideration of climate factors such as vegetation, cloud, and sea ice in modeling could bring large uncertainties in understanding the Arctic climate. Thus present thesis examines the contributions of vegetation and cloud to the Arctic amplification through modeling work with adopting a global dynamic vegetation model (DGVM) and improving physical processes related to sea ice and cloud.

First, modeling result from simulating the Community Climate System Model 3 (CCSM3) coupled with a DGVM indicates that potential vegetation change under a doubled CO₂ situation and its feedback have an influence on

surface warming over the Arctic/high-latitude region. This dissertation performed two baseline experiments under the present and doubling CO₂ concentration using the CCSM3-DGVM. Then, an additional simulation without DGVM was performed under doubling CO₂ concentration with the prescribed vegetation taken from the present CO₂ simulation. Model experiments indicate that a vegetation change in high-latitudes may induces substantial alternation of climate change in the Arctic/high-latitude during warm and cold seasons. When the interactive vegetation process is included in the future climate simulation, the warming in high-latitude continent appears to be significantly amplified. Furthermore, and the Arctic sea ice exhibits considerable decline both in areal extent and thickness associated with the vegetation feedback effect. The present results demonstrate that a conspicuous climatic change can take place in the Arctic region from the vegetation-climate feedback, and suggest a possible positive vegetation feedback over the Arctic and high-latitude region in association with anthropogenic global warming.

Next, diagnosis and modeling on recent Arctic cloud change were performed. This dissertation examines changes in Arctic cloud during winter (December to February) in recent three decades and their impacts on atmospheric circulation with multiple datasets from satellite and reanalysis products. From change point analysis applied to both datasets, it was shown that Arctic cloud

decreases gradually during the late 20th century and increases considerably after late 1990s. The gradual decrease and substantial increase in each period are also seen simultaneously in the temperature and moisture at lower troposphere over the Arctic. In particular, the recent profound cloud increasing emerges over the most Arctic and expands to higher altitude compared to decreasing period, accompanying increasing in precipitation. Between decreasing and increasing periods, the relationship between cloud and the Arctic Oscillation does not change, and the region where cloud increasing and moisture upward transport are linked to sea ice reducing moves from the margin to the center of the Arctic. Changes in surface conditions between two periods indicate that reduced sea ice cover in cloud-increasing period leads to an increase in turbulent fluxes from surface, a decrease in lower tropospheric static stability, and deepening of planetary boundary layer. As a result, these altered conditions provide a favorable condition for cloud to be more formed through enhancing upward moisture transport. In addition, these changes tighten the local relationship between cloud at lower troposphere and atmospheric states over the Arctic.

Diagnosis on recent cloud change suggests sea ice change could play a crucial role for changes in cloud and its effect on the Arctic climate. This dissertation investigates surface boundary condition related to sea ice change in order to obtain more accurate modeling result, in advance of modeling the

impact of sea ice on the cloud change. It is found that the atmospheric responses related to Arctic sea ice melt in the cold season (October–March) depend on sea ice fraction and are very sensitive to in-situ sea surface temperature (SST) from a series of atmospheric general circulation model (AGCM) simulations in which multiple combinations of SSTs and sea ice concentrations are prescribed in the Arctic Ocean. The amplitude of surface warming over the melted sea ice region is controlled by concurrent in-situ SST even if these simulations are forced by the same sea ice concentration. Much of the sensitivity of surface warming to in-situ SST are related with large changes in surface heat fluxes such as the outgoing long-wave flux in early winter (October–December) and the sensible and latent heat fluxes for the entire cold season. Vertical extension of surface warming and moistening is sensitive to these changes as well; the associated condensational heating modulates a static stability in the lower troposphere. Thus, changes in SST fields in AGCM simulations must be implemented with extra care, especially in the melted sea ice region in the Arctic. In addition, the statistical method in the thesis for adjusting SSTs in conjunction with a given sea ice change can help to model the atmospheric response to sea ice loss more accurately.

Finally, modeling result of recent Arctic climate change with refined surface boundary condition and cloud amount parameterization suggests that recent

changes in cloud and its effect on the Arctic climate are closely linked to surface condition change due to sea ice retreat even during winter. As seen in reanalyses, modeling result also describes that reduced sea ice cover leads to an increase in turbulent fluxes from surface, deepening of planetary boundary layer, and enhancing of convective process, thereby causing an increasing in cloud and closer relationship between cloud and local atmospheric state over the Arctic. Further investigations from the fifth phase the Coupled Model Intercomparison Project, of which the winter Arctic cloud increases and its impact on the Arctic becomes enhanced in future climate under global warming condition, also confirm this modeling result. The results from diagnosis and modeling emphasize that the cloud may amplify the surface warming over the Arctic during winter in recent decade, under sea ice retreat condition.

The modeling works in the thesis do not adopt fully dynamic ocean model and sea ice model, and this could be a limitation of the present thesis. The effect of vegetation feedback on the Arctic/sub-Arctic climate is examined with SOM and thermodynamical sea ice model. This approach gives an advantage of efficiency, but also could give less accurate result. For instance, momentum transported into the Arctic also increases owing to vegetation feedback, and this can act as mechanical forcing able to cause a deformation of sea ice. Therefore, an adopting full dynamical sea ice model could give a better understanding for

role of vegetation with more improved result because full dynamical sea ice model consider the process related to horizontal transport and mechanical redistribution of sea ice.

Likewise, the investigation of the impact of cloud on the Arctic climate does not consider the impact of cloud on sea ice change. Sea ice is only treated with surface boundary condition, thus interaction between cloud and sea ice is not considered in the modeling. However, it has been suggested that downwelling longwave radiation into sea ice also could affect properties in sea ice (Eisenman et al., 2007; Francis et al., 2005). Adopting full dynamical sea ice model, therefore, also could give a better understanding for role of cloud on recent Arctic climate change with more improved result.

It is known that using coupled global climate model (CGCM) with various component models could usually give better simulation result compared to using single component model. Thus, there has been and is being a long patient effort to improve the CGCM. While much effort exerted into adding new component model to the CGCM, from the modeling perspective, more accurate remapping process in coupling component models can be the vital improvement point. It is essential for CGCM to use remapping process in flux exchanges owing to diverse grid systems among component models. The bilinear and conservative remapping methods have been widely used for the remapping process, and

particularly the conservative remapping method has been more usually used owing to its higher order accuracy. However, while conceived accuracy of the conservative remapping method could be attained by using the 2nd order remapping coefficients, the coupler in most CGCMs currently uses only the 1st order remapping coefficients because of difficulty in implementing high order remapping process and massive computational time.

If the positive feedback process exists between component models, it is possible that the uncertainty due to using only the 1st order remapping coefficients may be amplified as coupling with remapping process repeated. Unfortunately, the Arctic has a well-known positive feedback process between atmosphere and cryosphere – sea ice albedo feedback process. Therefore, for the better simulation result with CGCM, further investigation on uncertainties in the CGCM due to lower order remapping processes, and implementation of coupling with higher order accuracy remapping process are suggested.

Thus, future modeling works of the present thesis could be the Arctic climate modeling with full oceanic and sea ice model, accompanying improved coupling process with more accurate remapping method. These works could give extension of understanding of the role of vegetation and cloud on the Arctic climate.

REFERENCES

- ACIA (2005) Arctic Climate Impact Assessment. Cambridge University Press.
- Alexander MA, Bhatt US, Walsh JE, Timlin MS, Miller JS, Scott JD (2004) The atmospheric response to realistic Arctic sea ice anomalies in an AGCM during winter. *J Climate* 17:890-905.
- Alexeev VA, Langen PL, Bates JR (2005) Polar amplification of surface warming on an aquaplanet in "ghost forcing" experiments without sea ice feedbacks. *Clim Dynam* 24:655-666.
- Andersson C, Pausata FSR, Jansen E, Risebrobakken B, Telford RJ (2010) Holocene trends in the foraminifer record from the Norwegian Sea and the North Atlantic Ocean. *Clim Past* 6:179-193.
- Beesley JA, Moritz RE (1999) Toward an explanation of the annual cycle of cloudiness over the Arctic ocean. *J Climate* 12:395-415.
- Bintanja R, Graverson RG, Hazeleger W (2011) Arctic winter warming amplified by the thermal inversion and consequent low infrared cooling to space. *Nat Geosci* 4:758-761.
- Bitz CM, Fu Q (2008) Arctic warming aloft is data set dependent. *Nature* 455:E3-E4.
- Bitz CM, Gent PR, Woodgate RA, Holland MM, Lindsay R (2006) The influence of sea ice on ocean heat uptake in response to increasing CO₂. *J Climate* 19:2437-2450.

- Boe J, Hall A, Qu X (2009) Current GCMs' Unrealistic Negative Feedback in the Arctic. *J Climate* 22:4682-4695.
- Bonan GB, Levis S (2006) Evaluating Aspects of the Community Land and Atmosphere Models (CLM3 and CAM3) Using a Dynamic Global Vegetation Model. *J Climate* 19:2290-2301.
- Bonan GB, Pollard D, Thompson SL (1992) Effects of Boreal Forest Vegetation on Global Climate. *Nature* 359:716-718.
- Brandefelt J, Otto-Bliesner BL (2009) Equilibration and variability in a Last Glacial Maximum climate simulation with CCSM3. *Geophys Res Lett* 36:-.
- Budikova D (2009) Role of Arctic sea ice in global atmospheric circulation: A review. *Global Planet Change* 68:149-163.
- Bunn AG, Goetz SJ, Kimball JS, Zhang K (2007) Northern High-Latitude Ecosystems Respond to Climate Change. *EOS* 88:333-340.
- Cavalieri DJ, Parkinson CL (2012) Arctic sea ice variability and trends, 1979-2010. *The Cryosphere* 6:881-889.
- Chapin FS, Sturm M, Serreze MC, McFadden JP, Key JR, Lloyd AH, McGuire AD, Rupp TS, Lynch AH, Schimel JP, Beringer J, Chapman WL, Epstein HE, Euskirchen ES, Hinzman LD, Jia G, Ping CL, Tape KD, Thompson CDC, Walker DA, Welker JM (2005) Role of land-surface changes in Arctic summer warming. *Science* 310:657-660.
- Chung CE, Räisänen P (2011) Origin of the Arctic warming in climate models. *Geophys Res Lett* 38:L21704. doi:21710.21029/22011gl049816.

- Collins WD, Bitz CM, Blackmon ML, Bonan GB, Bretherton CS, Carton JA, Chang P, Doney SC, Hack JJ, Henderson TB, Kiehl JT, Large WG, McKenna DS, Santer BD, Smith RD (2006) The Community Climate System Model version 3 (CCSM3). *J Climate* 19:2122-2143.
- Collins WD, Rasch P, Boville B, Hack J, McCaa J, Williamson D, Kiehl J, Briegleb B, Bitz C, Lin S-J, Zhang M, Dai Y (2004) Description of the NCAR Community Atmosphere Model (CAM 3.0): NCAR/TN-464+STR NCAR TECHNICAL NOTE. National Center For Atmospheric Research, Boulder, Colorado, p. 226.
- Curry JA, Rossow WB, Randall D, Schramm JL (1996) Overview of Arctic cloud and radiation characteristics. *J Climate* 9:1731-1764.
- Curry JA, Schramm JL, Serreze MC (1995) Water-Vapor Feedback over the Arctic-Ocean. *J Geophys Res-Atmos* 100:14223-14229.
- Cuzzone J, Vavrus S (2011) The relationships between Arctic sea ice and cloud-related variables in the ERA-Interim reanalysis and CCSM3. *Environ Res Lett* 6.
- Danabasoglu G, Gent PR (2009) Equilibrium Climate Sensitivity: Is It Accurate to Use a Slab Ocean Model? *J Climate* 22:2494-2499.
- Dee DP, Uppala S (2009) Variational bias correction of satellite radiance data in the ERA-Interim reanalysis. *Q J Roy Meteor Soc* 135:1830-1841.
- Dee DP, Uppala SM, Simmons AJ, Berrisford P, Poli P, Kobayashi S, Andrae U, Balmaseda MA, Balsamo G, Bauer P, Bechtold P, Beljaars ACM, van de Berg L, Bidlot J, Bormann N, Delsol C, Dragani R, Fuentes M, Geer AJ,

- Haimberger L, Healy SB, Hersbach H, Holm EV, Isaksen L, Kallberg P, Kohler M, Matricardi M, McNally AP, Monge-Sanz BM, Morcrette JJ, Park BK, Peubey C, de Rosnay P, Tavolato C, Thepaut JN, Vitart F (2011) The ERA-Interim reanalysis: configuration and performance of the data assimilation system. *Q J Roy Meteor Soc* 137:553-597.
- Deser C, Magnusdottir G, Saravanan R, Phillips A (2004) The effects of North Atlantic SST and sea ice anomalies on the winter circulation in CCM3. Part II: Direct and indirect components of the response. *J Climate* 17:877-889.
- Deser C, Tomas R, Alexander M, Lawrence D (2010) The Seasonal Atmospheric Response to Projected Arctic Sea Ice Loss in the Late Twenty-First Century. *J Climate* 23:333-351.
- Dethloff K, Rinke A, Benkel A, Koltzow M, Sokolova E, Saha SK, Handorf D, Dorn W, Rockel B, von Storch H, Haugen JE, Roed LP, Roeckner E, Christensen JH, Stendel M (2006) A dynamical link between the Arctic and the global climate system. *Geophys Res Lett* 33:L03703. doi:03710.01029/02005gl025245.
- Eastman R, Warren SG (2010a) Arctic Cloud Changes from Surface and Satellite Observations. *J Climate* 23:4233-4242.
- Eastman R, Warren SG (2010b) Interannual Variations of Arctic Cloud Types in Relation to Sea Ice. *J Climate* 23:4216-4232.
- Eisenman I, Untersteiner N, Wettlaufer JS (2007) On the reliability of simulated Arctic sea ice in global climate models. *Geophys Res Lett* 34:-.
- Eldrett JS, Greenwood DR, Harding IC, Huber M (2009) Increased seasonality

- through the Eocene to Oligocene transition in northern high latitudes. *Nature* 459:969-U991.
- Finnis J, Holland MM, Serreze MC, Cassano JJ (2007) Response of Northern Hemisphere extratropical cyclone activity and associated precipitation to climate change, as represented by the Community Climate System Model. *J Geophys Res-Biogeophys* 112:-.
- Foley JA, Kutzbach JE, Coe MT, Levis S (1994) Feedbacks between Climate and Boreal Forests during the Holocene Epoch. *Nature* 371:52-54.
- Foley JA, Prentice IC, Ramankutty N, Levis S, Pollard D, Sitch S, Haxeltine A (1996) An integrated biosphere model of land surface processes, terrestrial carbon balance, and vegetation dynamics. *Global Biogeochem Cy* 10:603-628.
- Folley JA (2005) Tipping points in the tundra. *Science* 310:627-628.
- Francis JA, Chan WH, Leathers DJ, Miller JR, Veron DE (2009) Winter Northern Hemisphere weather patterns remember summer Arctic sea-ice extent. *Geophys Res Lett* 36:L07503. doi:07510.01029/02009gl037274.
- Francis JA, Hunter E (2006) New insight into the disappearing Arctic sea ice. *Eos Trans. AGU* 87:509.
- Francis JA, Hunter E, Key JR, Wang XJ (2005) Clues to variability in Arctic minimum sea ice extent. *Geophys Res Lett* 32:-.
- Gerdes R (2006) Atmospheric response to changes in Arctic sea ice thickness. *Geophys Res Lett* 33:L18709. doi:18710.11029/12006gl027146.

- Goetz SJ, Bunn AG, Fiske GJ, Houghton RA (2005) Satellite-observed photosynthetic trends across boreal North America associated with climate and fire disturbance. *P Natl Acad Sci USA* 102:13521-13525.
- Gorodetskaya IV, Tremblay LB, Liepert B, Cane MA, Cullather RI (2008) The influence of cloud and surface properties on the Arctic Ocean shortwave radiation budget in coupled models. *J Climate* 21:866-882.
- Graversen RG (2006) Do changes in the midlatitude circulation have any impact on the Arctic surface air temperature trend? *J Climate* 19:5422-5438.
- Graversen RG, Mauritsen T, Tjernstrom M, Kallen E, Svensson G (2008) Vertical structure of recent Arctic warming. *Nature* 451:53-56.
- Graversen RG, Wang MH (2009) Polar amplification in a coupled climate model with locked albedo. *Clim Dynam* 33:629-643.
- Hack J, Caron J, Danabasoglu G, Oleson K (2006) CCSM-CAM3 Climate Simulation Sensitivity to Changes in Horizontal Resolution. *J Climate* 19:2267-2289.
- Holland MM, Bitz CM (2003) Polar amplification of climate change in coupled models. *Clim Dynam* 21:221-232.
- Honda M, Inoue J, Yamane S (2009) Influence of low Arctic sea-ice minima on anomalously cold Eurasian winters. *Geophys Res Lett* 36:Artn L08707. doi:08710.01029/02008gl037079.
- Intrieri JM, Fairall CW, Shupe MD, Persson POG, Andreas EL, Guest PS, Moritz RE (2002) An annual cycle of Arctic surface cloud forcing at SHEBA. *J*

Geophys Res-Oceans 107:-.

IPCC (2007) Climate change 2007: the physical science basis. Cambridge Univ Press.

Isaksen ISA, Gauss M, Myhre G, Walter Anthony KM, Ruppel C (2011) Strong atmospheric chemistry feedback to climate warming from Arctic methane emissions. *Global Biogeochem Cy* 25:GB2002.

Jaiser R, Dethloff K, Handorf D, Rinke A, Cohen J (2012) Impact of sea ice cover changes on the Northern Hemisphere atmospheric winter circulation. *Tellus A* 64.

Jeong J-H, Kug J-S, Kim B-M, Min S-K, Linderholm H, Ho C-H, Rayner D, Chen D, Jun S-Y (2012) Greening in the circumpolar high-latitude may amplify warming in the growing season. *Clim Dynam* 38:1421-1431.

Jeong S-J, Ho C-H, Kim K-Y, Kim J, Jeong J-H, Park T-W (2010) Potential impact of vegetation feedback on European heat waves in a 2 x CO₂ climate. *Climatic Change* 99:625-635.

Jeong S-J, Ho C-H, Park T-W, Kim J, Levis S (2011) Impact of vegetation feedback on the temperature and its diurnal range over the Northern Hemisphere during summer in a 2 × CO₂ climate. *Clim Dynam* 37:821-833.

Jia GSJ, Epstein HE, Walker DA (2003) Greening of arctic Alaska, 1981-2001. *Geophys Res Lett* 30:2067.

Jones CG, Wyser K, Ullerstig A, Willen U (2004) The Rossby Centre regional atmospheric climate model part II: Application to the Arctic climate. *Ambio*

33:211-220.

Jun S-Y, Ho C-H, Kim B-M, Jeong J-H (2013) Sensitivity of Arctic warming to sea surface temperature distribution over melted sea-ice region in atmospheric general circulation model experiments. *Clim Dynam*:1-15.

Karlsson J, Svensson G (2011) The simulation of Arctic clouds and their influence on the winter surface temperature in present-day climate in the CMIP3 multi-model dataset. *Clim Dynam* 36:623-635.

Kay JE, Gettelman A (2009) Cloud influence on and response to seasonal Arctic sea ice loss. *J Geophys Res-Atmos* 114:-.

Kiehl JT, Shields CA, Hack JJ, Collins WD (2006) The climate sensitivity of the Community Climate System Model version 3 (CCSM3). *J Climate* 19:2584-2596.

Kirkevåg A, Iversen T, Kristjánsson JE, Seland O, Debernard JB (2008) On the additivity of climate response to anthropogenic aerosols and CO₂, and the enhancement of future global warming by carbonaceous aerosols. *Tellus A* 60:513-527.

Lawrence DM, Slater AG, Romanovsky VE, Nicolsky DJ (2008a) Sensitivity of a model projection of near-surface permafrost degradation to soil column depth and representation of soil organic matter. *J Geophys Res-Earth* 113:-.

Lawrence DM, Slater AG, Tomas RA, Holland MM, Deser C (2008b) Accelerated Arctic land warming and permafrost degradation during rapid sea ice loss. *Geophys Res Lett* 35:-.

- Lee E, Chase TN, Lawrence PJ, Rajagopalan B (2008) Model assessment of the observed relationship between El Nino and the northern East Asian summer monsoon using the Community Climate System Model Community Atmosphere Model-Community Land Model version 3 (CAM-CLM3). *J Geophys Res-Atmos* 113:-.
- Levis S, Bonan GB, Vertenstein M, Oleson KW (2004) The Community Land Model's Dynamic Global Vegetation Model (CLM-DGVM): technical description and user's guide. Technical Note NCAR/TN-459+IA. National Center for Atmospheric Research, Boulder, Colorado, p. 50.
- Levis S, Foley JA, Pollard D (1999) Potential high-latitude vegetation feedbacks on CO₂-induced climate change. *Geophys Res Lett* 26:747-750.
- Liu Y, Key JR, Francis JA, Wang X (2007) Possible causes of decreasing cloud cover in the Arctic winter, 1982-2000. *Geophys Res Lett* 34:-.
- Liu Y, Key JR, Wang X (2008) The influence of changes in cloud cover on recent surface temperature trends in the Arctic. *J Climate* 21:705-715.
- Liu YH, Key JR, Wang XJ (2009) Influence of changes in sea ice concentration and cloud cover on recent Arctic surface temperature trends. *Geophys Res Lett* 36:-.
- Long SP, Ainsworth EA, Leakey ADB, Nosberger J, Ort DR (2006) Food for thought: Lower-than-expected crop yield stimulation with rising CO₂ concentrations. *Science* 312:1918-1921.
- Magnusdottir G, Deser C, Saravanan R (2004) The effects of North Atlantic SST and sea ice anomalies on the winter circulation in CCM3. Part I: Main

- features and storm track characteristics of the response. *J Climate* 17:857-876.
- McGregor S, Sen Gupta A, Holbrook NJ, Power SB (2009) The Modulation of ENSO Variability in CCSM3 by Extratropical Rossby Waves. *J Climate* 22:5839-5853.
- McMahon SM, Parker GG, Miller DR (2010) Evidence for a recent increase in forest growth. *Proc Natl Acad Sci U S A* 107:3611-3615.
- Meehl GA, Arblaster JM, Lawrence DM, Seth A, Schneider EK, Kirtman BP, Min D (2006a) Monsoon regimes in the CCSM3. *J Climate* 19:2482-2495.
- Meehl GA, Washington WM, Santer BD, Collins WD, Arblaster JM, Hu AX, Lawrence DM, Teng HY, Buja LE, Strand WG (2006b) Climate change projections for the twenty-first century and climate change commitment in the CCSM3. *J Climate* 19:2597-2616.
- Merkel U, Prange M, Schulz M (2010) ENSO variability and teleconnections during glacial climates. *Quaternary Sci Rev* 29:86-100.
- Miller JR, Chen YH, Russell GL, Francis JA (2007) Future regime shift in feedbacks during Arctic winter. *Geophys Res Lett* 34.
- Murray RJ, Simmonds I (1995) Responses of Climate and Cyclones to Reductions in Arctic Winter Sea-Ice. *J Geophys Res-Oceans* 100:4791-4806. doi:4710.1029/4794JC02206.
- Neale RB, Chen C-C, Lauritzen PH, Gettelman A, Park S, Williamson DL, Conley AJ, Garcia R, Kinnison D, Lamarque J-F, Marsh D, Mills M, Smith AK, Tilmes S, Vitt F, Morrison H, Cameron-Smith P, Collins WD, Iacono MJ,

- Easter RC, Ghan SJ, Liu X, Rasch PJ, Taylor MA (2012) Description of the NCAR Community Atmosphere Model (CAM 5.0). NCAR TECHNICAL NOTE NCAR/TN-486+STR National Center for Atmospheric Research, Boulder, Colorado, p. 274.
- Neale RB, Richter JH, Conley AJ, Park S, Lauritzen PH, Gettelman A, Williamson DL, Rasch PJ, Vavrus SJ, Taylor MA, Collins WD, Zhang M, Lin S-J (2011) Description of the NCAR Community Atmosphere Model (CAM4). NCAR Tech. Note NCAR/TN-4851STR. National Center for Atmospheric Research, Boulder, Colorado, p. 212.
- Newson RL (1973) Response of a General Circulation Model of Atmosphere to Removal of Arctic Ice-Cap. *Nature* 241:39-40.
- Notaro M, Liu ZY (2008) Statistical and dynamical assessment of vegetation feedbacks on climate over the boreal forest. *Clim Dynam* 31:691-712.
- Notaro M, Vavrus S, Liu Z (2007) Global Vegetation and Climate Change due to Future Increases in CO₂ as Projected by a Fully Coupled Model with Dynamic Vegetation*. *J Climate* 20:70-90.
- O'ishi R, Abe-Ouchi A (2009) Influence of dynamic vegetation on climate change arising from increasing CO₂. *Clim Dynam* 33:645-663.
- Overland JE, Wang MY (2010) Large-scale atmospheric circulation changes are associated with the recent loss of Arctic sea ice. *Tellus A* 62:1-9.
- Overpeck JT, Sturm M, Francis JA, Perovich DK, Serreze MC, Benner R, Carmack EC, Chapin FS, Gerlach SC, Hamilton LC, Hinzman LD, Holland MM, Huntington HP, Key JR, Lloyd AH, MacDonald GM, McFadden JP,

- Noone D, Prowse TD, Schlosser P, Vörösmarty C (2005) Arctic System on Trajectory to New, Seasonally Ice-Free State. *Eos Trans. AGU* 86:309-316.
- Palm SP, Strey ST, Spinhirne J, Markus T (2010) Influence of Arctic sea ice extent on polar cloud fraction and vertical structure and implications for regional climate. *J Geophys Res-Atmos* 115:-.
- Petoukhov V, Semenov VA (2010) A link between reduced Barents-Kara sea ice and cold winter extremes over northern continents. *Journal of Geophysical Research: Atmospheres* 115:D21111. doi:21110.21029/22009jd013568.
- Rampal P, Weiss J, Dubois C, Campin JM (2011) IPCC climate models do not capture Arctic sea ice drift acceleration: Consequences in terms of projected sea ice thinning and decline. *Journal of Geophysical Research: Oceans* 116:C00D07.
- Rayner NA, Parker DE, Horton EB, Folland CK, Alexander LV, Rowell DP, Kent EC, Kaplan A (2003) Global analyses of sea surface temperature, sea ice, and night marine air temperature since the late nineteenth century. *J Geophys Res* 108:4407. doi:4410.1029/2002JD002670.
- Reynolds RW, Rayner NA, Smith TM, Stokes DC, Wang WQ (2002) An improved in situ and satellite SST analysis for climate. *J Climate* 15:1609-1625.
- Rind D, Healy R, Parkinson C, Martinson D (1995) The role of sea ice in $2\times\text{CO}_2$ climate model sensitivity. Part I: the total influence of sea ice thickness and extent. *J Climate* 8:449-463.
- Saha S, Moorthi S, Pan HL, Wu XR, Wang JD, Nadiga S, Tripp P, Kistler R,

- Woollen J, Behringer D, Liu HX, Stokes D, Grumbine R, Gayno G, Wang J, Hou YT, Chuang HY, Juang HMH, Sela J, Iredell M, Treadon R, Kleist D, Van Delst P, Keyser D, Derber J, Ek M, Meng J, Wei HL, Yang RQ, Lord S, Van den Dool H, Kumar A, Wang WQ, Long C, Chelliah M, Xue Y, Huang BY, Schemm JK, Ebisuzaki W, Lin R, Xie PP, Chen MY, Zhou ST, Higgins W, Zou CZ, Liu QH, Chen Y, Han Y, Cucurull L, Reynolds RW, Rutledge G, Goldberg M (2010) The Ncep Climate Forecast System Reanalysis. *B Am Meteorol Soc* 91:1015-1057.
- Schneider EK, Fennessy MJ, Kinter JL (2009) A Statistical-Dynamical Estimate of Winter ENSO Teleconnections in a Future Climate. *J Climate* 22:6624-6638.
- Schweiger AJ, Lindsay RW, Francis JA, Key J, Intrieri JM, Shupe MD (2002) Validation of TOVS Path-P data during SHEBA. *J Geophys Res-Oceans* 107:-.
- Schweiger AJ, Lindsay RW, Vavrus S, Francis JA (2008) Relationships between Arctic sea ice and clouds during autumn. *J Climate* 21:4799-4810.
- Screen JA, Simmonds I (2010a) The central role of diminishing sea ice in recent Arctic temperature amplification. *Nature* 464:1334-1337.
- Screen JA, Simmonds I (2010b) Increasing fall-winter energy loss from the Arctic Ocean and its role in Arctic temperature amplification. *Geophys Res Lett* 37:L16707. doi:16710.11029/12010GL044136.
- Screen JA, Simmonds I, Deser C, Tomas R (2012) The Atmospheric Response to Three Decades of Observed Arctic Sea Ice Loss. *J Climate* 26:1230-1248.

- Seierstad IA, Bader J (2009) Impact of a projected future Arctic Sea Ice reduction on extratropical storminess and the NAO. *Clim Dynam* 33:937-943.
- Semmler T, McGrath R, Wang S (2012) The impact of Arctic sea ice on the Arctic energy budget and on the climate of the Northern mid-latitudes. *Clim Dynam* 39:2675-2694.
- Serreze MC, Barry RG (2009) *The Arctic Climate System*. Cambridge University Press.
- Serreze MC, Francis JA (2006) The arctic amplification debate. *Climatic Change* 76:241-264.
- Serreze MC, Walsh JE, Chapin FS, Osterkamp T, Dyurgerov M, Romanovsky V, Oechel WC, Morison J, Zhang T, Barry RG (2000) Observational evidence of recent change in the northern high-latitude environment. *Climatic Change* 46:159-207.
- Shellito CJ, Lamarque JF, Sloan LC (2009) Early Eocene Arctic climate sensitivity to pCO₂ and basin geography. *Geophys Res Lett* 36:-.
- Shupe MD, Intrieri JM (2004) Cloud radiative forcing of the Arctic surface: The influence of cloud properties, surface albedo, and solar zenith angle. *J Climate* 17:616-628.
- Singarayer JS, Bamber JL, Valdes PJ (2006) Twenty-first-century climate impacts from a declining Arctic sea ice cover. *J Climate* 19:1109-1125.
- Singarayer JS, Valdes PJ, Bamber JL (2005) The atmospheric impact of uncertainties in recent Arctic sea ice reconstructions. *J Climate* 18:3996-4012.

- Sinha A, Harries JE (1995) Water-Vapor and Greenhouse Trapping - the Role of Far-Infrared Absorption. *Geophys Res Lett* 22:2147-2150.
- Sitch S, Smith B, Prentice IC, Arneth A, Bondeau A, Cramer W, Kaplan JO, Levis S, Lucht W, Sykes MT, Thonicke K, Venevsky S (2003) Evaluation of ecosystem dynamics, plant geography and terrestrial carbon cycling in the LPJ dynamic global vegetation model. *Global Change Biol* 9:161-185.
- Skific N, Francis JA, Cassano JJ (2009a) Attribution of Projected Changes in Atmospheric Moisture Transport in the Arctic: A Self-Organizing Map Perspective. *J Climate* 22:4135-4153.
- Skific N, Francis JA, Cassano JJ (2009b) Attribution of Seasonal and Regional Changes in Arctic Moisture Convergence. *J Climate* 22:5115-5134.
- Stokes GM, Schwartz SE (1994) The Atmospheric Radiation - Measurement (Arm) Program - Programmatic Background and Design of the Cloud and Radiation Test-Bed. *B Am Meteorol Soc* 75:1201-1221.
- Stroeve J, Holland MM, Meier W, Scambos T, Serreze M (2007) Arctic sea ice decline: Faster than forecast. *Geophys Res Lett* 34.
- Stroeve JC, Maslanik J, Serreze MC, Rigor I, Meier W, Fowler C (2011) Sea ice response to an extreme negative phase of the Arctic Oscillation during winter 2009/2010. *Geophys Res Lett* 38:L02502.
- Stroeve JC, Serreze MC, Holland MM, Kay JE, Malanik J, Barrett AP (2012) The Arctic's rapidly shrinking sea ice cover: a research synthesis. *Climatic Change* 110:1005-1027.

- Sturm M, Holmgren J, McFadden JP, Liston GE, Chapin FS, Racine CH (2001) Snow–Shrub Interactions in Arctic Tundra: A Hypothesis with Climatic Implications. *J Climate* 14:336-344.
- Swann AL, Fung IY, Levis S, Bonan GB, Doney SC (2009) Changes in Arctic vegetation amplify high-latitude warming through the greenhouse effect. *PNAS*.
- Swann AL, Fung IY, Levis S, Bonan GB, Doney SC (2010) Changes in Arctic vegetation amplify high-latitude warming through the greenhouse effect. *PNAS* Natl Acad Sci USA 107:1295-1300.
- Tape K, Sturm M, Racine C (2006) The evidence for shrub expansion in Northern Alaska and the Pan-Arctic. *Glob Change Biol* 12:686-702.
- Teng HY, Washington WM, Meehl GA, Buja LE, Strand GW (2006) Twenty-first century Arctic climate change in the CCSM3 IPCC scenario simulations. *Clim Dynam* 26:601-616.
- Thompson DWJ, Wallace JM (1998) The Arctic Oscillation signature in the wintertime geopotential height and temperature fields. *Geophys Res Lett* 25:1297-1300.
- Thompson SL, Pollard D (1995) A Global Climate Model (Genesis) with a Land-Surface Transfer Scheme (Lsx) .1. Present Climate Simulation. *J Climate* 8:732-761.
- Tomé AR, Miranda PMA (2004) Piecewise linear fitting and trend changing points of climate parameters. *Geophys Res Lett* 31:L02207.

- Trenberth KE, Caron JM (2001) Estimates of Meridional Atmosphere and Ocean Heat Transports. *J Climate* 14:3433-3443.
- Uppala SM, Kallberg PW, Simmons AJ, Andrae U, Bechtold VD, Fiorino M, Gibson JK, Haseler J, Hernandez A, Kelly GA, Li X, Onogi K, Saarinen S, Sokka N, Allan RP, Andersson E, Arpe K, Balmaseda MA, Beljaars ACM, Van De Berg L, Bidlot J, Bormann N, Caires S, Chevallier F, Dethof A, Dragosavac M, Fisher M, Fuentes M, Hagemann S, Holm E, Hoskins BJ, Isaksen L, Janssen PAEM, Jenne R, McNally AP, Mahfouf JF, Morcrette JJ, Rayner NA, Saunders RW, Simon P, Sterl A, Trenberth KE, Untch A, Vasiljevic D, Viterbo P, Woollen J (2005) The ERA-40 re-analysis. *Q J Roy Meteor Soc* 131:2961-3012.
- Vavrus S (2004) The impact of cloud feedbacks on Arctic climate under greenhouse forcing. *J Climate* 17:603-615.
- Vavrus S, Holland MM, Bailey DA (2011a) Changes in Arctic clouds during intervals of rapid sea ice loss. *Clim Dynam* 36:1475-1489.
- Vavrus S, Waliser D (2008) An Improved Parametrization for Simulating Arctic Cloud Amount in the CCSM3 Climate Model. *J Climate* 21:5673-5687.
- Vavrus S, Waliser D, Schweiger A, Francis J (2009) Simulations of 20th and 21st century Arctic cloud amount in the global climate models assessed in the IPCC AR4. *Clim Dynam* 33:1099-1115.
- Vavrus SJ, Bhatt US, Alexeev VA (2011b) Factors Influencing Simulated Changes in Future Arctic Cloudiness. *J Climate* 24:4817-4830.
- Walsh JE, Chapman WL, Portis DH (2009) Arctic Cloud Fraction and Radiative

- Fluxes in Atmospheric Reanalyses. *J Climate* 22:2316-2334.
- Walsh JE, Vavrus SJ, Chapman WL (2005) Workshop on Modeling of the Arctic Atmosphere. *B Am Meteorol Soc* 86:845-852.
- Wang XJ, Key JR (2003) Recent trends in arctic surface, cloud, and radiation properties from space. *Science* 299:1725-1728.
- Wang XJ, Key JR (2005a) Arctic surface, cloud, and radiation properties based on the AVHRR Polar Pathfinder dataset. Part I: Spatial and temporal characteristics. *J Climate* 18:2558-2574.
- Wang XJ, Key JR (2005b) Arctic surface, cloud, and radiation properties based on the AVHRR Polar Pathfinder dataset. Part II: Recent trends. *J Climate* 18:2575-2593.
- Warshaw M, Rapp RP (1973) An experiment on the sensitivity of a global circulation model. *J Appl Meteorol Clim* 12:43-49.
- Wetherald RT, Manabe S (1988) Cloud Feedback Processes in a General-Circulation Model. *J Atmos Sci* 45:1397-1415.
- Winton M (2011) Do Climate Models Underestimate the Sensitivity of Northern Hemisphere Sea Ice Cover? *J Climate* 24:3924-3934.
- Winton M, Takahashi K, Held IM (2010) Importance of Ocean Heat Uptake Efficacy to Transient Climate Change. *J Climate* 23:2333-2344.
- Xin XG, Zhou TJ, Yu RC (2008) The Arctic Oscillation in coupled climate models. *Chinese J Geophys-Ch* 51:337-351.

- Yoshida Y, Maruyama K, Takahara H (2008) Global Warming Projections Using the Community Climate System Model, CCSM3. *Nec Tech J* 3:73-77.
- Yu JY, Sun FP, Kao HY (2009) Contributions of Indian Ocean and Monsoon Biases to the Excessive Biennial ENSO in CCSM3. *J Climate* 22:1850-1858.
- Zhang T, Sun DZ, Neale R, Rasch PJ (2009) An Evaluation of ENSO Asymmetry in the Community Climate System Models: A View from the Subsurface. *J Climate* 22:5933-5961.
- Zygmuntowska M, Mauritsen T, Quaas J, Kaleschke L (2012) Arctic Clouds and Surface Radiation – a critical comparison of satellite retrievals and the ERA-Interim reanalysis. *Atmos. Chem. Phys.* 12:6667-6677.

국문초록

최근 수 십 년간 북극 지역에서는 전구 평균 기온 상승보다 더 큰 기온 상승이 발생하였다. 북극 증폭 (Arctic amplification) 이라 불리는 이 북극지역의 강한 기온 상승 현상에 다양한 기후 요소가 영향을 미칠 수 있음이 여러 연구를 통해 밝혀지고 있다. 본 연구에서는 전구 식생역학모델 (dynamic global vegetation model)의 기후모델에의 접합과 구름모수화과정 및 해빙 해수면 경계조건을 개선한 모델링을 통해 식생과 구름이 이러한 북극의 기후 변화에 미치는 영향에 대하여 살펴보았다.

전구역학식생모델을 접합한 기후모델을 이용한 이산화탄소 배증 실험 결과, 온실기체 증가에 따른 고위도 지역의 식생 증가가 북극지역의 기온 상승에 기여하는 것으로 나타난다. 이산화탄소 배증실험에서 역학전구식생모델은 이산화탄소 배증시 북아메리카, 유라시아 대륙 북부의 고위도 지역의 식생 증가를 모의하였다. 식생의 변화를 고려하지 않고 현재 기후에서 모의된 식생분포를 고정한 이산화탄소 배증 실험결과와 비교하였을 때, 이러한 식생 증가는 식생성장 계절에서의 고위도 대륙지역의 기온 상승을 야기하였으며 이에 따라 북극으로의 대기중 북향 수송 에너지 역시 증가하였다. 결국 식생의 변화가 고려된 실험에서 가을철 북극지역의 해빙은 면적과 두께 모두 크게 감소하였으며 이에 따라 북극지역의 기온 역시 크게 상승하였다. 이 결과는 최근 위성자료 등을 통해 관측된 고위도 지역의 식생의 증가가 양의 되먹임 과정을 통해 북극지역의 기온 상승 및 해빙 감소에 기여했을 가능성을 암시한다.

재분석자료와 위성자료 분석과 개선된 기후모델링 실험을 통해 살펴본 결과, 최근 겨울철 북극지역의 해빙 감소와 이에 연관된 북극의 기후시스템의 변화가 북극지역의 구름 증가에 기여하며 이에 따라 북극지역의 구름이 북극지역의 기온 상승에 미치는 영향이 커지는 것으로 나타난다. 재분석자료와 위성자료의 북극지역 겨울철 평균 지면대기온도, 운량의 변화 경향은 1997/1998년을 기점으로 약한 감소 경향에서 강한 증가 경향으로 변화하였다. 겨울철 해빙 역시 1997/1998년을 기점으로 급격하게 감소하기 시작하였다. 북극지역 평균 해빙에 대한 구름수분량의 회귀분석 결과 1997/1998년 이전 시기는 해빙 변화에 대한 구름수분량의 변화가 북극지역 경계에 나타남에 반해 1997/1998년 이후는 북극지역의 중앙에서 나타난다. 두 시기의 평균 대기장의 차이를 살펴보면 1997/1998년 이후 시기에 해빙의 감소, 지면대기온도의 증가, 하층 안정도의 감소, 행성경계층의 확장, 대기경압성의 발달이 발생하였으며 이러한 북극지역의 대기조건의 변화는 국지대류 및 저기압 발생에 호조건을 제공한다. 따라서 1997/1998년 이후 시기에 해빙의 감소와 북극지역의 운량의 증가가 더욱 밀접하게 연관되며, 북극지역 평균 하층운량과 북극지역 동서방향 평균 기온 및 비습의 회귀분석 결과 역시 이러한 관계의 변화를 제시하고 있다.

이러한 최근 북극지역 해빙감소와 운량 증가 메커니즘을 개선된 대기모델 실험에서 확인하였다. 먼저 해빙 변화에 대한 보다 정확한 대기모델의 경계조건을 얻기 위하여 해빙 변화에 대한 해수면온도를 북극지역의 해빙 면적과 해수면온도의 분포 관계에서 계수 다항식 근사 (polynomial fitting)를 통하여 얻어진 3차 다항식을 이용하여 보정

하였다. 이 보정 방안을 이용한 대기모델 실험 결과는 해수의 어는점을 이용하는 전통적 보정 방식에 비하여 관측에 더 가까운 대기의 반응을 모의하였다. 다음으로 보다 정확한 운량의 변화를 모의하기 위하여 기존 연구에서 제안된 FREEZEDRY 운량모수화 방안을 대기모델에 접합하고 성능을 확인하였다. 이 운량모수화 방안을 이용하였을 때 북극지역 겨울철 운량의 과다모의 경향과 운량-기온 관계가 개선된 모의 결과를 얻었다. 이 계수 다항식 근사 방안과 운량모수화 방안의 접합을 통해 대기모델 실험 결과, 관측에서 나타난 겨울철 해빙의 감소가 지면대기온도 증가, 하층안정도 감소, 행성경계층의 확장, 대기경압성의 증가 등의 대기조건의 변화를 야기하고, 이에 따라 운량 역시 증가함을 확인하였다. 이에 따라 해빙이 감소하는 경우 운량이 하층기온 상승에 미치는 영향 역시 커짐을 확인하였다. 이 해빙의 감소와 운량의 증가, 이에 따른 운량과 주변 기후요소와의 관계변화는 제 5차 결합기후모델비교사업 (coupled model intercomparison project phase 5)에 참여한 모델들의 미래기후실험 결과 앙상블 평균에서도 마찬가지로 나타나고 있다. 즉 재분석 자료와 모델 실험 결과들은 해빙이 감소하는 조건에서 겨울철 북극지역의 구름이 지면대기온도와 하층대기의 기온 증가에 더욱 기여할 수 있음을 제시한다.

주요어: 북극, 북극중폭, 기후모델링, 식생, 구름, 해빙

학 번: 2008-30822



저작자표시-비영리-변경금지 2.0 대한민국

이용자는 아래의 조건을 따르는 경우에 한하여 자유롭게

- 이 저작물을 복제, 배포, 전송, 전시, 공연 및 방송할 수 있습니다.

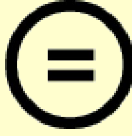
다음과 같은 조건을 따라야 합니다:



저작자표시. 귀하는 원저작자를 표시하여야 합니다.



비영리. 귀하는 이 저작물을 영리 목적으로 이용할 수 없습니다.



변경금지. 귀하는 이 저작물을 개작, 변형 또는 가공할 수 없습니다.

- 귀하는, 이 저작물의 재이용이나 배포의 경우, 이 저작물에 적용된 이용허락조건을 명확하게 나타내어야 합니다.
- 저작권자로부터 별도의 허가를 받으면 이러한 조건들은 적용되지 않습니다.

저작권법에 따른 이용자의 권리는 위의 내용에 의하여 영향을 받지 않습니다.

이것은 [이용허락규약\(Legal Code\)](#)을 이해하기 쉽게 요약한 것입니다.

[Disclaimer](#)

Thesis for a Ph. D. Degree

Role of Vegetation and Cloud on Arctic
Climate Change: A Modeling Study

북극지역에서 식생과 구름이 기후변화에 미치는
영향의 모델링 연구

Sang-Yoon Jun

February 2014

School of Earth and Environmental Sciences
Graduate School
Seoul National University

이학박사학위논문

북극지역에서 식생과 구름이 기후변화에
미치는 영향의 모델링 연구

Role of Vegetation and Cloud on Arctic Climate Change:
A Modeling Study

2014년 2월

서울대학교 대학원

지구환경과학부

전 상 운

Role of Vegetation and Cloud on Arctic Climate Change: A Modeling Study

by
Sang-Yoon Jun

Dissertation Submitted to the Faculty of the Graduate School of the
Seoul National University in Partial Fulfillment of the Requirement
for the Degree of Doctor of Philosophy

Degree Awarded:
February 2014

Advisory committee:

Professor	Rokjin Park, Chair
Professor	Chang-Hoi Ho, Advisor
Doctor	Seong-Joong Kim
Professor	Soon-Il An
Professor	Myong-In Lee

북극지역에서 식생과 구름이 기후변화에 미치는
영향의 모델링 연구
Role of Vegetation and Cloud on Arctic Climate Change:
A Modeling Study

지도교수 허 창 회

이 논문을 이학박사 학위논문으로 제출함
2013년 10월

서울대학교 대학원
지구환경과학부
전 상 윤

전 상 윤 의 이학박사 학위논문을 인준함
2013년 12월

위 원 장 _____ (인)
부위원장 _____ (인)
위 원 _____ (인)
위 원 _____ (인)
위 원 _____ (인)

ABSTRACT

The Arctic has experienced substantial warming in recent decades of which degree and rate is much larger than global averages. This phenomenon, which is also widely predicted from future climate modeling for several climate change assessment reports of the Intergovernmental Panels for Climate Change, is called as the Arctic amplification. Various climate factors on the globe could contribute to the amplified warming over the Arctic because of the highly sensitive Arctic climate system and the northward transport into the high latitude region. Much of understanding for these contributing factors come from modeling study because of lack of observation datasets owing to severe weather and climate conditions of the Arctic. In particular, less consideration of climate factors such as vegetation, cloud, and sea ice in modeling could bring large uncertainties in understanding the Arctic climate. Thus present thesis examines the contributions of vegetation and cloud to the Arctic amplification through modeling work with adopting a global dynamic vegetation model (DGVM) and improving physical processes related to sea ice and cloud.

First, modeling result from simulating the Community Climate System Model 3 (CCSM3) coupled with a DGVM indicates that potential vegetation change under a doubled CO₂ situation and its feedback have an influence on

surface warming over the Arctic/high-latitude region. This dissertation performed two baseline experiments under the present and doubling CO₂ concentration using the CCSM3-DGVM. Then, an additional simulation without DGVM was performed under doubling CO₂ concentration with the prescribed vegetation taken from the present CO₂ simulation. Model experiments indicate that a vegetation change in high-latitudes may induce substantial alteration of climate in the Arctic/high-latitude during warm and cold seasons. When the interactive vegetation process is included in the future climate simulation, vegetation in high-latitudes increases during growing season and the warming in the Arctic and high-latitude continent appears to be significantly amplified. Furthermore, and the Arctic sea ice exhibits considerable decline both in areal extent and thickness associated with the vegetation feedback effect. The present results demonstrate that a conspicuous climatic change can take place in the Arctic region from the vegetation-climate feedback, and suggest a possible positive vegetation feedback over the Arctic and high-latitude region in association with anthropogenic global warming.

Next, diagnosis and modeling on recent Arctic cloud change are conducted. The dissertation first examines changes in Arctic cloud during winter (December to February) in recent three decades and their impacts on atmospheric circulation with multiple datasets from satellite and reanalysis products. From change point

analysis applied to both datasets, it was shown that Arctic cloud decreases gradually during the late 20th century and increases considerably after late 1990s. The gradual decrease and substantial increase in each period are also seen simultaneously in the temperature and moisture at lower troposphere over the Arctic. In particular, the recent profound cloud increasing emerges over the most Arctic and expands to higher altitude compared to decreasing period, accompanying increasing in precipitation. Between decreasing and increasing periods, the relationship between cloud and the Arctic Oscillation does not change, and the region where cloud increasing and moisture upward transport are linked to sea ice reducing moves from the margin to the center of the Arctic. Changes in surface conditions between two periods indicate that reduced sea ice cover in cloud-increasing period leads to an increase in turbulent fluxes from surface, a decrease in lower tropospheric static stability, and deepening of planetary boundary layer. As a result, these altered conditions provide a favorable condition for cloud to be more formed through enhancing upward moisture transport. In addition, these changes tighten the local relationship between cloud at lower troposphere and atmospheric states over the Arctic. Diagnosis on recent cloud change suggests that sea ice change could play a crucial role on changes in cloud and its effect on the Arctic climate, also suggests that further modeling is needed due to weakness in datasets.

The modeling of the impact of sea ice on recent cloud change first performs an investigation of surface boundary condition related to sea ice change in order to obtain more accurate modeling result. It is found that the atmospheric responses related to Arctic sea ice melt in the cold season (October–March) depend on sea ice fraction and are very sensitive to *in-situ* sea surface temperature (SST) from a series of atmospheric general circulation model (AGCM) simulations in which multiple combinations of SSTs and sea ice concentrations are prescribed in the Arctic Ocean. The amplitude of surface warming over the melted sea ice region is controlled by concurrent *in-situ* SST even if these simulations are forced by the same sea ice concentration. Much of the sensitivity of surface warming to *in-situ* SST are related with large changes in surface heat fluxes such as the outgoing long-wave flux in early winter (October–December) and the sensible and latent heat fluxes for the entire cold season. Vertical extension of surface warming and moistening is sensitive to these changes as well; the associated condensational heating modulates a static stability in the lower troposphere. Thus, changes in SST fields in AGCM simulations must be implemented with extra care, especially in the melted sea ice region in the Arctic. In addition, the statistical method in the thesis for adjusting SSTs in conjunction with a given sea ice change can help to model the atmospheric response to sea ice loss more accurately.

Finally, modeling result of recent Arctic climate change with refined surface boundary condition and cloud amount parameterization suggests that recent changes in cloud and its effect on the Arctic climate are closely linked to surface condition change due to sea ice retreat even during winter. As seen in reanalyses, modeling result also describes that reduced sea ice cover leads to an increase in turbulent fluxes from surface, deepening of planetary boundary layer, and enhancing of convective process, thereby causing an increasing in cloud and closer relationship between cloud and local atmospheric state over the Arctic. Further investigation from the fifth phase the Coupled Model Intercomparison Project, of which the winter Arctic cloud increases and its impact on the Arctic becomes enhanced in future climate under global warming condition, also confirms this modeling result. The results from diagnosis and modeling emphasize that the cloud may amplify the surface warming over the Arctic during winter in recent decade, under sea ice retreat condition.

Keywords: Arctic, Arctic amplification, climate modeling, vegetation, cloud, sea ice

Student number: 2008-30822

TABLE OF CONTENTS

Abstract	i
Table of Contents	vi
List of Tables	viii
List of Figures	ix
1. Introduction	1
1.1. Background	1
1.2. Motivation and Objectives	4
1.3. Thesis Organization.....	8
2. Model and Data	9
2.1. Model	9
2.2. Data	13
3. Modeling the role of vegetation on the Arctic warming under greenhouse warming	17
3.1. Vegetation over the high-latitudinal region and its change	17
3.2. Modeling vegetation change and its effect under greenhouse warming 19	
3.3. The vegetation change under a doubled CO ₂ climate	21
3.4. Vegetation feedback effect on SAT and circulation changes	24
3.5. Sea ice change and atmospheric northward energy transport	30

3.6. Discussion	37
4. Modeling the role of cloud on the recent Arctic warming during winter	39
4.1. Recent change in the winter Arctic cloud.....	39
4.1.1. Year-to-year variation and trends in cloud-related variables.....	43
4.1.2. Effect of AO on the change in Arctic cloud	51
4.1.3. Effect of sea ice retreat on recent changes in Arctic cloud	53
4.1.4. Discussion	60
4.2. Refinement of surface boundary condition for reduced sea ice in AGCM Experiment	76
4.2.1. Surface condition according to sea ice change for AGCM Experiment	76
4.2.2. Experimental Design.....	80
4.2.3. Responses in surface air temperature and heat fluxes.....	84
4.2.4. Vertical structure of responses in temperature and specific humidity	91
4.2.5. Discussion	95
4.3. Modeling the change in cloud and its effect in relation to sea ice	115
4.3.1. FREEZEDRY cloud amount parameterization	115
4.3.2. Response over the Arctic on reduced sea ice cover in AGCM Experiment	118
4.3.3. Discussion	121
5. Summary and Discussion	130
References	137

LIST OF TABLES

Table 2.1 Description of the CMIP5 models used in this study.....	16
Table 3.1 Change in model simulated variables by vegetation feedback effect (<i>F-FPV</i>).....	36
Table 4.1 Mean, standard deviation, and trends of total cloud fraction over the Arctic Ocean (north of 67°N) in each dataset.....	64
Table 4.2 Mean, standard deviation, and trend of surface skin temperature over the Arctic Ocean (north of 67°N) in each dataset.	65
Table 4.3 The 3rd polynomial fitting coefficients for the relationship between SST and sea ice fraction for each month during the cold season.....	100
Table 4.4 Summary of surface conditions of experiments in this study.	101

LIST OF FIGURES

- Fig. 3.1 Mean leaf area index (LAI) in growing season (May to September) for a) present (P) and b) future (F) simulation, and c) the fractional coverage of plant species (NET: needleleaf evergreen tree, BDT: broadleaf deciduous tree, C3: grasses with C3 pathway. T, B, and Arc in the suffix indicate temperate, boreal, and the Arctic respectively) over high-latitude, north of 60°N. The LAI represent the leaf abundance, the fractional area of plant's leaf surface relative to the surface area.23
- Fig. 3.2 (left panel) SAT difference between *F* and *P* simulation (upper) and *FPV* and *P* simulation (lower). (right panel) zonal mean of SAT difference between *F* and *FPV* simulation.28
- Fig. 3.3 Zonal mean temperature (shading) and u-wind (contour) changes by vegetation feedback effect (*F-FPV*) in JJA and SON.29
- Fig. 3.4 Shading indicates simulated average sea ice extent and thickness for September to October in *P* simulation. Lines in the left panel indicate sea ice extents where the ocean is covered with more than 15% sea ice. White line is the observed sea ice extent averaged from 1981-2000 HadISST data. Lines in the right panel indicate 25cm levels of mean sea ice thickness.33
- Fig. 3.5 (left panel) *NET* change by vegetation feedback effect (*F-FPV*). (right panel) changes in the components of *NET* at 70°N. 10-day running average is applied for the time dimension. Here atmospheric energy is estimated by moist static energy – summation of atmospheric latent, potential, and internal energy.34
- Fig. 3.6 Zonal mean *NET* change by vegetation feedback effect (*F-FPV*).35

- Fig. 4.1 Time-series of (a) cloud amount, (b) surface temperature, (c) sea ice cover over the Arctic Ocean (north of 67°N), and (d) AO index in winter (December to February) from the NCEP CFSR, ERA-Interim, APP-x, and TPP datasets. Trend lines are denoted with dashed line. Time series of cloud amount, surface temperature, and sea ice cover are re-scaled to have the mean and standard deviation of ERA-Interim for comparison.66
- Fig. 4.2 Changing trends in winter total cloud amount and surface air temperature during late 20th century (1979–1997) and early 21st century (1998–present) from the ERA-Interim and NCEP CFSR. Stippled region indicates that trend is significant at the 95% confidence level. Oblique and cross checked region in c and g (d and h) indicate that region sea ice cover is increasing (decreasing) with above (below) 0.2 %/year and 0.5 %/year, respectively.67
- Fig. 4.3 (left panels) changing trends in zonal-averaged winter temperature (shading) and specific humidity (contour) during late 20th century (1979–1997) and early 21st century (1998–present) from the ERA-Interim and NCEP CFSR. (right panels) same as left panels except for cloud water contents (shading) and fractional cloud cover (contour).68
- Fig. 4.4 Zonal-averaged total northward moisture transport ($vq + v'q'$, shading) and northward transport by mean flow (vq , contour) at 67°N.69
- Fig. 4.5 Changing trends in winter evaporation and precipitation during late 20th century (1979–1997) and early 21st century (1998–present) from the ERA-Interim and NCEP CFSR. Stippled region indicates that trend is significant at the 95% confidence level.70
- Fig. 4.6 Regressions of the AO index with zonal-averaged (a) cloud water

content [10^6 kg kg^{-1}], (b) horizontal moisture convergence [$10^9 \text{ kg kg}^{-1} \text{ s}^{-1}$], and (c) upward moisture transport [$10^5 \text{ kg Pa kg}^{-1} \text{ s}^{-1}$] from the ERA-interim and NCEP CFSR. Stipple regions indicate that values are significant at the 95% confidence level. 71

Fig. 4.7 Partial correlations of sea ice cover averaged over the Arctic Ocean (north of 67°N) with zonal-averaged cloud water content (shading) and mean upward moisture transport (contour) independent on the AO index during the late 20th century and the early 21st century from the ERA-interim and NCEP CFSR. Stippled (cross-checked) regions indicate that values with shading (contour) are significant at the 95% confidence level. 72

Fig. 4.8 Differences in (a and e) 850 hPa thickness (shading) and surface air temperature (contour), (b and f) PBL height (shading) and sea ice fraction (contour), (c and g) longwave cloud radiative forcing (shading) and cloud amount (contour), and sea level pressure (shading) and 500 hPa geopotential (contour) between averages for the early 21st century and the late 20th century. Stippled region indicates differences in shading values are significant at the 95% confidence level. 73

Fig. 4.9 Regression of winter low-level cloud amount [%] averaged over the Arctic Ocean (North of 67°N) with zonally averaged temperature (shading, [K]) and specific humidity (contour, [g kg^{-1}]) during late 20th century (1979 – 1997) and early 21st century (1998 – present) from the ERA-Interim and NCEP CFSR. All trends are removed. Stippled and cross-checked regions indicate that regression is significant at the 95% confidence level. 74

Fig. 4.10 Regression of winter low-level cloud amount averaged over the Arctic Ocean (North of 67°N) with sea level pressure (shading, [hPa]) and geopotential at 500 hPa (contour, [$\text{m}^2 \text{ s}^{-2}$]) during the late 20th century

(1979 – 1997) and the early 21st century (1998 – present) from the ERA-Interim and NCEP CFSR. All trends are removed in calculation. Stippled and cross-checked regions indicate that regressions are significant at the 95% confidence level.	75
Fig. 4.11 Scatter plot between sea ice concentration (SIC; fraction) and sea surface temperature (SST) over the Arctic (north of 60°N) for the cold season (October through March) of the period 1982–2000 from OISST v2. White lines indicate the third-degree polynomial fitting between SIC below 0.9 fraction and SST, in each month.	102
Fig. 4.12 Differences of sea surface temperature (shade) and sea ice concentration (contour) boundary conditions from (a and e) CTRL, (b and f) CONV, and (c and g) POLY experiments compared to the baseline experiment during early winter (October-November-December) and late winter (January-February-March); (d and h) Differences between mean sea surface temperature during early and late winters for 2006–2010 and 1982–2000 from the OISST v2. Differences are plotted only over the region where sea ice reduced above 0.01 fraction. In all panels, the contour interval is 0.1 fraction.	103
Fig. 4.13 Change in surface air temperature from (a) CTRL, (b) CONV, (c) POLY compared to the baseline experiment during the cold season, and (d) 2 m air temperature difference between 2006–2010 and 1982–2000 during the cold season from the ERA-Interim data.	104
Fig. 4.14 Change in surface air temperature from (a) CONV and (b) POLY compared to CTRL experiment during the cold season. Oblique and cross regions indicate that surface air temperature response is significant at the 90% and 95% confidence level, respectively.	105

- Fig. 4.15 Changes in net longwave flux (positive in the upward direction), sensible heat flux, and latent heat flux at the surface from CTRL (contour in all figures) compared to the baseline experiment, and changes in (a–c) CONV and (d–f) POLY experiments compared to CTRL experiment (shade in all figure) during the cold season. Contour interval is 5 W m^{-2} . Oblique and cross regions indicate that surface fluxes are significant at the 90% and 95% confidence level, respectively..... 106
- Fig. 4.16 Monthly changes in (a) net longwave flux (positive in the upward direction), (b) sensible heat flux, and (c) latent heat flux averaged over the Arctic Ocean (north of 67°N) from CTRL, CONV, and POLY experiments compared to the baseline experiment..... 107
- Fig. 4.17 Vertical profiles in temperature and specific humidity averaged over the Arctic Ocean (north of 67°N) in the baseline, CTRL, CONV, and POLY experiments during early and later winter (left panel) and their differences to the baseline experiment (right panel)..... 108
- Fig. 4.18 Changes in zonal-averaged heating by longwave radiation, diffusion, and moist processes during the cold season. Contour in the figure indicates a change between CTRL and the baseline experiments, and shade indicates the change in CONV and POLY against CTRL. Contour interval is 0.03 K day^{-1} . Oblique and cross regions indicate that surface fluxes are significant at the 90% and 95% confidence level, respectively..... 109
- Fig. 4.19 Changes in zonal-averaged temperature (shade) and specific humidity (contour) during early winter (October–November–December) and late winter (January–February–March) from CTRL, CONV, and POLY experiments compared to the baseline experiment. Oblique and cross regions indicate that surface fluxes are significant at the 90% and 95%

confidence level, respectively; (d and h) changes in the same variables for the periods 2006–2010 and 1982–2000 from the ERA-Interim data. Contour interval is 0.03 g kg^{-1} 110

Fig. 4.20 Change in surface air temperature from CTRL compared to the baseline experiment (contour), and changes in (a) POLY, (b) HadISST over the MSR, and (c) OISSTv2 over the MSR compared to CTRL (shade) during the cold season. Contour interval is 0.5 K. Oblique and cross regions indicate that surface air temperature response is significant at the 90% and 95% confidence level, respectively. 111

Fig. 4.21 Comparisons between simulated SST (model; left figure in each panel) and adjusted SST by polynomial fitting with SIC change (fitting; right figure in each panel) among 14 model results with future experiment of the RCP4.5 scenario in the fifth phase of the Climate Model Intercomparison Project. Model differences are calculated with simulated SSTs averaged for 2051–2055 and simulated SSTs averaged for 2006–2010. Fitting differences are calculated with fitted SSTs by using polynomial coefficients in the POLY method, SIC values averaged for 2051–2055 and simulated SSTs averaged for 2006–2010. Shading indicates sea surface temperature, and contour indicates sea ice concentration with an interval of 0.1. 112

Fig. 4.22 (a) relative humidity, (b) layered cloud amount by cloud amount parameterization in CAM3, and (c) layered cloud amount by FREEZEDRY modified parameterization under varying in temperature and specific humidity. 124

Fig. 4.23 Low level cloud amount during winter from (a) CAM3 original cloud amount parameterization, (b) FREEZEDRY cloud amount parameterization, and (c) their difference. 125

- Fig. 4.24 Changes in (a) surface air temperature (contour) and 850 hPa thickness (shading), (b) sea ice cover (contour) and planetary boundary layer height (shading), (b) total cloud amount (contour) and longwave cloud radiative forcing (shading), and (c) 500 hPa geopotential (contour) and sea level pressure (shading) from SIC experiment compared to CTRL experiment.126
- Fig. 4.25 Changes in (a) zonal-averaged temperature (contour) and specific humidity (shading), (b) heating by diffusion (contour) and moistening process (shading), and (c) cloud amount (contour) and regressed temperature of low-level cloud amount over the Arctic (shading) from SIC experiment compared to CTRL experiment.....127
- Fig. 4.26 Annual cycles of changes in (a) surface air temperature, (b) cloud amount, (c) longwave cloud radiative forcing, (d) shortwave cloud radiative forcing, (e) latent heat flux, and (f) sensible heat flux averaged over the Arctic (north of 70°N) between RCP4.5 and PIctrl experiments from climate models in the CMIP5. Solid thick lines in each figure indicate their ensemble mean values.....128
- Fig. 4.27 Annual cycles of regressions of (a) cloud amount onto surface air temperature, and (b) surface air temperature onto cloud amount averaged over the Arctic (north of 70°N) from PIctrl experiment, and (c) cloud amount onto surface air temperature, and (d) surface air temperature onto cloud amount from RCP4.5 experiment in the CMIP5. Solid thick lines indicate their ensemble mean values.....129

1. INTRODUCTION

1.1. Background

The Arctic is the northern polar component of the global climate system, the coldest region in the Northern Hemisphere. The Arctic is characterized by severe climate system during winter due to a low amount or absence of sunlight in winter and long days during summer. The absence of sunlight during cold season induces extremely low temperature, and the cryosphere, which is present as snow, ice sheets, glaciers, sea ice, and permafrost, becomes a prominent feature of the Arctic. In particular, a high reflectivity of the cryosphere makes the Arctic climate highly sensitive system passively through the ice-albedo feedback. It could help unusually large and rapid climate change by small temperature changes in the Arctic (ACIA, 2005).

In Earth's radiation budget, the Arctic is a less receiver for net solar radiative flux than lower latitudinal region because of an incoming angle of solar radiation. In the annual averages of top of atmosphere (TOA) radiation budget from the Earth Radiation Budget Experiment (ERBE), the region between about 38°N and 38°S receives more radiation than it emits to space. Poleward regions of these latitudes, the earth emits more radiation than it receives (Trenberth and Caron, 2001). The imbalance in energy budget along latitude implies that there

must be poleward transports of energy by the atmosphere and oceans that warm the Arctic region in order to keep global energy budget in balance.

These major characteristics, a highly sensitive climate system of the Arctic and an existence of poleward energy transport into the Arctic, could bring a unique phenomenon for the Arctic under the global climate change. The globe has experienced a large increasing in surface air temperature since the mid-1800s called as 'global warming', which might be caused by increasing in concentration of greenhouse gases (IPCC, 2007). Under the global warming, the Arctic has experienced larger warming almost twice as large as the global average increasing rate. This phenomenon is known as the 'Arctic amplification' (Graversen, 2006; Holland and Bitz, 2003; Serreze and Francis, 2006). Global warming may reinforce poleward energy transport by atmosphere and ocean (Alexeev et al., 2005; Bitz et al., 2006; Graversen et al., 2008), and the warming could be amplified by highly sensitive climate system of the Arctic (Bintanja et al., 2011; Boe et al., 2009; Screen and Simmonds, 2010a). Consequently, warming over the Arctic becomes larger than that over the globe.

Although major underlying cause for the Arctic amplification between the sensitive Arctic climate system due to the cryosphere and enhanced poleward energy transport is in debate (Bitz and Fu, 2008; Graversen et al., 2008; Screen and Simmonds, 2010a; Serreze and Francis, 2006), numerous studies have

attempted to find the other factors which affect the Arctic amplification. The cloud, which could compose positive process over the Arctic, has received much attention as one of amplifying factor from the earlier studies (Curry et al., 1996; Wetherald and Manabe, 1988). Water vapor feedback also has attracted attention for the factor since mid-1990s (Curry et al., 1995; Sinha and Harries, 1995). Recent studies have persisted in investigating the effect of these factors focused on earlier (Graversen and Wang, 2009; Vavrus, 2004; Vavrus et al., 2009), and tried to find the effect of other factors such as surface inversion at near surface over the Arctic (Bintanja et al., 2011; Boe et al., 2009), vegetation over the high-latitude region (Chapin et al., 2005; Swann et al., 2010), ocean heat uptake (Bitz et al., 2006; Winton et al., 2010), chemical feedback by methane emission in the Arctic region (Isaksen et al., 2011), and remotely induced warming from lower latitude (Chung and Räisänen, 2011).

These studies, which investigate the effect of various factors on the Arctic amplification, utilize a numerical model broadly. There might be two major reasons why the modeling is extensively adopted. First, because of extreme weather and climate condition over the Arctic, observational data are quite limited. In particular, extremely harmful condition in cold season causes hardship in both surface and satellite observations. Next, because the Arctic is the highly complex and sensitive system which has many climatic elements to

affect each other, modeling study can be an efficient way to investigate the isolated effect of climate factor on the Arctic climate. Namely, much of our current understanding of the Arctic climate system comes from numerical models (Serreze and Barry, 2009).

However, extreme weather and complex climate conditions also bring large difficulties into modeling the Arctic (Walsh et al., 2005). In intercomparison of multi-model results, it has been reported that the Arctic region has large discrepancies in principle variables such as surface air temperature (SAT) among the models (IPCC, 2007). This might be caused by the uncertainties in the cloud and related surface energy budget over the Arctic (Vavrus and Waliser, 2008; Walsh et al., 2005), and unrealistic longwave feedback at the near surface (Boe et al., 2009). In addition, uncertainties in the properties of sea ice also could bring a wide sensitivity into coupled models (Rampal et al., 2011; Winton, 2011). Moreover, the important physical elements excluded in the Arctic modeling such as glacier could induce error into the Arctic modeling. Namely, for the Arctic, while modeling is one of the most important tools for understanding the climate system, modeling result must always be handled with appropriate caveats.

1.2. Motivation and Objectives

Nevertheless, the modeling can give a great motivation to the study on the

Arctic. As modeling becomes refined and modeling area becomes extended, an understanding on the Arctic could grow. For instance, because the effect of vegetation on the Arctic warming could not be fully understood without interaction with other climatic elements, earlier modeling studies could investigate fragmentary effect of vegetation. Meanwhile, recent land surface model includes dynamical vegetation process, thus we can investigate the role of vegetation on the Arctic climate in much detail (Swann et al., 2010). In addition, reducing uncertainties by improving cloud properties over the Arctic also gives better understanding for the role of cloud on the Arctic climate system (Vavrus et al., 2011a; Vavrus and Waliser, 2008; Vavrus et al., 2011b). In other words, the Arctic climate modeling with refinement and extension of processes of climatic elements may facilitate more detailed study for the Arctic.

The role of vegetation on the Arctic warming still remains as one of challenges in modeling study on the Arctic. Warming and moistening over the Arctic and high latitudes provide a favorable condition for vegetation to grow. In practice, recent observations suggest that the shrubs and grasses in the Arctic tundra and trees in the boreal forests have expanded more northward and increased in its growth during recent decades (Bunn et al., 2007; Goetz et al., 2005; Jia et al., 2003; McMahon et al., 2010). An increasing in vegetation has a positive feedback effect – more warming with more vegetation growth, which is

mainly caused by decreased surface albedo as relatively darker vegetation cover replaces snow-covered or barren surface of high-reflectivity (Levis et al., 1999; Notaro and Liu, 2008; Notaro et al., 2007; O'ishi and Abe-Ouchi, 2009). Thus, the vegetation may, in turn, amplify the warming over the high latitudinal regions under global warming.

Although it is evident that such vegetation-feedbacks may provoke profound consequences in the Arctic climate system, much mechanism are still poorly understood due to lack of physical understanding and observations. In addition, only a few climate models include dynamic vegetation models, and most climate models' future climate predictions – even multi-model climate model predictions of the Intergovernmental Panels on Climate Change (IPCC) the Fourth Assessment Report (AR4) (IPCC, 2007) – neglect the vegetation feedback effect. Thus, modeling work with dynamic vegetation model could promote our understanding for role of the vegetation on the Arctic warming. In a chapter 3, the dissertation examines the role of vegetation on the Arctic climate under global warming condition by performing the doubled CO₂ simulation with dynamic vegetation model.

As mentioned previously, the cloud has been attracted attention as one of the major amplifying factors for the Arctic warming from earlier studies. However, much of understanding for the role of cloud on the Arctic climate

change still remains uncertain. In particular, for the cold season when uncertainties in both observation and modeling become stronger, only a few studies have focused on the change and the role of cloud under the Arctic climate (Liu et al., 2007; Miller et al., 2007).

The lack of studies for the winter Arctic cloud also is also seen in the recent Arctic climate change. Since the late 1990s, the accelerated melting of sea ice and associated ice-albedo feedback led to considerable warming throughout the troposphere (Screen and Simmonds, 2010a) and even caused hemispheric-scale atmospheric circulation changes (Francis et al., 2009; Overland and Wang, 2010). These changes are conspicuous especially during winter (Screen and Simmonds, 2010b), and numerous studies have pointed out the cloud as possible cause for amplifying the Arctic warming in winter because cloud-radiation feedback process works positively due to absence of solar radiation (Graversen et al., 2008; Graversen and Wang, 2009; Palm et al., 2010).

However, previous studies for the Arctic cloud with respect to recent Arctic climate change have been concentrated in melting season although winter Arctic cloud could play a crucial role on the recent Arctic warming (Cuzzone and Vavrus, 2011; Kay and Gettelman, 2009; Palm et al., 2010; Schweiger et al., 2008). Accordingly, whereas much of role of Arctic sea ice loss for the associated changes in Arctic clouds in melting season have been investigated, the

change in cloud and its impact on the Arctic climate system according to recent Arctic change during winter still remains poorly understood. Thus it is necessary to understand the change and effect of winter Arctic cloud in recent Arctic climate. In a chapter 4, this dissertation further diagnose the change in cloud and its impact on the Arctic during winter in recent decades, and model the recent Arctic change related to cloud with refinement in surface condition and modified cloud amount parameterization.

1.3. Thesis Organization

This dissertation is organized as the following.

Chapter 2 describes the model and data used in this thesis. Chapter 3 denotes the role of vegetation on the Arctic climate change under global warming condition by modeling work with dynamic vegetation model. Chapter 4 reveals the diagnosis and modeling on the change in cloud and its impact on the Arctic during winter in recent decades. Modeling works to improve modeling result are also documented. Lastly, the results of this dissertation are summarized, and the limitation of the study and possible future works are also discussed in Chapter 5.

2. MODEL AND DATA

2.1. Model

For modeling the role of vegetation and cloud on the Arctic climate change, the Community Climate System Model version 3 (CCSM3; Collins et al., 2006) is used. The CCSM3 is a fully coupled climate model with component models representing atmosphere, ocean, land surface, and sea ice, allowing researchers to conduct fundamental research into the earth's past, present and future climate states. The CCSM3 is a one of models participating the Coupled Model Intercomparison Project phase 3 (CMIP3) for the IPCC AR4, and the performance of CCSM3 for simulating global and regional climate system has been verified by numerous studies – El Niño/Southern Oscillation (McGregor et al., 2009; Merkel et al., 2010; Schneider et al., 2009; Zhang et al., 2009), regional climate such as monsoon and storm track (Finnis et al., 2007; Lee et al., 2008; Meehl et al., 2006a; Yu et al., 2009), global warming by greenhouse gases (Kiehl et al., 2006; Kirkevag et al., 2008; Meehl et al., 2006b; Yoshida et al., 2008), and paleo-climate (Andersson et al., 2010; Brandefelt and Otto-Bliesner, 2009; Eldrett et al., 2009; Shellito et al., 2009). In addition, numerous studies also have been done for the Arctic climate with giving much of knowledge on the Arctic climate system (Deser et al., 2010; Gorodetskaya et al., 2008;

Graversen and Wang, 2009; Lawrence et al., 2008a; Lawrence et al., 2008b; Skific et al., 2009a, b; Teng et al., 2006; Vavrus and Waliser, 2008; Xin et al., 2008).

This study utilizes the CCSM3 by using two main component models and two additional models in each main component model instead of using fully coupled model. First, the Community Atmosphere Model version 3 (CAM3), the atmospheric component of CCSM3, and the Community Land Model version 3 (CLM3), the land surface component of CCSM3, are used to simulate atmosphere and land surface, respectively. These two component models are used to study the role of both vegetation and cloud on the Arctic climate change.

Next, for investigating the role of vegetation, the Community Land Model's Dynamic Global Vegetation Model (CLM-DGVM), which simulates the distribution and structure of natural vegetation dynamically, is coupled to CLM3. The CLM-DGVM is based on the Lund–Potsdam–Jena (LPJ) DGVM (Sitch et al., 2003) and the IBIS which provides plant phenology to the CLM3 (Foley et al., 1996). It simulates the biogeographic distributions of potential vegetation plant functional types (PFTs) as a response of environmental conditions such as temperature, growing degree days, and precipitation. These climatic variables determine the survival and establishment of PFTs (Levis et al., 2004). The CLM-DGVM has been used in numerous studies for investigating the change in

vegetation and its effect on climate system for past, present and future climate (Bonan and Levis, 2006; Jeong et al., 2012; Jeong et al., 2010; Jeong et al., 2011; Notaro et al., 2007).

In addition to CLM-DGVM, the mixed-layer slab ocean model (SOM) is coupled to CAM3 for calculating prognostic ocean mixed-layer temperature instead of using the full-layered dynamical ocean and sea ice model. The governing equation for the slab mixed-layer temperature, which is usually treated as sea surface temperature (SST) in SOM, is

$$\rho_o C_o h_o \frac{\partial T_o}{\partial t} = (1 - A)F + Q + AF_{oi} + (1 - A)F_{fz} \quad (2.1)$$

where T_o is the ocean mixed layer temperature, ρ_o is the density of ocean water, C_o is the heat capacity of ocean water, h_o is the annual mean ocean mixed layer depth (m), A is the fraction of the ocean covered by sea ice, F is the net atmosphere to ocean heat flux (Wm^{-2}), Q is the internal ocean mixed layer heat flux (Wm^{-2}), F_{oi} is the heat exchanged with the sea ice (Wm^{-2}) and F_{fz} is the heat gained when sea ice grows over open water (Wm^{-2}).

In addition to ocean mixed layer model, thermodynamical sea ice model coupled to SOM calculates the prognostic fractional cover and thickness of sea ice. Sea ice thickness is calculated by following equations:

$$\frac{dh_i}{dt} = \frac{F_{TOP}}{q} + \frac{F_{LH}}{-q + \rho_i L_v} \quad (2.2)$$

$$\frac{dh_i}{dt} = \frac{F_{BOT}}{q} + \frac{k}{q} \frac{dT}{dz} \quad (2.3)$$

where F_{TOP} is heat flux from ice surface, h_i is the ice thickness, ρ_i is the ice density, q is the energy of melting of sea ice, F_{BOT} is the heat flux from the ocean to the ice, k is the thermal conductivity, and z is the vertical coordinate. In addition, sea ice cover A is prognostically calculated with three separate equations:

$$q_f \frac{\partial h_{new}}{\partial t} = F_{fz} (1 - A) \quad (2.4)$$

$$\left(A - \frac{\partial A}{\partial t} \right)^2 = \frac{A^2}{h_i} \left(h - \frac{\partial h_i}{\partial t} \right) \quad (2.5)$$

$$\frac{\partial A}{\partial t} = A \frac{F_{SID}}{E_{TOT}} \quad (2.6)$$

where q_f is the energy of melting for new ice growth, h_{new} is the thickness of the new ice, F_{SID} is the total flux from lateral boundary, and E_{TOT} is total energy of melting of snow and ice.

As the equilibrium climate sensitivity of the CCSM3 with SOM to anthropogenic forcing is known to be almost similar to that from fully-coupled version of CCSM3 (Danabasoglu and Gent, 2009; Kiehl et al., 2006). Therefore the using SOM gives an advantage of reducing computational time and bias reduction in remapping process between different grid systems compared to

using fully coupled model with ocean and sea ice models.

2.2. Data

The ERA-Interim, the latest European Centre for Medium-Range Weather Forecast (ECMWF) reanalysis, covers the period from the January 1979 to present with 0.75° by 0.75° horizontal resolution and 37 vertical levels. In the ERA-Interim, notable improvements have been made in its hydrological cycle by updating data assimilation system which newly includes rain-affected Special Sensor Microwave Image (SSM/I) radiances with updated cloud and convection schemes. In addition, a new bias correction to satellite radiances led to improvement in representing magnitude and vertical structure of temperature accurately with respect to the radiosonde observations over the Arctic (Dee and Uppala, 2009). These provide good performance of ERA-Interim in simulating accurate amount and properties of clouds in the Arctic (Dee et al., 2011; Walsh et al., 2009). The ERA-Interim provides two kind of horizontal resolution – full resolution (0.75° by 0.75°) and low resolution (1.5° by 1.5°), and low resolution dataset is used in this study.

The NCEP CFSR, a new reanalysis provided by the NCEP recently, covers the period from the January 1979 to December 2009 with 0.5° by 0.5° horizontal resolution and 37 vertical levels. The NCEP CFSR is produced by a coupled

forecast system model which has T382 (about 38 km) horizontal resolution and hybrid vertical sigma coordinate with 64 levels. The NCEP CFSR has many improvements in data quality by introducing a new satellite bias correction method with direct assimilation of radiances, and in prognostic cloud water from condensation based on diagnostic cloud cover compared to the previous version of the NCEP reanalyses (Saha et al., 2010). A better performance of the cloud data in the reanalysis from the NCEP in the Arctic region has been evaluated in the NARR reanalysis, which has 32 km horizontal resolution but covers limited area of the Arctic (Walsh et al., 2009). The NCEP CFSR also provides various horizontal resolutions – 0.5° by 0.5°, 1.5° by 1.5°, and 2.5° by 2.5°, and we use 2.5° by 2.5° horizontal resolution in this study.

For validation of the used reanalyses, we utilize clouds and surface temperature data from two long-term satellite observations – APP-x (Wang and Key, 2005a) and the Television and Infrared Observation Satellite (TIROS) Operational Vertical Sounder (TOVS) Polar Pathfinder (TPP) (Schweiger et al., 2002). These data were utilized for many previous studies on the Arctic cloud (Eastman and Warren, 2010a; Liu et al., 2007; Liu et al., 2009; Schweiger et al., 2008; Wang and Key, 2003, 2005a, b). The APP-x composites are a collection of products for both poles, consisting of calibrated satellite channel data and derived parameters at a 25 km spatial resolution. Skin temperature, cloud mask,

and clear sky surface albedo are provided from five AVHRR channels for the period 1982–2004. The APP-x provides daily composites at 04:00 and 14:00 local solar time (LST). We use monthly cloud and surface skin temperature data averaged from only 14:00 LST in daily dataset, but results from the data at 04:00 are very similar. The TPP dataset is another long-term satellite observation including atmospheric temperature, water vapor, skin surface temperature, total effective cloud fraction, cloud top pressure and temperature. Data are available for the period 1980–2005 with a resolution of 100 km. We use monthly cloud and surface skin temperature based on 1200 UTC daily values.

For validation of our modeling result, we use modeling outputs from the fifth phase of the Coupled Model Intercomparison Project (CMIP5). We use sea ice concentration and sea surface temperature (SST) in 14 model results from the RCP4.5 future simulation for checking the usability of our polynomial fitting method to generate SST distribution with respect to sea ice distribution. In addition, in order to check whether cloud increases during winter, total cloud amount, surface air temperature, CRF, and sensible and latent fluxes in 30 model results from the PIconrol and RCP4.5 simulations are used. Descriptions of all used CMIP5 models are summarized in Table 2.1.

Table 2.1 Description of the CMIP5 models used in this study.

Model Name	Institute	Country	Resolution
ACCESS1-0	CSIRO-BOM	Australia	192 × 145
ACCESS1-3	CSIRO-BOM	Australia	192 × 145
BCC-CSM1-1	BCC	China	128 × 64
BNU-ESM	BNU	China	128 × 64
CCSM4	NCAR	USA	288 × 192
CESM1-BGC	NSF-DOE-NCAR	USA	288 × 192
CSIRO-Mk3.6	CSIRO-QCCCE	Australia	192 × 96
FGOALS-G2	LASG-CESS	China	128 × 60
GFDL-CM3	NOAA GFDL	USA	144 × 90
GFDL-ESM2G	NOAA GFDL	USA	144 × 90
GFDL-ESM2M	NOAA GFDL	USA	144 × 90
GISS-E2-H	NASA-GISS	USA	144 × 90
GISS-E2-H-CC	NASA-GISS	USA	144 × 90
GISS-E2-R	NASA-GISS	USA	144 × 90
GISS-E2-R-CC	NASA-GISS	USA	144 × 90
HadGEM2-CC	MOHC	UK	192 × 145
HadGEM2-ES	MOHC	UK	192 × 145
INMCM4	INM	Russia	180 × 120
IPSL-CM5A-LR	IPSL	France	96 × 96
IPSL-CM5A-MR	IPSL	France	144 × 143
IPSL-CM5B-LR	IPSL	France	96 × 96
MIROC4h	MIROC	Japan	640 × 320
MIROC5	MIROC	Japan	256 × 128
MIROC-ESM	MIROC	Japan	128 × 64
MIROC-ESM-CHEM	MIROC	Japan	128 × 64
MPI-ESM-LR	MPI-M	Germany	192 × 96
MPI-ESM-MR	MPI-M	Germany	192 × 96
MRI-CGCM3	MRI	Japan	320 × 160
NorESM1-M	NCC	Norway	144 × 96
NorESM1-ME	NCC	Norway	144 × 96

3. MODELING THE ROLE OF VEGETATION ON THE ARCTIC WARMING UNDER GREENHOUSE WARMING

3.1. Vegetation over the high-latitude region and its change

The Arctic and northern high-latitude region have experienced substantial climate warming in recent decades, and its degree and pace is much larger and faster than the global average (ACIA, 2005). The extent of sea ice cover in the Arctic Sea and snow-cover in the sub-Arctic landmasses have reached their lowest recorded levels, and it is likely that associated feedback processes have exacerbated the warming (Chapin et al., 2005; Overpeck et al., 2005; Serreze et al., 2000). Accompanying with this warming is conspicuous change in vegetation in the Arctic and high-latitude regions. Contrasting to our great anxiety to it, anthropogenic climate change seems to provide the vegetation in the harsh Arctic climate environment with more pleasant conditions for living – higher temperature and increased water availability over longer growing season and fertilization by elevated CO₂ level. Much attention has been paid with this vegetation change, because it may, in turn, lead to considerable changes in surface energy budget and hydrological cycle. Therefore it has been widely

perceived that this vegetation-climate feedback has a great potential to alter natural or anthropogenic climate change, having different feedback effects depending on regional vegetation type and climate characteristics (Bonan et al., 1992; Chapin et al., 2005; Folley, 2005; Levis et al., 1999; Notaro and Liu, 2008).

Previous modeling studies have emphasized the potential significance of vegetation feedback on climate model's responses to anthropogenic and natural forcings in recent centuries, and to paleoclimatic perturbations (Bonan et al., 1992; Foley et al., 1994; Notaro et al., 2007). Regarding the recent warming in the Arctic and high-latitude climate, climate models generally indicate that the vegetation changes have a positive feedback effect – more warming with more vegetation growth, which is mainly caused by decreased surface albedo (reflectivity of the surface to sunlight) as relatively darker vegetation cover replaces snow-covered or barren surface of high-reflectivity (Levis et al., 1999; Notaro and Liu, 2008; Notaro et al., 2007; O'ishi and Abe-Ouchi, 2009). In addition, more suggested are an increased greenhouse effect by increased atmospheric water vapor from increased evapotranspiration and more ice-melt in the Arctic reinforcing both the Arctic warming and more vegetation growth (Swann et al., 2009).

Here we present the possible vegetation feedback effect on the Arctic and high-latitude climate under the anthropogenic climate change. Taking advantages

of the vegetation-climate coupled model, the potential vegetation change under doubled CO₂ concentration and its feedback effects on surface temperature and associated energy budgets in the Arctic/high-latitude climate system were investigated. In addition to the local feedback effect, the remote influence of vegetation change on the Arctic sea and sea ice through atmospheric energy transports and associated feedback mechanism are primary foci of present study.

3.2. Modeling vegetation change and its effect under greenhouse warming

For modeling vegetation change and its effect, CAM3, CLM3, and CLM-DGVM are utilized. The mechanistic parameterization of large-scale vegetation processes in CLM-DGVM simulates the distribution and structure of natural vegetation, and therefore synchronous climate-vegetation coupling enables to consider the two-way feedback between climate and vegetation. If not coupled to the CLM-DGVM, the CAM3 and CLM3 can be run with prescribed vegetation, where the fractional distribution of plant species and seasonal cycle of plant's leaf abundance are fixed during model simulation years. We utilized this CCSM3's functionality to be run with/without CLM-DGVM to isolate the vegetation feedback effect.

First, we performed two baseline experiments *P* and *F*, representing

‘Present’ and ‘Future’ respectively. 355 *ppmv* and 710 *ppmv* CO₂ concentration were used for the present and future simulation respectively. Each model simulation was run for 150 model years, and results for the last 30 years are utilized. Then, an additional ‘future’ simulation – *FPV* was performed. The *FPV* is identical to *F* simulation except performed with the prescribed vegetation taken from the *P* simulation. Namely, vegetation change caused by overlying climate change is not allowed in the *FPV* simulation. Therefore the difference between *F* and *FPV* is only contributed by vegetation changes caused by CO₂ doubling. Here we simply estimated the ‘vegetation feedback effect’ under CO₂-doubled climate change as *F* minus *FPV*, and the ‘all effect’ including CO₂-doubling and climate-vegetation feedback effects as *F* minus *P*.

The equilibrium climate sensitivity of annual and global averaged surface air temperature change (Δ SAT) associated with a doubling CO₂ (355 to 710 *ppmv*) was estimated as 2.78°C when all effect was considered (*F* vs. *P*), and 2.51°C when vegetation feedback effect was not considered (*FPV* vs. *P*). Both values are comparable to the sensitivity to a CO₂ doubling estimated by the CCSM3 with full dynamical ocean (without vegetation feedback) – 2.47°C and the transient simulation for IPCC AR4 under A1B emission scenario – 2.78°C (IPCC, 2007; Kiehl et al., 2006). Over the Arctic/high-latitudes (north of 60°N), the Δ SAT change becomes much higher compared to the global average; 5.53°C

when all effect was considered (F vs. P), and 3.92°C when vegetation feedback effect was not considered (FPV vs. P).

3.3. The vegetation change under a doubled CO_2 climate

We first examined potential vegetation over the Arctic and high-latitude region under present (P) and future (F) climate condition simulated by CLM-DGVM (Fig. 3.1). Overall, the replacement of low-vegetated land to densely grass-covered surface and the northward expansion and enhanced growth of boreal trees are salient. Over the northern high-latitude land, where the severe cold climate is the limiting factor for vegetation's growth, all simulated plant species have increased in their areal coverage and leave growth (leaf area index) during the warm season. In particular, increase in the coverage of the Arctic grass (+17%) and boreal deciduous tree species (+10%) are prominent. The most notable change is the encroachment of in the northern parts of continents where the major permafrost regions are located in the present climate. It is likely that the strong surface warming boosts the cold season temperature above the threshold for the establishment and survival of some plants species. Also it is plausible that the increase in available moisture and CO_2 fertilization effect contribute to this remarkable change. A larger CO_2 fertilization effect may have promoted the photosynthetic activity of vegetation owing to more available

moisture supply from the increased precipitation and the thawing of soil-ice in the permafrost region (Lawrence et al., 2008a; Long et al., 2006). But it should be noted that the simulated potential vegetation has discrepancies against observed vegetation. The CLM-DGVM tends to underestimate the forest cover but overestimate grass cover (Bonan and Levis, 2006), and this is also the case in the simulated vegetation in northern high-latitudes. Another important discrepancy is the missing treatment of the shrub species despite of its importance in the vegetation ecosystem in the sub-Arctic region. Recent observation indicated that an explosive shrub encroachment to the Arctic tundra in the northernmost part of continents is one of prominent vegetation change associated with the rapid climate warming (ACIA, 2005; Tape et al., 2006). However, the grass species seem to undertake the shrub's role in the present CLM-DGVM simulation results. Compared to the grass in tundra, shrubs have a lower albedo and a stronger interaction with snow, and therefore give a stronger positive feedback effect on the climate warming (Chapin et al., 2005; Sturm et al., 2001). Despite of these discrepancies, our simulation results indicating more greening in the Arctic/high-latitudes under climatic changes induced by the elevated CO₂ are generally consistent with observed trends and other model's predictions.

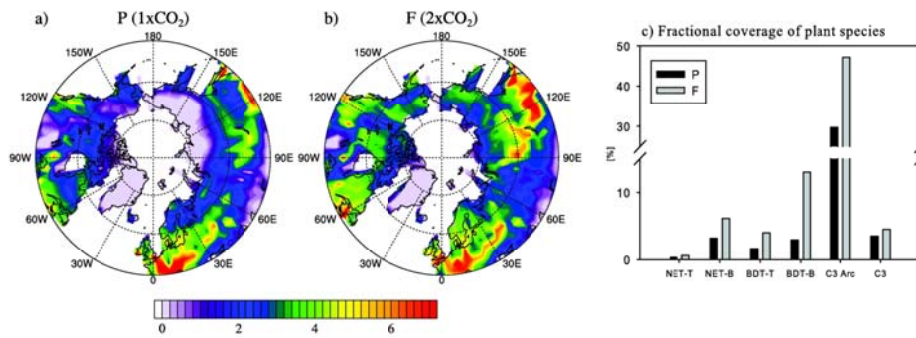


Fig. 3.1 Mean leaf area index (LAI) in growing season (May to September) for a) present (P) and b) future (F) simulation, and c) the fractional coverage of plant species (NET: needleleaf evergreen tree, BDT: broadleaf deciduous tree, C3: grasses with C3 pathway. T, B, and Arc in the suffix indicate temperate, boreal, and the Arctic respectively) over high-latitude, north of 60°N. The LAI represent the leaf abundance, the fractional area of plant's leaf surface relative to the surface area.

3.4. Vegetation feedback effect on SAT and circulation changes

Vegetation change in the high-latitudes induces substantial alternation of climate change in the Arctic/high-latitude in the warming seasons through winter. Figure 3.2 compares the simulated SAT changes under a doubling CO₂ concentration with/without the interactive vegetation. When the interactive vegetation is included in the future climate simulation, the warming in high-latitude continent appears to be substantially amplified. In summer, additional 2 to 3°K warming can be detectable over northern high-latitudes area where the major vegetation change is found. In autumn, this vegetation-related additional warming in land region becomes weaker, but it spreads over the entire Arctic sea. Seen from the direct estimation of vegetation feedback effect ($F\text{-FPV}$) on the zonal mean ΔSAT , interestingly, vegetation-related warm shows a northward propagation pattern of the warm season warming in high-latitude toward the Arctic region in autumn through winter.

The warming in spring to summer is mostly contributed by a great increase of absorbed shortwave radiation (SW, solar radiation) at surface: +6.93 W/m² in MAM and +16.82 W/m² in JJA. With relatively smaller increase net longwave radiation (LW, terrestrial radiation): -1.84 W/m² in MAM and -6.52 W/m² in JJA, the net absorbed radiation increases is +5.09 W/m² in MAM and +10.3 W/m² in JJA at surface. These surplus radiative energy is mostly transferred to sensible

(MAM: +1.12 and JJA: +5.08 W/m²) and latent heat (MAM: +2.31 and JJA: +6.47 W/m²) increases, which contributes to the strong surface warming (+1.58 and +2.53°K for land north of 60°N). In spring to early summer, the surface albedo decrease (-7.34% in MAM) by the replacement of snow-covered surface by vegetation (-6.17% snowcover change in MAM) appear to induce the increased absorption of SW at surface. The low cloud change associated with vegetation feedback effect seems to be another contributor to the increased SW absorption particularly in summer. Because low cloud has high-reflectivity to incoming SW, the notable decrease in low cloud in summer (-8.85%) may lead to more incoming SW at surface. We also note that high cloud amount slightly increases over all seasons, but is thought to be effective on the LW change. Being almost transparent to SW radiation, high cloud is known to invoke greenhouse effect by absorbing and re-emitting LW radiation (Vavrus, 2004). Thus high cloud increase seems to partly offset the increased LW emission at warmer and less ice-covered surface, which may also contribute surface warming.

The vegetation-induced changes are not only confined to near-surface, but significantly alter the tropospheric temperature and associated atmospheric circulation. Figure 3.3 represent vertical structure of temperature and zonal wind change associated with vegetation feedback effect. In summer, the vegetation-induced near-surface warming well extends above to mid-troposphere and also

northward over the Arctic sea; about 1.5°C air temperature increase can be found almost at 400 hPa in the Arctic/high-latitudes. Probably relatively weak vertical atmospheric stability in summer leads to the upward energy transport by vertical mixing process, while it is highly prevented by the strong atmospheric stability in the Arctic climate system during the rest of year. There is relatively modest warming at the near surface in the Arctic sea, which implies the large consumption of energy to melt sea ice and warm the upper ocean (Serreze and Francis, 2006). In autumn, the lower- to mid-tropospheric warming originated from high-latitude land surface is almost vanished, but substantial warming is found over the Arctic sea ice, mostly confined near surface. This lower-tropospheric warming pattern evokes the typical characteristic of the Arctic amplification when sea ice feedback mechanism provokes the near surface warming in cold season. Namely, as the Arctic atmosphere becomes very stably stratified, weak atmospheric vertical mixing traps the large warming signal to near surface. Accompanying with this tropospheric temperature change, the atmospheric zonal wind shows substantial change. Overall pattern is the weakening of tropospheric westerlies in the mid- to high-latitude in the south of maximum warming. As the center of maximum warming moves to the Arctic in autumn, the negative zonal mean wind pattern also moves northward. The change in westerlies and warming seems to be well consistent with the thermal

wind relationship. Also expected is the positive geopotential height (or pressure) anomaly in the mid- to high-latitudes, which may also contribute the decrease of low cloud in summer.

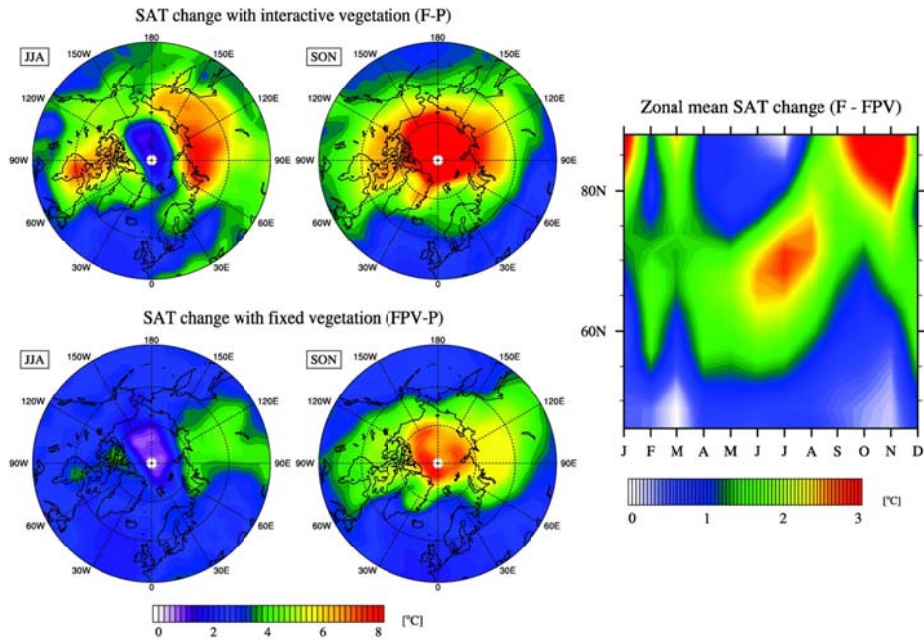


Fig. 3.2 (left panel) SAT difference between F and P simulation (upper) and FPV and P simulation (lower). (right panel) zonal mean of SAT difference between F and FPV simulation.

Zonal mean T and U difference (F - FPV)

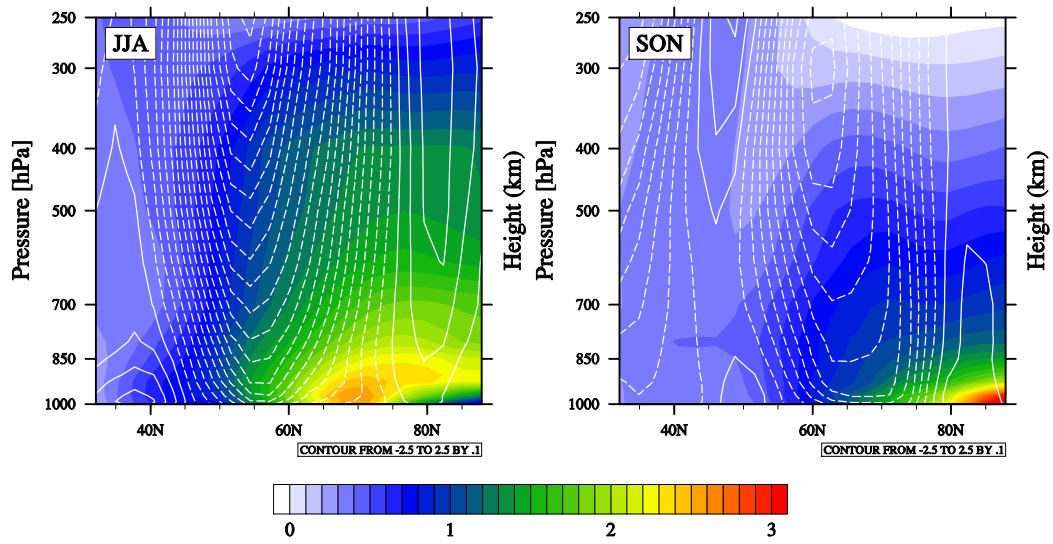


Fig. 3.3 Zonal mean temperature (shading) and u-wind (contour) changes by vegetation feedback effect (F - FPV) in JJA and SON.

3.5. Sea ice change and atmospheric northward energy transport

Easily expected from the temperature change, the Arctic sea ice exhibits considerable decline both in areal extent and thickness associated with the vegetation feedback effect. Much more decrease in sea ice extent and thickness are found owing to vegetation feedback effect (Figure 3.4 and Table 3.1). The greatest change in the Arctic sea ice is found in autumn, when the extent and thickness of sea ice reaches its minimum in a year, showing about 24% and -13cm decrease in areal extent and thickness respectively. The direct cause of this sea ice change may lie in the warmer atmospheric air (JJA: 1.60°K and SON: 2.15°K) and warmer ocean (JJA: 1.48°K and SON: 0.93°K). In summer, the positive feedback between the reduced sea ice extent (-10.57%) and more absorbed SW radiation (9.61 W/m²) may give the largest effect on the oceanic temperature rise, whereas the negative feedback effect from increased surface LW radiation is relatively modest (-1.43 W/m²). As a consequence, more latent heat (3.13 W/m²) and sensible heat (0.80 W/m²) release are emitted from the warmer and more opened Arctic Ocean. It is obvious that such energy fluxes associated with sea ice changes eventually cause the near-surface warming, of which processes exhibit a typical mechanism of sea ice feedback to invoke the Arctic amplification of surface warming.

Given that the horizontal energy transport within land surface is almost

negligible, the atmospheric transport of excess heat to the Arctic region could be the only mechanism to connect the vegetation-related warming in the continents with the remote changes in the Arctic sea. Actually, atmospheric circulation change and associated energy transports are important process accounting for the amplification of tropospheric warming in the Arctic region (Graversen, 2006; Graversen and Wang, 2009; Serreze and Francis, 2006). Figure 3.5 shows the tropospheric northward atmospheric energy transport (NET) change by the vegetation feedback effect. Zonal mean change of NET pattern appears well consistent with temperature change; the maximum NET occurs over and to the north of surface warming in the high-latitude land from spring through summer. This indicates that the surplus sensible energy and moisture from the increased vegetation activity are transported by atmosphere, presumably through strong atmospheric eddy activities in the high-latitudes. Seen at 70°N roughly about boundary between the Arctic sea and surrounding continents, the contribution of internal energy transport explains about half of total NET change, and the latent and potential energy transport explain the other half. Like as the temperature change, the increased NET well extends to mid- to upper-troposphere in summer (Fig. 3.6), which may contribute the considerable warming in the mid to upper troposphere in the Arctic region as well as near surface warming.

The maximum of NET increase is in summer but that of Arctic warming

occurs in autumn through winter. This lagged response is related with the seasonal cycle of the Arctic sea ice and associated the latent heat release/absorption. As the Arctic sea ice reaches its minimum around in September to October both in areal extent and thickness, the large amount of surplus energy input by NET in summer is consumed by the heat absorption to melt the Arctic sea ice as well as to warm the upper ocean. We estimated the latent heat content change by the Arctic sea ice loss associated with the vegetation feedback, manifested as an equivalent temperature change attained if the latent energy is used to warm the upper mixed layer of the Arctic Ocean. The heat content change by sea ice is found to be substantial; it is estimated as larger than that by warming of mixed layer ocean throughout a year. The maximum occurs in summer when the NET is largest in the Arctic region, and become smaller in winter through spring. Recalling that the Arctic sea ice begins to refreeze from mid-autumn, this is consistent with the less sea ice refreezing in the cold season.

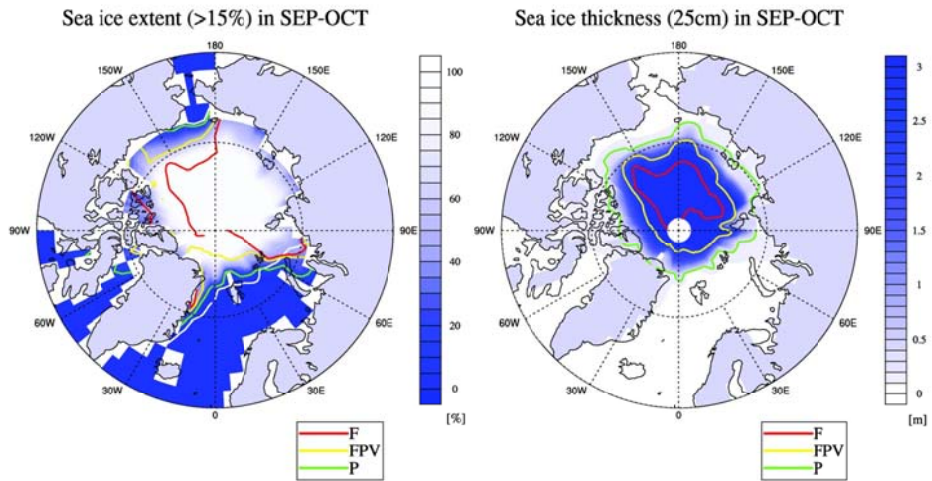


Fig. 3.4 Shading indicates simulated average sea ice extent and thickness for September to October in *P* simulation. Lines in the left panel indicate sea ice extents where the ocean is covered with more than 15% sea ice. White line is the observed sea ice extent averaged from 1981-2000 HadISST data. Lines in the right panel indicate 25cm levels of mean sea ice thickness.

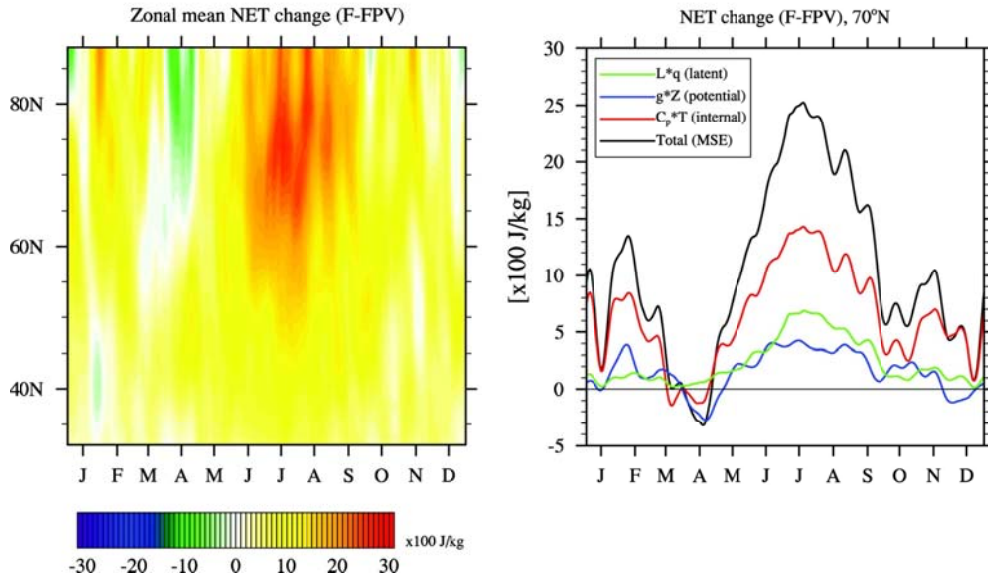


Fig. 3.5 (left panel) *NET* change by vegetation feedback effect (*F-FPV*). (right panel) changes in the components of *NET* at 70°N. 10-day running average is applied for the time dimension. Here atmospheric energy is estimated by moist static energy – summation of atmospheric latent, potential, and internal energy.

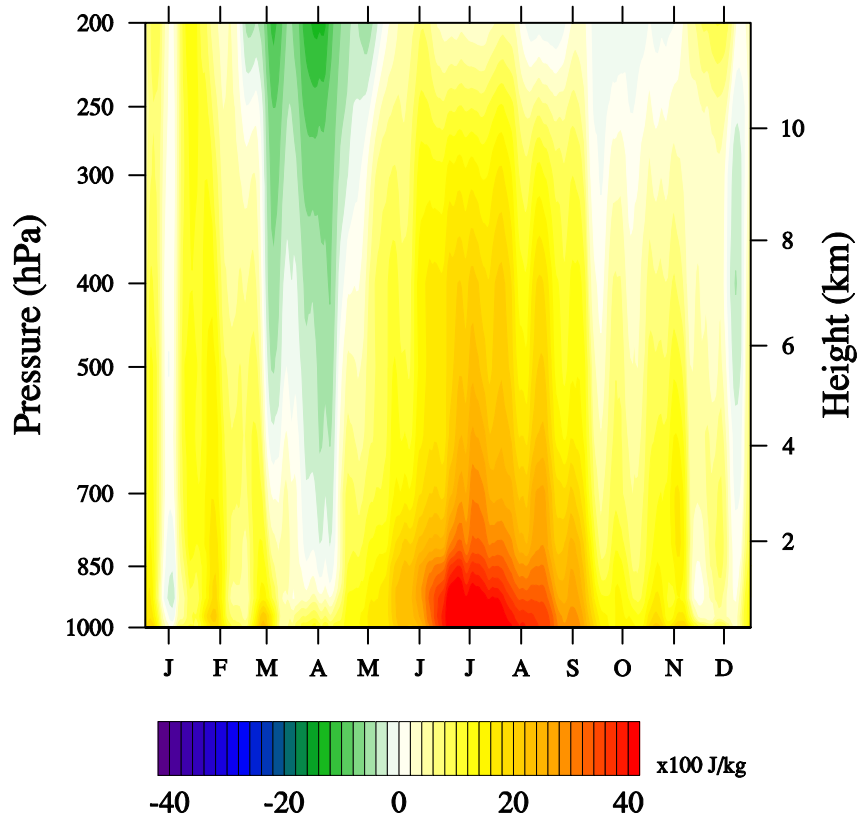


Fig. 3.6 Zonal mean NET change by vegetation feedback effect ($F-FPV$).

Table 3.1 Change in model simulated variables by vegetation feedback effect (*F-FPV*).

Variables	High-latitude land (north of 60°N)				Arctic sea (north of 70°N)			
	MAM	JJA	SON	DJF	MAM	JJA	SON	DJF
Sfc air temperature [K]	1.58	2.53	1.28	1.46	1.24	1.60	2.15	1.37
Net SW [Wm^{-2}]	6.93	16.82	0.24	0.22	1.72	9.61	0.49	0.00
Net LW [Wm^{-2}]	-1.84	-6.52	0.28	0.40	-0.23	-1.43	-0.99	-1.08
Latent heat [Wm^{-2}]	2.31	6.47	1.59	0.65	1.02	3.13	1.79	1.51
Sensible heat [Wm^{-2}]	1.12	5.08	-0.54	-0.13	-0.09	0.80	-0.35	0.75
Low cloud [%]	-1.93	-8.85	0.41	1.21	0.24	-2.21	0.40	-0.05
High cloud [%]	2.00	1.71	1.51	1.24	1.35	1.41	0.35	0.65
Sea ice extent [%]	-	-	-	-	-0.86	-10.57	-24.13	-1.64
Sea ice thickness [cm]	-	-	-	-	-7.64	-14.42	-13.37	-9.50
Oceanic temperature [K]	-	-	-	-	0.15	1.48	0.93	0.18
Snowcover fraction [%]	-6.17	-2.49	-3.46	-2.59	-	-	-	-

Values represent the climatological mean difference between the F and FPV simulation.

3.6. Discussion

Present modeling results clearly demonstrated that conspicuous climatic change can be arisen in the Arctic region from the vegetation-climate feedback. However, it should be noted again that the simulated vegetation and its change could be highly model-dependant, and limitations of CLM-DGVM restrict the direct application of present results to recorded climate change. Above all, anthropogenic vegetation change is not considered in the chosen modeling system. Because the CLM-DGVM only simulates the ‘potential’ vegetation under idealized present and future conditions, vegetation change from urbanization, deforestation, and cultivation were not taken into account despite of its huge impacts on the local vegetation biosphere. Also important limitation to note is that the carbon cycle is not considered in the present modeling system, despites profound impacts are anticipated in company with vegetation change. In the Arctic climate system, for instance, the enhanced carbon uptake by more vegetation activity may counteract the warming, and also possible is that the methane release from vegetation activity and accelerated thawing of permafrost may amplify the warming. There are still many controversial issues on the ecosystem-climate interaction under climate change, that need to be further accessed in order to increase the fidelity of our climate prediction. In addition, limitations also lie in the utilization of SOM instead of full-depth ocean

dynamics. Either possible changes in meridional transport of energy by ocean circulation or the redistribution of sea ice were not simulated, although it has a great potential to affect the vegetation-climate feedback process.

Most climate models underestimate the surface warming and Arctic sea ice loss in recent decades after late 1990s. This partly seems to be due to unrealistic, excessive negative LW feedback of climate models (Boe et al., 2009), but the reason is still controversial (Rampal et al., 2011; Stroeve et al., 2007; Winton, 2011). Our finding implies that the exclusion of vegetation-feedback in climate model can be one of underlying causes. This could not be examined due to the limitation of experiment design, but the transient simulations with fully-coupled ocean model may address this issue.

4. MODELING THE ROLE OF CLOUD ON THE RECENT ARCTIC WARMING DURING WINTER

4.1. Recent change in the winter Arctic cloud

The existence of cloud has immediate impacts on the surface radiation balance. Due to its unique physical properties, clouds tend to warm the surface by absorbing and re-emitting longwave radiation from the Earth's surface. At the same time, clouds have cooling effect by reflecting incoming shortwave radiation from space. These radiative properties of cloud are known to be very important for the Arctic climate and weather system and its change (Curry et al., 1996). Clouds cover the Arctic region by more than 50% throughout the year (Eastman and Warren, 2010a), interacting with other atmospheric and oceanic variables of Arctic climate system (Francis and Hunter, 2006; Schweiger et al., 2008). During the wintertime over Arctic region, net cloud radiative forcing (CRF) at surface is about $+20 \text{ W m}^{-2}$ in spite of nearly zero incoming solar radiation, which is due to the strong long wave radiative effect of Arctic cloud (Shupe and Intrieri, 2004). Therefore wintertime surface air temperature is largely controlled by Arctic clouds and a coherent change of Arctic clouds and surface temperature has been suggested by various observations. For instance,

Wang and Key (2003) reported that the both Arctic clouds and surface temperature have decreased by $-5.7 \text{ \% decade}^{-1}$ and $-0.34 \text{ K decade}^{-1}$, respectively, for the period 1982–1999 from APP-x data. Liu et al. (2009) found that change in Arctic clouds accounts for a cooling trend at surface at a rate of $-0.91 \text{ K decade}^{-1}$ for the period 1982–2004 from the same satellite product.

On the other hand, Arctic clouds are greatly affected by surface conditions as well. Curry et al. (1996) showed that the formation of Arctic clouds is enhanced by surface warming through enhanced turbulent heat fluxes and horizontal and vertical advection, suggesting a positive feedback effect to surface temperature. Vavrus (2004) argued that this positive feedback process plays a crucial role in amplifying Arctic warming under increased greenhouse forcing. Other studies have noted that variation of winter Arctic clouds in recent decades was much affected by large-scale atmospheric circulation in addition to the radiative feedback effect; Liu et al. (2007) showed that moisture convergence induced by large-scale atmospheric circulation change over the Nansen Basin and the Barents and Kara Seas had significant impacts on Arctic clouds during 1982–2000. Eastman and Warren (2010b) noted that the cloudiness in the Arctic is highly associated with the variation of Arctic Oscillation (AO) (Thompson and Wallace, 1998), a hemispheric pattern of atmospheric circulation anomalies.

Since the late 1990s, the Arctic climate has been exposed to radical changes.

The accelerated melting of sea ice and associated ice-albedo feedback led to considerable warming throughout the troposphere (Screen and Simmonds, 2010a) and even caused hemispheric-scale atmospheric circulation changes (Francis et al., 2009; Overland and Wang, 2010). These changes are conspicuous especially during early winter (Screen and Simmonds, 2010b). Numerous studies pointed out the cloud as possible cause for amplifying the Arctic warming in winter because cloud-radiative feedback process works positively due to absence of solar radiation (Graversen et al., 2008; Graversen and Wang, 2009; Palm et al., 2010).

However, previous studies for the Arctic cloud with respect to recent Arctic climate change have been concentrated in melting season although winter Arctic cloud could play a crucial role on the recent Arctic warming (Cuzzone and Vavrus, 2011; Kay and Gettelman, 2009; Palm et al., 2010; Schweiger et al., 2008). Accordingly, whereas much of role of Arctic sea ice loss for the associated changes in Arctic clouds in melting season have been investigated, the change in cloud and its impact on the Arctic climate system according to recent Arctic change during winter still remains poorly understood. Thus it is necessary to more understand the change and effect of winter Arctic cloud in recent Arctic climate.

The lack of study on winter Arctic cloud is mainly due to harmful weather and climate condition in Arctic winter (ACIA, 2005). Examining changes in

clouds and its feedback in winter is very difficult because extremely cold and dry conditions lead to large detection error in observation. Still there is large discrepancy in the interannual variation and even long-term trends of cloud cover observations among different satellites and surface measurement (Eastman and Warren, 2010a). In addition, the extreme condition also gives uncertainty to modeling for simulating the Arctic cloud (Vavrus and Waliser, 2008; Walsh et al., 2005).

Considering the uncertainties in cloud data from satellite products, cloud information from the reanalysis might be a useful complementary to study the Arctic clouds and associated feedback effects. Schweiger et al. (2008), for instance, used cloud data from the 40-yr the ECMWF Re-Analysis (ERA40) (Uppala et al., 2005) to investigate the relationship between the sea ice and cloud cover during autumn. Walsh et al. (2009) compared the fraction and radiative forcing of Arctic clouds estimated from four different reanalysis datasets with an observational dataset from the Atmospheric Radiation Measurement Program (ARM) (Stokes and Schwartz, 1994). They suggested that the reanalysis models could simulate cloud radiative forcing correctly when the cloud amount was simulated correctly.

Thus we examine the variation of Arctic clouds during winter (December through February) for the recent 3 decades from two reanalyses: ERA-Interim

reanalysis and NCEP CFSR. Long-term trends in Arctic cloud for the recent decades, and coherent changes in atmospheric variables (e.g., temperature and moisture) and large-scale atmospheric circulations are examined.

4.1.1. Year-to-year variation and trends in cloud-related variables

We examine overall changes in total cloud cover, surface temperature and sea ice cover during winter over the Arctic Ocean (oceanic and sea ice covered region in the north of 67°N), and AO index for last three decades (Fig. 4.1). The trends in cloud amount and surface temperature from all datasets are summarized in Tables 4.1 and 4.2. In considering the large differences in the mean and variability among the dataset (Table 4.1), each time-series in Fig. 4.1 is re-scaled to have the mean and standard deviation of the ERA-Interim for the period 1979–2011 for comparison. The most notable feature of the Arctic cloud amount variation for the analysis period is the long-term trend change occurred around the end of the 20th century. The Arctic cloud amount showed a clear negative trend for the last two decades in the 20th century but it was turned to a positive trend around the 2000s. Although the interannual variation of the Arctic cloud amount exhibits little consistency among datasets, even between two satellites ($r = -0.08$ for the period 1982–2004), these long-term trends and their changes agree fairly well with each other only except the APP-x which shows continuous

decrease until the mid 2000s. The variations in surface temperature and sea ice fraction are negatively correlated ($r = -0.86$ in the ERA-Interim and -0.80 in the NCEP CFSR). Interestingly, the surface temperature and sea ice cover in the Arctic seem to also have a notable trend change concurrent with the cloud amount. There was a weak decreasing (increasing) or nearly neutral trend in surface temperature (sea ice cover) for the 1980s to 1997 but it was replaced by a strong increasing (decreasing) trend from 1998 to 2011. This is commonly found in the both reanalyses. Here the APP-x again exhibits quite different long-term variation from other datasets.

We check whether there actually exists trend change in these year-to-year variations in late 1990s by performing the change point analysis (Tomé and Miranda, 2004). As a result, year-to-year variations of cloud amount, surface temperature, and sea ice cover have breakpoints to trend changes in late 1990s. In variation of the cloud, trend is changed in 1997 (NCEP CFSR) and 2000 (ERA-Interim). The trends of surface temperature and sea ice cover from both reanalyses also are changed in 1997 and 1998, respectively. Considering the concurrent trend changes in cloud and surface temperature around year 1997 and 1998, we divide whole period into two periods including the late 20th century (1979–1997, hereinafter L20C) and including the early 21st century (1998–present, hereinafter E21C).

In spatial distributions of linear trends in clouds over the Arctic during both L20C and E21C, clear trend changes appear between two periods (Figs. 4.2a–b, and 4.2e–f). Both reanalyses show consistent significant decrease in cloud amount over the Kara Sea, Laptev Sea, East Siberian Sea, north of the Queen Elizabeth Islands and central Arctic for the L20C, but the tendency is larger in the ERA-Interim. Satellite datasets also show similar decrease over the Arctic for the same period. In the E21C both reanalyses show increasing cloud amount over the most of the Arctic Ocean but regions of large increase slightly differ between the two reanalyses. The ERA-Interim shows significant increasing trend over the Kara Sea, Laptev Sea, East Siberian Sea, north of the Queen Elizabeth Islands, and Baffin Bay, but the NCEP CSFR does not show significant increasing trend mostly over the Kara Sea, north of the Queen Elizabeth Islands, Baffin Bay. The difference in significant regions for the E21C may be partly due to slightly different periods in two reanalyses (the ERA-Interim covers three more years: 2009–2011); the statistically significant regions for the period 1998–2008 are more similar.

Spatial pattern and strength of the cloud amount change consort with surface air temperature (SAT; 2-meter air temperature) changes in the Arctic Ocean (Figs. 4.2c–d, and 4.2g–h). Surface skin temperature is used in Fig. 4.1 for the comparison with satellite data, but we hereinafter use SAT rather than

surface skin temperature. During the L20C, both reanalyses show general cooling trend over the Arctic Ocean with significant cooling over the central Arctic, north of Queen Elizabeth Islands, East Siberian Sea, and Chukchi Sea. In the E21C, SAT shows prominent warming trend over the most Arctic Ocean and also over high-latitude continents. The significant warming trend is found over the Kara, East Siberian, and Chukchi Seas, and northern Greenland in both reanalyses (Figs. 4.2d and 4.2h). Most of these regions also are experiencing large sea ice retreat (see region with oblique lines in Fig. 4.2). However, very strong warming trend is found over the Barents Sea in both datasets, where a prominent decrease in sea ice is found in winter (Cavalieri and Parkinson, 2012), while vivid increasing in total cloud amount is not found over this region. Over this region, low level cloud cover decreases while mid level cloud increases during the E21C (figure not shown). Schweiger et al. (2008) suggested that less sea ice cover could affect decreasing in low level cloud and increasing in mid level cloud through changing in boundary layer height and static stability during autumn. The Barents Sea is relatively warmer than other Arctic regions because it is located at the location contacting with warm Atlantic water. In addition, over the Barents Sea, the PBL height increases and static stability decreases significantly during the E21C. Consequently, similar mechanism may underlie between changes in total cloud cover and SAT.

Trends in vertical distribution of zonal-averaged temperature, specific humidity, and cloud water content also show that there are gradual decreasing during the L20C and large increasing during E21C over the Arctic (Fig. 4.3). Although vertical distributions in temperature from two reanalyses are slightly different during L20C in weak warming region, weak cooling is dominant whole troposphere over the Arctic. The weak cooling trend over the Arctic is changed to substantial warming trend with particularly strong warming at near surface in the vicinity of 80°N during the E21C. This strong increasing at near surface is also found in the trend of specific humidity for same period. During the E21C, vigorous moistening trend occurs at surface over the 70-80°N and spreads to entire lower troposphere over the Arctic while weak drying trend is found at lower troposphere.

Changes in cloud properties are also observed mainly at the lower troposphere with the same manner of moisture change. In particular, vertical distributions of trends in cloud water content along with latitude in both reanalyses and both periods are almost analogous to each other. Trends during the L20C from both reanalyses reveal weak decreasing at near surface over around 70°N and relatively stronger decreasing over central Arctic (80–90°N). A spatial distribution of trend in cloud cover is consistent with cloud water content; strong decrease occurs primarily at near surface over the central Arctic. During

the E21C, explosive increasing in cloud water content compared to change in the L20C occurs at lower troposphere and the increasing spreads to mid-troposphere. In particular, both reanalyses show that cloud water content increases mainly at altitude of around 900 hPa over the most Arctic region. In addition, cloud water content above 900 hPa to about 500 hPa is also largely increasing. Meanwhile, the differences between reanalyses are observed at surface over central Arctic with larger amount of observed in the ERA-Interim.

The major distinctions in cloud change between in the E21C compared to the L20C are the different trend and vertical extent of cloud water content. The gradual decrease and steep increase are also observed in temperature and moisture change. However, spatial pattern in cloud water content change resembles that of humidity more than temperature. This implies that cloud trend might be closely linked to variation of moisture budget over the Arctic. Previous studies have noted this relationship; moisture inflow to the Arctic could be primarily attributable to cloud variation (Beesley and Moritz, 1999; Curry et al., 1996; Liu et al., 2007). Thus, we examine the contribution of moisture transport to the Arctic Ocean through northward moisture transport ($\bar{v}\bar{q} + v'q'$) at 67°N. Properly, as expected, the variation in total moisture inflow to the Arctic at 67°N with height resembles that in moisture over the Arctic (Fig. 4.4). In particular, moisture transport also presents largely increasing after winter of 1997/1998.

Tendency to vertical extension in cloud water content implies that other cloud type besides stratiform cloud can be more formed. Eastman and Warren (2010b) found that an increasing in formation of cumulonimbus and stratus over the Arctic Ocean is correlated with sea ice reduce even in winter based on long-term surface observation. They found that this kind of cloud type increases under low-ice cover winter by comparing cases in low-ice covered years and high-ice covered years. Thus, considering recent substantially reduced sea ice, the increasing in cloud water content during the E21C might indicate increases in low level stratus at about 900 hPa and cumulonimbus above 900 hPa.

Trend changes in precipitation and evaporation over the Arctic Ocean also suggest the possibility of increasing in cumulonimbus. Figure 4.5 shows spatial distribution of changing trend of evaporation and total precipitation over the Arctic Ocean during each period. Both evaporation and precipitation show decreasing during L20C and increasing during E21C over the most Arctic Ocean similarly with temperature and cloud amount. Trend in precipitation change appear more largely than evaporation for both periods, and this tendency that precipitation is larger than evaporation becomes stronger during the E21C. Difference between precipitation and evaporation averaged over the Arctic Ocean increases during the E21C. This also implies that formation of precipitating cloud such as cumulonimbus and nimbostratus increases during this

period.

Moreover, the spatial distributions of trend in evaporation and precipitation during the E21C are almost analogous to each other. Significant increasing in both variables emerges over the Kara, Laptev, East Siberian, and Chukchi Seas. These coherent changes in evaporation and precipitation are different from the L20C. This suggests that local hydrological cycle is being enhanced during the E21C. Additionally, the region where total cloud cover increases significantly is also consistent to these regions (Fig. 4.2). In this process, the relationship between cloud and surface condition could be closer through enhanced local hydrological cycle. We also find that the coherent change between SAT and cloud is being tightened in the E21C in Fig. 4.1. Correlation coefficients between SAT and cloud amount averaged over the Arctic Ocean increase in the E21C compared to the L20C: 0.68 to 0.81 in the ERA-Interim, 0.42 to 0.66 in the CFSR. Furthermore, the changing trends in the E21C also become larger than those in the L20C (Tables 4.1 and 4.2). Major underlying physical basis for the coherent changes in SAT and cloud cover is the cloud radiative effect (Liu et al., 2008; Wang and Key, 2005a). However, it can be suggested that the other factors such as the large-scale circulation change and substantial sea ice retreat can affect the tightened coherent change in SAT and cloud in the E21C.

4.1.2. Effect of AO on the change in Arctic cloud

The large-scale advective process also contributes to the variation of Arctic cloud in addition to local feedback processes (Eastman and Warren, 2010b; Liu et al., 2007; Wang and Key, 2005b). Thus, cloud change between the L20C and E21C also could be affected by the large-scale atmospheric circulation change. In particular, during the E21C, the large-scale circulation also has shown a notable change in association with sea ice melting (Overland and Wang, 2010). The AO, which represents the variation of large-scale atmospheric circulation over the Arctic, turned into opposite phase in this period (Stroeve et al., 2011). This implies that the phase change in the AO could affect trend change between two periods. Therefore, we examine the relationship between the Arctic cloud and the AO and its changes between two periods.

In the last three decades, the AO showed a clear interdecadal variation. The positive AO phase was dominant during the L20C including prominent positive trend from the 1980s to 1990s. However, the trend was sharply changed to neutral to weak negative in the 2000s and extreme negative AO in the recent years (Fig. 4.1d). The change in temperature-cloud relationship between two periods could be affected by the change in AO phase due to vertical and horizontal moisture flux associated with the AO.

In the both reanalyses the AO index is positively correlated with cloud water

content over mid- and upper troposphere and negatively correlated with that at near surface (Figs. 4.6a and 4.6d) and similarly with surface observation from Eastman and Warren (2010b). This contrasting relationship between low and upper tropospheric cloud is equally found in both L20C and E21C periods, suggesting that intrinsic relationship between cloud and the AO might be not much affected by recent changes in large-scale circulation and surface conditions. Examining moisture fluxes associated with AO, it seems that that lower clouds are affected more by horizontal moisture flux while upper clouds are affected more by vertical moisture flux from the lowest level of troposphere (Figs. 4.6b–c, and e–f). The horizontal moisture convergence is negatively correlated with the AO at the lower troposphere over the subarctic latitudes (60–75°N). In contrast, vertical moisture transport is positively correlated with the AO over the sub Arctic (60–75°N) and central Arctic (80–90°N) at the whole troposphere. This is associated with the low (high) pressure anomalies in the positive (negative) AO phase. The anomalous low pressure above planetary boundary layers supports lifting of moisture but leads to the divergence in the sub Arctic. This can strengthen cloud formation above near surface over the central Arctic while horizontal moisture divergence at lower troposphere decreases low clouds.

In the same manner to relationship between cloud water content and AO index, the moisture transport associated with the AO presented in Fig. 4.6 is also

found in both L20C and E21C periods. Namely, AO-related moisture transport does not change between two periods. This suggests that the AO contributes to the interannual variation of cloud mainly through its phase; the phase of wintertime AO changed from negative to positive in the L20C, but it was changed to decreasing trend in the E21C. Because low-level cloud mostly accounts for the total cloud amount, low-level moisture convergence associated with the AO might be mainly linked to cloud change in each period. In addition, it also suggests that the AO-related moisture transport has a weak effect on change in cloud and its relation to surrounding atmospheric states.

4.1.3. Effect of sea ice retreat on recent changes in Arctic cloud

The recent change in Arctic cloud during the E21C seems to be more linked to the change in Arctic surface than change in large-scale circulation represented with AO. This implies that change during the E21C could be more directly linked with accelerated sea ice retreat. Therefore, we examine change in cloud water content and upward moisture transport in relation to sea ice cover during the two periods. To minimize the correlation from the AO, we calculated the partial correlation between sea ice cover averaged over the Arctic Ocean and zonal-averaged cloud water content/upward moisture transport independent from the AO index during the L20C and E21C. First, cloud water content at troposphere is

tightly associated with sea ice fraction over the Arctic Ocean for the both L20C and E21C (Fig. 4.7). In particular, cloud water content at lower troposphere below 700 hPa is more closely linked to surface conditions. Surface evaporation, horizontal moisture flux, and longwave CRF may be major causes for this binding at lower troposphere (Beesley and Moritz, 1999; Shupe and Intrieri, 2004).

Comparing relationships between the L20C and E21C, strengthening of relationship over the local Arctic occurs for the E21C. At lower troposphere, significantly correlated region over the Arctic margin during the L20C moves and extends to the central Arctic during the E21C. Contrastingly, significant correlation between cloud water content and sea ice reduction at most troposphere over the Arctic margin (70–80°N) during the L20C disappears in the E21C. In addition, cloud water content at upper troposphere above 700 hPa over the central Arctic (80–90°N) is positively correlated to sea ice during the L20C (Figs. 6a and 6c), but it becomes to be negatively correlated to sea ice during the E21C same as cloud water content at the Arctic margin (Figs. 6b and 6d). Namely, during the E21C, the effect of sea ice on cloud at lower troposphere over the central Arctic becomes to be reinforced while effect on upper troposphere over the Arctic becomes weaker.

On the relationship of sea ice fraction with cloud water content, vertical

moisture transport seems to play an important role (see contour in Fig. 4.7). During the L20C, upward moisture transport is positively correlated with sea ice reduction over the Arctic margin, and negatively correlated over the central Arctic in common to correlation of cloud water content. It seems to be plausible that the ice-reduced surface condition might be linked to the increase in cloud water content through upward moisture transport. In addition, the significant linkages among sea ice reduction, cloud water content and vertical moisture flux at near the top of troposphere bring the hint of the possibility that these linkages are bound under large-scale circulation during the L20C. During the E21C, the influence of sea ice on vertical moisture transport move to the higher Arctic (75–90°N). The northward expansion of correlated region to higher Arctic is also seen in cloud water content. In addition, the change in upward moisture transport related to sea ice during the E21C is also consistent with the vertical expansion in cloud water content during the E21C in Fig. 4.3. Perhaps, enhanced upward moisture transport over this region might contribute to an increase in cumulonimbus over the Arctic.

The change in upward moisture transport related to sea ice during the E21C suggests that there could be surface condition change which enhances upward moisture transport over the central Arctic. At the surface, a decreasing in static stability and deepening in planetary boundary layer (PBL) could contribute to

this change as suggested for autumn by Schweiger et al. (2008). In Fig. 4.8, we examine changes in 850 hPa thickness ($\theta_{850 \text{ hPa}} - \theta_{1000 \text{ hPa}}$) and PBL height between the E21C and L20C. It is found that 850 hPa thickness and PBL height averaged for the E21C are larger than those for the L20C over the most Arctic Ocean. In particular, both reanalyses show that the Barents Sea, which region sea ice cover reduces substantially during the E21C, experiences significant changes in thickness and PBL height. These indicate that sea ice retreat induces increasing in PBL height and decreasing in static stability (increasing in thickness) even during winter. This also implies that upward moisture transport might be enhanced corresponding to these changes.

Meanwhile, two reanalyses show slightly different features over the Arctic Ocean except the Barents Sea. Although the ERA-Interim shows that atmospheric thickness expansion during the E21C occurs significantly over the most Arctic Ocean and PBL height increases over the Eurasian margins of the Arctic Ocean (Figs. 4.8a and 4.8b), the CFSR shows that the increases in atmospheric thickness and PBL height are limited in the vicinity of the Barents Sea (Figs. 4.8e and 4.8f). The discrepancy between two datasets seems to be mainly due to difference in sea ice change between two datasets. First, the ERA-Interim has three more years which period has experienced substantial sea ice retreat than the CFSR. In addition, the CFSR has less sea ice cover over the

Arctic than ERA-Interim during the L20C (Fig. 4.1c). Consequently, an amount of reduce sea ice during the E21C is smaller in the CFSR than the ERA-Interim. As a result, weaker changes at surface appear in the CFSR compared to the ERA-Interim. However, despite of this discrepancy, the relationship between sea ice retreat and near surface change is found consistently in both datasets. The increases in PBL height and atmospheric thickness are mainly found in sea ice retreated regions in each datasets (contour in Figs. 4.8b and 4.8f).

In addition, alterations in surface condition and cloud amount could bring a change in effect of cloud on surface, and this could amplify the change at surface. Figures 4.8c and 4.8g present the difference in CRF between two periods. Both datasets show that significant increase in CRF during the E21C occurs over the Barents Sea. As examined with PBL height and atmospheric thickness, this region has experienced substantial surface warming and consequent surface condition change due to sea ice retreat. According to surface warming outgoing longwave radiation increases, thus CRF increases because of more trapping increased longwave radiation by cloud. In addition, increased cloud amount also reinforces CRF. Consequently, the surface, in turn, can be more warmed. On the other hand, the large discrepancy between two datasets is also found in CRF over the Arctic Ocean except the Barent Sea in similar manner to PBL height and atmospheric thickness. This also seems to be linked to different change in sea ice

cover between two datasets.

The differences in sea level pressure and 500 hPa geopotential between two periods present the development of high pressure system across the Eurasian side of the Arctic Ocean and Eurasia continent (Figs. 4.8d and 4.8h). Significant change in sea level pressure appears over the Eurasian continent around 90°E from only the ERA-Interim, and 500 hPa geopotential near this region also shows large increases during the E21C. Larger differences from ERA-Interim are also probably relevant to difference in sea ice cover between datasets. It has been suggested that the development of winter high pressure over the Eurasian continent around 90°E is linked to sea ice melting (Jaiser et al., 2012), and the recent dipole-like atmospheric structure over the Arctic could contribute to modification of large-scale circulation patterns (Overland and Wang, 2010). Perhaps, recent change in vertical moisture transport related to sea ice may be closely linked with this pressure system change.

The overall changes in the Arctic climate between two periods also could induce the change in the impact of clouds on recent Arctic climate. Figure 4.9 presents the regression of zonally averaged air temperature and specific humidity onto low level cloud cover (below 750 hPa) averaged over the entire Arctic with removing the trends. Here we choose low-level clouds as it mostly accounts for total cloud cover and have strongest radiative effect at the surface (Eastman and

Warren, 2010b; Intrieri et al., 2002; Shupe and Intrieri, 2004). Overall, the underlying positive relationship between the cloud and SAT is found to be largely similar in both periods, but there is important difference between two periods. During the L20C, low-level cloud in the Arctic is positively correlated with lower tropospheric (below 700 hPa) temperature over the southern part of Arctic (60–75°N) rather than the central Arctic. In the E21C, contrastingly, the center of temperature associated with clouds moves to the high Arctic, north of 70°N with strengthened amplitude of the relationship. Atmospheric moisture exhibits positive relationship with the low-level cloud change similar to the temperature change pattern. Moreover, the positive relationship between low-level cloud and temperature more vertically extends further to mid- to even upper-troposphere above 500 hPa. In other words, the local connection between cloud and temperature/moisture over the Arctic became much tightened in the E21C.

Relationship between low-level cloud and atmospheric states in the L20C presented in Figs. 4.9a and 4.9c reflects the mechanism between cloud and the moisture over the marginal Arctic suggested by Liu et al. (2007). Arctic low clouds show largest correlation with subarctic moisture and temperature and the pattern seems to represent the influence of northward moisture fluxes to the Arctic. During the E21C, however, the changed pattern of strengthened local

connection presented in Figs. 4.9b and 4.9d implies that cloud might be more associated with profound changes in the Arctic climate system for this period – explosive warming and moistening associated with accelerated melting of sea ice. The strong surface warming would cause lower tropospheric warming and sea ice retreat might reinforce moistening by increased evaporation more over the central Arctic region. Warming and moistening of lower troposphere associated with melting sea ice might greatly reduce the atmospheric stability. Consequently, the near-surface warming could more easily propagate to mid- to upper troposphere by enhanced turbulent mixing and upward motion. In addition, this might reinforce increases in formation of precipitating cloud and precipitation, thus the local connection between clouds and temperature/moisture, in turn, is much tightened over the Arctic. This suggests that the impact of cloud on warming and moistening at lower troposphere over the local Arctic could be strengthened under sea ice retreated condition.

4.1.4. Discussion

We examined the long-term variations of cloud and its relationship to atmospheric state over the Arctic during winter for recent three decades, particularly focusing on changes for the early 21st century in relation to sea ice retreat. Two state-of-the-art reanalyses present that cloud decreases gradually

during late 20th century and increases largely in the 21st century. Coherent changes in each period also are found in temperature and moisture at lower troposphere, and the relation of cloud to local atmospheric states becomes stronger during the increasing period. Surface condition change due to reduced sea ice cover seems to be the major cause for the increasing in cloud and change in relationship between cloud and environmental atmospheric state. Reduced sea ice cover leads to an increasing in surface fluxes, a decrease in lower-tropospheric static stability, and deepening of planetary boundary layer. Consequently, low level stratiform cloud and convective cloud can be more formed over the more opened ocean. This reinforces the cloud radiative effect and precipitation over the Arctic, and, in turn, the local relationship between cloud at lower troposphere and atmospheric states becomes strengthened.

We divided whole analysis period into two periods with criterion based on the year of changing trends oppositely. In interannual variation of cloud amount, the change point analysis indicates that the criterion year could be 1997 or 2000. We checked both years as criterion to divide periods, and the results including relationship between cloud and surrounding atmospheric state are almost analogous to each other. In particular, most characteristics in sea ice melting period do not change. This result also emphasizes the role of sea ice retreat on recent Arctic climate changes related to cloud.

We compare cloud data from reanalyses with satellite data retrieved from APP-x and TOVS which cover the late 20th century, but we do not use recent cloud data retrieved from CloudSat and CALIPSO. Because this study focuses on long-term change more than decade, we think that data consistency in homogeneous dataset might give more reliable result to this study. For a similar reason, we choose satellite datasets which covers more than two decades for comparison. Recent satellite cloud dataset has relatively short-term period, so we do not compare with this dataset. However, Zygmuntowska et al. (2012) has mentioned that there are large discrepancy in winter cloud data between the ERA-Interim and recent satellite retrievals from CloudSat and CALIPSO from comparison for 4 years (2006–2009). Although the domains defined for the Arctic cloud are slightly different from this study, this suggests that more careful interpretation for result in this study should be needed.

Lastly, although the result of this study and prior studies suggest that the atmospheric circulation on cloud change plays also important role, the role of the atmospheric circulation is not investigated in detail. We examine interannual variation of sea level pressure and geopotential at 500 hPa in association with low level cloud (Fig. 4.10). Both analyses show that the variation in low level cloud is mainly related to low pressure over the most Arctic Ocean during the L20C. The relationship between low level cloud and pressure system over the

Arctic during the L20C indicates the low level cloud forms more frequently under low pressure system over the Arctic region. This relation between winter Arctic cloud and low pressure system is consistent with the result of prior study (see Fig. 3 in Liu et al. (2007)). During the E21C, the variation in low level cloud becomes to be related with high pressure system across the Eurasian coastal region and the Siberia region and low pressure over the central and North American side of the Arctic, which forms dipole-like structure. The dipole-like spatial pattern related to low level cloud during the E21C is also shown in geopotential at 500 hPa more clearly. The dipole-like pattern with high pressure over the Eurasian continent around 90°E and the low pressure over the Arctic Ocean is also seen in difference between two periods (Fig. 4.8). These resemblances strongly suggest that this dipole-like pressure system will be closely linked to recent variation of the Arctic winter cloud. Maybe, the factors such as storm track and cyclone activity related to this structure could affect the cloud formation over the Arctic.

Table 4.1 Mean, standard deviation, and trends of total cloud fraction over the Arctic Ocean (north of 67°N) in each dataset.

	mean (%)	standard deviation (%)	trend (% decade ⁻¹)		
			whole period	20th century	21st century
ERA-Interim	87.47	3.35	-1.39^{**} (1979–2011)	-5.08^{**} (1979–1997)	5.51^{**} (1998–2011)
NCEP CFSR	81.89	2.41	-1.36^{**} (1979–2008)	-2.43^{**} (1979–1997)	4.46^{**} (1998–2008)
TPP-x	72.67	7.38	-2.09 (1980–2005)	-3.06 (1980–1997)	19.66^{**} (1998–2005)
APP-x	70.55	8.12	-8.86^{**} (1982–2004)	-12.23^{**} (1982–1997)	-24.96[*] (1998–2004)

* significant at 90% confidence level

** significant at 95% confidence level

Table 4.2 Mean, standard deviation, and trend of surface skin temperature over the Arctic Ocean (north of 67°N) in each dataset.

	mean (K)	standard deviation (K)	trend (K decade ⁻¹)		
			whole period	20th century	21st century
ERA-Interim	253.91	1.51	0.88[*] (1979–2011)	-0.88^{**} (1979–1997)	2.80[*] (1998–2011)
NCEP CFSR	252.32	1.23	0.67^{**} (1979–2009)	-0.49 (1979–1997)	2.42^{**} (1998–2008)
TPP-x	248.82	1.25	0.67^{**} (1980–2005)	-0.33 (1980–1997)	4.81[*] (1998–2005)
APP-x	251.26	1.26	-1.20^{**} (1982–2004)	-2.27^{**} (1982–1997)	-3.03 (1998–2004)

* significant at 90% confidence level

** significant at 95% confidence level

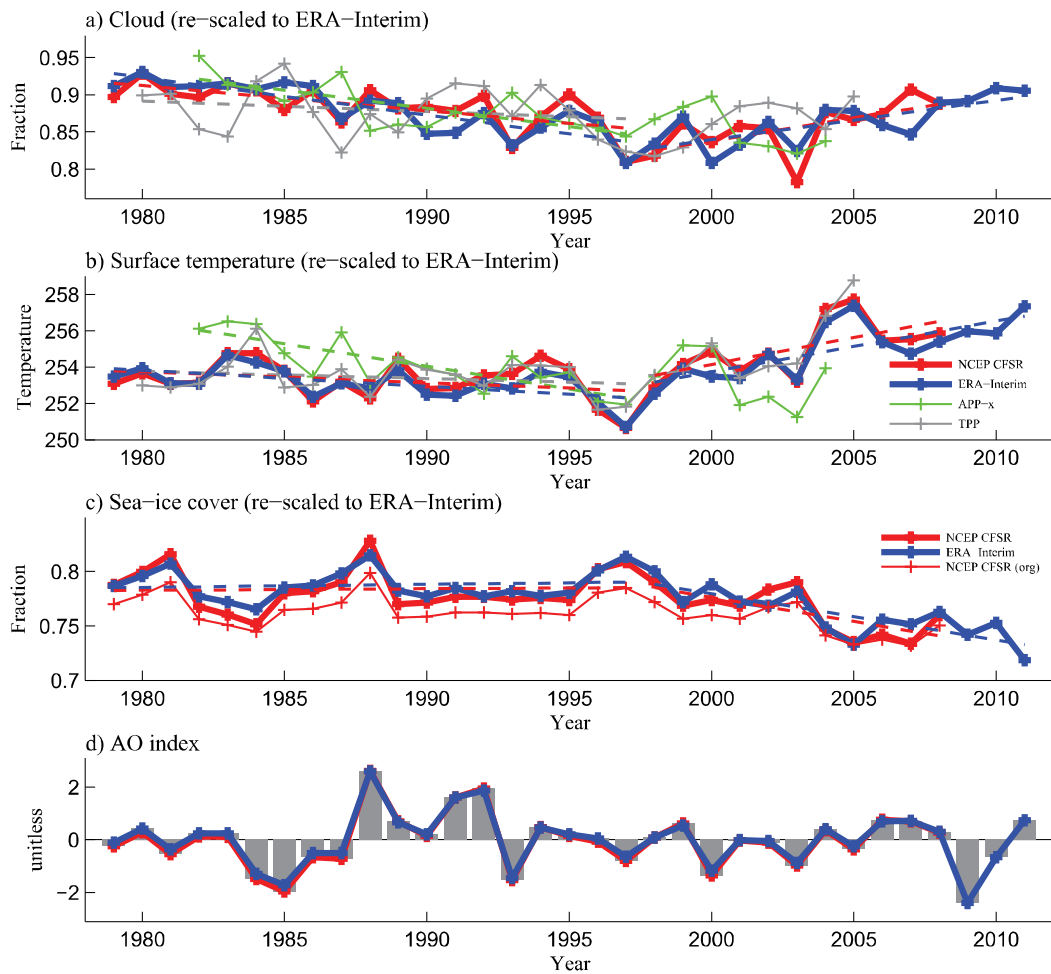


Fig. 4.1 Time-series of (a) cloud amount, (b) surface temperature, (c) sea ice cover over the Arctic Ocean (north of 67°N), and (d) AO index in winter (December to February) from the NCEP CFSR, ERA-Interim, APP-x, and TPP datasets. Trend lines are denoted with dashed line. Time series of cloud amount, surface temperature, and sea ice cover are re-scaled to have the mean and standard deviation of ERA-Interim for comparison.

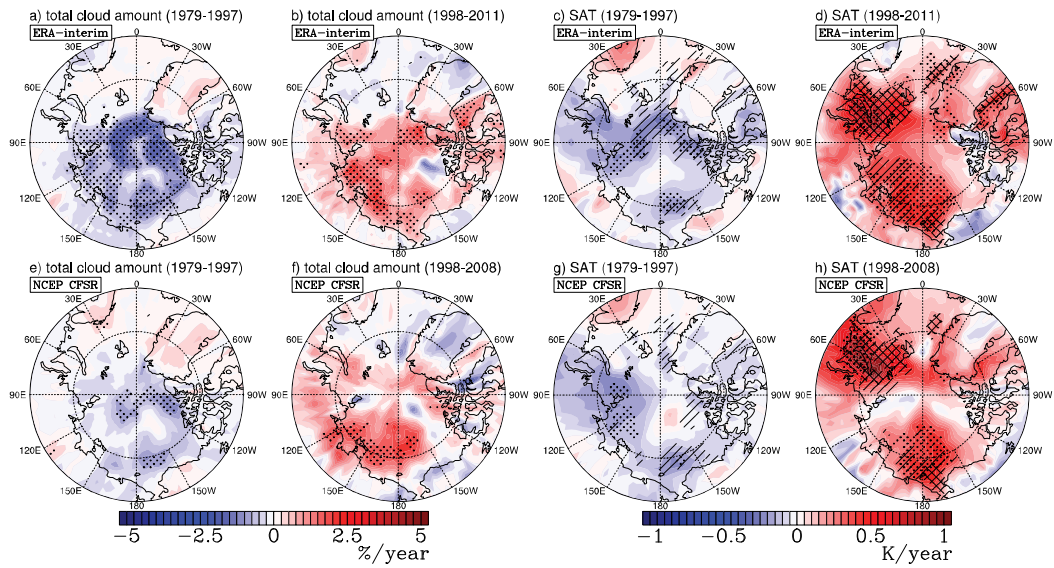


Fig. 4.2 Changing trends in winter total cloud amount and surface air temperature during late 20th century (1979–1997) and early 21st century (1998–present) from the ERA-Interim and NCEP CFSR. Stippled region indicates that trend is significant at the 95% confidence level. Oblique and cross checked region in c and g (d and h) indicate that region sea ice cover is increasing (decreasing) with above (below) 0.2 %/year and 0.5 %/year, respectively.

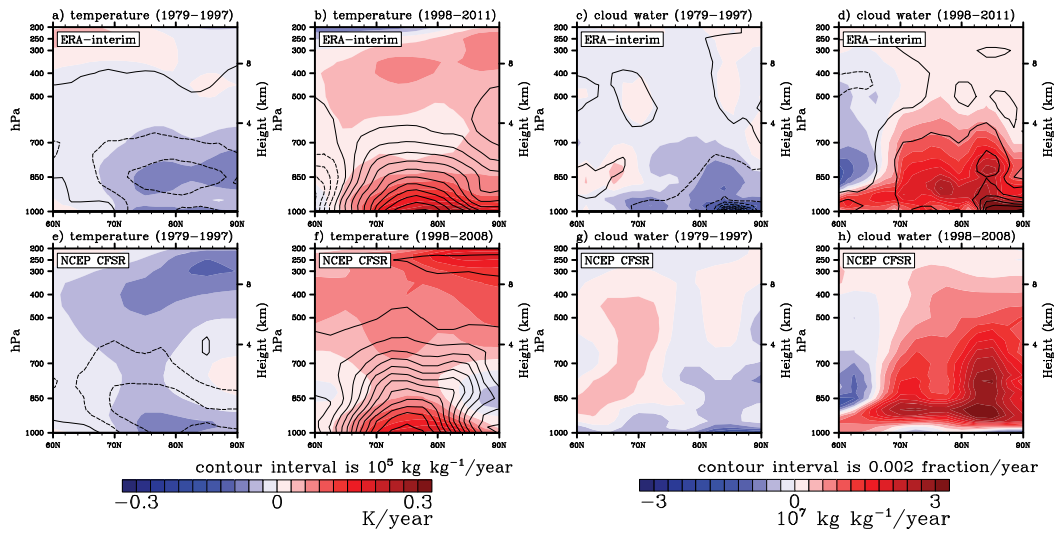


Fig. 4.3 (left panels) changing trends in zonal-averaged winter temperature (shading) and specific humidity (contour) during late 20th century (1979–1997) and early 21st century (1998–present) from the ERA-Interim and NCEP CFSR. (right panels) same as left panels except for cloud water contents (shading) and fractional cloud cover (contour).

northward moisture transport at 67N

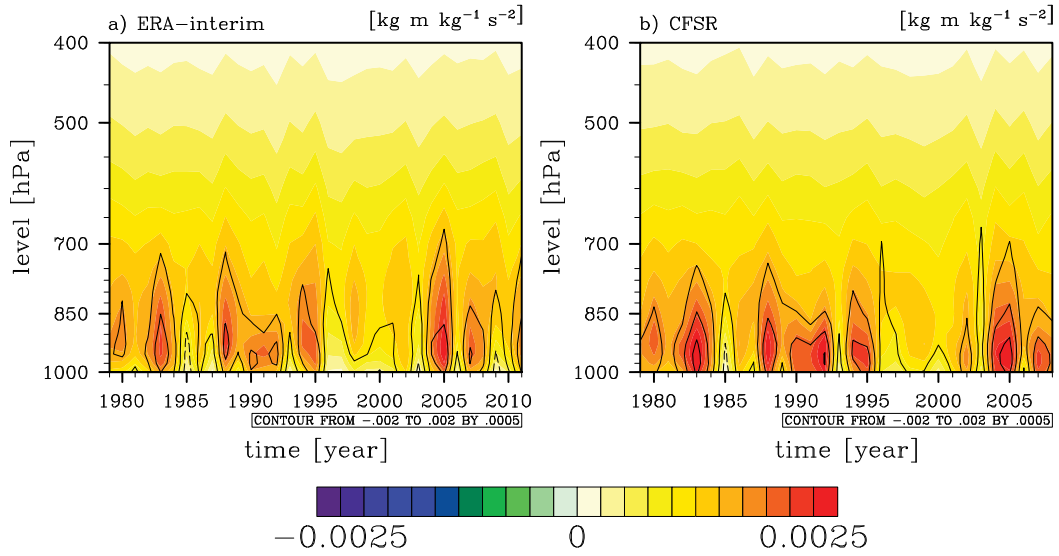


Fig. 4.4 Zonal-averaged total northward moisture transport ($\bar{v}\bar{q} + v'q'$, shading) and northward transport by mean flow ($\bar{v}\bar{q}$, contour) at 67°N.

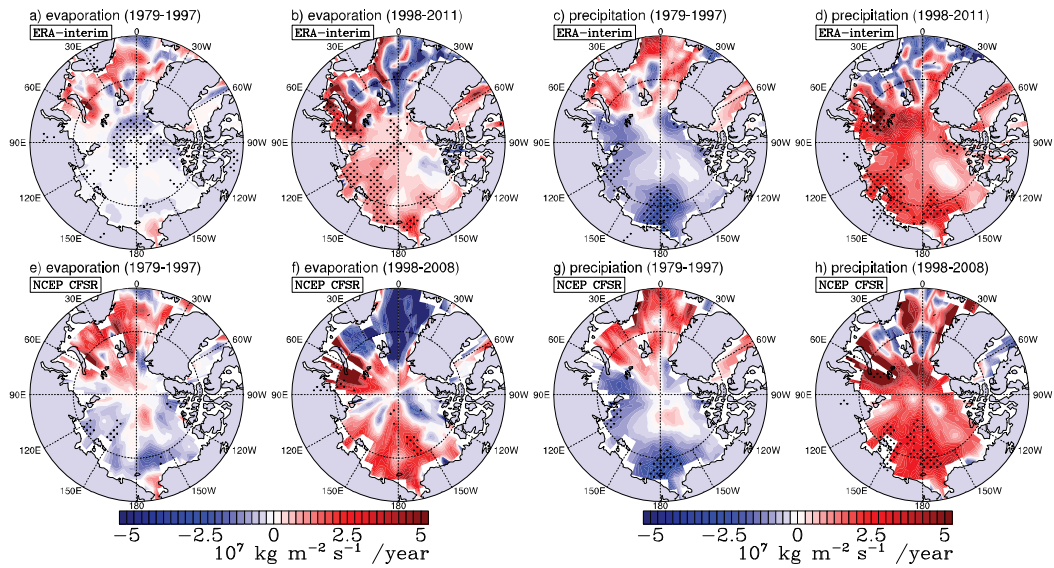


Fig. 4.5 Changing trends in winter evaporation and precipitation during late 20th century (1979–1997) and early 21st century (1998–present) from the ERA-Interim and NCEP CFSR. Stippled region indicates that trend is significant at the 95% confidence level.

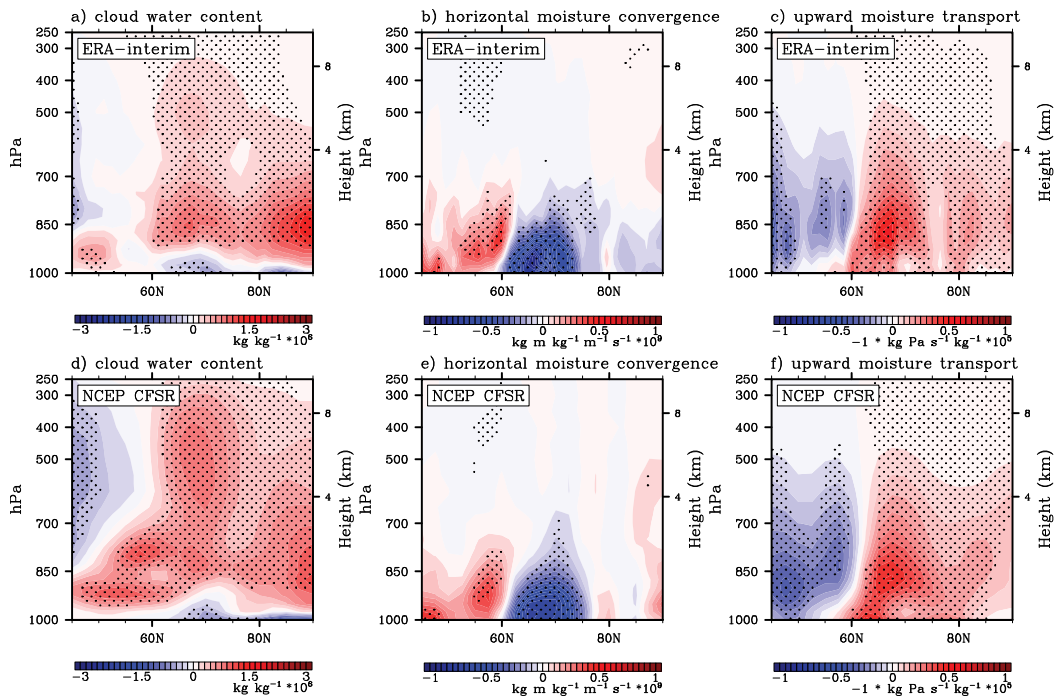


Fig. 4.6 Regressions of the AO index with zonal-averaged (a) cloud water content [10^6 kg kg^{-1}], (b) horizontal moisture convergence [$10^9 \text{ kg kg}^{-1} \text{ s}^{-1}$], and (c) upward moisture transport [$10^5 \text{ kg Pa kg}^{-1} \text{ s}^{-1}$] from the ERA-interim and NCEP CFSR. Stipple regions indicate that values are significant at the 95% confidence level.

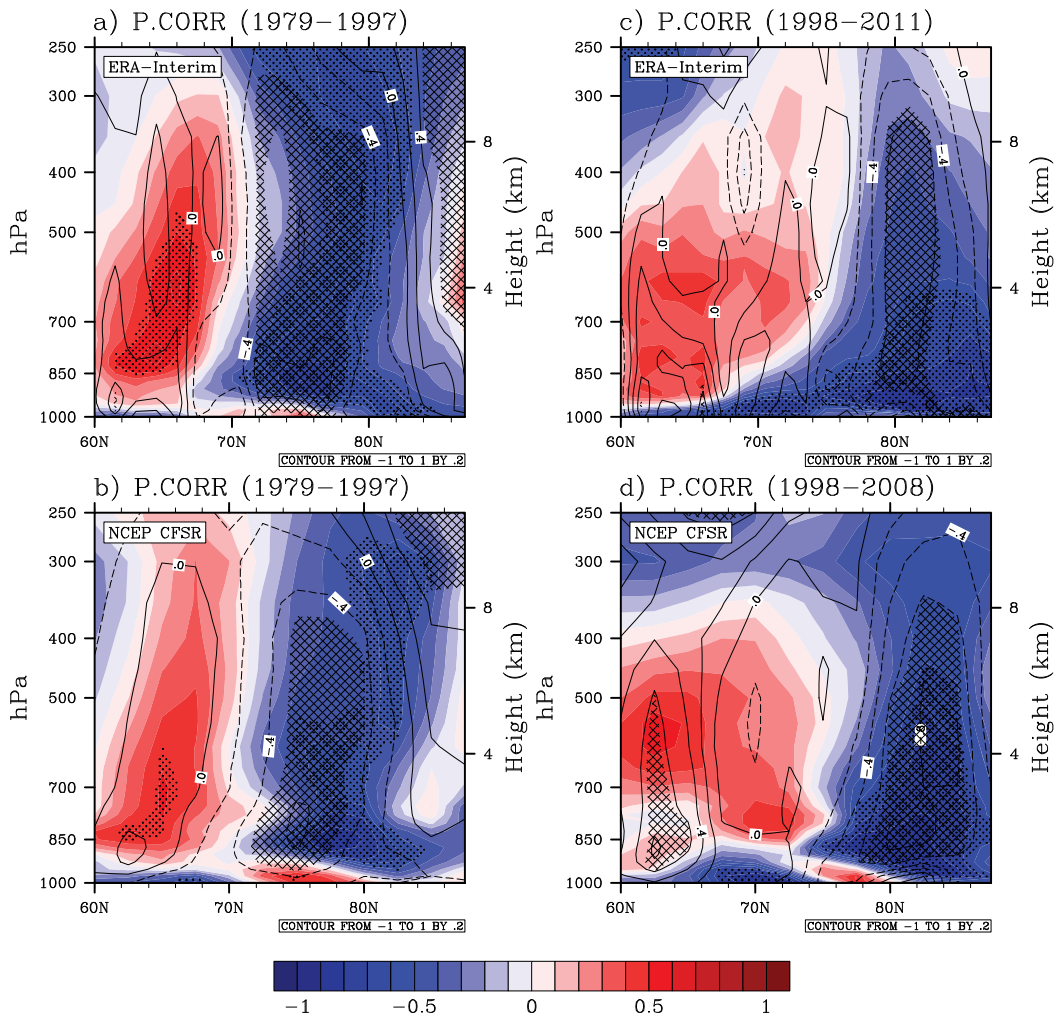


Fig. 4.7 Partial correlations of sea ice cover averaged over the Arctic Ocean (north of 67°N) with zonal-averaged cloud water content (shading) and mean upward moisture transport (contour) independent on the AO index during the late 20th century and the early 21st century from the ERA-interim and NCEP CFSR. Stippled (cross-checked) regions indicate that values with shading (contour) are significant at the 95% confidence level.

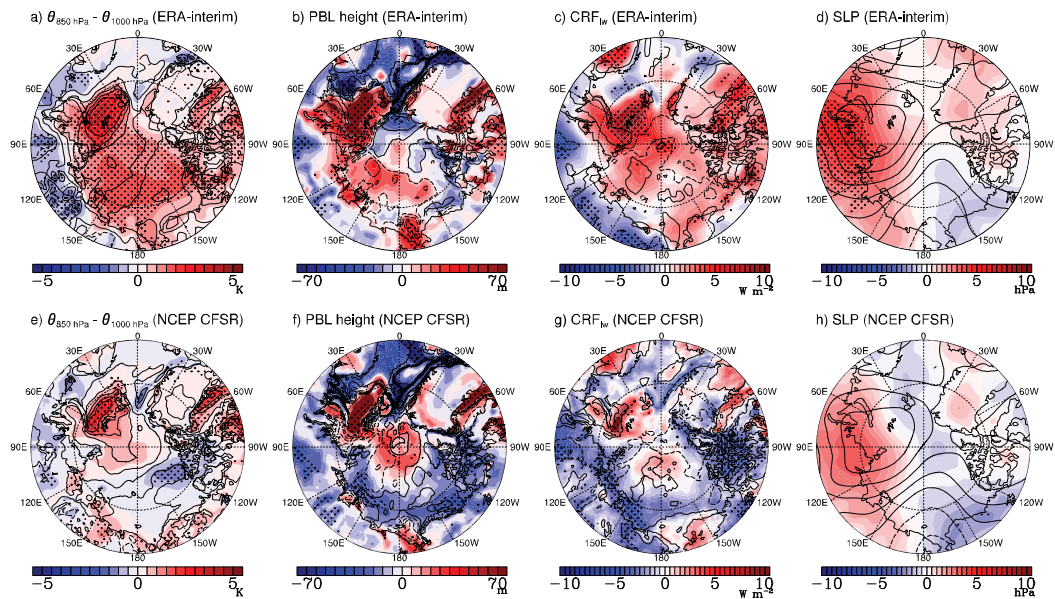


Fig. 4.8 Differences in (a and e) 850 hPa thickness (shading) and surface air temperature (contour), (b and f) PBL height (shading) and sea ice fraction (contour), (c and g) longwave cloud radiative forcing (shading) and cloud amount (contour), and sea level pressure (shading) and 500 hPa geopotential (contour) between averages for the early 21st century and the late 20th century. Stippled region indicates differences in shading values are significant at the 95% confidence level.

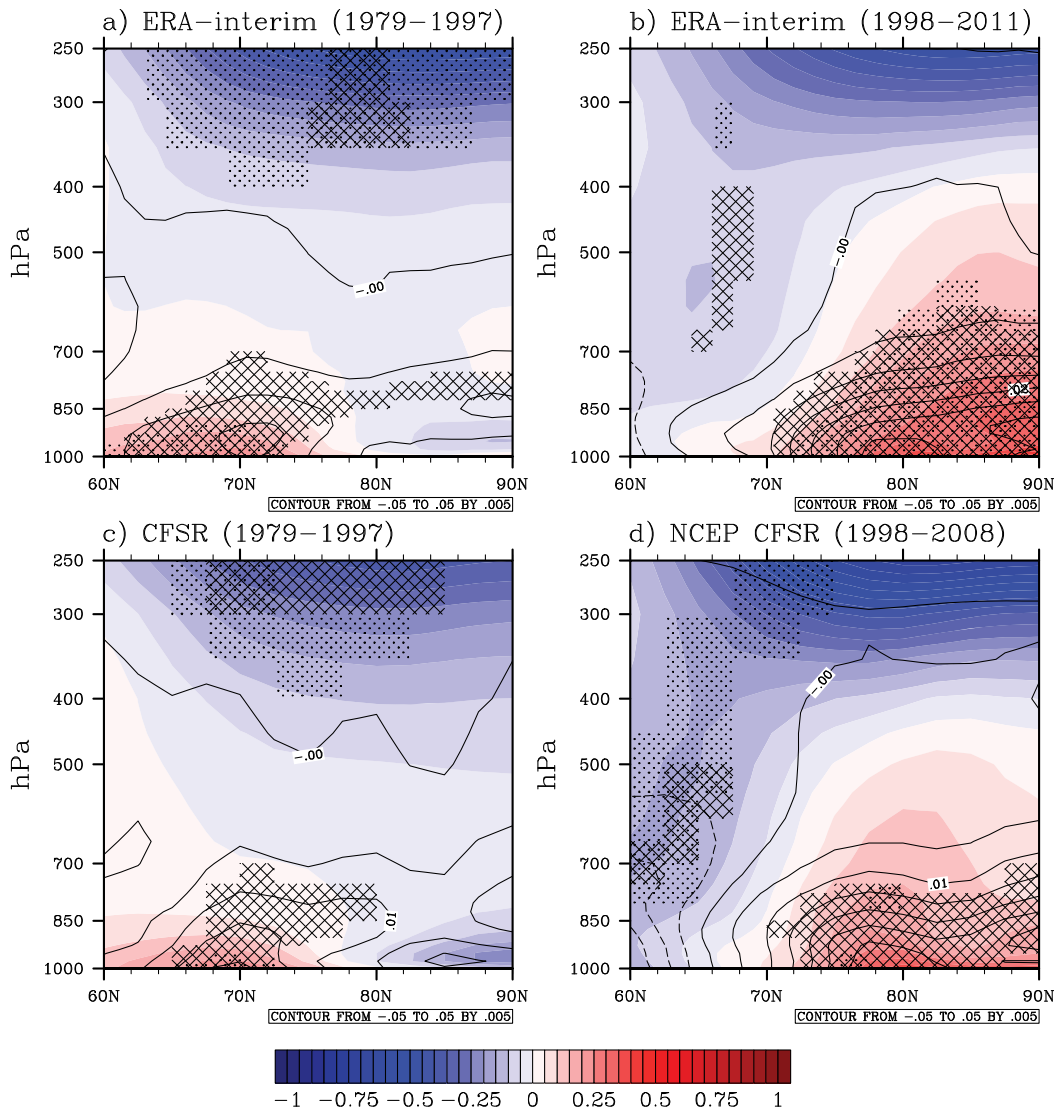


Fig. 4.9 Regression of winter low-level cloud amount [%] averaged over the Arctic Ocean (North of 67°N) with zonally averaged temperature (shading, [K]) and specific humidity (contour, [g kg⁻¹]) during late 20th century (1979 – 1997) and early 21st century (1998 – present) from the ERA-Interim and NCEP CFSR. All trends are removed. Stippled and cross-checked regions indicate that regression is significant at the 95% confidence level.

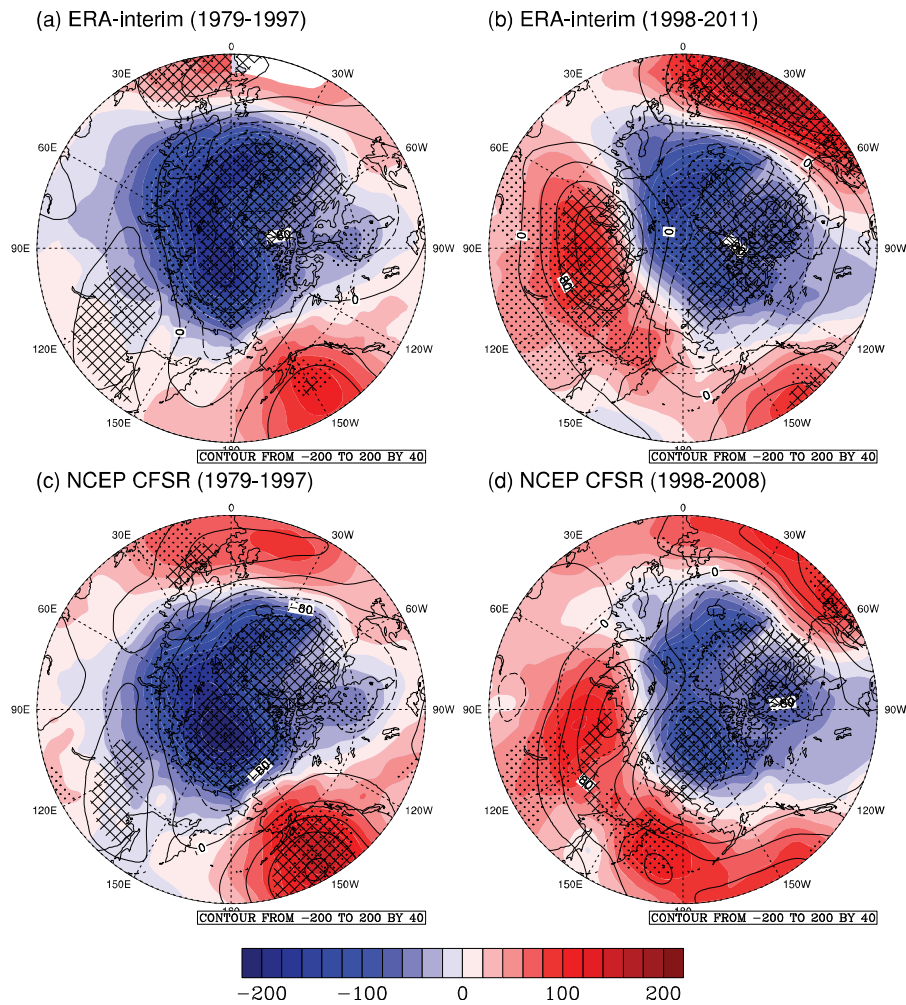


Fig. 4.10 Regression of winter low-level cloud amount averaged over the Arctic Ocean (North of 67°N) with sea level pressure (shading, [hPa]) and geopotential at 500 hPa (contour, [$\text{m}^2 \text{s}^{-2}$]) during the late 20th century (1979 – 1997) and the early 21st century (1998 – present) from the ERA-Interim and NCEP CFSR. All trends are removed in calculation. Stippled and cross-checked regions indicate that regressions are significant at the 95% confidence level.

4.2. Refinement of surface boundary condition for reduced sea ice in AGCM Experiment

A diagnosis on recent cloud change from reanalysis and satellite datasets in previous chapter suggests that surface condition change owing to reduced sea ice cover might play a crucial role on recent changes in cloud and its relation to adjacent atmospheric states over the Arctic during winter. Thus, we attempt to confirm these consequences through modeling work which examines the impact of the areal change in sea ice on the Arctic climate with atmospheric general circulation model (AGCM).

In this modeling, the accurate surface condition according to sea ice change is very important because of the highly sensitive Arctic climate system (Singarayer et al., 2005). The CAM3 uses SST and sea ice fractional coverage as oceanic surface boundary condition, and thus it is demanded evaluating a proper SST distribution according to sea ice change for more accurate surface boundary condition. Therefore, prior to modeling impact of the areal change in sea ice on the Arctic climate, we first examine the sensitivity of SST distribution on the Arctic climate and find proper method to generate the SST distribution according to sea ice change.

4.2.1. Surface condition according to sea ice change for AGCM

Experiment

The change of Arctic sea ice, particularly in the areal extent (i.e., the change of open ocean area occupied by water surface), is known to affect the Arctic and sub-Arctic climate from local temperature change in the Arctic during the boreal winter (Screen and Simmonds, 2010b) to winter weather patterns and large-scale atmospheric circulations over the midlatitudes (Francis et al., 2009; Overland and Wang, 2010). Thus, many previous studies have investigated the impact of Arctic sea ice on large-scale environments over the Northern Hemisphere using AGCMs (Budikova, 2009).

These studies have focused mainly on the atmospheric sensitivity to the changes in sea ice extent. In early 1970s, several studies examined the atmospheric response to a complete removal of Arctic sea ice (Newson, 1973; Warshaw and Rapp, 1973). Murray and Simmonds (1995) performed a perpetual January simulation by gradually reducing sea ice coverage; their results suggest that Arctic sea ice extent is non-linearly related to the changes in the 850 hPa temperature over the Arctic and mid-latitude westerlies. Alexander et al. (2004) correlated large-scale atmospheric teleconnection patterns, such as the Arctic Oscillation/North Atlantic Oscillation (AO/NAO), to anomalous sea ice cover. Deser et al. (2004) investigated an AO/NAO-type atmospheric response to changes in North Atlantic sea ice and sea surface temperature (SST) conditions

based on observations spanning over a 40-year period. Screen et al. (2012) suggested that the response pattern of atmospheric circulation in early winter to sea ice loss in the last three decades resembles the NAO negative phase. This NAO-type atmospheric response is also found in future climate projections under reduced Arctic sea ice conditions (Deser et al., 2010; Seierstad and Bader, 2009).

Arctic atmospheric response to local changes in sea ice conditions is quite sensitive and non-linear (Singarayer et al., 2005). To account for this sensitivity, researchers have been specifying more detailed and observation-based sea ice conditions in AGCM experiments. For instance, both the thickness and fractional coverage of sea ice are used to specify surface boundary conditions (Gerdes, 2006; Rind et al., 1995). Dethloff et al. (2006) achieved a realistic surface air temperature (SAT) simulation for the Arctic using an improved sea ice albedo scheme.

Changes in sea ice concentration (SIC) are a primary factor in driving atmospheric changes by inducing dramatic changes in energy and moisture exchanges between the sea surface and the lower troposphere. Based on this, a number of previous studies have investigated atmospheric responses to altered SIC (Alexander et al., 2004; Magnusdottir et al., 2004; Semmler et al., 2012; Singarayer et al., 2006). Typically, SST in the melted sea ice region (MSR) is estimated by using SST values at the adjacent grids (Alexander et al., 2004) or

by using sea ice surface temperature (Semmler et al., 2012); none of earlier studies use SIC fraction in the estimation of the SST over MSR.

This earlier approach in estimating SSTs in MSR is rather unrealistic and may produce erroneous results. As the sea ice and ocean interact, their changes are always concurrent. For instance, the heat absorbed by the Arctic Ocean when covered with broken sea ice is used in part to melt sea ice and in part to increase SST. Thus, the oceanic area exhibiting significant reduction in SIC is expected to show a significant increase in local SST. Because heat fluxes between two interfaces (i.e., atmosphere and ocean surface) increase the temperature difference between the two interfaces; the increased SST provides more heat and moisture fluxes into the lower troposphere. Hence, accurate determination of local SST in a region where SIC exhibits dramatic decreases is essential for improving the simulations in sea ice model experiments.

This study shows that the atmospheric response associated with sea ice variability depends on SIC, and the response is very sensitive to *in-situ* SST distributions. To isolate the atmospheric response to SSTs in a given SIC change, we compare the results from multiple AGCM simulations generated using various SST conditions in MSR. Model configurations for the sensitivity include: (1) no SST change; (2) SST adjusted by averaging a long-term climatology with a constant value for the lowest ice-free SST; and (3) SST from a statistical fitting

concurrent with the *in-situ* observed SIC. By comparing the three corresponding sensitivity experiments, we have examined the atmospheric responses during the cold season (October through March) and changes in the associated surface-heat fluxes.

4.2.2. Experimental Design

The version used in this study is configured with a finite volume dynamics core having a $4^\circ \times 5^\circ$ horizontal resolution and 26 vertical levels. Previous studies suggested that the sensitivity of the atmospheric response to surface boundary and doubling-CO₂ conditions in the CAM3 version increases with spatial resolution (Hack et al., 2006; Kiehl et al., 2006). Thus, results from this type of experiment using the model can vary according to the spatial resolutions; relatively low resolution used in this study may give results derived from conditions of relatively lower sensitivity.

To assess atmospheric responses to SST changes in MSR, a series of CAM3 experiments have been performed; one baseline and three sensitivity experiments. The baseline experiment prescribes the monthly climatological seasonal cycles of SST and SIC from the National Oceanic and Atmospheric Administration Optimum Interpolation version 2 (OISSTv2) (Reynolds et al., 2002) for 1982–2000. The three sensitivity runs employ the same reduced SIC averaged over

2006–2010, but with different MSR SST conditions. It is noted that, for the period 2006–2010, there is a dramatic decrease in Arctic sea ice extent in winter (Stroeve et al., 2012).

In the three sensitivity experiments, MSR is defined as the region where the time-mean SIC for 2006–2010 is reduced by over 1% compared to that for 1982–2000. Local SSTs are specified over MSR as follows: the first experiment (hereafter CTRL) prescribes the same SST field as in the baseline run in conjunction with the reduced SIC. The second experiment (hereafter CONV) adjusts SST at the MSR grid points using average of the mean climatological SSTs for 1982–2000 and the minimum value of -0.8°C . This method is designed to follow the conventional approach of Alexander et al. (2004) where the SST in grids adjacent to the sea ice is constrained with the average of value of -0.8°C (the lowest ice-free SST) and the warmest climatological SST in adjacent grid boxes. In the third experiment (hereafter POLY), the MSR SSTs are estimated to be more physically associated with the given sea ice reduction using a statistical relationship between SIC and SST over MSR derived from a 3rd-order polynomial regression method.

Figure 4.11 presents a scatter plot of the observed relationship between SST and SIC over the ocean, north of 60°N for the cold seasons (October through March) for the period 1982–2000. In general, regions of larger sea ice cover

show relatively colder SSTs, close to the sea-water freezing point (around -1.8°C); SSTs over areas with small sea ice cover vary widely. White lines in the figure represent a 3rd-degree polynomial fit to the observed data. These polynomials are calculated using data over the regions of $\text{SIC} < 0.9$. SSTs where $\text{SIC} > 0.9$ are excluded as SSTs over such regions are approximately constant (i.e. -1.8°C). These polynomials represent the seasonal variation reasonably in the relationship between the two variables (SST and SIC). This fitting method is currently applied to adjust bias in the Hadley Centre Sea ice and Sea Surface Temperature data (HadISST) using a 2nd-degree polynomial to estimate SSTs over MSR where SST observations are absent (Rayner et al., 2003). In our POLY experiment, SSTs over MSR are specified based on the third-degree polynomial fits; the SST corresponding to the given SIC from the fitting line is chosen as the SST over MSR. Table 4.3 presents the polynomial fitting coefficients between the two variables in the POLY experiment during the cold season.

The baseline and three sensitivity experiments have been run for 250 years by prescribing the annual cycles of SST- and SIC fields corresponding to each experiment as described above. In this study, we focused on the cold season responses when the atmospheric local response to an altered boundary condition is known to be strongest (Screen and Simmonds, 2010b; Screen et al., 2012). Table 4.4 summarizes the monthly-mean values of SST and SIC during the cold

season, averaged over the Arctic Ocean to the north of 67°N in all experiments. As expected, among the sensitivity experiments, POLY had mean values of SST for 2006–2010 that are closest to those obtained by the OISSTv2 product. The mean SST in CONV in October is considerably colder than in POLY; the colder SSTs in CONV affects values in autumn and December, perhaps because the method used in CONV is originally designed to model atmospheric response during December-January-February (Alexander et al., 2004).

Figure 4.12 shows the SIC differences between the sensitivity and baseline experiments (contour in all panels). Also shown are the SST differences in CONV (shading, Figs. 4.12b and 4.12f) and POLY (shading, Figs. 4.12c and 4.12g) from CTRL in early winter (October–December) (Figs. 2a–2d) and late winter (January–March) (Figs. 4.12e–h). Note that SSTs in CONV and POLY are explicitly calculated using the local SIC value. For comparison, the SST changes in OISSTv2 between 2006–2010 and 1982–2000 are presented in (Figs. 4.12d and 4.12h for the corresponding periods. In terms of the pattern and amplitude of SST anomalies, results from POLY are most similar to observations. Compared to POLY, CONV has apparently smaller SST increases over most of MSR. In addition, colder SSTs are generally found in the Barents Sea indicating that CONV is unable to capture the SST changes associated with the recent decline in early and late winter (Figs. 4.12b and 4.12f). Previous studies have noted that

SIC changes over the Barents Sea and Kara Sea play a crucial role in modulating large-scale atmospheric circulations (Honda et al., 2009; Petoukhov and Semenov, 2010). Thus, these results imply that using SST values adjusted to the lowest SST in the ice-free region cannot generate proper atmospheric responses because warming over the Barents and Kara Seas is much weaker than the observed. More detailed examination of early winter conditions shows that, over most of the Arctic Ocean, POLY captures the SST increase associated with the SIC decrease better than CONV (Figs. 4.12b and 4.12c). However, warming over the Barents Sea in POLY is overestimated compared to the observation (Figs. 4.12c and 4.12d). In late winter, CONV presents excessive warming over the Kara Sea and Laptev Sea (Figs. 4.12f and 4.12h). In contrast, those for POLY in late winter are closer to the observed SST changes associated with the changes in SIC. Still, a stronger warming tendency appears over the Barents Sea (Figs. 4.12g and 4.12h).

4.2.3. Responses in surface air temperature and heat fluxes

We first compare the CTRL with the baseline results to examine the SAT response related solely with changing sea ice conditions and fixed climatological SST (Fig. 4.13a). During the cold season, the reduced SIC induces overall warming over the Eurasian margins of the Arctic Ocean and Hudson Bay by

more than 1 K, with particularly strong warming over the Barents Sea of approximately 3 K. This spatial variation in SAT response also appears in CONV and POLY. Compared to CTRL, POLY shows stronger the warming over the Barents Sea; both CONV and POLY show further horizontal expansions of warming to the Eurasian margins (Figs. 4.13b and 4.13c). With the same SIC changes, the mean SAT difference between 2006–2010 and 1982–2000 is estimated from the ERA-Interim. The estimate shows warming > 3 K over major sea ice reduced regions and extreme warming > 6 K over the Barents Sea (Fig. 4.13d). All three experiments yield smaller warming compared to the ERA-Interim data, perhaps due to weaker internal variability since the results obtained in this study is the mean response averaged over much longer period than the averaging period of the ERA-Interim data. In addition, the lack of heat transport from lower latitudes in the three sensitivity experiments can be another reason for this weaker warming because they use the climatological SSTs where SIC does not change.

In Fig. 4.14, we compare SAT responses in CONV and POLY against CTRL. Under the same SIC change, SAT in POLY differs significantly from that in CONV. CONV generates slightly weaker SAT responses compared to CTRL over most of the Arctic Ocean, except for weak warming of about 0.2 K over the Chukchi Sea (Fig. 4.14a), consistently with the prescribed colder SSTs in the

Barents Sea and warmer SSTs in the Chukchi Sea in CONV (Figs. 4.12b and 4.12f). In contrast, POLY generates significant warming of 0.2 K over most of the Arctic Ocean, particularly by as much as 0.4 K over the Barents Sea (Fig. 4.14b). Considering the changes found in the ERA-Interim reanalysis data, POLY appears to simulate SAT response over the Arctic more reasonably, in both intensity and spatial distribution, than CONV. Even though warming in POLY is weaker than the observed, our results suggest that a careful choice of the SST field based on statistical estimation can improve model response. In addition, the relatively weaker warming found in the experiments, even in POLY, emphasizes that heat transport from lower latitudes is a major cause of Arctic warming (Chung and Räisänen, 2011; Graversen et al., 2008).

Screen and Simmonds (2010b) showed that, during the cold season, recent Arctic warming is largely associated with enhanced surface heat fluxes over the region of reduced sea ice. Here, we examine the changes in surface heat fluxes associated with SST distributions that might be closely associated with SAT responses. CAM3 formulates surface fluxes in the sea ice covered region as follows (Collins et al., 2004),

$$F_{LWUP} = \varepsilon\sigma_{sb}T_s^4 - (1 - \varepsilon)F_{LWDN} \quad (4.1)$$

$$F_{SW} = \rho_a c_a r_h u^* (T_s - \theta_a) \quad (4.2)$$

$$F_{LH} = \rho_a (L_i + L_v) r_e u^* (\bar{q} - q_a) \quad (4.3)$$

where, the upwelling longwave flux is F_{LWUP} ; sensible heat flux is F_{SH} ; latent heat flux is F_{LH} ; downwelling longwave flux is F_{LWDN} ; longwave emissivity is ε ; Stefan-Boltzmann constant is σ_{sb} , specific heat of air is c_a , exchange coefficients for sensible and latent heat are r_h and r_e , respectively; and latent heat of fusion of ice and vaporization are L_i and L_v , respectively. At the lowest model layer, the air density is ρ_a ; potential temperature is θ_a ; and specific humidity q_a . At the surface, the temperature is T_s ; friction velocity is u^* ; and saturation specific humidity is \bar{q}^* . In the equations, all surface fluxes are defined to be positive in upward direction.

When the ocean surface previously occupied by sea ice becomes warmer, MSR experiences a significant increase in surface fluxes. In Fig. 4.15, all of the SIC change experiments show a consistent increase in surface fluxes over MSR (see contours in the figure). Net longwave flux ($F_{LWUP} + F_{LWDN}$) increases over the Barents Sea, Laptev Sea, and East Siberian Sea; these regions also experience large increases in sensible (F_{SH}) and latent (F_{LH}) heat fluxes. In particular, a large reduction in sea ice over the Barents Sea leads to increases in both sensible and latent heat fluxes. Elsewhere, in the inner-Arctic, especially over the northeast of Greenland and Queen Elizabeth Islands, the sea ice expanded region undergoes a conspicuous decrease in sensible heat flux of more than 1 W m^{-2} . This occurs in all three experiments (contour in the Figs. 4.15b and 4.15e) due mainly to the

cold surface temperatures over the sea ice expanded region which are colder than in the baseline experiment.

In CONV and POLY, warmer SSTs increase the outgoing longwave flux as well as the sensible and latent heat fluxes. Compared to CTRL, POLY shows significant and larger increases in surface fluxes over most MSRs (Figs. 4.15d–f) than CONV (Figs. 4.15a–c). These increases in surface fluxes in POLY are roughly proportional to the reduction of sea ice because fluxes increase most over the Barents Sea and north of the Chukchi Sea and considerably less elsewhere. In particular, increases in the surface fluxes over the Barents Sea were above 3 W m^{-2} . These changes over MSR in POLY are significant at the 95% confidence level.

The SAT responses obtained in the three experiments are well explained by increases in surface flux changes. Surface flux changes might have different monthly variations due to diverse dependencies of the fluxes on the seasonal evolution of SST. Because longwave flux increases in proportion to the fourth power of SST, as indicated by Eq. (4.1), an increase in longwave flux becomes larger in early winter than in late winter because the early winter has a considerably warmer SST value. In Fig. 4.16a, changes in net longwave flux are largest over the Arctic Ocean, exceeding 3.6 W m^{-2} , and represent warmer SST conditions in October. In November, all experiments show a stronger longwave

flux, 2 W m^{-2} more than in the baseline experiment. Afterwards, the net longwave flux changes become much weaker as the Arctic becomes colder. Thus, differences among all methods are nearly zero in February and March; the impact of longwave flux is concentrated in the two months, October and November.

Changes in sensible heat flux for all experiments remain in a similar range of $1\text{--}2 \text{ W m}^{-2}$ in every month, except for October; the change is relatively small in October compared to the changes in other cold months (Fig. 4.16b). In Eq. (4.2), sensible heat flux mainly depends on the difference between the potential temperature at the lowest atmospheric level and the surface temperature. The temperature differences in all experiments closely match observed sensible heat fluxes during all cold months. These differences are smallest in October, although SST anomalies in all experiments are largest in October compared to the baseline experiment.

Among experiments, the sensible heat flux in POLY is consistently larger than that in CTRL during the whole cold season. However, sensible heat flux in CONV is smaller than that in CTRL for several months (Fig. 4.16b). This feature is coupled tightly to the SST change in MSR, especially over the Barents Sea. The SST in POLY bears a more accurate warming signal, corresponding to a reduction in SIC, while SST in MSR CONV is colder than in CTRL for most

periods. This SST difference occurs throughout the entire winter (see Fig. 4.12) and follows the sensible heat flux difference between CONV and CTRL quite well.

Changes in latent heat flux are more sensitive to changes in SST conditions than are other fluxes throughout the cold season in the models. As shown in Eq. (4.3), latent heat flux depends mainly on the difference between specific humidity in the lowest layer and saturated specific humidity at the surface. In the annual cycle, both the specific humidity at the lowest model layer and the saturated specific humidity at the surface have maximum values in July and August. However, saturated specific humidity declines more gradually in association with declines of SIC. Consequently, the latent heat flux over the Arctic peaks in October and declines through the remaining cold season. In addition, because specific humidity in the lowest layer changes least in all three sensitivity experiments, changes in the saturated specific humidity at the surface is more responsible than other factors for increasing latent heat fluxes. Because saturated specific humidity at the surface increases exponentially with SST, different SST distributions in each sensitivity experiments contribute largely to the differences in latent heat fluxes among the sensitivity experiments during the cold season (Fig. 4.16c).

In CTRL, CONV and POLY, changes in fluxes over the Arctic Ocean

average to 1.09, 1.01, and 1.42 W m^{-2} for net longwave flux, 1.32, 1.19, and 1.65 W m^{-2} for sensible heat fluxes, and 1.32, 1.26, and 1.73 W m^{-2} for latent heat fluxes, respectively. Different SST conditions yield changes in all surface fluxes, and latent heat fluxes are most sensitive to SST conditions in the cold season. Among the surface flux differences between POLY and CTRL, those for latent heat fluxes are significant at the 90% confidence level during the entire cold season. The sensible heat fluxes in October, November, and March, and the longwave fluxes in October and March are also significant at the 90% confidence level. In contrast, most differences between CONV and CTRL are not statistically significant. The longwave fluxes in November and January and latent heat flux in October are significant at the 90% confidence level.

4.2.4. Vertical structure of responses in temperature and specific humidity

The changes in surface fluxes related to SST eventually affect the vertical distributions of temperature and humidity, which, in turn, affects the atmospheric response to SIC and SST changes. Figure 4.17 shows the vertical profiles of temperature and specific humidity and their changes among the three experiments during early and late winter. For both periods, vertically extended warming and moistening are commonly found in all three sensitivity experiments. The effects of surface-induced warming and moistening on lower troposphere are

larger with warmer SSTs. CTRL and CONV generate similar magnitudes of warming and moistening near the surface compared to the baseline experiment, and POLY generates warming and moistening greater than the other two experiments. During late winter, CONV also generates lower tropospheric warming greater than CTRL (Fig. 4.17b) with larger surface flux differences (Fig. 4.16).

Near-surface warming in the sea ice reduced experiments is linked mainly to longwave radiation and sensible heat fluxes. First, longwave radiation flux from the surface is greater in MSR (Figs. 4.15a and 4.15d) and possibly warms the lower troposphere if the atmosphere absorbs the longwave flux. Over the Arctic, this effect of longwave flux can be stronger near the surface because of the abundance of longwave-absorbing low-cloud cover that reemits longwave radiation to the surface during the cold season (Curry et al., 1996). Figures 4.18a and 4.18d show longwave radiative heating at troposphere based on the SST change: CTRL generates larger longwave radiative heating over the Arctic region than baseline experiment (contour). CONV induces rather cooling compared to CTRL, and POLY induces weaker warming than CTRL (shade). Meanwhile, the difference in longwave radiative heating at lower troposphere between CONV (POLY) and CTRL is relatively weak compared to heating by other processes (Fig. 4.18). This may have been caused by seasonal variations in the Arctic

longwave radiation; longwave radiative heating in lower troposphere is effective only during early winter due to extremely cold conditions at the near surface during middle and late winters (Fig. 4.16a). In addition, longwave radiative heating in the lower troposphere does not represent the only effect of longwave emissions at the surface. Because it presents the difference in longwave radiative heating in equilibrium state, longwave radiative heating results from the total effects of factors that contribute to the temperature change in the lower troposphere. Thus, the effect of change in longwave radiation at surface could be underestimated in Figs. 4.18a and 4.18d.

Turbulent heat diffusion in lower troposphere below 850 hPa over 70°–80°N suggests that changes in sensible heat fluxes mainly contribute to the near-surface warming (Figs. 4.18b and 4.18e). CTRL induces greater diffusive heating in the lower troposphere than the baseline experiment. CONV generates greater diffusive heating than CTRL, and POLY generates even greater heating than CONV. In particular, diffusive heating effects associated with different SST conditions appear to induce stronger lower atmospheric warming, as compared to the effects from longwave radiation. The difference in sensible heat flux among our experiments became larger during late winter (Fig. 4.16b) and it appears that the different vertical temperature profiles between early and late winter, especially shown in the difference between CTRL and CONV, might be

influenced by sensible heat flux (Figs. 4.17a and 4.17b).

POLY simulates cooling near the surface and heating in the troposphere by moist processes that is the largest and most significant among experiments (Fig. 4.18f). In particular, tropospheric heating via moist processes over MSR (70–80°N) in POLY reaches around the 500 hPa level, much higher when compared to the altitude in CONV (Fig. 4.18c). This vertical extension of heating by moist processes should be affected by the strengthened vertical moisture transport such as shallow convection. Large increases in the surface fluxes and associated warming and moistening induces a decrease in static stability and thickening of the planetary boundary layer. The decrease in static stability occurs through an enhanced vertical mixing of heat and moisture that, consequently, contributes to warming and moistening in the mid-troposphere. This destabilization effect associated with the increase in surface fluxes has been suggested by observational relationships between an increase in mid-level cloud cover and a decrease in SIC during early winter (Schweiger et al., 2008).

In addition to affecting vertical propagation, warmer SST conditions over MSR can spread warming and moistening further into the mid-latitudes, even under the same sea ice condition. Figure 4.19 shows a vertical cross-section of changes in the zonal-averaged temperature (shade) and specific humidity (contours) during early and late winter for each method. It also shows

observational changes. As SST becomes warmer from CTRL to POLY, warming reaches a high altitude and spreads farther south to mid-latitudes, with a corresponding change in specific humidity. In particular, the SST condition in POLY leads to warming and moistening even to the mid-latitudes as south as 45°N (Figs. 4.19c and 4.19g). According to ERA-Interim, warming and moistening over the high latitudes, particularly amplified warming and moistening over the Arctic, occur between the cold seasons for 2006–2010 and 1982–2000 (Figs. 4.19d and 4.19h). Therefore, the strong warming and moistening over the Northern Hemisphere in POLY, are closest to the recent observed changes in the Arctic and high-latitude regions. In particular, among the experiments, POLY simulates well the vertically and horizontally expanded warming during both early and late winters as captured in ERA-Interim data (Figs. 4.19c and 4.19g). It has been suggested that these changes in the lower troposphere is linked closely with recent drastic sea ice melt (Screen and Simmonds, 2010a); the present results support this linkage.

4.2.5. Discussion

Sensitivity of atmospheric warming in response to the SST for reduced SIC in the Arctic Ocean has been examined. It has been found that temperature and moisture responses in the lower troposphere over the Arctic are sensitive to even a small amount of SST changes under the same sea ice condition. Warmer SSTs

generate substantially stronger warming near the surface, which expands vertically and horizontally compared to colder SST conditions with the same SIC. Surface heat fluxes play crucial roles in shaping these different atmospheric responses. Longwave radiation and sensible and latent heat fluxes perceptively respond to different SST conditions. Averaged over the entire cold season, latent and sensible heat fluxes are more responsible for altered atmospheric responses than longwave radiation. In particular, distribution of atmospheric heating into diffusive and condensational processes implies that sensible heat fluxes affect near-surface warming, and latent heat fluxes affect the warming in the mid-troposphere above 800 hPa. Static stability is decreased, and the air-column expands vertically due to warming and moistening in the lower troposphere.

This study suggests that the SST field in POLY may be most suitable for examining the effect of sea ice change on the climate over the Arctic and surrounding regions as the results in POLY compares most closely with observations based on recent observational changes and in terms of larger impact on the atmosphere, vertically and horizontally. Thus, the SST adjusting methodology used in POLY can be recommended for examining the effect of sea ice condition changes, including realistic and artificial changes. Meanwhile, because a part of SSTs used in the ERA-Interim is adjusted with sea ice concentration, a similarity between result from POLY and the ERA-Interim may

come from adjusting method. This suggests that present modeling result should be handled more carefully.

To address the validity of the polynomial fitting method more clearly, we have conducted additional experiments using observed and prescribed SSTs and comparing results with POLY (Fig. 4.20). For comparison, two different SST conditions, HadISST and OISSTv2, have been used over MSR. Comparison of the mean atmospheric surface air temperature response to the SST difference for the two periods (2006–2010 versus 1982–2000) against HadISST, POLY can capture qualitatively similar features, supporting the use of the polynomial fitting method (Figs. 4.20a–b). Rather unexpectedly, the SAT response from OISSTv2 is significantly different than that from HadISST (Figs. 4.20b–c). These results show that atmospheric circulation responses sensitively to small SST changes in the Arctic Ocean. It is also noted that the quality of SST observations over MSR is poor in both products and also is subjected to statistical fitting using slightly different methods (Appendix B in Rayner et al. (2003)).

The polynomial fitting method can be more useful for studies that do not use observed SST data, e.g., examining certain sea ice melting trends on the paleo- or future climates. To examine the usability of the POLY method for future climate projection studies, we have applied our polynomial fitting coefficients to 14 model results from future experiments of RCP 4.5 scenarios in

CMIP5. We have generated SST conditions by applying the polynomial coefficients to SIC differences between 2051–2055 and 2006–2010, and compared the generated SSTs with simulated SSTs (Fig. 4.21). As shown in the figure, the polynomial fitting method successfully reproduces the simulated SST distribution well in the sea ice retreated region. The method also well captures the SST warming pattern in most of these models, although the estimated SST is slightly warmer than the simulated ones. Among the models, the estimation method gives the best match for GFDL-CM3, GFDL-ESM2G, MIROC5, MRI-CGCM3, and NorESM1-M.

Warming and moistening responses in troposphere in our study, even in POLY, are still weaker than the observed (see Fig. 4.19), basically due to the difference in internal variability based on the differences in the averaging periods for the observed and simulated records. Nevertheless, this can occur if recent tropospheric warming and moistening over the Arctic is induced by additional factors other than sea ice retreat. For example, heat and moisture can be transported from the lower latitudes to the Arctic by atmospheric and oceanic circulations that also contribute to Arctic warming and moistening (Alexeev et al., 2005; Chung and Räisänen, 2011; Graversen et al., 2008). Perhaps, given the weak responses obtained in this study compared to observations, contributions from other factors are larger. This situation can be explored in additional

experiments using the observed global SST conditions for 2006–2010, which can replicate well the recent vertical warming structure that extends to the upper troposphere. This result also implies that there can be another important factor, in addition to melting sea ice, which contributes to the recently observed tropospheric warming over the Arctic. The SST condition over middle or lower latitudes can be one such factor.

Table 4.3 The 3rd polynomial fitting coefficients for the relationship between SST and sea ice fraction for each month during the cold season.

	Oct	Nov	Dec	Jan	Feb	Mar
a	1.4573	1.1727	1.4012	1.3413	1.1103	1.1486
b	-4.248	-4.716	-4.5208	-3.7716	-3.1089	-3.3505
c	3.3636	5.7375	6.0431	5.4956	4.3157	4.2713
d	-2.626	-4.278	-5.1979	-5.4454	-4.6410	-4.3526

* $y = \mathbf{a} + \mathbf{b}x + \mathbf{c}x^2 + \mathbf{d}x^3 + \varepsilon$ where x and y are sea ice (fraction) and SST ($^{\circ}\text{C}$), respectively, and ε is residual.

Table 4.4 Summary of surface conditions of experiments in this study.

Experiment	Sea ice	SST	SST averaged over the Arctic Ocean (north of 67°N, °C)						
			OC T	NO V	DEC	JAN	FEB	MA R	OND JFM
Baseline	averaged annual cycle for 1982–2000	averaged annual cycle for 1982–2000	0.10	-0.65	-0.89	-1.01	-1.08	-1.08	-0.77
CTRL		same as baseline	0.10	-0.65	-0.89	-1.01	-1.08	-1.08	-0.77
CONV	averaged annual cycle for 2006–2010	adjusted to average of climatology for 1982–2000 and -0.8°C	0.10	-0.56	-0.82	-0.93	-1.00	-1.01	-0.70
POLY		adjusted to the 3rd degree polynomial fitted SST where sea ice fraction is melted to below 0.9	0.47	-0.50	-0.80	-0.92	-1.01	-1.02	-0.63
*2006–2010	averaged annual cycle for 2006–2010	averaged annual cycle for 2006–2010	0.38	-0.49	-0.78	-0.88	-0.97	-1.03	-0.63

*only for comparison

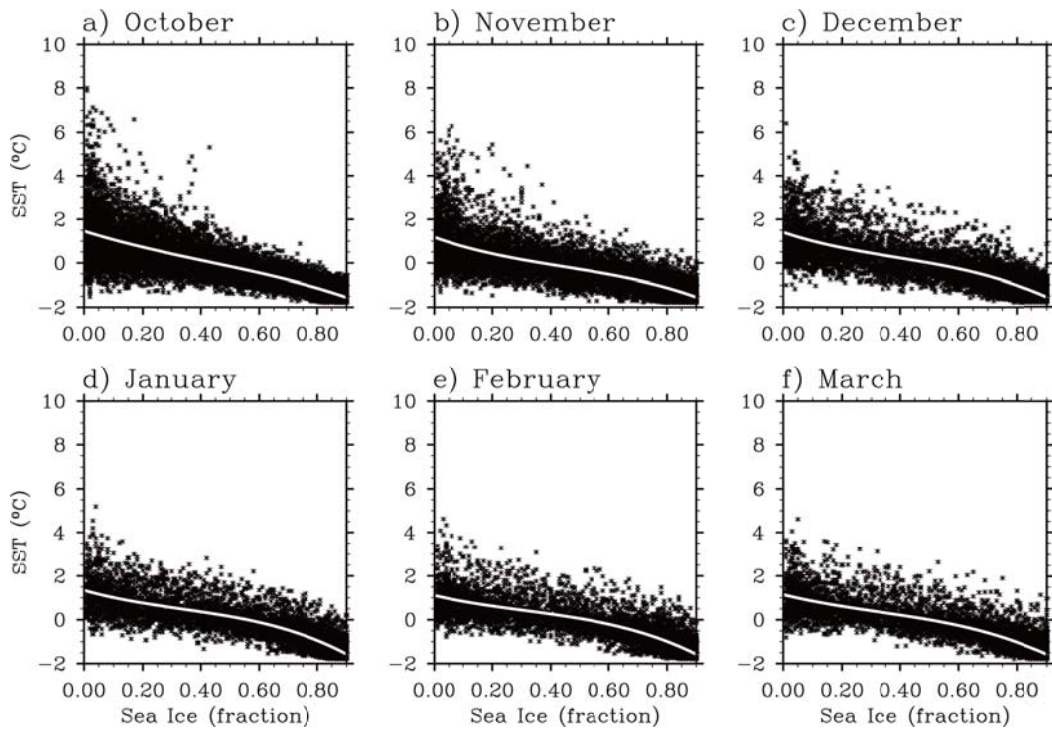
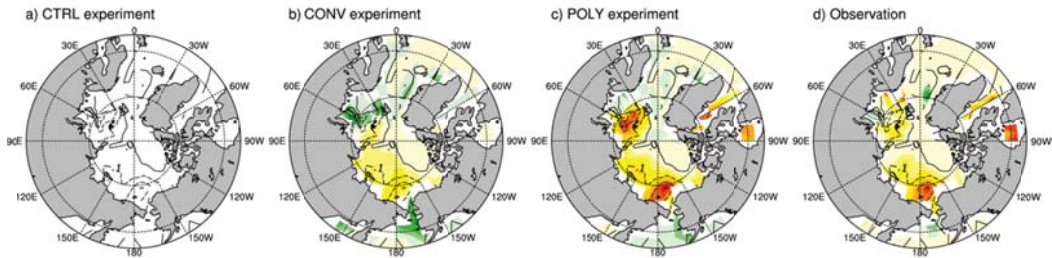


Fig. 4.11 Scatter plot between sea ice concentration (SIC; fraction) and sea surface temperature (SST) over the Arctic (north of 60°N) for the cold season (October through March) of the period 1982–2000 from OISST v2. White lines indicate the third-degree polynomial fitting between SIC below 0.9 fraction and SST, in each month.

Early winter (October–November–December)



Late Winter (January–February–March)

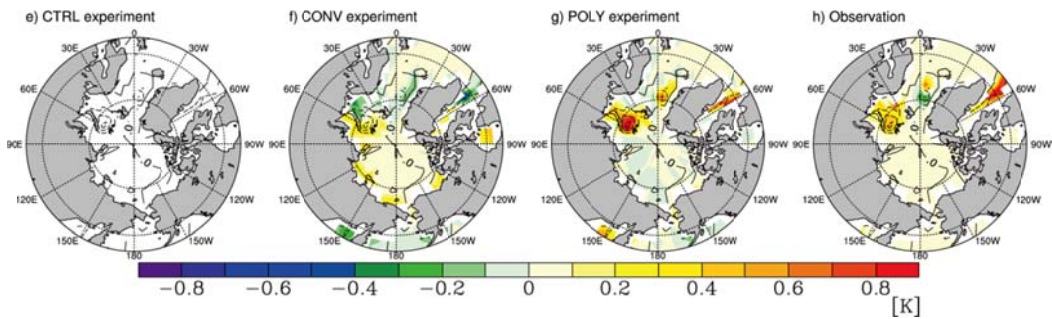


Fig. 4.12 Differences of sea surface temperature (shade) and sea ice concentration (contour) boundary conditions from (a and e) CTRL, (b and f) CONV, and (c and g) POLY experiments compared to the baseline experiment during early winter (October–November–December) and late winter (January–February–March); (d and h) Differences between mean sea surface temperature during early and late winters for 2006–2010 and 1982–2000 from the OISST v2. Differences are plotted only over the region where sea ice reduced above 0.01 fraction. In all panels, the contour interval is 0.1 fraction.

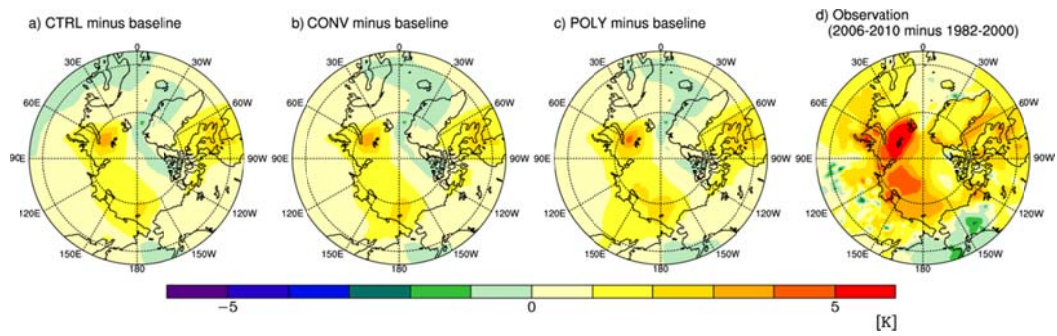


Fig. 4.13 Change in surface air temperature from (a) CTRL, (b) CONV, (c) POLY compared to the baseline experiment during the cold season, and (d) 2 m air temperature difference between 2006–2010 and 1982–2000 during the cold season from the ERA-Interim data.

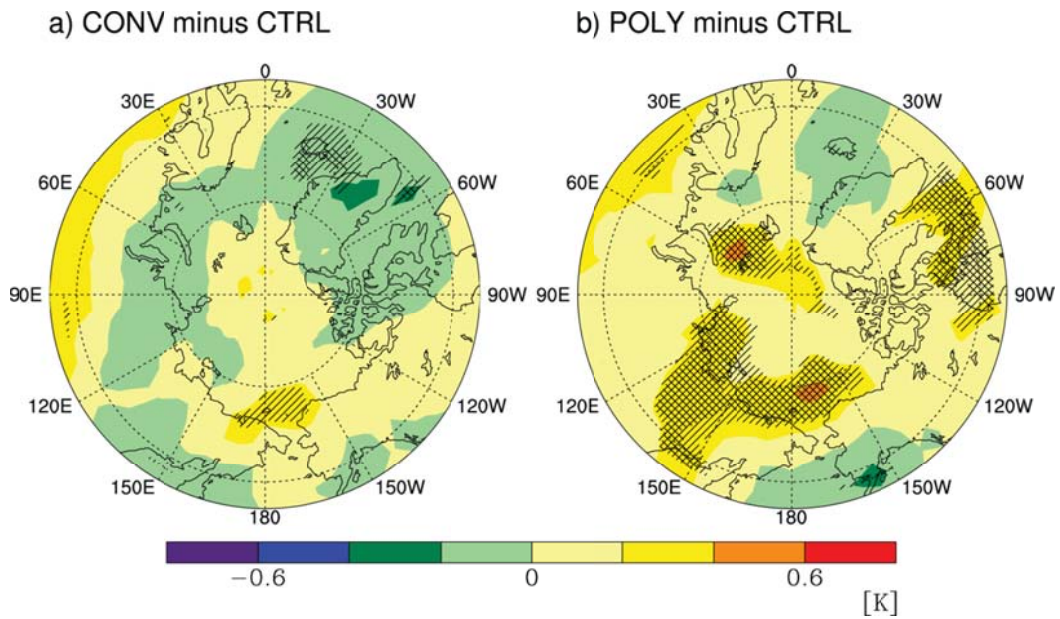


Fig. 4.14 Change in surface air temperature from (a) CONV and (b) POLY compared to CTRL experiment during the cold season. Oblique and cross regions indicate that surface air temperature response is significant at the 90% and 95% confidence level, respectively.

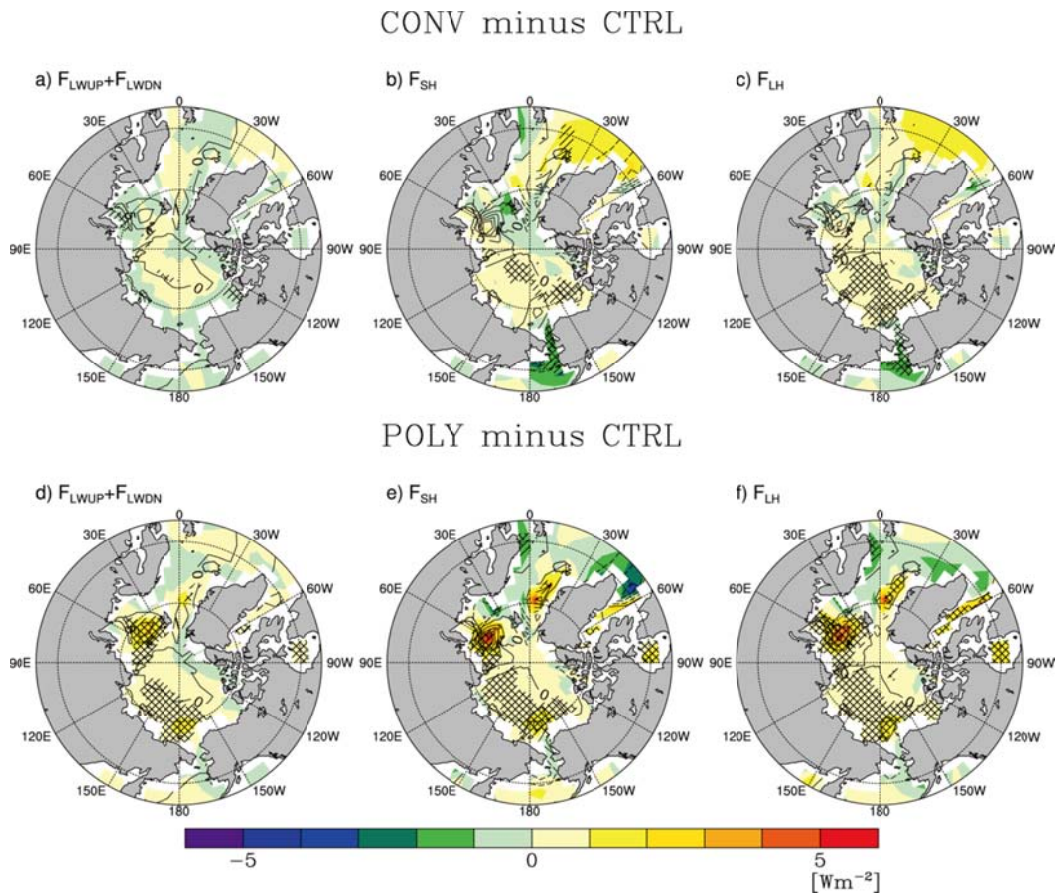


Fig. 4.15 Changes in net longwave flux (positive in the upward direction), sensible heat flux, and latent heat flux at the surface from CTRL (contour in all figures) compared to the baseline experiment, and changes in (a–c) CONV and (d–f) POLY experiments compared to CTRL experiment (shade in all figure) during the cold season. Contour interval is 5 W m^{-2} . Oblique and cross regions indicate that surface fluxes are significant at the 90% and 95% confidence level, respectively.

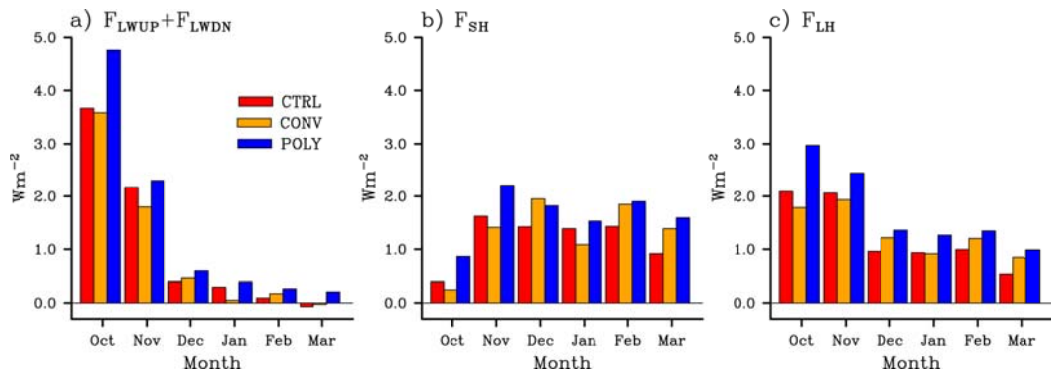


Fig. 4.16 Monthly changes in (a) net longwave flux (positive in the upward direction), (b) sensible heat flux, and (c) latent heat flux averaged over the Arctic Ocean (north of 67°N) from CTRL, CONV, and POLY experiments compared to the baseline experiment.

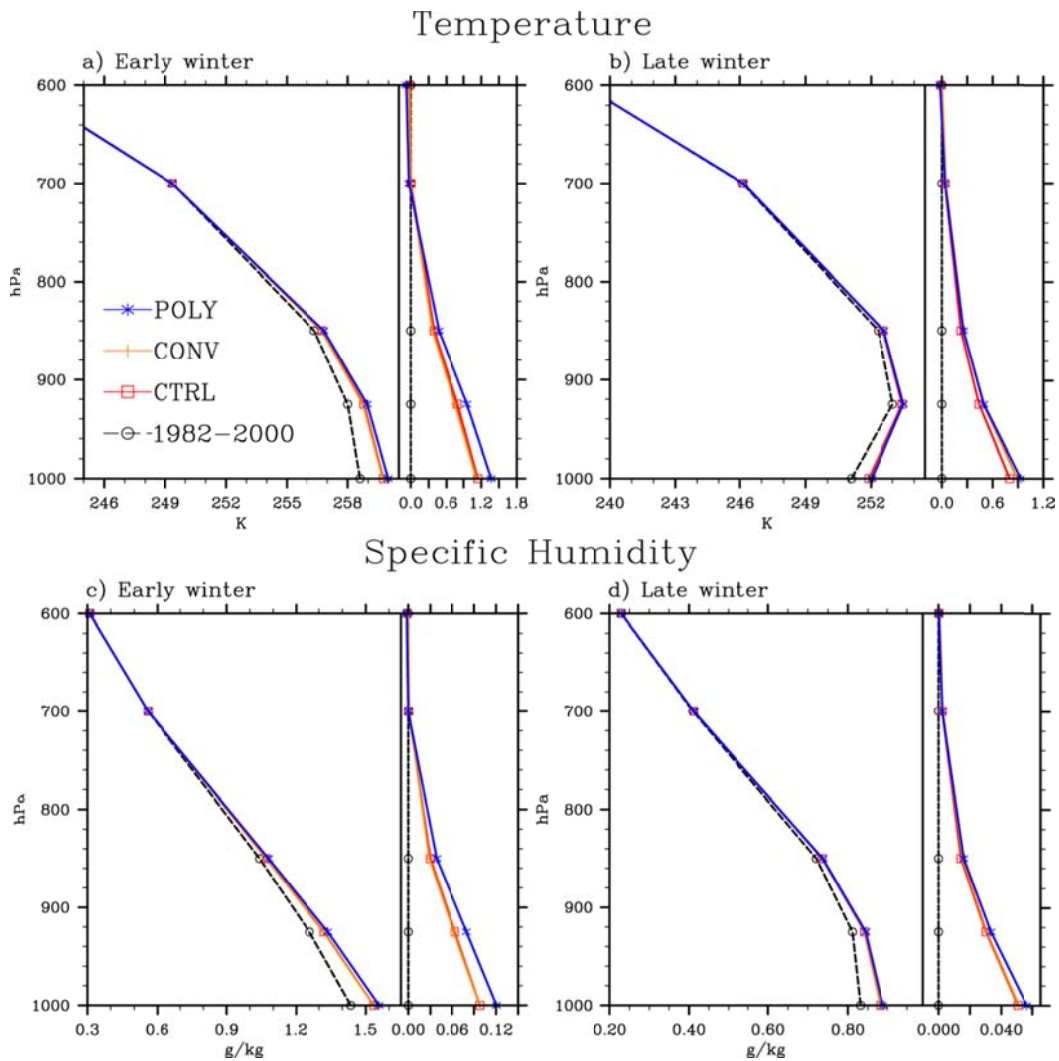


Fig. 4.17 Vertical profiles in temperature and specific humidity averaged over the Arctic Ocean (north of 67°N) in the baseline, CTRL, CONV, and POLY experiments during early and later winter (left panel) and their differences to the baseline experiment (right panel).

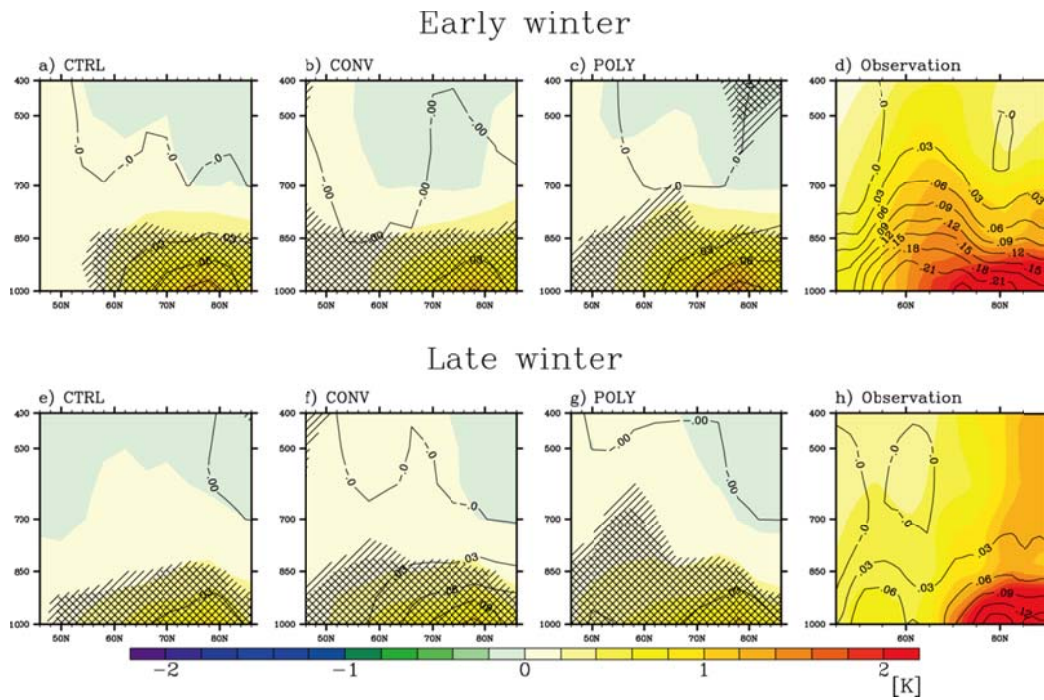


Fig. 4.19 Changes in zonal-averaged temperature (shade) and specific humidity (contour) during early winter (October–November–December) and late winter (January–February–March) from CTRL, CONV, and POLY experiments compared to the baseline experiment. Oblique and cross regions indicate that surface fluxes are significant at the 90% and 95% confidence level, respectively; (d and h) changes in the same variables for the periods 2006–2010 and 1982–2000 from the ERA-Interim data. Contour interval is 0.03 g kg^{-1} .

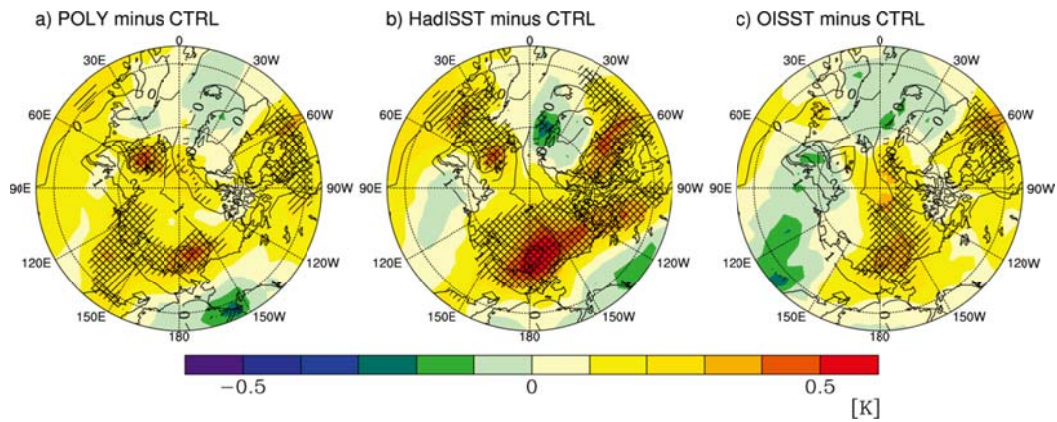


Fig. 4.20 Change in surface air temperature from CTRL compared to the baseline experiment (contour), and changes in (a) POLY, (b) HadISST over the MSR, and (c) OISSTv2 over the MSR compared to CTRL (shade) during the cold season. Contour interval is 0.5 K. Oblique and cross regions indicate that surface air temperature response is significant at the 90% and 95% confidence level, respectively.

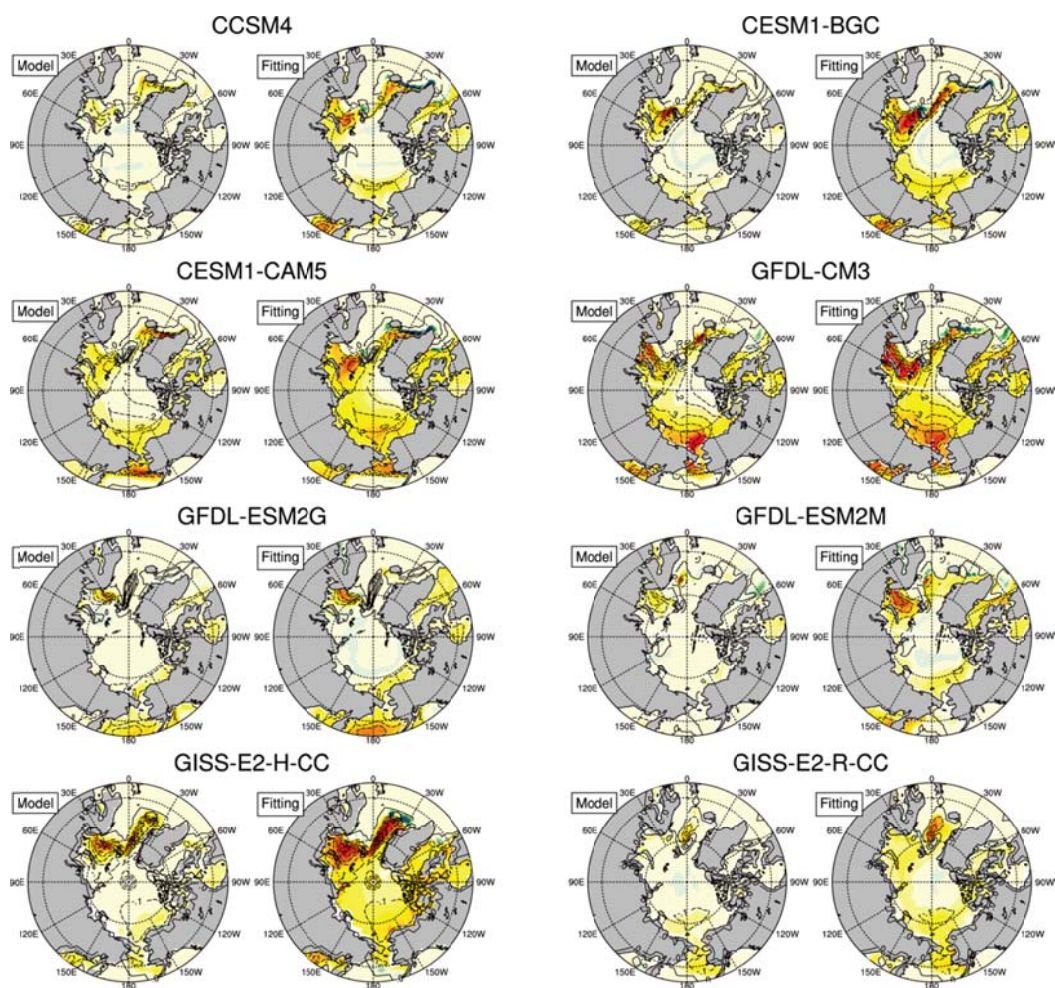


Fig. 4.21 Comparisons between simulated SST (model; left figure in each panel) and adjusted SST by polynomial fitting with SIC change (fitting; right figure in each panel) among 14 model results with future experiment of the RCP4.5 scenario in the fifth phase of the Climate Model Intercomparison Project. Model differences are calculated with simulated SSTs averaged for 2051–2055 and simulated SSTs averaged for 2006–2010. Fitting differences are calculated with fitted SSTs by using polynomial coefficients in the POLY method, SIC values averaged for 2051–2055 and simulated SSTs averaged for

2006–2010. Shading indicates sea surface temperature, and contour indicates sea ice concentration with an interval of 0.1.

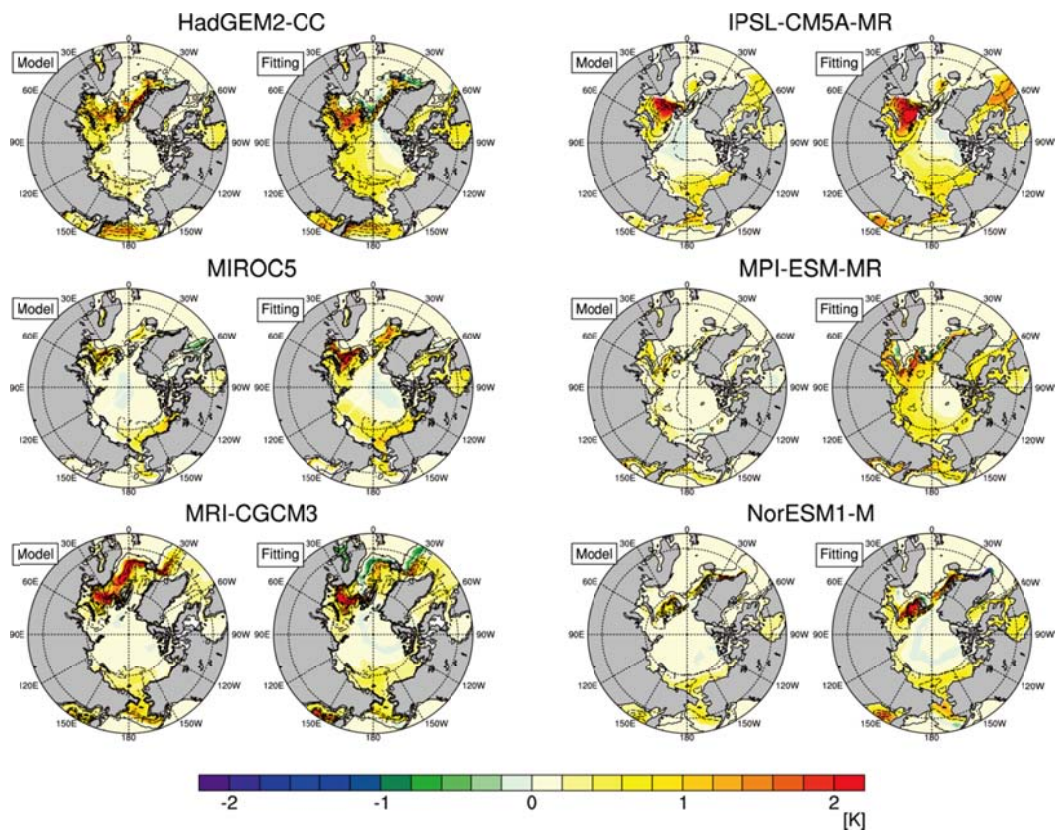


Fig. 4.21. (continued)

4.3. Modeling the change in cloud and its effect in relation to sea ice

As mentioned earlier, much of GCMs have difficulty in simulating cloud amount in the Arctic region (Jones et al., 2004; Vavrus and Waliser, 2008; Vavrus et al., 2009; Walsh et al., 2005), thereby displaying a large discrepancy in total cloud amount among models, particularly during winter (Karlsson and Svensson, 2011). Jones et al. (2004) has indicated climate models commonly produce excessive wintertime Arctic clouds, particularly at low levels, an error attributed to an insufficient treatment of cloud processes unique to polar region. It is known that the CAM3 also produce excessive low level cloud over the Arctic during cold season (Vavrus and Waliser, 2008). Since the focus of modeling work is cloud change in relation to sea ice, we adopt modified cloud amount parameterization into our modeling the impact of reduced sea ice on the recent Arctic climate change.

4.3.1. FREEZEDRY cloud amount parameterization

For improving parameterization of the Arctic low cloud, Vavrus and Waliser (2008) suggests the “FREEZEDRY” parameterization, which is designed to alleviate the bias of excessive low clouds during polar winter by reducing the cloud amount under very dry conditions. The CAM3 uses three types of cloud amount parameterizations: convective cloud, marine-stratus cloud, and layered

cloud. In these, layered cloud amount parameterization is used for low-level cloud in winter Arctic. Current layered cloud fraction in the CAM3 is function of relative humidity as follow:

$$f = \left[\frac{(RH - RH_{MIN})}{(1 - RH_{MIN})} \right]^2 \quad (4.4)$$

However this type of formula is not well suited for high latitudes, particularly the extremely cold and dry atmospheric conditions typical of polar winter. Thompson and Pollard (1995) suggests that reducing the relative humidity-derived low cloud fraction (f) when the gridbox mean specific humidity (q) falls below a threshold value (0.003 kg kg^{-1}):

$$f = f \times \left[\max(0.15, \min\left(1.0, \frac{q}{0.003}\right)) \right] \quad (4.5)$$

Thus, the originally calculated cloud fraction is only adjusted under very dry atmospheric conditions, in which case the low cloud amount is reduced by as much as 85% of its relative humidity-based value. Figure 4.22 presents relative humidity, layered cloud fraction in original CAM3, and layered cloud fraction by FREEZEDRY parameterization under varying temperature and specific humidity. Relative humidity is calculated with equation by Magnus approximation based on the Clausius-Clapeyron relationship. Figure 4.22a indicates that air becomes

supersaturated easily by less moisture under extremely cold condition. Thus, the CAM3 simulated excessively large amount in Arctic cloud in these condition (Fig. 4.22b). The FREEZEDRY modification, in meeting its own purpose, generates less cloud amount than original CAM3 under dry and cold conditions (Fig. 4.22c). Vavrus and Waliser (2008) performed simulation by using CCSM3 adopted the FREEZEDRY parameterization, and gained enhanced result with reduced polar low cloud in similar with observations.

We also perform 50 years test simulations with the original CAM3 and modified with FREEZEDRY parameterization in order to check whether adaptation has been done correctly and confirm the performance of FREEZEDRY parameterization. Figure 4.23 describes spatial distributions of low level cloud amount during winter from simulations with original cloud amount parameterization and FREEZEDRY parameterization. The FREEZEDRY parameterization successfully reduces a large amount of low level cloud over the Arctic and continents at high latitudes where are cold and dry during winter.

In addition, FREEZEDRY parameterization has another effect besides its own purpose that removes excessive cloud amount. In most extremely cold and dry region (below about 260 K and 3 g/kg), the original CAM3 always generates almost maximum cloud amount (Fig. 4.22b). In contrast, in this region, FREEZEDRY parameterization generates changed cloud amount by gradually

reduced with specific humidity (Fig. 4.22c). This effect could generate stronger relationship between temperature and cloud. In original CAM3, cloud amount has few or no response to temperature change during winter. It always generates almost maximum cloud under cold and dry condition during winter. However, in the FREEZEDRY parameterization, temperature change could bring change in cloud amount as well. Thus, tropospheric warming could be linked to increases in winter cloud. The FREEZEDRY modified cloud amount parameterization is currently adopted in recent fourth and fifth versions of CAM (Neale et al., 2012; Neale et al., 2011).

4.3.2. Response over the Arctic on reduced sea ice cover in AGCM

Experiment

To examine whether sea ice retreat is a key factor for changes in cloud and its relationship to environmental atmospheric states during recent decade, we perform AGCM experiments with sea ice retreat condition. We perform two 50 year experiments configured with a finite volume core having a 2x2.5 horizontal resolution; baseline and sensitivity experiments. For more realistic cloud amount simulation, we adopt the FREEZEDRY cloud amount parameterization for the cloud. The baseline experiment (hereinafter SIC_CTRL) uses monthly climatological SST and sea ice concentration from the OISSTv2 for 1982–2000,

and under CO₂ concentration of 369 ppmv. Sensitivity experiment (hereinafter SIC_REDUCE) is performed for same 50 year to examine effects of recent sea ice retreat. The SIC_REDUCE experiment prescribes reduced sea ice condition in the Arctic averaged over 2006–2010, with SST condition adjusted befittingly with reduced sea ice concentration by method suggested in earlier chapter.

First, modeling result shows that surface air temperature, PBL height, total cloud amount, longwave CRF increase mainly over the sea ice retreated region in SIC_REDUCE experiment compared to SIC_CTRL experiment. The Barents, Kara, Chukchi Seas, where sea ice reduces largely, induce large increases in these variables (Fig. 4.24). These changes related to sea ice retreat between experiments are consistent to differences between E21C and L20C in reanalyses (Fig. 4.8). In addition, atmospheric pressure system also resembles differences in reanalyses; high pressure system develops across the Eurasian side of the Arctic Ocean and Eurasia continent (Fig. 4.24c).

In addition, sea ice retreat induces tropospheric warming and moistening over the Arctic region during winter (Fig. 4.25a). Reduced sea ice is sufficient to increase temperature and specific humidity even under same CO₂ concentration with SIC_CTRL experiment. This might be because surface condition change by sea ice retreat supplies sufficient heat and moisture to troposphere by turbulent and radiative fluxes during cold season (Jun et al., 2013; Screen and Simmonds,

2010b). We examine the effect of change in turbulent heat fluxes due to sea ice retreat on atmosphere through atmospheric heating by diffusion and moistening process among experiments (Figure 4.25b). The diffusive heating over the sea ice retreated region (65–80°N) warms air at near surface, with particularly strong diffusive heating at around 80°N where sea ice cover reduces largely. In contrast, heating by moistening process cools air at near surface and warms air above cooling region. It is found that warming region by moistening becomes higher where sea ice cover reduced more (around 80°N). This indicates that evaporation and convection can occur more frequently over the sea ice retreat region, and convection over more opened ocean can be deeper. Namely, sea ice retreat leads to increase in PBL height and decrease in static stability at near surface by diffusive heating, and this could help frequency and strength of convection to be increased.

SIC_REDUCE experiment shows that an increase in cloud amount occurs over most Arctic regions with larger increasing, and its spatial distribution resembles heating distribution by moistening process (see contour in Fig. 4.25c). The region where strong condensation (heating by moistening) occurs also shows clearly the increasing in cloud amount. This result supports recent increasing in cloud above 900 hPa in both reanalyses. Meanwhile, the disparity between changes in cloud amount and moistening process is a larger increase in

cloud amount over the central Arctic region. Over this region, climatological temperature is extremely low, and increasing in moisture is relatively larger than increasing in temperature (Fig. 4.25a). This leads to large increasing in relative humidity, thus cloud can be more formed easily at this region.

The stronger increasing over the central Arctic region is also found in the change in relationship between low level cloud and zonal-averaged temperature. The relationship becomes stronger over the most Arctic region (north of 60°N), and the relationship becomes much stronger over the central Arctic compared to SIC_CTRL experiment (sea shading in Fig. 4.25c). In reanalyses, the enhancement in relationship between cloud and temperature over the central Arctic becomes stronger during the E21C (Fig. 4.9). Modeling results from sensitivity experiments well reproduce the relationship change over the Arctic during the E21C, and this suggests that sea ice retreat could induce the increasing in cloud amount and the enhancement of the effect of cloud on the Arctic climate in winter.

4.3.3. Discussion

Modeling result strongly suggests that recent changes in cloud and atmospheric state over the Arctic are associated with sea ice retreat. In AGCM experiments, reduced sea ice cover leads to an increasing in surface fluxes, a

decrease in lower-tropospheric static stability, and deepening of planetary boundary layer as seen in the Arctic surface during recent decade. Consequently, cloud in most Arctic troposphere increases according to reduced sea ice. In particular, modeling result also suggests that convection could be deeper where sea ice reduces more largely even during winter. Eventually, an increasing in cloud reinforces the CRF and precipitation over the Arctic, and, the local relationship between cloud at lower troposphere and atmospheric states, in turn, also becomes strengthened.

Modeling result in this study differs from prior modeling work in Vavrus et al. (2011a). Vavrus et al. (2011a) investigated cloud change in the case of rapid sea ice decline from CCSM3 future climate simulation. Their result presents that winter cloud decreases during rapid sea ice loss. Although major decreasing occurs in mid and high level cloud, low level cloud also decreases. In contrast, modeling result in this study shows the increasing in cloud under sea ice reduced condition. The difference between two modeling results is mainly due to cloud amount parameterization in each model. Both studies use same CAM3 for simulating atmosphere, but we utilize the modified cloud amount parameterization which is designed to reduce exceeded cloud amount at low level. This might produce different cloud response to sea ice retreat.

Meanwhile, much of modeling results predict that the Arctic warming under

global warming accompanies an increasing in winter Arctic cloud. Most climate models and their ensemble mean values in the CMIP3 predict that cloud increases during winter in future climate simulation (Vavrus et al., 2009). In future experiment from the CMIP5, most climate models also predict that cloud increases and its relationship to SAT is also closer during winter (Figs. 4.26 and 4.27). Most models and their ensemble mean from the CMIP5 predict that strong surface warming emerges over the Arctic during winter in future (RCP4.5 experiment) compared to present climate (PIcontrol experiment). Additionally, cloud amount also increases during cold season with the strongest increasing in November. Similarly to our experimental results, sensible and latent heat fluxes also increase largely during winter, and this may play an important role for increasing cloud (Fig. 4.26). In addition, longwave CRF increases largely during winter (Fig. 4.26c), and relationship between cloud and surface also becomes closer in future climate (Fig. 4.27).

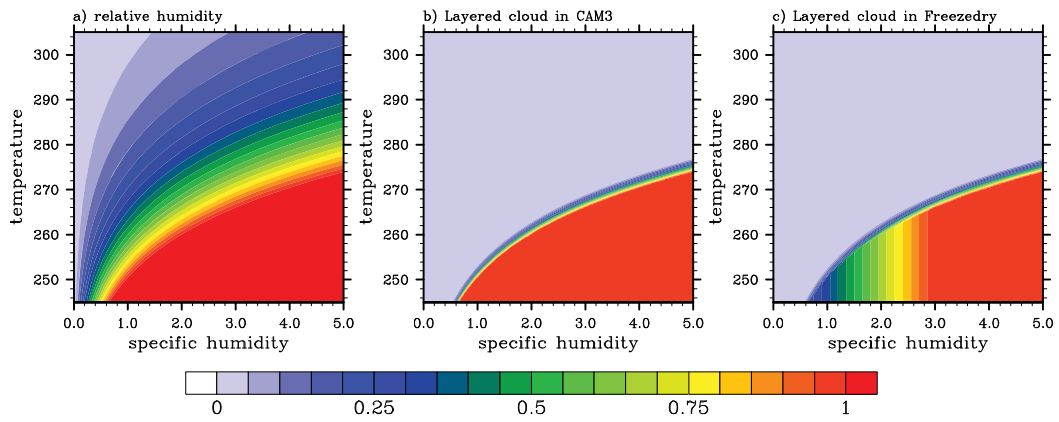


Fig. 4.22 (a) relative humidity, (b) layered cloud amount by cloud amount parameterization in CAM3, and (c) layered cloud amount by FREEZEDRY modified parameterization under varying in temperature and specific humidity.

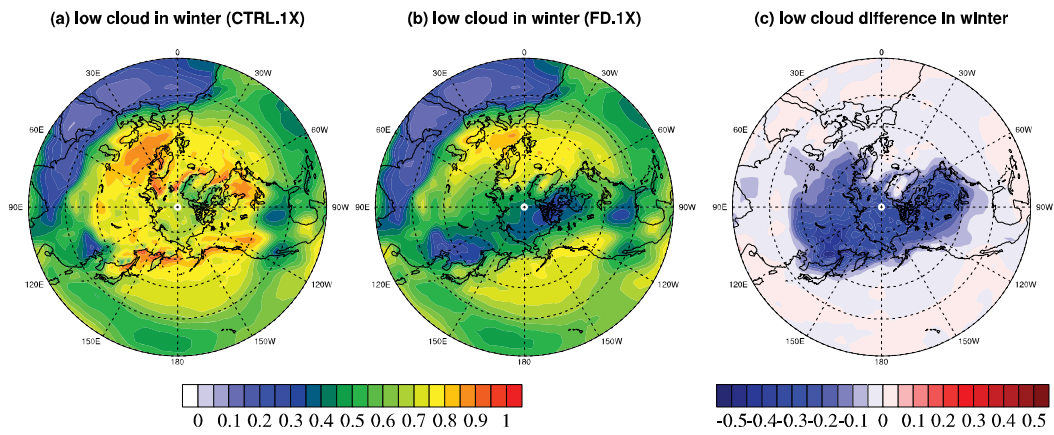


Fig. 4.23 Low level cloud amount during winter from (a) CAM3 original cloud amount parameterization, (b) FREEZEDRY cloud amount parameterization, and (c) their difference.

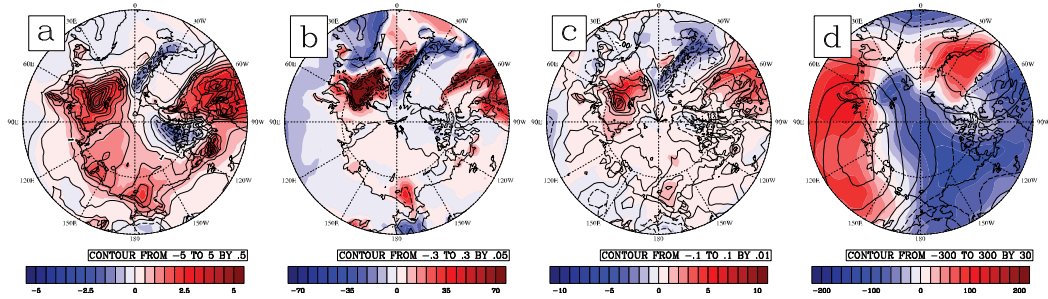


Fig. 4.24 Changes in (a) surface air temperature (contour) and 850 hPa thickness (shading), (b) sea ice cover (contour) and planetary boundary layer height (shading), (b) total cloud amount (contour) and longwave cloud radiative forcing (shading), and (c) 500 hPa geopotential (contour) and sea level pressure (shading) from SIC experiment compared to CTRL experiment.

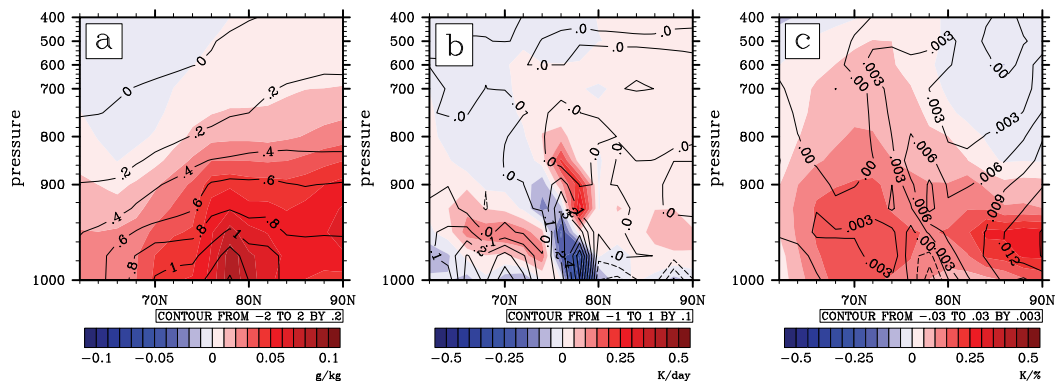


Fig. 4.25 Changes in (a) zonal-averaged temperature (contour) and specific humidity (shading), (b) heating by diffusion (contour) and moistening process (shading), and (c) cloud amount (contour) and regressed temperature of low-level cloud amount over the Arctic (shading) from SIC experiment compared to CTRL experiment.

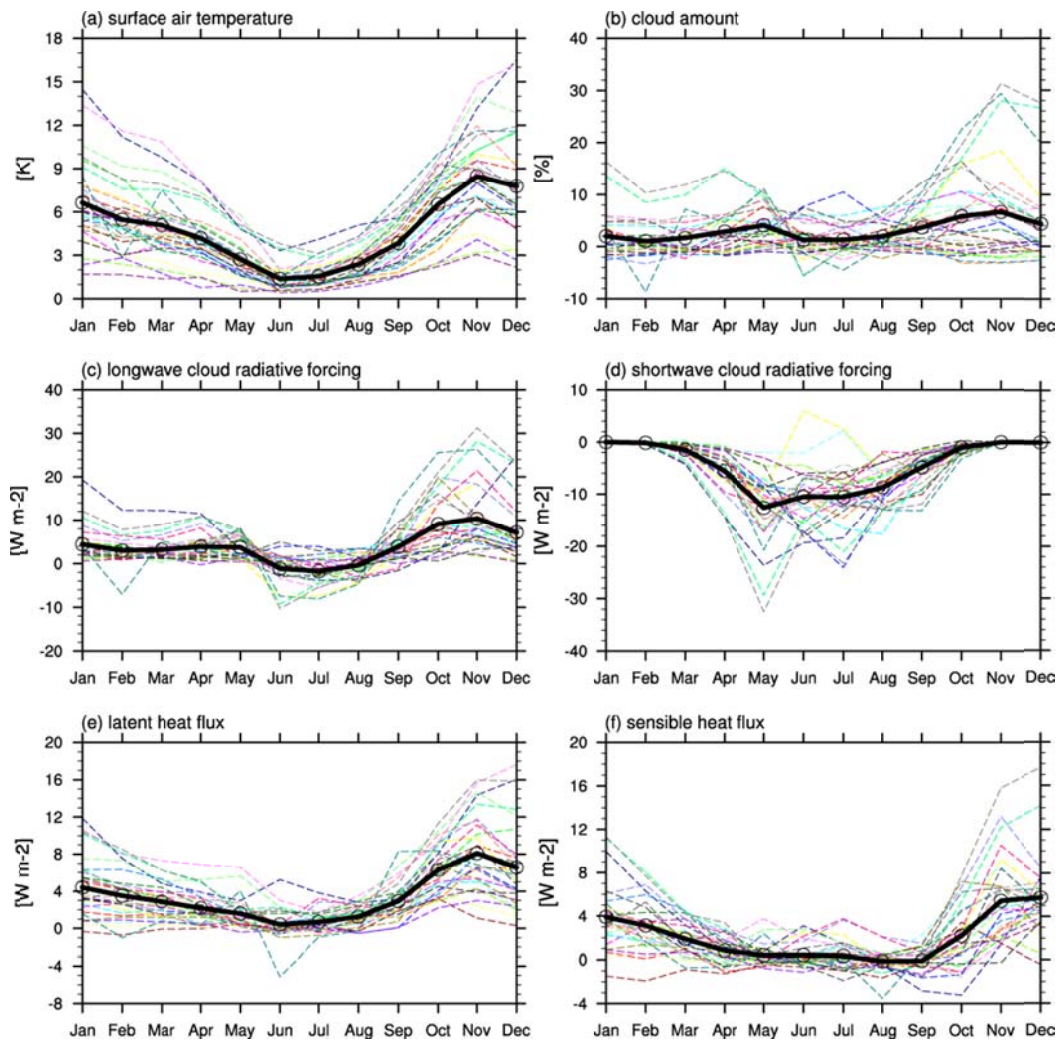


Fig. 4.26 Annual cycles of changes in (a) surface air temperature, (b) cloud amount, (c) longwave cloud radiative forcing, (d) shortwave cloud radiative forcing, (e) latent heat flux, and (f) sensible heat flux averaged over the Arctic (north of 70°N) between RCP4.5 and P1ctrl experiments from climate models in the CMIP5. Solid thick lines in each figure indicate their ensemble mean values.

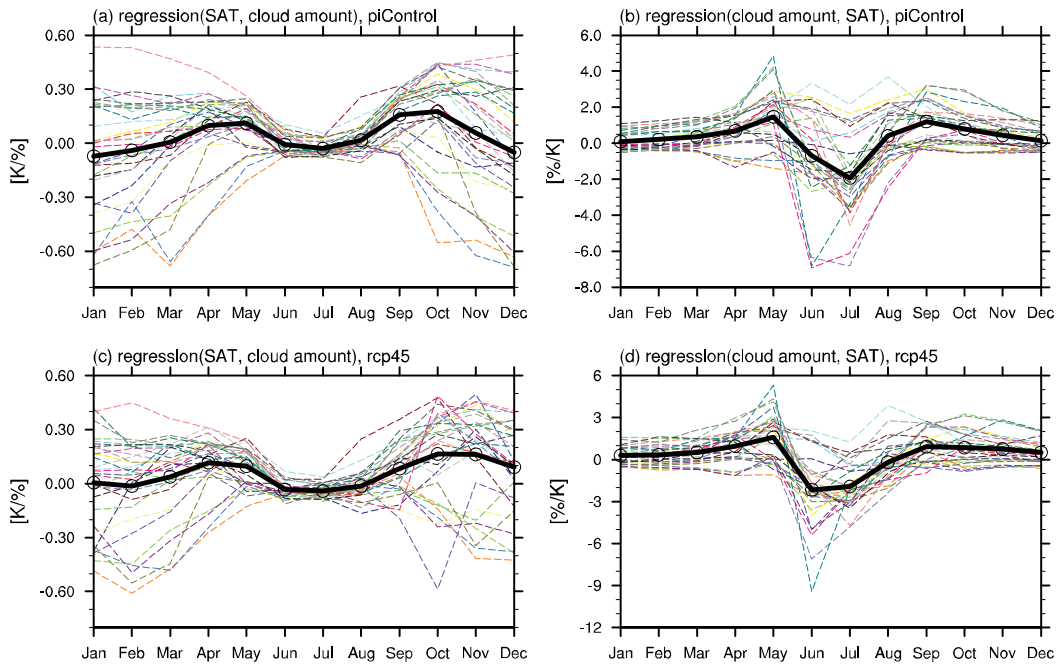


Fig. 4.27 Annual cycles of regressions of (a) cloud amount onto surface air temperature, and (b) surface air temperature onto cloud amount averaged over the Arctic (north of 70°N) from PIctrl experiment, and (c) cloud amount onto surface air temperature, and (d) surface air temperature onto cloud amount from RCP4.5 experiment in the CMIP5. Solid thick lines indicate their ensemble mean values.

5. SUMMARY AND DISCUSSION

The Arctic has experienced substantial warming in recent decades of which degree and rate is much larger than global averages. This phenomenon, which is also widely predicted from future climate modeling for several climate change assessment reports of the Intergovernmental Panels for Climate Change, is called as the Arctic amplification. Various climate factors on the globe could contribute to the amplified warming over the Arctic because of the highly sensitive Arctic climate system and the northward transport into the high latitude region. Much of understanding for these contributing factors come from modeling study because of lack of observation datasets owing to severe weather and climate conditions of the Arctic. In particular, less consideration of climate factors such as vegetation, cloud, and sea ice in modeling could bring large uncertainties in understanding the Arctic climate. Thus present thesis examines the contributions of vegetation and cloud to the Arctic amplification through modeling work with adopting a global dynamic vegetation model (DGVM) and improving physical processes related to sea ice and cloud.

First, modeling result from simulating the Community Climate System Model 3 (CCSM3) coupled with a DGVM indicates that potential vegetation change under a doubled CO₂ situation and its feedback have an influence on

surface warming over the Arctic/high-latitude region. This dissertation performed two baseline experiments under the present and doubling CO₂ concentration using the CCSM3-DGVM. Then, an additional simulation without DGVM was performed under doubling CO₂ concentration with the prescribed vegetation taken from the present CO₂ simulation. Model experiments indicate that a vegetation change in high-latitudes may induces substantial alternation of climate change in the Arctic/high-latitude during warm and cold seasons. When the interactive vegetation process is included in the future climate simulation, the warming in high-latitude continent appears to be significantly amplified. Furthermore, and the Arctic sea ice exhibits considerable decline both in areal extent and thickness associated with the vegetation feedback effect. The present results demonstrate that a conspicuous climatic change can take place in the Arctic region from the vegetation-climate feedback, and suggest a possible positive vegetation feedback over the Arctic and high-latitude region in association with anthropogenic global warming.

Next, diagnosis and modeling on recent Arctic cloud change were performed. This dissertation examines changes in Arctic cloud during winter (December to February) in recent three decades and their impacts on atmospheric circulation with multiple datasets from satellite and reanalysis products. From change point analysis applied to both datasets, it was shown that Arctic cloud

decreases gradually during the late 20th century and increases considerably after late 1990s. The gradual decrease and substantial increase in each period are also seen simultaneously in the temperature and moisture at lower troposphere over the Arctic. In particular, the recent profound cloud increasing emerges over the most Arctic and expands to higher altitude compared to decreasing period, accompanying increasing in precipitation. Between decreasing and increasing periods, the relationship between cloud and the Arctic Oscillation does not change, and the region where cloud increasing and moisture upward transport are linked to sea ice reducing moves from the margin to the center of the Arctic. Changes in surface conditions between two periods indicate that reduced sea ice cover in cloud-increasing period leads to an increase in turbulent fluxes from surface, a decrease in lower tropospheric static stability, and deepening of planetary boundary layer. As a result, these altered conditions provide a favorable condition for cloud to be more formed through enhancing upward moisture transport. In addition, these changes tighten the local relationship between cloud at lower troposphere and atmospheric states over the Arctic.

Diagnosis on recent cloud change suggests sea ice change could play a crucial role for changes in cloud and its effect on the Arctic climate. This dissertation investigates surface boundary condition related to sea ice change in order to obtain more accurate modeling result, in advance of modeling the

impact of sea ice on the cloud change. It is found that the atmospheric responses related to Arctic sea ice melt in the cold season (October–March) depend on sea ice fraction and are very sensitive to in-situ sea surface temperature (SST) from a series of atmospheric general circulation model (AGCM) simulations in which multiple combinations of SSTs and sea ice concentrations are prescribed in the Arctic Ocean. The amplitude of surface warming over the melted sea ice region is controlled by concurrent in-situ SST even if these simulations are forced by the same sea ice concentration. Much of the sensitivity of surface warming to in-situ SST are related with large changes in surface heat fluxes such as the outgoing long-wave flux in early winter (October–December) and the sensible and latent heat fluxes for the entire cold season. Vertical extension of surface warming and moistening is sensitive to these changes as well; the associated condensational heating modulates a static stability in the lower troposphere. Thus, changes in SST fields in AGCM simulations must be implemented with extra care, especially in the melted sea ice region in the Arctic. In addition, the statistical method in the thesis for adjusting SSTs in conjunction with a given sea ice change can help to model the atmospheric response to sea ice loss more accurately.

Finally, modeling result of recent Arctic climate change with refined surface boundary condition and cloud amount parameterization suggests that recent

changes in cloud and its effect on the Arctic climate are closely linked to surface condition change due to sea ice retreat even during winter. As seen in reanalyses, modeling result also describes that reduced sea ice cover leads to an increase in turbulent fluxes from surface, deepening of planetary boundary layer, and enhancing of convective process, thereby causing an increasing in cloud and closer relationship between cloud and local atmospheric state over the Arctic. Further investigations from the fifth phase the Coupled Model Intercomparison Project, of which the winter Arctic cloud increases and its impact on the Arctic becomes enhanced in future climate under global warming condition, also confirm this modeling result. The results from diagnosis and modeling emphasize that the cloud may amplify the surface warming over the Arctic during winter in recent decade, under sea ice retreat condition.

The modeling works in the thesis do not adopt fully dynamic ocean model and sea ice model, and this could be a limitation of the present thesis. The effect of vegetation feedback on the Arctic/sub-Arctic climate is examined with SOM and thermodynamical sea ice model. This approach gives an advantage of efficiency, but also could give less accurate result. For instance, momentum transported into the Arctic also increases owing to vegetation feedback, and this can act as mechanical forcing able to cause a deformation of sea ice. Therefore, an adopting full dynamical sea ice model could give a better understanding for

role of vegetation with more improved result because full dynamical sea ice model consider the process related to horizontal transport and mechanical redistribution of sea ice.

Likewise, the investigation of the impact of cloud on the Arctic climate does not consider the impact of cloud on sea ice change. Sea ice is only treated with surface boundary condition, thus interaction between cloud and sea ice is not considered in the modeling. However, it has been suggested that downwelling longwave radiation into sea ice also could affect properties in sea ice (Eisenman et al., 2007; Francis et al., 2005). Adopting full dynamical sea ice model, therefore, also could give a better understanding for role of cloud on recent Arctic climate change with more improved result.

It is known that using coupled global climate model (CGCM) with various component models could usually give better simulation result compared to using single component model. Thus, there has been and is being a long patient effort to improve the CGCM. While much effort exerted into adding new component model to the CGCM, from the modeling perspective, more accurate remapping process in coupling component models can be the vital improvement point. It is essential for CGCM to use remapping process in flux exchanges owing to diverse grid systems among component models. The bilinear and conservative remapping methods have been widely used for the remapping process, and

particularly the conservative remapping method has been more usually used owing to its higher order accuracy. However, while conceived accuracy of the conservative remapping method could be attained by using the 2nd order remapping coefficients, the coupler in most CGCMs currently uses only the 1st order remapping coefficients because of difficulty in implementing high order remapping process and massive computational time.

If the positive feedback process exists between component models, it is possible that the uncertainty due to using only the 1st order remapping coefficients may be amplified as coupling with remapping process repeated. Unfortunately, the Arctic has a well-known positive feedback process between atmosphere and cryosphere – sea ice albedo feedback process. Therefore, for the better simulation result with CGCM, further investigation on uncertainties in the CGCM due to lower order remapping processes, and implementation of coupling with higher order accuracy remapping process are suggested.

Thus, future modeling works of the present thesis could be the Arctic climate modeling with full oceanic and sea ice model, accompanying improved coupling process with more accurate remapping method. These works could give extension of understanding of the role of vegetation and cloud on the Arctic climate.

REFERENCES

- ACIA (2005) Arctic Climate Impact Assessment. Cambridge University Press.
- Alexander MA, Bhatt US, Walsh JE, Timlin MS, Miller JS, Scott JD (2004) The atmospheric response to realistic Arctic sea ice anomalies in an AGCM during winter. *J Climate* 17:890-905.
- Alexeev VA, Langen PL, Bates JR (2005) Polar amplification of surface warming on an aquaplanet in "ghost forcing" experiments without sea ice feedbacks. *Clim Dynam* 24:655-666.
- Andersson C, Pausata FSR, Jansen E, Risebrobakken B, Telford RJ (2010) Holocene trends in the foraminifer record from the Norwegian Sea and the North Atlantic Ocean. *Clim Past* 6:179-193.
- Beesley JA, Moritz RE (1999) Toward an explanation of the annual cycle of cloudiness over the Arctic ocean. *J Climate* 12:395-415.
- Bintanja R, Graverson RG, Hazeleger W (2011) Arctic winter warming amplified by the thermal inversion and consequent low infrared cooling to space. *Nat Geosci* 4:758-761.
- Bitz CM, Fu Q (2008) Arctic warming aloft is data set dependent. *Nature* 455:E3-E4.
- Bitz CM, Gent PR, Woodgate RA, Holland MM, Lindsay R (2006) The influence of sea ice on ocean heat uptake in response to increasing CO₂. *J Climate* 19:2437-2450.

- Boe J, Hall A, Qu X (2009) Current GCMs' Unrealistic Negative Feedback in the Arctic. *J Climate* 22:4682-4695.
- Bonan GB, Levis S (2006) Evaluating Aspects of the Community Land and Atmosphere Models (CLM3 and CAM3) Using a Dynamic Global Vegetation Model. *J Climate* 19:2290-2301.
- Bonan GB, Pollard D, Thompson SL (1992) Effects of Boreal Forest Vegetation on Global Climate. *Nature* 359:716-718.
- Brandefelt J, Otto-Bliesner BL (2009) Equilibration and variability in a Last Glacial Maximum climate simulation with CCSM3. *Geophys Res Lett* 36:-.
- Budikova D (2009) Role of Arctic sea ice in global atmospheric circulation: A review. *Global Planet Change* 68:149-163.
- Bunn AG, Goetz SJ, Kimball JS, Zhang K (2007) Northern High-Latitude Ecosystems Respond to Climate Change. *EOS* 88:333-340.
- Cavalieri DJ, Parkinson CL (2012) Arctic sea ice variability and trends, 1979-2010. *The Cryosphere* 6:881-889.
- Chapin FS, Sturm M, Serreze MC, McFadden JP, Key JR, Lloyd AH, McGuire AD, Rupp TS, Lynch AH, Schimel JP, Beringer J, Chapman WL, Epstein HE, Euskirchen ES, Hinzman LD, Jia G, Ping CL, Tape KD, Thompson CDC, Walker DA, Welker JM (2005) Role of land-surface changes in Arctic summer warming. *Science* 310:657-660.
- Chung CE, Räisänen P (2011) Origin of the Arctic warming in climate models. *Geophys Res Lett* 38:L21704. doi:21710.21029/22011gl049816.

- Collins WD, Bitz CM, Blackmon ML, Bonan GB, Bretherton CS, Carton JA, Chang P, Doney SC, Hack JJ, Henderson TB, Kiehl JT, Large WG, McKenna DS, Santer BD, Smith RD (2006) The Community Climate System Model version 3 (CCSM3). *J Climate* 19:2122-2143.
- Collins WD, Rasch P, Boville B, Hack J, McCaa J, Williamson D, Kiehl J, Briegleb B, Bitz C, Lin S-J, Zhang M, Dai Y (2004) Description of the NCAR Community Atmosphere Model (CAM 3.0): NCAR/TN-464+STR NCAR TECHNICAL NOTE. National Center For Atmospheric Research, Boulder, Colorado, p. 226.
- Curry JA, Rossow WB, Randall D, Schramm JL (1996) Overview of Arctic cloud and radiation characteristics. *J Climate* 9:1731-1764.
- Curry JA, Schramm JL, Serreze MC (1995) Water-Vapor Feedback over the Arctic-Ocean. *J Geophys Res-Atmos* 100:14223-14229.
- Cuzzone J, Vavrus S (2011) The relationships between Arctic sea ice and cloud-related variables in the ERA-Interim reanalysis and CCSM3. *Environ Res Lett* 6.
- Danabasoglu G, Gent PR (2009) Equilibrium Climate Sensitivity: Is It Accurate to Use a Slab Ocean Model? *J Climate* 22:2494-2499.
- Dee DP, Uppala S (2009) Variational bias correction of satellite radiance data in the ERA-Interim reanalysis. *Q J Roy Meteor Soc* 135:1830-1841.
- Dee DP, Uppala SM, Simmons AJ, Berrisford P, Poli P, Kobayashi S, Andrae U, Balmaseda MA, Balsamo G, Bauer P, Bechtold P, Beljaars ACM, van de Berg L, Bidlot J, Bormann N, Delsol C, Dragani R, Fuentes M, Geer AJ,

- Haimberger L, Healy SB, Hersbach H, Holm EV, Isaksen L, Kallberg P, Kohler M, Matricardi M, McNally AP, Monge-Sanz BM, Morcrette JJ, Park BK, Peubey C, de Rosnay P, Tavolato C, Thepaut JN, Vitart F (2011) The ERA-Interim reanalysis: configuration and performance of the data assimilation system. *Q J Roy Meteor Soc* 137:553-597.
- Deser C, Magnusdottir G, Saravanan R, Phillips A (2004) The effects of North Atlantic SST and sea ice anomalies on the winter circulation in CCM3. Part II: Direct and indirect components of the response. *J Climate* 17:877-889.
- Deser C, Tomas R, Alexander M, Lawrence D (2010) The Seasonal Atmospheric Response to Projected Arctic Sea Ice Loss in the Late Twenty-First Century. *J Climate* 23:333-351.
- Dethloff K, Rinke A, Benkel A, Koltzow M, Sokolova E, Saha SK, Handorf D, Dorn W, Rockel B, von Storch H, Haugen JE, Roed LP, Roeckner E, Christensen JH, Stendel M (2006) A dynamical link between the Arctic and the global climate system. *Geophys Res Lett* 33:L03703. doi:03710.01029/02005gl025245.
- Eastman R, Warren SG (2010a) Arctic Cloud Changes from Surface and Satellite Observations. *J Climate* 23:4233-4242.
- Eastman R, Warren SG (2010b) Interannual Variations of Arctic Cloud Types in Relation to Sea Ice. *J Climate* 23:4216-4232.
- Eisenman I, Untersteiner N, Wettlaufer JS (2007) On the reliability of simulated Arctic sea ice in global climate models. *Geophys Res Lett* 34:-.
- Eldrett JS, Greenwood DR, Harding IC, Huber M (2009) Increased seasonality

- through the Eocene to Oligocene transition in northern high latitudes. *Nature* 459:969-U991.
- Finnis J, Holland MM, Serreze MC, Cassano JJ (2007) Response of Northern Hemisphere extratropical cyclone activity and associated precipitation to climate change, as represented by the Community Climate System Model. *J Geophys Res-Biogeophys* 112:-.
- Foley JA, Kutzbach JE, Coe MT, Levis S (1994) Feedbacks between Climate and Boreal Forests during the Holocene Epoch. *Nature* 371:52-54.
- Foley JA, Prentice IC, Ramankutty N, Levis S, Pollard D, Sitch S, Haxeltine A (1996) An integrated biosphere model of land surface processes, terrestrial carbon balance, and vegetation dynamics. *Global Biogeochem Cy* 10:603-628.
- Folley JA (2005) Tipping points in the tundra. *Science* 310:627-628.
- Francis JA, Chan WH, Leathers DJ, Miller JR, Veron DE (2009) Winter Northern Hemisphere weather patterns remember summer Arctic sea-ice extent. *Geophys Res Lett* 36:L07503. doi:07510.01029/02009gl037274.
- Francis JA, Hunter E (2006) New insight into the disappearing Arctic sea ice. *Eos Trans. AGU* 87:509.
- Francis JA, Hunter E, Key JR, Wang XJ (2005) Clues to variability in Arctic minimum sea ice extent. *Geophys Res Lett* 32:-.
- Gerdes R (2006) Atmospheric response to changes in Arctic sea ice thickness. *Geophys Res Lett* 33:L18709. doi:18710.11029/12006gl027146.

- Goetz SJ, Bunn AG, Fiske GJ, Houghton RA (2005) Satellite-observed photosynthetic trends across boreal North America associated with climate and fire disturbance. *P Natl Acad Sci USA* 102:13521-13525.
- Gorodetskaya IV, Tremblay LB, Liepert B, Cane MA, Cullather RI (2008) The influence of cloud and surface properties on the Arctic Ocean shortwave radiation budget in coupled models. *J Climate* 21:866-882.
- Graversen RG (2006) Do changes in the midlatitude circulation have any impact on the Arctic surface air temperature trend? *J Climate* 19:5422-5438.
- Graversen RG, Mauritsen T, Tjernstrom M, Kallen E, Svensson G (2008) Vertical structure of recent Arctic warming. *Nature* 451:53-56.
- Graversen RG, Wang MH (2009) Polar amplification in a coupled climate model with locked albedo. *Clim Dynam* 33:629-643.
- Hack J, Caron J, Danabasoglu G, Oleson K (2006) CCSM-CAM3 Climate Simulation Sensitivity to Changes in Horizontal Resolution. *J Climate* 19:2267-2289.
- Holland MM, Bitz CM (2003) Polar amplification of climate change in coupled models. *Clim Dynam* 21:221-232.
- Honda M, Inoue J, Yamane S (2009) Influence of low Arctic sea-ice minima on anomalously cold Eurasian winters. *Geophys Res Lett* 36:Artn L08707. doi:08710.01029/02008gl037079.
- Intrieri JM, Fairall CW, Shupe MD, Persson POG, Andreas EL, Guest PS, Moritz RE (2002) An annual cycle of Arctic surface cloud forcing at SHEBA. *J*

Geophys Res-Oceans 107:-.

IPCC (2007) Climate change 2007: the physical science basis. Cambridge Univ Press.

Isaksen ISA, Gauss M, Myhre G, Walter Anthony KM, Ruppel C (2011) Strong atmospheric chemistry feedback to climate warming from Arctic methane emissions. *Global Biogeochem Cy* 25:GB2002.

Jaiser R, Dethloff K, Handorf D, Rinke A, Cohen J (2012) Impact of sea ice cover changes on the Northern Hemisphere atmospheric winter circulation. *Tellus A* 64.

Jeong J-H, Kug J-S, Kim B-M, Min S-K, Linderholm H, Ho C-H, Rayner D, Chen D, Jun S-Y (2012) Greening in the circumpolar high-latitude may amplify warming in the growing season. *Clim Dynam* 38:1421-1431.

Jeong S-J, Ho C-H, Kim K-Y, Kim J, Jeong J-H, Park T-W (2010) Potential impact of vegetation feedback on European heat waves in a 2 x CO₂ climate. *Climatic Change* 99:625-635.

Jeong S-J, Ho C-H, Park T-W, Kim J, Levis S (2011) Impact of vegetation feedback on the temperature and its diurnal range over the Northern Hemisphere during summer in a 2 × CO₂ climate. *Clim Dynam* 37:821-833.

Jia GSJ, Epstein HE, Walker DA (2003) Greening of arctic Alaska, 1981-2001. *Geophys Res Lett* 30:2067.

Jones CG, Wyser K, Ullerstig A, Willen U (2004) The Rossby Centre regional atmospheric climate model part II: Application to the Arctic climate. *Ambio*

33:211-220.

Jun S-Y, Ho C-H, Kim B-M, Jeong J-H (2013) Sensitivity of Arctic warming to sea surface temperature distribution over melted sea-ice region in atmospheric general circulation model experiments. *Clim Dynam*:1-15.

Karlsson J, Svensson G (2011) The simulation of Arctic clouds and their influence on the winter surface temperature in present-day climate in the CMIP3 multi-model dataset. *Clim Dynam* 36:623-635.

Kay JE, Gettelman A (2009) Cloud influence on and response to seasonal Arctic sea ice loss. *J Geophys Res-Atmos* 114:-.

Kiehl JT, Shields CA, Hack JJ, Collins WD (2006) The climate sensitivity of the Community Climate System Model version 3 (CCSM3). *J Climate* 19:2584-2596.

Kirkevåg A, Iversen T, Kristjánsson JE, Seland O, Debernard JB (2008) On the additivity of climate response to anthropogenic aerosols and CO₂, and the enhancement of future global warming by carbonaceous aerosols. *Tellus A* 60:513-527.

Lawrence DM, Slater AG, Romanovsky VE, Nicolsky DJ (2008a) Sensitivity of a model projection of near-surface permafrost degradation to soil column depth and representation of soil organic matter. *J Geophys Res-Earth* 113:-.

Lawrence DM, Slater AG, Tomas RA, Holland MM, Deser C (2008b) Accelerated Arctic land warming and permafrost degradation during rapid sea ice loss. *Geophys Res Lett* 35:-.

- Lee E, Chase TN, Lawrence PJ, Rajagopalan B (2008) Model assessment of the observed relationship between El Nino and the northern East Asian summer monsoon using the Community Climate System Model Community Atmosphere Model-Community Land Model version 3 (CAM-CLM3). *J Geophys Res-Atmos* 113:-.
- Levis S, Bonan GB, Vertenstein M, Oleson KW (2004) The Community Land Model's Dynamic Global Vegetation Model (CLM-DGVM): technical description and user's guide. Technical Note NCAR/TN-459+IA. National Center for Atmospheric Research, Boulder, Colorado, p. 50.
- Levis S, Foley JA, Pollard D (1999) Potential high-latitude vegetation feedbacks on CO₂-induced climate change. *Geophys Res Lett* 26:747-750.
- Liu Y, Key JR, Francis JA, Wang X (2007) Possible causes of decreasing cloud cover in the Arctic winter, 1982-2000. *Geophys Res Lett* 34:-.
- Liu Y, Key JR, Wang X (2008) The influence of changes in cloud cover on recent surface temperature trends in the Arctic. *J Climate* 21:705-715.
- Liu YH, Key JR, Wang XJ (2009) Influence of changes in sea ice concentration and cloud cover on recent Arctic surface temperature trends. *Geophys Res Lett* 36:-.
- Long SP, Ainsworth EA, Leakey ADB, Nosberger J, Ort DR (2006) Food for thought: Lower-than-expected crop yield stimulation with rising CO₂ concentrations. *Science* 312:1918-1921.
- Magnusdottir G, Deser C, Saravanan R (2004) The effects of North Atlantic SST and sea ice anomalies on the winter circulation in CCM3. Part I: Main

- features and storm track characteristics of the response. *J Climate* 17:857-876.
- McGregor S, Sen Gupta A, Holbrook NJ, Power SB (2009) The Modulation of ENSO Variability in CCSM3 by Extratropical Rossby Waves. *J Climate* 22:5839-5853.
- McMahon SM, Parker GG, Miller DR (2010) Evidence for a recent increase in forest growth. *Proc Natl Acad Sci U S A* 107:3611-3615.
- Meehl GA, Arblaster JM, Lawrence DM, Seth A, Schneider EK, Kirtman BP, Min D (2006a) Monsoon regimes in the CCSM3. *J Climate* 19:2482-2495.
- Meehl GA, Washington WM, Santer BD, Collins WD, Arblaster JM, Hu AX, Lawrence DM, Teng HY, Buja LE, Strand WG (2006b) Climate change projections for the twenty-first century and climate change commitment in the CCSM3. *J Climate* 19:2597-2616.
- Merkel U, Prange M, Schulz M (2010) ENSO variability and teleconnections during glacial climates. *Quaternary Sci Rev* 29:86-100.
- Miller JR, Chen YH, Russell GL, Francis JA (2007) Future regime shift in feedbacks during Arctic winter. *Geophys Res Lett* 34.
- Murray RJ, Simmonds I (1995) Responses of Climate and Cyclones to Reductions in Arctic Winter Sea-Ice. *J Geophys Res-Oceans* 100:4791-4806. doi:4710.1029/4794JC02206.
- Neale RB, Chen C-C, Lauritzen PH, Gettelman A, Park S, Williamson DL, Conley AJ, Garcia R, Kinnison D, Lamarque J-F, Marsh D, Mills M, Smith AK, Tilmes S, Vitt F, Morrison H, Cameron-Smith P, Collins WD, Iacono MJ,

- Easter RC, Ghan SJ, Liu X, Rasch PJ, Taylor MA (2012) Description of the NCAR Community Atmosphere Model (CAM 5.0). NCAR TECHNICAL NOTE NCAR/TN-486+STR National Center for Atmospheric Research, Boulder, Colorado, p. 274.
- Neale RB, Richter JH, Conley AJ, Park S, Lauritzen PH, Gettelman A, Williamson DL, Rasch PJ, Vavrus SJ, Taylor MA, Collins WD, Zhang M, Lin S-J (2011) Description of the NCAR Community Atmosphere Model (CAM4). NCAR Tech. Note NCAR/TN-4851STR. National Center for Atmospheric Research, Boulder, Colorado, p. 212.
- Newson RL (1973) Response of a General Circulation Model of Atmosphere to Removal of Arctic Ice-Cap. *Nature* 241:39-40.
- Notaro M, Liu ZY (2008) Statistical and dynamical assessment of vegetation feedbacks on climate over the boreal forest. *Clim Dynam* 31:691-712.
- Notaro M, Vavrus S, Liu Z (2007) Global Vegetation and Climate Change due to Future Increases in CO₂ as Projected by a Fully Coupled Model with Dynamic Vegetation*. *J Climate* 20:70-90.
- O'ishi R, Abe-Ouchi A (2009) Influence of dynamic vegetation on climate change arising from increasing CO₂. *Clim Dynam* 33:645-663.
- Overland JE, Wang MY (2010) Large-scale atmospheric circulation changes are associated with the recent loss of Arctic sea ice. *Tellus A* 62:1-9.
- Overpeck JT, Sturm M, Francis JA, Perovich DK, Serreze MC, Benner R, Carmack EC, Chapin FS, Gerlach SC, Hamilton LC, Hinzman LD, Holland MM, Huntington HP, Key JR, Lloyd AH, MacDonald GM, McFadden JP,

- Noone D, Prowse TD, Schlosser P, Vörösmarty C (2005) Arctic System on Trajectory to New, Seasonally Ice-Free State. *Eos Trans. AGU* 86:309-316.
- Palm SP, Strey ST, Spinhirne J, Markus T (2010) Influence of Arctic sea ice extent on polar cloud fraction and vertical structure and implications for regional climate. *J Geophys Res-Atmos* 115:-.
- Petoukhov V, Semenov VA (2010) A link between reduced Barents-Kara sea ice and cold winter extremes over northern continents. *Journal of Geophysical Research: Atmospheres* 115:D21111. doi:21110.21029/22009jd013568.
- Rampal P, Weiss J, Dubois C, Campin JM (2011) IPCC climate models do not capture Arctic sea ice drift acceleration: Consequences in terms of projected sea ice thinning and decline. *Journal of Geophysical Research: Oceans* 116:C00D07.
- Rayner NA, Parker DE, Horton EB, Folland CK, Alexander LV, Rowell DP, Kent EC, Kaplan A (2003) Global analyses of sea surface temperature, sea ice, and night marine air temperature since the late nineteenth century. *J Geophys Res* 108:4407. doi:4410.1029/2002JD002670.
- Reynolds RW, Rayner NA, Smith TM, Stokes DC, Wang WQ (2002) An improved in situ and satellite SST analysis for climate. *J Climate* 15:1609-1625.
- Rind D, Healy R, Parkinson C, Martinson D (1995) The role of sea ice in 2×CO₂ climate model sensitivity. Part I: the total influence of sea ice thickness and extent. *J Climate* 8:449-463.
- Saha S, Moorthi S, Pan HL, Wu XR, Wang JD, Nadiga S, Tripp P, Kistler R,

- Woollen J, Behringer D, Liu HX, Stokes D, Grumbine R, Gayno G, Wang J, Hou YT, Chuang HY, Juang HMH, Sela J, Iredell M, Treadon R, Kleist D, Van Delst P, Keyser D, Derber J, Ek M, Meng J, Wei HL, Yang RQ, Lord S, Van den Dool H, Kumar A, Wang WQ, Long C, Chelliah M, Xue Y, Huang BY, Schemm JK, Ebisuzaki W, Lin R, Xie PP, Chen MY, Zhou ST, Higgins W, Zou CZ, Liu QH, Chen Y, Han Y, Cucurull L, Reynolds RW, Rutledge G, Goldberg M (2010) The Ncep Climate Forecast System Reanalysis. *B Am Meteorol Soc* 91:1015-1057.
- Schneider EK, Fennessy MJ, Kinter JL (2009) A Statistical-Dynamical Estimate of Winter ENSO Teleconnections in a Future Climate. *J Climate* 22:6624-6638.
- Schweiger AJ, Lindsay RW, Francis JA, Key J, Intrieri JM, Shupe MD (2002) Validation of TOVS Path-P data during SHEBA. *J Geophys Res-Oceans* 107:-.
- Schweiger AJ, Lindsay RW, Vavrus S, Francis JA (2008) Relationships between Arctic sea ice and clouds during autumn. *J Climate* 21:4799-4810.
- Screen JA, Simmonds I (2010a) The central role of diminishing sea ice in recent Arctic temperature amplification. *Nature* 464:1334-1337.
- Screen JA, Simmonds I (2010b) Increasing fall-winter energy loss from the Arctic Ocean and its role in Arctic temperature amplification. *Geophys Res Lett* 37:L16707. doi:16710.11029/12010GL044136.
- Screen JA, Simmonds I, Deser C, Tomas R (2012) The Atmospheric Response to Three Decades of Observed Arctic Sea Ice Loss. *J Climate* 26:1230-1248.

- Seierstad IA, Bader J (2009) Impact of a projected future Arctic Sea Ice reduction on extratropical storminess and the NAO. *Clim Dynam* 33:937-943.
- Semmler T, McGrath R, Wang S (2012) The impact of Arctic sea ice on the Arctic energy budget and on the climate of the Northern mid-latitudes. *Clim Dynam* 39:2675-2694.
- Serreze MC, Barry RG (2009) *The Arctic Climate System*. Cambridge University Press.
- Serreze MC, Francis JA (2006) The arctic amplification debate. *Climatic Change* 76:241-264.
- Serreze MC, Walsh JE, Chapin FS, Osterkamp T, Dyurgerov M, Romanovsky V, Oechel WC, Morison J, Zhang T, Barry RG (2000) Observational evidence of recent change in the northern high-latitude environment. *Climatic Change* 46:159-207.
- Shellito CJ, Lamarque JF, Sloan LC (2009) Early Eocene Arctic climate sensitivity to pCO₂ and basin geography. *Geophys Res Lett* 36:-.
- Shupe MD, Intrieri JM (2004) Cloud radiative forcing of the Arctic surface: The influence of cloud properties, surface albedo, and solar zenith angle. *J Climate* 17:616-628.
- Singarayer JS, Bamber JL, Valdes PJ (2006) Twenty-first-century climate impacts from a declining Arctic sea ice cover. *J Climate* 19:1109-1125.
- Singarayer JS, Valdes PJ, Bamber JL (2005) The atmospheric impact of uncertainties in recent Arctic sea ice reconstructions. *J Climate* 18:3996-4012.

- Sinha A, Harries JE (1995) Water-Vapor and Greenhouse Trapping - the Role of Far-Infrared Absorption. *Geophys Res Lett* 22:2147-2150.
- Sitch S, Smith B, Prentice IC, Arneth A, Bondeau A, Cramer W, Kaplan JO, Levis S, Lucht W, Sykes MT, Thonicke K, Venevsky S (2003) Evaluation of ecosystem dynamics, plant geography and terrestrial carbon cycling in the LPJ dynamic global vegetation model. *Global Change Biol* 9:161-185.
- Skific N, Francis JA, Cassano JJ (2009a) Attribution of Projected Changes in Atmospheric Moisture Transport in the Arctic: A Self-Organizing Map Perspective. *J Climate* 22:4135-4153.
- Skific N, Francis JA, Cassano JJ (2009b) Attribution of Seasonal and Regional Changes in Arctic Moisture Convergence. *J Climate* 22:5115-5134.
- Stokes GM, Schwartz SE (1994) The Atmospheric Radiation - Measurement (Arm) Program - Programmatic Background and Design of the Cloud and Radiation Test-Bed. *B Am Meteorol Soc* 75:1201-1221.
- Stroeve J, Holland MM, Meier W, Scambos T, Serreze M (2007) Arctic sea ice decline: Faster than forecast. *Geophys Res Lett* 34.
- Stroeve JC, Maslanik J, Serreze MC, Rigor I, Meier W, Fowler C (2011) Sea ice response to an extreme negative phase of the Arctic Oscillation during winter 2009/2010. *Geophys Res Lett* 38:L02502.
- Stroeve JC, Serreze MC, Holland MM, Kay JE, Malanik J, Barrett AP (2012) The Arctic's rapidly shrinking sea ice cover: a research synthesis. *Climatic Change* 110:1005-1027.

- Sturm M, Holmgren J, McFadden JP, Liston GE, Chapin FS, Racine CH (2001) Snow–Shrub Interactions in Arctic Tundra: A Hypothesis with Climatic Implications. *J Climate* 14:336-344.
- Swann AL, Fung IY, Levis S, Bonan GB, Doney SC (2009) Changes in Arctic vegetation amplify high-latitude warming through the greenhouse effect. *PNAS*.
- Swann AL, Fung IY, Levis S, Bonan GB, Doney SC (2010) Changes in Arctic vegetation amplify high-latitude warming through the greenhouse effect. *PNAS* Natl Acad Sci USA 107:1295-1300.
- Tape K, Sturm M, Racine C (2006) The evidence for shrub expansion in Northern Alaska and the Pan-Arctic. *Glob Change Biol* 12:686-702.
- Teng HY, Washington WM, Meehl GA, Buja LE, Strand GW (2006) Twenty-first century Arctic climate change in the CCSM3 IPCC scenario simulations. *Clim Dynam* 26:601-616.
- Thompson DWJ, Wallace JM (1998) The Arctic Oscillation signature in the wintertime geopotential height and temperature fields. *Geophys Res Lett* 25:1297-1300.
- Thompson SL, Pollard D (1995) A Global Climate Model (Genesis) with a Land-Surface Transfer Scheme (Lsx) .1. Present Climate Simulation. *J Climate* 8:732-761.
- Tomé AR, Miranda PMA (2004) Piecewise linear fitting and trend changing points of climate parameters. *Geophys Res Lett* 31:L02207.

- Trenberth KE, Caron JM (2001) Estimates of Meridional Atmosphere and Ocean Heat Transports. *J Climate* 14:3433-3443.
- Uppala SM, Kallberg PW, Simmons AJ, Andrae U, Bechtold VD, Fiorino M, Gibson JK, Haseler J, Hernandez A, Kelly GA, Li X, Onogi K, Saarinen S, Sokka N, Allan RP, Andersson E, Arpe K, Balmaseda MA, Beljaars ACM, Van De Berg L, Bidlot J, Bormann N, Caires S, Chevallier F, Dethof A, Dragosavac M, Fisher M, Fuentes M, Hagemann S, Holm E, Hoskins BJ, Isaksen L, Janssen PAEM, Jenne R, McNally AP, Mahfouf JF, Morcrette JJ, Rayner NA, Saunders RW, Simon P, Sterl A, Trenberth KE, Untch A, Vasiljevic D, Viterbo P, Woollen J (2005) The ERA-40 re-analysis. *Q J Roy Meteor Soc* 131:2961-3012.
- Vavrus S (2004) The impact of cloud feedbacks on Arctic climate under greenhouse forcing. *J Climate* 17:603-615.
- Vavrus S, Holland MM, Bailey DA (2011a) Changes in Arctic clouds during intervals of rapid sea ice loss. *Clim Dynam* 36:1475-1489.
- Vavrus S, Waliser D (2008) An Improved Parametrization for Simulating Arctic Cloud Amount in the CCSM3 Climate Model. *J Climate* 21:5673-5687.
- Vavrus S, Waliser D, Schweiger A, Francis J (2009) Simulations of 20th and 21st century Arctic cloud amount in the global climate models assessed in the IPCC AR4. *Clim Dynam* 33:1099-1115.
- Vavrus SJ, Bhatt US, Alexeev VA (2011b) Factors Influencing Simulated Changes in Future Arctic Cloudiness. *J Climate* 24:4817-4830.
- Walsh JE, Chapman WL, Portis DH (2009) Arctic Cloud Fraction and Radiative

- Fluxes in Atmospheric Reanalyses. *J Climate* 22:2316-2334.
- Walsh JE, Vavrus SJ, Chapman WL (2005) Workshop on Modeling of the Arctic Atmosphere. *B Am Meteorol Soc* 86:845-852.
- Wang XJ, Key JR (2003) Recent trends in arctic surface, cloud, and radiation properties from space. *Science* 299:1725-1728.
- Wang XJ, Key JR (2005a) Arctic surface, cloud, and radiation properties based on the AVHRR Polar Pathfinder dataset. Part I: Spatial and temporal characteristics. *J Climate* 18:2558-2574.
- Wang XJ, Key JR (2005b) Arctic surface, cloud, and radiation properties based on the AVHRR Polar Pathfinder dataset. Part II: Recent trends. *J Climate* 18:2575-2593.
- Warshaw M, Rapp RP (1973) An experiment on the sensitivity of a global circulation model. *J Appl Meteorol Clim* 12:43-49.
- Wetherald RT, Manabe S (1988) Cloud Feedback Processes in a General-Circulation Model. *J Atmos Sci* 45:1397-1415.
- Winton M (2011) Do Climate Models Underestimate the Sensitivity of Northern Hemisphere Sea Ice Cover? *J Climate* 24:3924-3934.
- Winton M, Takahashi K, Held IM (2010) Importance of Ocean Heat Uptake Efficacy to Transient Climate Change. *J Climate* 23:2333-2344.
- Xin XG, Zhou TJ, Yu RC (2008) The Arctic Oscillation in coupled climate models. *Chinese J Geophys-Ch* 51:337-351.

- Yoshida Y, Maruyama K, Takahara H (2008) Global Warming Projections Using the Community Climate System Model, CCSM3. *Nec Tech J* 3:73-77.
- Yu JY, Sun FP, Kao HY (2009) Contributions of Indian Ocean and Monsoon Biases to the Excessive Biennial ENSO in CCSM3. *J Climate* 22:1850-1858.
- Zhang T, Sun DZ, Neale R, Rasch PJ (2009) An Evaluation of ENSO Asymmetry in the Community Climate System Models: A View from the Subsurface. *J Climate* 22:5933-5961.
- Zygmuntowska M, Mauritsen T, Quaas J, Kaleschke L (2012) Arctic Clouds and Surface Radiation – a critical comparison of satellite retrievals and the ERA-Interim reanalysis. *Atmos. Chem. Phys.* 12:6667-6677.

국문초록

최근 수 십 년간 북극 지역에서는 전구 평균 기온 상승보다 더 큰 기온 상승이 발생하였다. 북극 증폭 (Arctic amplification) 이라 불리는 이 북극지역의 강한 기온 상승 현상에 다양한 기후 요소가 영향을 미칠 수 있음이 여러 연구를 통해 밝혀지고 있다. 본 연구에서는 전구 식생역학모델 (dynamic global vegetation model)의 기후모델에의 접합과 구름모수화과정 및 해빙 해수면 경계조건을 개선한 모델링을 통해 식생과 구름이 이러한 북극의 기후 변화에 미치는 영향에 대하여 살펴보았다.

전구역학식생모델을 접합한 기후모델을 이용한 이산화탄소 배증 실험 결과, 온실기체 증가에 따른 고위도 지역의 식생 증가가 북극지역의 기온 상승에 기여하는 것으로 나타난다. 이산화탄소 배증실험에서 역학전구식생모델은 이산화탄소 배증시 북아메리카, 유라시아 대륙 북부의 고위도 지역의 식생 증가를 모의하였다. 식생의 변화를 고려하지 않고 현재 기후에서 모의된 식생분포를 고정한 이산화탄소 배증 실험결과와 비교하였을 때, 이러한 식생 증가는 식생성장 계절에서의 고위도 대륙지역의 기온 상승을 야기하였으며 이에 따라 북극으로의 대기중 북향 수송 에너지 역시 증가하였다. 결국 식생의 변화가 고려된 실험에서 가을철 북극지역의 해빙은 면적과 두께 모두 크게 감소하였으며 이에 따라 북극지역의 기온 역시 크게 상승하였다. 이 결과는 최근 위성자료 등을 통해 관측된 고위도 지역의 식생의 증가가 양의 되먹임 과정을 통해 북극지역의 기온 상승 및 해빙 감소에 기여했을 가능성을 암시한다.

재분석자료와 위성자료 분석과 개선된 기후모델링 실험을 통해 살펴본 결과, 최근 겨울철 북극지역의 해빙 감소와 이에 연관된 북극의 기후시스템의 변화가 북극지역의 구름 증가에 기여하며 이에 따라 북극지역의 구름이 북극지역의 기온 상승에 미치는 영향이 커지는 것으로 나타난다. 재분석자료와 위성자료의 북극지역 겨울철 평균 지면대기온도, 운량의 변화 경향은 1997/1998년을 기점으로 약한 감소 경향에서 강한 증가 경향으로 변화하였다. 겨울철 해빙 역시 1997/1998년을 기점으로 급격하게 감소하기 시작하였다. 북극지역 평균 해빙에 대한 구름수분량의 회귀분석 결과 1997/1998년 이전 시기는 해빙 변화에 대한 구름수분량의 변화가 북극지역 경계에 나타남에 반해 1997/1998년 이후는 북극지역의 중앙에서 나타난다. 두 시기의 평균 대기장의 차이를 살펴보면 1997/1998년 이후 시기에 해빙의 감소, 지면대기온도의 증가, 하층 안정도의 감소, 행성경계층의 확장, 대기경압성의 발달이 발생하였으며 이러한 북극지역의 대기조건의 변화는 국지대류 및 저기압 발생에 호조건을 제공한다. 따라서 1997/1998년 이후 시기에 해빙의 감소와 북극지역의 운량의 증가가 더욱 밀접하게 연관되며, 북극지역 평균 하층운량과 북극지역 동서방향 평균 기온 및 비습의 회귀분석 결과 역시 이러한 관계의 변화를 제시하고 있다.

이러한 최근 북극지역 해빙감소와 운량 증가 메커니즘을 개선된 대기모델 실험에서 확인하였다. 먼저 해빙 변화에 대한 보다 정확한 대기모델의 경계조건을 얻기 위하여 해빙 변화에 대한 해수면온도를 북극지역의 해빙 면적과 해수면온도의 분포 관계에서 계수 다항식 근사 (polynomial fitting)를 통하여 얻어진 3차 다항식을 이용하여 보정

하였다. 이 보정 방안을 이용한 대기모델 실험 결과는 해수의 어는점을 이용하는 전통적 보정 방식에 비하여 관측에 더 가까운 대기의 반응을 모의하였다. 다음으로 보다 정확한 운량의 변화를 모의하기 위하여 기존 연구에서 제안된 FREEZEDRY 운량모수화 방안을 대기모델에 접합하고 성능을 확인하였다. 이 운량모수화 방안을 이용하였을 때 북극지역 겨울철 운량의 과다모의 경향과 운량-기온 관계가 개선된 모의 결과를 얻었다. 이 계수 다항식 근사 방안과 운량모수화 방안의 접합을 통해 대기모델 실험 결과, 관측에서 나타난 겨울철 해빙의 감소가 지면대기온도 증가, 하층안정도 감소, 행성경계층의 확장, 대기경압성의 증가 등의 대기조건의 변화를 야기하고, 이에 따라 운량 역시 증가함을 확인하였다. 이에 따라 해빙이 감소하는 경우 운량이 하층기온 상승에 미치는 영향 역시 커짐을 확인하였다. 이 해빙의 감소와 운량의 증가, 이에 따른 운량과 주변 기후요소와의 관계변화는 제 5차 결합기후모델비교사업 (coupled model intercomparison project phase 5)에 참여한 모델들의 미래기후실험 결과 앙상블 평균에서도 마찬가지로 나타나고 있다. 즉 재분석 자료와 모델 실험 결과들은 해빙이 감소하는 조건에서 겨울철 북극지역의 구름이 지면대기온도와 하층대기의 기온 증가에 더욱 기여할 수 있음을 제시한다.

주요어: 북극, 북극중폭, 기후모델링, 식생, 구름, 해빙

학 번: 2008-30822